ISSN 0915-9916

Readout

HORIBA Technical Reports

May 2023 No. 57

特集　次世代環境・エネルギーへの取組

2022 堀場雅夫賞

カーボンニュートラル社会に向けた水素の利活用に貢献する分析・計測技術

HORIBA

https://www.horiba.com/jp/publications/readout/

Readout
HORIBA Technical Reports
May 2023 No.57

カーボンニュートラル社会実現への動きは世界的に加速しており，環境保全と産業発展の両立に向けてエネルギー分野でのイノベーションが期待されています。今号では，対象分野を「カーボンニュートラル社会に向けた水素の利活用に貢献する分析・計測技術」にした堀場雅夫賞と持続可能な社会の実現に貢献するHORIBAの技術や取り組みについて紹介します。

■表紙写真
撮影：写真家　松井秀雄氏
（二科会写真部　会員）
藤の花が咲き誇る姿を求めて，中部地方の庭園を尋ねました。雨の中に立ち込める花の香りと共に，花の色や木々の緑を満喫し，満ち足りた心持ちになりました。

■誌名について
誌名 Readout（リードアウト）には，「当社が創造・育成した製品・技術を広く世にお知らせし，多くの皆様に読み取っていただきたい」という願いが込められています。

特集 次世代環境・エネルギーへの取組
2022 堀場雅夫賞
カーボンニュートラル社会に向けた水素の利活用に貢献する分析・計測技術

Readout
HORIBA Technical Reports
May 2023 No.57

Next Generation Environmental and Energy Initiatives
2022 Masao Horiba Awards

Analytical and measurement technologies that contribute to the use of hydrogen for a decarbonized society

Realizing a carbon neutral society is accelerating worldwide and innovation in the energy field is expected to help achieve both environmental conservation and industrial development. This issue will introduce the Masao Horiba Awards, under the theme of "Analytical and measurement technologies that contribute to the use of hydrogen for a decarbonized society," as well as HORIBA's technologies and initiatives that contribute to the realization of a sustainable society.

In search of fully bloomed wisteria flowers, I visited a garden in the Chubu region. I enjoyed the colors of the flowers and the greenery of the trees along with the fragrance of the flowers in the rain.
-Photographer MATSUI Hideo-
(Member of Nikakai Association of Photographers)

Name of this Journal

This Journal is named "Readout" in the hope that "the products and technology we have created and developed will be read out and so become widely known".

水素エネルギー社会の展望

中村 博司
NAKAMURA Hiroshi
株式会社堀場製作所
コーポレートオフィサー(執行役員)
開発本部　本部長
博士(工学)
Corporate Officer
Chief Technology Officer
R&D Division General Manager
HORIBA, Ltd.
Doctor of Engineering

新型コロナウイルスの感染拡大は，世界中で多くの国々が経済活動の停滞をもたらし，2020年の実質GDP成長率はマイナス6.3％と第2次世界大戦後最大の落ち込みを記録しました。しかし，この危機への対応策として，多くの国々は環境に配慮した持続可能な経済対策を取り入れることを決めました。欧州連合は，「グリーンリカバリー」施策を打ち出し，「欧州グリーンディール」を発表し，2030年までに温室効果ガス排出量を半減し，2050年には実質ゼロにすることを目標としました。欧州復興基金の創設も発表され，環境に配慮した政策を支援するための基金として注目されました。米国もバイデン政権に移行し，環境に配慮した政策を打ち出し，G7サミットにおいて温室効果ガス排出量を2030年までに半減することを表明しました。

2050年に「カーボンニュートラル」を実現するためには，再生可能エネルギーを一次エネルギーとして生産された水素「グリーン水素」が不可欠であるとして，欧州委員会は「欧州の気候中立に向けた水素戦略」を発表しました。この戦略では，2024年までに少なくとも6 GW，2030年までに40 GWの水電解による水素製造設備を設置することを目標としました。ドイツやフランスも，国家戦略を策定し，2030年までにそれぞれ5 GW，6.5 GWの水素製造能力を持つことを目指し，多額の投資を計画しています。

注目されている「水素」の産業利用の歴史は非常に古く，1900年初頭に開発されたハーバーボッシュ法で，窒素と水素からアンモニアを生産することによって化学肥料の大量生産を可能にしたことは20世紀以降の人口急増を支えてきました。現在でも，アンモニア製造の他，石油精製，石油化学製品に多く利用されています。しかしながら，2020年の段階で，産業利用される水素の95％が化石燃料の水蒸気改質によって製造される，いわゆる「グレー水素」と言われるもので，製造時にCO_2を排出します。

カーボンニュートラルを実現するために，再度注目をされている水素は，不安定な電力供給が課題である太陽光や風力発電などの再生可能エネルギーから作られる

「グリーン水素」であり，その利用方法は従来の産業利用に加え，燃料電池を用いて再度電力に変換する方法の他，燃料電池車の燃料としての利用，製鉄での水素還元，あるいは水素を直接燃焼させる水素エンジンや，運びやすいアンモニアに変換した後にガスタービン発電で利用するなど，その利用方法も多岐に渡って研究されています。

HORIBAの創業製品であるpHメーターは，水素の利活用には欠かせない電気化学反応を応用したものであり，さらにカーボンニュートラル社会の実現に欠かせない触媒技術は，創業者の堀場雅夫の先代である堀場信吉が京都大学の研究者として1900年代初めにドイツから学び，日本の化学工学発展を支えました。堀場製作所の創業時やそれ以前から関わりのあった研究や技術が，水素の利活用という今の社会課題への取組にも繋がっているとも言えます。また，1990年代後半から，自動車産業でブームとなっていた燃料電池車開発向けに，水素，水分の直接計測や，燃料改質ガスあるいは水素燃焼ガスの計測技術の開発を行ってきました。さらに，2018年にドイツ，ザクセンアンハルト州に位置するFuelCon社を買収し，HORIBA FuelCon（HFC）社として，燃料電池，水電解の研究・開発用評価装置，製造装置および生産品質検査装置まで，ポートフォリオを拡大しました。そして，2023年1月にはHFC社において生産能力を3倍に拡張した新工場「e-HUB」（**Figure 1**）の稼働を開始し，欧州における急速な水電解装置の製造，評価装置の需要に対応しています。

水素は，他のエネルギー源と比較しても単位質量あたりでは非常に高いエネルギー密度を持ちます。液体1 Lのガソリンと同じエネルギーを得るためには，気体で約3,000 Lの水素が必要とされますが，質量に換算すると，750 gのガソリンに対して水素は270 gとなります。ちなみに，このエネルギーを現在のリチウムイオンバッテリーに貯めるためには，その100倍の約27 kgもの質量が必要になります。このように比較しても単位質量あたりでは非常に高いエネルギー密度を持つことから，質量が重要なファクターであるモビリティのエネルギー源やエネルギー輸送の手段としても，潜在的な可能性を持っていると言えます。一方で，標準状態において気体であるが故に取り扱いが難しく，また電気，熱，あるいはe-Fuelなど他のエネルギーへ変換する際の効率の低さなど，実用化・商用化に向けての技術課題は多岐に渡ります。

HORIBAが持つ分析計測技術が燃料電池や水電解装置の新規材料探索から水素燃焼技術の開発，水素と二酸化炭素から効率的に合成燃料を作成するための触媒開発に活用されることで，カーボンニュートラル社会の実現に一翼を担えるよう貢献していきたいと考えています。

Figure 1　新施設「HORIBA eHUB」外観

＊編集局注：本内容は特段の記載がない限り，本誌発行年時点での自社調査に基づいて記載しています。

カーボンニュートラル実現のシナリオ

Scenarios for Realizing Carbon Neutrality

山地 憲治
YAMAJI Kenji
公益財団法人 地球環境産業技術研究機構(RITE)
理事長
工学博士
President
Research Institute of Innovative Technology for the Earth (RITE)
Dr. Eng.

地球温暖化問題は人類全体で長期の時間をかけて取り組むべきグローバルな課題である。単に温暖化問題だけに取組むのではなく，SDGs(持続可能な発展への国連目標)の17ゴールやわが国のエネルギー政策の基本目標である3つのE(エネルギー安全保障，経済効率性，環境の適合)などをバランスよく実現していく必要がある。SDGsの達成に向けた社会イノベーションによってCO_2排出のベースラインを下げ，そこに技術イノベーションによって電気や水素のようなクリーンな二次エネルギーをCO_2排出なく生産し，効率的に利用するシステムを構築すれば，地球温暖化問題を解決するカーボンニュートラル実現へのシナリオが描ける。

Outline of scenarios for realizing carbon neutrality is described. Climate change is a global problem to be tackled with long-term perspectives. Not only carbon neutrality, but also 17 SDGs (Sustainable Development Goals) set by United Nations and 3E (energy security, economic efficiency, and environmental compatibility) targets of Japan's energy policy must be realized. Carbon neutrality scenarios will be realized through wide range innovations, namely social innovations to reduce baseline CO_2 emissions, and technological innovations such as carbon free electricity, hydrogen, and negative emission technologies.

はじめに

2022年2月から始まったロシア軍のウクライナ侵攻は深刻なエネルギー危機を招いている。1970年代の2度にわたる石油危機との大きな違いは，今回の危機は世界全体が地球温暖化対策としてカーボンニュートラル(脱炭素)実現を目指して大きく動き出した中で発生したことである。もちろん，その他にも当時との違いは多くある。石油だけでなく天然ガスや石炭の価格も高騰していること，途上国のエネルギー需要が先進国より大きくなっていることなどである。

ウクライナ侵攻の前にも，脱炭素化の動きや新型コロナウィルス感染拡大による需要減などにより化石資源開発が抑制され，エネルギー価格は上昇基調にあった。そこにウクライナ侵攻である。ロシアは世界最大の天然ガス輸出国であり，石油・石炭でも3位以内に入っている。ロシアへの制裁で，欧州等へのロシアのエネルギー輸出は急減したが，中国やインドなどの新興国が輸入していて複雑な様相を見せている。特に深刻なのは欧州の天然ガスで2022年のスポット価格は2年前の10倍の水準になっている。欧州は今後LNG(液化天然ガス)の輸入を増やすと見込まれ，LNGの取り合いが始まっており，LNG価格も急騰している。これは途上国における石炭から天然ガスへの転換を阻み，地球温暖化対策の障害となる。このようなエネルギー危機の中でも地球温暖化対策を止めるわけにはいかない。

地球温暖化問題の解決のためには，最終的には温室効果ガスの正味排出ゼロ(カーボンニュートラル)を実現する必要がある。パリ協定の長期目標では「世界的な平均気温上昇を産業革命前に比べて2℃より十分低く保つとともに，1.5℃に抑える努力を追求する」とし，そのため，世界の温室効果ガスの排出量を今世紀後半に実質(正味)ゼロにする脱炭素社会，つまりカーボンニュートラル実現が目標とされていた。ただし，IPCCの1.5℃目標に関する特別報告(2018年)では，1.5℃目標達成には2050年までにカーボンニュートラル実現が必要とされ，これが契機となって欧州を先導役として長期目標を2050年カーボンニュートラルに引き上げる動きが始まった。バイデン政権下の米国をはじめ，カーボンニュートラル2050年実現への野心度向上は瞬

く間に世界に広がった。いまやパリ協定の努力目標が本目標になりつつある。わが国の温室効果ガス排出量の8割以上がエネルギー起源のCO_2である。本稿では，エネルギー危機の中でのカーボンニュートラル実現について考える。

イノベーションで実現するカーボンニュートラル

カーボンニュートラルを最適に実現するエネルギーシステムでは，技術と社会の両面の様々なイノベーションを動員する必要がある。中心になるのは，クリーンで効率的な利用ができる2次エネルギー媒体であり，現状では電気，将来的には燃料・熱利用として水素が活躍すると思われる。電気と水素を中心に置き，各種イノベーションを配置したカーボンニュートラル実現の構図を**Figure 1**に示す。

電気と水素は様々な資源から生産できるので，技術イノベーションによって低炭素化・脱炭素化が可能である。CCUS（CO_2回収・利用・貯留））技術を想定すれば，原子力や再生可能エネルギーの利用だけでなく，化石資源の活用も排除されない。ただし，今後太陽光発電や風力発電のような出力が自然変動する電源が大規模に導入されると見込まれるので，電解水素での貯蔵（PtG）を含め蓄電技術の役割が重要になる。また，自然変動電源を連系する電力ネットワークには柔軟性や強靭性が求められる。

電気の利用は，デジタル社会の進展，運輸部門の電化やヒートポンプによる熱供給の増加によって今後も継続して増大すると思われる。太陽光発電やコージェネなどの分散型電源や電動自動車の蓄電池，ヒートポンプ給湯器の貯湯槽など需要側に置かれたエネルギー設備の活用も進むだろう。

送配電事業の制度も電力システム改革によって大きく変化しつつあり，需要に合わせた電力供給という従来の姿から，需給一体となったネットワーク形成・運用へと変化していくと思われる。デジタル技術の活用がこのようなネットワーク革新を支えていくことになる。

産業部門では更なる電化の促進も需要であるが，水素の活用が期待される。2022年の堀場雅夫賞の対象分野も水素の利活用に貢献する分析・計測技術だった。水素は，燃料電池での利用に加えて，燃料アンモニアとしての利用も含めた燃焼発電や熱利用，さらにはカーボンリサイクルの進展に伴って種々の合成燃料や化学物質合成の原料としての需要が増加すると見込まれる。もちろん，ここで使われる水素はCO_2フリーで製造される必要がある。

また，超スマート社会（ソサエティ5.0）によってシェアリング・サーキュラーエコノミーが実現すれば，情報によるエネルギー・物質の代替によってエネルギー需要の大幅な低減が実現するだけでなく，エネルギーと情報のシステム統合がさらに進み，需要側に置かれた設備等の分散型資源が一層効率よく活用されることになるだろう。スマホのように，アプリケーションソフトによって様々な機能を実現する情報機器は今後も増え続け，情報によるエネルギー・物質の代替は機器レベルでも進むと思われる。結果として，電化とデジタル化による革命的エネルギー節約が実現する可能性が描ける。もっとも，ブロックチェーンなど情報処理に伴う電力需要増大に対応する必要があり，量子コンピュータなど情報分野でのイノベーションとの連携を図る必要がある。

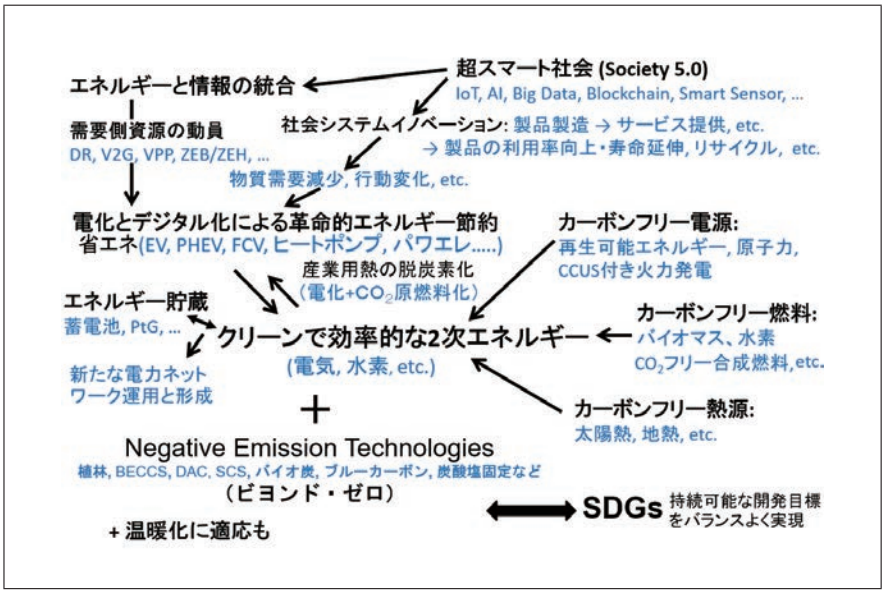

Figure 1　カーボンニュートラル実現の構図

製鉄やセメント製造，化学工業，農業など人間の経済活動全体を俯瞰すれば，以上のような対策をすべて実施しても温室効果ガスの排出ゼロを実現することは困難と思われる。従って，植林やDAC（大気からのCO_2回収），BECCS（CCS（CO_2回収・貯留）を伴うバイオマスエネルギー利用），廃コンクリートなどを利用したCO_2の鉱物固定化など，大気からCO_2を回収する技術も備えておく必要がある。

その上で，起こりうる温暖化への適応と，SDGs（持続可能な発展への国連目標）における温暖化問題以外のゴール実現とのバランスを図っていく必要がある。より幅広い視点に立てば，SDGsの達成に向けた社会イノベーションによってCO_2排出のベースラインを下げ，そこに技術イノベーションによって電気や水素のようなクリーンな二次エネルギーをCO_2排出なく生産し，効率的に利用するシステムを構築すれば，地球温暖化問題解決の展望が開ける。

原子力による3つのEの再建

原子力については様々な意見があるが，CO_2を排出しないエネルギーとして温暖化対策に有効な技術であることは確かである。2022年8月のGX（グリーントランスフォーメーション）実行会議で，わが国は原子力の本格活用に向けてリプレイスや新増設を進める姿勢を鮮明にした。国は既設原子力発電所の再稼働を前面に立って進めることを表明し，運転期間延長や次世代炉開発についても具体的に動き始めた。2023年2月には，わが国政府はGX実現に向けた基本方針を閣議決定し，脱炭素成長型経済構造への円滑な移行の推進に関する法律案を取りまとめている。

ロシア軍のウクライナ侵攻を受けて，地球温暖化対策に偏っていたエネルギー政策において，エネルギー安全保障や経済性の重要性が再確認され，エネルギー安全保障，経済性，環境対策の3つのEを同時に達成するという政策の基本方針が改めて認識されつつある。この中で，政治的理由から避けてきた原子力政策について国が積極的に取り組み始めたことは注目される。

しかし，原子力を取り巻く厳しい現実は変わらない。リアリズムをもって重点政策を絞り込まないと原子力復活は期待できない。その点では，再稼働や運転期間の延長は当然行うべきと考えるが，次世代原子炉の開発には危うさを感じる。人材開発には新増設が必要なことは確かだが，これは安全性を高めた革新型軽水炉で対応すればよい。次世代炉の議論の中で疑問を感じるのは，相変わらず高速炉や核融合が取り上げられていることである。これらは何れも国家プロジェクトや国際共同開発によって進められてきたが，50年を超える開発を経ても実用化というゴールに届いていない。

1950年代後半から高速増殖炉や高温ガス炉，溶融塩炉など様々なタイプの原子炉開発が行われてきたが，結局60年代に軽水炉が実用化され世界で導入が進んだ。ガス炉を開発して実用化した英国も今後の新設炉には軽水炉を選んでいる。

次世代炉の中で私が注目しているのはSMR（スモール・モジュラー・リアクター）である。SMRでは，小型原子炉を量産することで，安全性向上とともに量産による経済性を実現できると期待されている。原子炉を小型化すると容積に対して表面積が大きくなり，大型炉より冷えやすくなる。これを固有安全性が向上するという。一方，モジュールとは，規格が統一された部材一式を工場で生産してユニットとして組み立て，現地ではこのユニットをさらに組み合わせて建設するする生産方式である。プレハブ住宅をイメージすればよい。従来の原子力発電所は，同じ設計型式でも建設は現場で行う一点ものだった。SMRでは工場生産する部分がほとんどになるので，高い品質管理や工期短縮が期待できる。

SMRというコンセプトは実は昔からあった。いずれも実現しなかったが，私の記憶では1980年代にGEがPRISMという名前のナトリウム冷却高速炉を開発していた。ドイツが開発した高温ガス炉を南アフリカでモジュール炉として建設する計画もあった。しかし，実用化している軽水炉との競合には勝てなかった。

今回再び脚光を浴びているSMRの中でも小型軽水炉を使う構想に将来性があると考えている。というのは，小型軽水炉は潜水艦や航空母艦，砕氷船の動力として既に実用化しているからだ。わが国の「むつ」を含め舶用軽水炉開発の歴史は長い。軍用や砕氷船以外で舶用小型炉が実用化しなかったのは，原子力への懸念から市場が展開できなかったという社会的理由が大きい。しかし，小型発電炉なら，僻地での利用や移動可能な発電船としての利用も視野に入る。軽水炉のSMR展開に期待している。

視野拡大の重要性

カーボンニュートラル実現のための様々な技術と社会のイノベーションの動員には，視野の拡大が必要である。空間的広がりでは，地域社会の取り組みから国際連携，業界や需要区分を連携するセクターカップリングまで様々な取り組みが必要になる。時間軸では，カーボンニュートラル実現に至る移行期での取り組みも重要になる。カーボンニュートラル実現には，技術や社会，地域経済や国際政治など，幅広い視点から取り組む必要がある。

しかし，現実は厳しい。2021年11月のCOP26については，わが国が化石賞を受賞したことが繰り返し報道されたが，受賞理由は岸田文雄首相が水素やアンモニアを利用した「火力発電のゼロエミッション化」を表明したことだった。その他にもノルウェーはCCS（CO_2回収・貯留）を進めていること，フランスは原子力の新設を表明したことにより化石賞を受賞している。火力のゼロエミッション化もCCSも原子力も地球温暖化対策の重要な手段である。カーボンニュートラルという高い目標の実現には，このように特定技術を排除して選択肢を狭めることは大きな障害になる。

そもそも地球温暖化問題には，対策の負担は地域ごとに発生するが，対策による利益は世界全体に裨益するという構造がある。このような構造を持つ問題に対処するには，世界全体で連携した行動を維持することが極めて重要である。主要国が離脱するような状況を作るとか，特定技術を排除することは，連携を破壊し，地球温暖化対策の自滅を招く。世界の脱炭素実現のような厳しい目標の実現には，技術や文化の多様性を認め，すべての対策を総動員する必要がある。

また，カーボンニュートラル実現には，水素利用やCCUSのようなCO_2削減に直接寄与する個別の革新技術に加えて，デジタル技術やパワーエレクトロニクス，分析・計測技術，バイオ技術，都市管理技術など，一見するとCO_2削減と関係が無いように見える汎用性の高い共通基盤技術の活用も必要である。

GX（グリーントランスフォーメーション）政策の展開

グリーン成長戦略とか，クリーンエネルギー戦略とか，ここ数年様々なニックネームの付いた政策が提唱されてきたが，これらの流れがGX（グリーントランスフォーメーション）実行会議で束ねられつつある。エネルギー安定供給と共に達成する脱炭素とか，再エネと共に原子力も最大限活用するとか，エネルギー・環境政策が本来持つべき総合的取組みが具体的な政策の姿を伴って見え始めた。政府は20兆円のGX経済移行債を準備してカーボンニュートラル実現に向けて150兆円の民間投資の誘導を図ろうとしている。

国民の支持が高い再エネ主力電源化やカーボンニュートラルを掲げることは政治的に容易だが，エネルギー安定供給実現や原子力活用に言及することには政治的困難が伴っていた。ロシア軍のウクライナ侵攻などを契機とした燃料価格の高騰や供給不安への高まりが後押ししたことは確かだが，当面国政選挙の予定がなく政権の安定性が予見できたことも重要な要素だったはずである。その点で，GX実行会議のとりまとめは政治決断の賜物と言えるだろう。

しかし，多様な内容が含まれていて，GX実行会議とりまとめ案の具体化には困難が予想される。例えば，成長志向型カーボンプライシングの導入，具体的には排出量取引（GX-ETS）と炭素賦課金の導入が提案されているが，導入のタイミングや有償オークションのルール作りなど制度の詳細は大まかにしか示されていない。また，カーボンプライシングの収入をGX経済移行債の償還財源に使うとしているが，具体的な仕組みの規模や導入時期などは示されていない。

一般的に，政策手段はアメとムチに分けられる。今回の例でいえば，カーボンプライシングはムチ，GX経済移行債はアメである。アメとムチをうまく組み合わせたと言えなくもないが，具体的な政策の中身が確定していない現状では手放しでは褒められない。再エネ電源の導入比率を義務付けるRPS（リニューアブル・ポートフォリオ・スタンダード）やFIT（再エネ電気固定価格買取制度）の制度設計など再エネ政策に関わってきたが，制度の詳細の重要性を痛感している。「神は細部に宿る」と言われるように，多くの利害関係者が複雑に絡まる問題への対応には，政策の具体的な詳細が重要であることを指摘しておきたい。

おわりに

地球温暖化問題は人類全体で100年単位の長期の時間をかけて取り組むべきグローバルな課題である。持続可能な未来を拓くためには，単に温暖化問題だけに取組むのではなく，国連が掲げるSDGsの17ゴールやわが国のエネルギー政策の基本目標である3つのE（エネルギー安全保障，経済効率性，環境保全性）などをバランスよく実現していく必要がある。

本稿で概要を示したように，SDGsの達成に向けた社会イノベーションによってCO_2排出のベースラインを下げ，そこに技術イノベーションによって電気や水素のようなクリーンな二次エネルギーをCO_2排出なく生産し，効率的に利用するシステムを構築すれば，地球温暖化問題解決のシナリオが描ける。

2022 堀場雅夫賞　受賞内容

堀場雅夫賞について

堀場雅夫賞は，国内外の大学または公的な試験研究機関において，分析・計測およびその応用に関する科学技術分野で顕著な業績を挙げつつある研究者・技術者を奨励表彰するものです。

対象分野

カーボンニュートラル社会に向けた水素の利活用に貢献する分析・計測技術

審査委員会（敬称略，順不同）

● 審査委員長

山地 憲治	公益財団法人 地球環境産業技術研究機構（RITE）理事長 東京大学名誉教授，グリーンイノベーション戦略推進会議 座長

● 審査委員

石谷 治	東京工業大学 理学院化学系 教授 広島大学 先進理工系科学研究科 特任教授（兼任） カーボン・エネルギーコントロール社会協議会（CanApple）共同代表
石原 達己	九州大学 カーボンニュートラル・エネルギー国際研究所 教授 一般社団法人 日本固体イオニクス学会 会長
里川 重夫	成蹊大学 理工学部 教授 一般社団法人 水素エネルギー協会 理事・副会長

● 海外審査委員

Scott Samuelsen （スコット・サミュエルセン）	カリフォルニア大学アーバイン校（アメリカ）教授 Mechanical and Aerospace Engineering

● 社内審査委員

水野 裕介	株式会社堀場製作所 ビジネスインキュベーション本部 Alternative Energy Conversionセンター Alternative Energy Conversion部 部長
花木 保成	株式会社堀場製作所 ビジネスインキュベーション本部 Alternative Energy Conversionセンター 新エネルギー技術担当マネジャー

堀場雅夫賞受賞

国立大学法人東海国立大学機構　名古屋大学 大学院工学研究科
化学システム工学専攻
特任准教授

佐藤 勝俊 氏

【受賞研究題目】

原子分解能電子顕微鏡解析で先導する新しい窒素還元サイトのデザイン

国立大学法人東海国立大学機構　名古屋大学 大学院工学研究科
電子工学専攻
教授

高橋 康史 氏

【受賞研究題目】

触媒活性サイトの実空間イメージングに資する電気化学セル顕微鏡の開発

東北大学
多元物質科学研究所
准教授

中村 崇司 氏

【受賞研究題目】

電気化学に基づく欠陥エンジニアリング技術の開発

特別賞受賞

九州大学
カーボンニュートラル・エネルギー　国際研究所
准教授

髙橋 幸奈 氏

【受賞研究題目】

太陽光をエネルギー源としたプラズモン誘起電荷分離による高効率水素発生システムの開発

カールスルーエ工科大学
ヘルムホルツ研究所 ウルム校
テニュアトラック教授

ヘルゲ・ゼーレン・シュタイン 氏

【受賞研究題目】

相関分光法及び研究室規模製造による データ駆動材質発見の加速及びスケールアップ製作

＊ 編集局注：本内容は特段の記載がない限り，受賞時点での自社調査に基づいて記載しています。

Design of Novel Catalytic Nitrogen Reduction Sites Based on Atomic-Resolution Electron Microscopic Analysis

原子分解能電子顕微鏡解析で先導する新しい窒素還元サイトのデザイン

SATO Katsutoshi
佐藤 勝俊

Understanding the structure and chemical state of the active sites is important for the development of highly active catalysts. However, it is difficult to conduct the necessary analyses without exposing reduced catalyst to air, which can alter its structure. We have developed a means of loading reduced catalysts into analytical instruments, such as transmission electron microscopes and various spectroscopic detectors, that avoids exposing the catalyst to the air. Using our non-air-exposure analysis technique, we were able to investigate the nitrogen reduction sites of novel ammonia synthesis catalysts and elucidate the synergistic mechanisms between the catalysts' structures and chemical states. These analyses ultimately allowed us to develop catalysts with high activities at the low temperatures needed for ammonia synthesis using renewable energy. We expect that our non-air-exposure analysis technique will become an important tool for the development of novel catalytic reaction processes, particularly those related to the use of ammonia as a hydrogen carrier, which is an important milestone for establishment of a carbon-neutral society.

高活性な新規触媒の開発のためには，活性点の構造と化学状態を詳細に解析して作用機構を明らかにし，新しい活性点のデザインへと結びつける必要がある。我々は近年進展が目覚ましい収差補正透過型電子顕微鏡と各種分光検出器による観察・分析技術に注目し，大気非暴露分析の手法を組み合わせて，「触媒の活性点そのものを原子レベルの分解能で直接解析」する手法として確立した。この手法を用いて，再生可能エネルギーの利用を志向したアンモニア合成触媒のための窒素還元サイトの研究に取り組み，高活性な窒素還元サイトの実現に必要な構造と化学状態の相乗的な作用機構を明らかにした。さらには顕微解析の結果から着想を得て，実用に適した酸化物系の材料をベースにした世界最高レベルの活性を示す触媒を複数開発した。これらの触媒の開発はアンモニアの水素キャリアとして利用拡大と，水素流通ネットワークの構築につながるものであり，将来のカーボンニュートラル社会構築に資する重要な成果であるといえる。

Introduction

Design of active sites is essential for the development of highly active catalysts. X-ray diffraction, X-ray absorption spectroscopy, infrared spectroscopy, and Raman spectroscopy are powerful tools for the characterization of heterogeneous catalysts; however, these techniques cannot directly capture the structure and characteristics of the active site because they provide only average information. Transmission electron microscopy (TEM) has the advantage of position-selective observation of targets; however, in the study of supported catalysts, where the size of the active site is below the nanoscale and the structure is too disordered, electron microscopy has traditionally played only a supplementary role for observing morphology and measuring particle size. In recent years, technological innovations such as increased resolution by using spherical aberration correctors and the ability to conduct highly sensitive elemental analyses by using large-area energy-dispersive X-ray fluorescence (EDX) detectors have greatly improved what can be achieved with TEM. Adding to these innovations, we have developed a

sample-loading technique that allows simultaneous observation of the structure and chemical state of the active sites of heterogeneous supported metal catalysts at the atomic-level.

Recently, hydrogen carriers have attracted attention as means of storing and transporting renewable energy. One such hydrogen carrier is ammonia, because of its high energy density (12.8 GJ m^{-3}), high hydrogen content (17.6 wt%), ease of liquefaction and suitability for storage and transportation, and the fact that it can be used to produce hydrogen without emission of CO_2.[1] Ammonia is produced industrially via the Haber-Bosch process using double-promoted iron catalysts. However, the currently available catalysts are all optimized for large-scale processes operating at high temperatures and pressures, meaning their performances are insufficient for processes that are powered by renewable energy and conducted under much milder conditions. Thus, to address the need for novel ammonia synthesis catalysts, we used our non-air-exposure analysis technique to conduct analyses and develop several catalysts with ammonia synthesis activities superior to those of conventional catalysts. Here, we discuss our sample-loading technique and the development of our improved catalysts.

Outline of our sample-loading technique

In heterogeneous catalysts, active sites are usually formed on the catalyst surface during activation (reduction). However, when these active sites are exposed to air, their structure and chemical state are changed by reaction with atmospheric oxygen and water vapor. For example, Ce^{4+} is reduced to Ce^{3+} under high-temperature, reductive conditions, but Ce^{3+} is extremely sensitive to oxygen and is easily oxidized back to Ce^{4+} upon contact with air. Therefore, the state of the active site cannot be analyzed by TEM by using the usual sample preparation method of grinding and grid preparation in air.

To address this issue, we developed an approach that uses a glove box and special airtight sample holder to prevent the catalyst from being exposed to the air (Figure 1). In brief, after activation (reduction), the catalyst is moved to a glove box filled with an inert gas. Once inside the glove box, the catalyst is placed within the airtight receptacle of a special sample holder. The sample holder is then removed from the glove box and loaded into the TEM instrument. This operation allows the activated catalyst to be introduced into the optical tube of the TEM instrument without exposing it to air, and to be observed and analyzed while maintaining its surface structure and state after reduction.

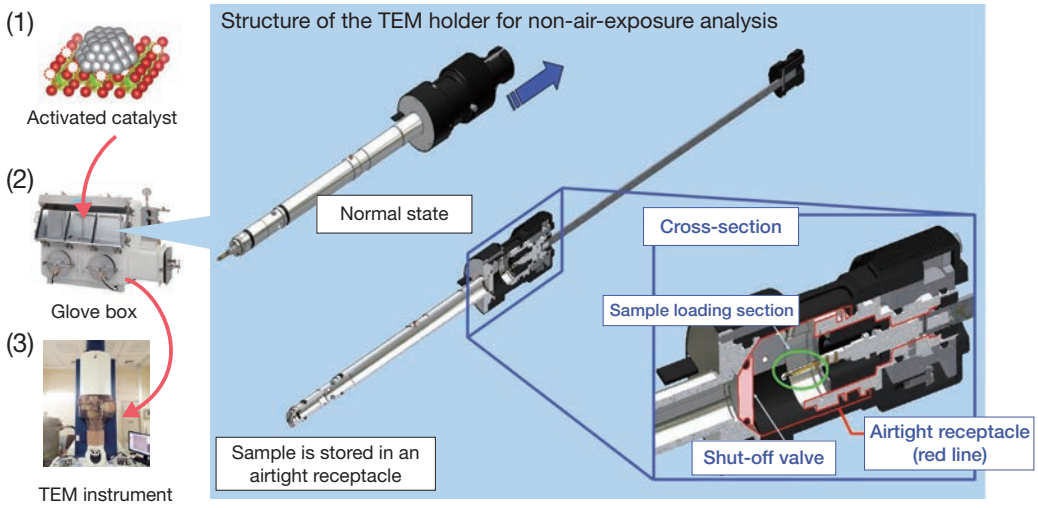

Figure 1 Overview of the sample-loading technique and a schematic showing the structure of the sample holder.
(1) The catalyst is activated (reduced) and then moved to a glove box filled with an inert gas.
(2) The catalyst is then placed within the airtight receptacle of a special sample holder.
(3) The sample holder is then removed from the glove box and inserted into the transmission electron microscope for analysis.

Example application: Supported Ru catalysts

Under mild conditions, supported ruthenium (Ru) catalysts show higher ammonia synthesis activity than the usual double-promoted iron catalysts.[1-3] We developed a cerium-lanthanum composite oxide supported Ru catalyst ($Ru/La_{0.5}Ce_{0.5}O_{1.75}$) and found that this catalyst exhibited better activity than conventional supported Ru catalysts; this higher activity was achieved by reducing the catalyst at 650°C, which is a much higher temperature than that used for the reduction of conventional ammonia-synthesis catalysts such as $Ru/Cs^{+}/MgO$ and Ru/CeO_2.[4]

Using our non-air-exposure analysis technique, we were able to observe the elemental composition of the surface of the $Ru/La_{0.5}Ce_{0.5}O_{1.75}$ catalyst by using an EDX detector and to examine the electronic state of Ce by using an electron-energy-loss spectroscopy (EELS) detector (Figure 2). EELS analysis revealed that Ce^{3+} was more abundant near the surface of the support (Figure 2c). In addition, detailed analysis of the interface between the Ru nanoparticles and the / $/La_{0.5}Ce_{0.5}O_{1.75}$ support revealed that it was Ce^{+3} rich (Figure 2d, e). The rate-determining step in ammonia synthesis is dissociation of the N_2 molecule. To promote this dissociation, electrons can be donated to N_2 molecules adsorbed on the catalyst surface. Our analysis indicated that Ru adjacent to Ce^{3+} was a strong nitrogen reduction site because Ce^{3+} is in a more electron-rich state than is Ce^{4+}.

From our study of the Ru/ $La_{0.5}Ce_{0.5}O_{1.75}$ catalyst, we formulated a guiding principle for catalyst preparation, which is that reduction at high temperature induces the dynamics of the support and produces an active site at the interface with Ru. Following this guiding principle, we prepared a barium (Ba)-doped $La_{0.5}Ce_{0.5}O_{1.75}$ support, loaded it with Ru, and subjected it to high-temperature reduction, which afforded a $Ru/Ba/LaCeO_x$ catalyst with world-class ammonia synthesis performance.[5] We then subjected the reduced catalyst to TEM analysis (Figure 3). We found that the majority of the surface of the Ru nanoparticle was covered with nanosized oxides of low crystallinity (nanofractions) (Figure 3a) and that these nanofractions contained Ba, La, Ce^{4+}, and Ce^{+3} (Figure 3b). These elements have strong electron-donating ability; therefore, the Ru atoms adjacent to the nanofractions showed strong ability to donate electrons to nitrogen and high activity for nitrogen reduction. In addition, Ba was found to play a major role in the formation of these unique structures. The surface of the support is destabilized during the high-temperature reduction by forming a composite oxide incorporating Ba^{2+} with a large ionic radius. To reduce their own surface energy, the resulting composite oxides migrate to the surface of the Ru nanoparticles as nanofractions. Like Ce^{3+}, Ba is also extremely sensitive to atmospheric oxygen and water vapor; therefore, our non-air-exposure sample-loading technique proved useful for clarifying the structure and formation of the active site.

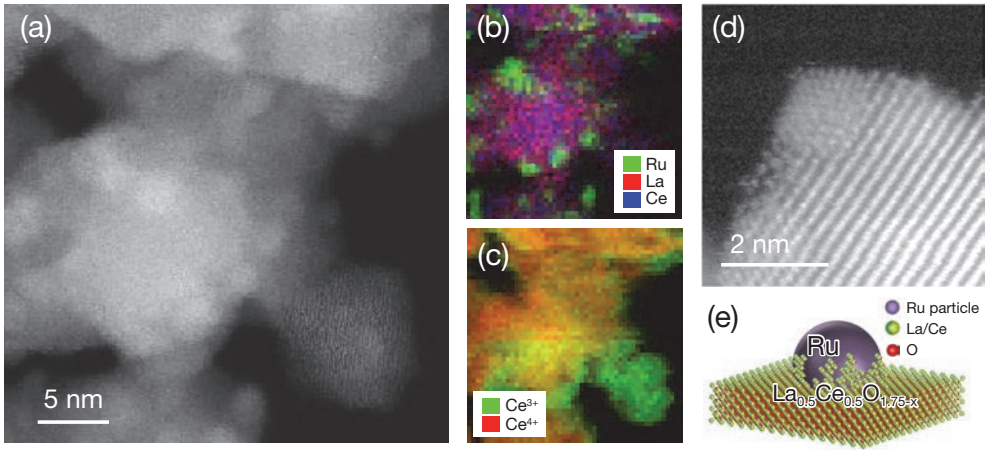

Figure 2 Microscopic analysis of Ru/ $La_{0.5}Ce_{0.5}O_{1.75}$ without exposure to air.
(a) High-angle annular dark-field (HAADF) image. (b) Elemental map of the catalyst, as determined by energy-dispersive X-ray fluorescence analysis. (c) Color map of the valence state of Ce, as determined by electron energy loss spectroscopy. (d) Atomic-resolution HAADF image of an Ru nanoparticle. (e) Schematic illustration of the Ru/L $La_{0.5}Ce_{0.5}O_{1.75}$ surface after reduction.

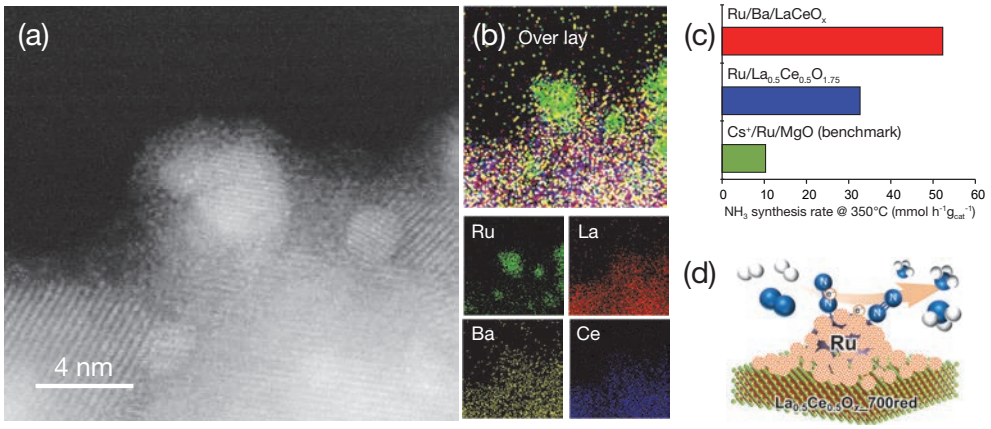

Figure 3 Microscopic analysis of Ru/Ba/LaCeO$_X$ without exposure to air. (a) Atomic-resolution high-angle annular dark-field image of the area around several Ru nanoparticles. (b) Elemental map of the catalyst, as determined by energy-dispersive X-ray fluorescence analysis. (c) Ammonia synthesis activity of Ru/Ba/LaCeO$_x$, Ru/La$_{0.5}$Ce$_{0.5}$O$_{1.75}$, and Cs+/Ru/MgO. Reaction conditions: 1.0 MPa, SV = 72,000 mL h^{-1} gcat^{-1}, N_2/H_2 = 1/3. (d) Schematic illustration of the active site of Ru/Ba/LaCeO$_x$ after reduction.

Example application: Supported non-noble metal (Co) catalysts

We next extended our investigation to supported non-noble metal catalysts and found that Co@BaO/MgO, with magnesium oxide (MgO) as the support, exhibited very good ammonia synthesis activity.[6] Co@BaO/MgO not only achieved higher activity than conventional Co catalysts (250 times higher reaction rate per active site), but also surpassed that of an Ru-based benchmark catalyst (Figure 4). Elemental mapping revealed that the catalyst surface contained a structure comprising Co nanoparticles covered by nanofractions of BaO (Figure 4a). Results of first-principles calculations suggest that formation of this structure promotes dissociation of adsorbed nitrogen as a result of most of the Co nanoparticle surface's becoming electron-rich from electron donation by BaO. Further microscopic analyses revealed the mechanism underlying the formation of the active sites: During high-temperature reduction, Ba species with low melting points are generated and dispersed over the support; Co nanoparticles then collect the Ba species as they are moved across the support by thermal vibrations, resulting in deposition of a BaO nanofraction on the surface of the Co nanoparticles.

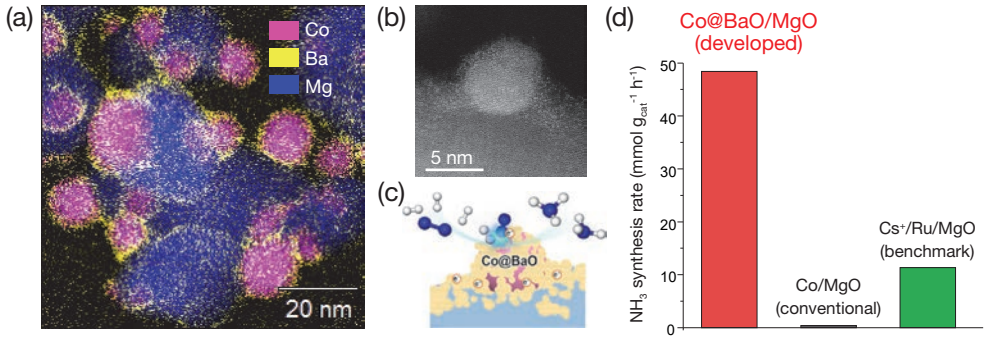

Figure 4 Microscopic analysis of Co@BaO/MgO. (a) Elemental map of the catalyst without exposure to air, as determined by energy-dispersive X-ray fluorescence analysis. (b) Atomic-resolution high-angle annular dark-field image of the area around several Co nanoparticles. (c) Schematic illustration of the surface of Co@BaO/MgO after reduction. (d) Ammonia synthesis activity of Co@BaO/MgO, Co/MgO, and Cs$^+$/Ru/MgO. Reaction condition: 1.0 MPa, SV = 72,000 mL h^{-1} gcat^{-1}, N_2/H_2 = 1/3, 350°C.

Conclusion

Precise design of active sites is important for the development of highly active catalysts. Using our non-air-exposure analysis technique, we successfully developed several highly active catalysts for ammonia synthesis. We expect that our analysis technique will contribute to elucidating further guiding principles for the design of active sites, and to the realization of highly active catalysts for a broad range of reactions.

References

[1] K. Sato, K. Nagaoka, Boosting Ammonia Synthesis under Mild Reaction Conditions by Precise Control of the Basic Oxide-Ru Interface, Chem. Lett., 50 (2021) 687-696.

[2] K. Sato, K. Imamura, Y. Kawano, S. Miyahara, T. Yamamoto, S. Matsumura, K. Nagaoka, A low-crystalline ruthenium nano-layer supported on praseodymium oxide as an active catalyst for ammonia synthesis, Chem. Sci., 8 (2017) 674-679.

[3] S. Miyahara, K. Sato, Y. Kawano, K. Imamura, Y. Ogura, K. Tsujimaru, K. Nagaoka, Ammonia synthesis over lanthanoid-oxide supported ruthenium catalysts, Catal. Today, 376 (2021) 36-40

[4] Y. Ogura, K. Sato, S. Miyahara, Y. Kawano, T. Toriyama, T. Yamamoto, S. Matsumura, S. Hosokawa, K. Nagaoka, Efficient ammonia synthesis over a $Ru/La_{0.5}Ce_{0.5}O_{1.75}$ catalyst pre-reduced at high temperature, Chem. Sci., 9 (2018) 2230-2237.

[5] K. Sato, S. Miyahara, Y. Ogura, K. Tsujimaru, Y. Wada, T. Toriyama, T. Yamamoto, S. Matsumura, K. Nagaoka, Surface Dynamics for Creating Highly Active Ru Sites for Ammonia Synthesis: Accumulation of a Low-Crystalline, Oxygen-Deficient Nanofraction, ACS Sustainable Chem. Eng., 8 (2020) 2726-2734.

[6] K. Sato, S. Miyahara, K. Tsujimaru, Y. Wada, T. Toriyama, T. Yamamoto, S. Matsumura, K. Inazu, H. Mohri, T. Iwasa, T. Taketsugu, K. Nagaoka, Barium Oxide Encapsulating Cobalt Nanoparticles Supported on Magnesium Oxide: Active Non-Noble Metal Catalysts for Ammonia Synthesis under Mild Reaction Conditions, ACS Catal., 11 (2021) 13050-13061.

Dr. SATO Katsutoshi

佐藤 勝俊

Designated Associate Professor,
Department of Chemical Systems Engineering,
Graduate School of Engineering,
Nagoya University

Development of the Electrochemical Imaging Technology for Visualizing Catalytic Active Site

触媒活性サイトの電気化学イメージング技術の開発

TAKAHASHI Yasufumi
高橋 康史

To develop high-performance catalysts, it is important to understand the relationship between the micro/nanoscale structures of catalysts and catalytic activity. Catalytic reactions progress in multiple steps, such as diffusion, adsorption, and dissociation of molecules in solution. Therefore, local operando measurement technology in liquid is indispensable for visualizing catalytic active sites. To visualize the catalytic active site, a nanopipette filled with electrolyte is used to form a nanoscale electrochemical cell on the sample by developing scanning electrochemical cell microscopy (SECCM). Using this technique, we visualized the catalytically active sites of MoS_2 nanosheets, which are expected to catalyze the hydrogen evolution reaction.

高性能な触媒を開発するうえで，触媒のマイクロ・ナノスケールの構造と触媒活性の関係を理解することは重要である。触媒反応では，溶液中での分子の拡散・吸着・解離など，マルチステップで反応が進行するため，触媒活性サイトを可視化するには，液中での局所的なオペランド計測技術が不可欠である。そこで，電解液を充填したナノピペットを用いてサンプル上にナノスケールの電気化学セルを形成する。さらに走査型プローブ顕微鏡技術を応用することで，試料表面の触媒活性サイトを可視化する走査型電気化学セル顕微鏡（SECCM）を開発した。この手法を用いて，水素生成の触媒として期待されるMoS_2ナノシートの触媒活性サイトを可視化した。

Introduction

To slow global warming, reducing CO_2 emissions is essential. Among them, electrochemical hydrogen evolution reaction (HER) is one of the key technologies to produce hydrogen known as a clean energy source. Platinum (Pt) is the catalyst that can efficiently generate hydrogen. Since the price of Pt is high, the development of a catalyst to replace Pt is desired.

Two-dimensional (2D) layered transitional metal dichalcogenides[*1], molybdenum disulfide (MoS_2) is one of the most promising precious rare metal-free catalysts for HER.[1] To improve the catalytic activity of MoS_2, significant efforts have been made in terms of conductivity improvement, chemical doping, phase transition, strain, and defect engineering.[2] Quantitatively identifying and characterizing catalytically active sites in MoS_2 are critically important for understanding the catalysis of MoS_2. However, it is still difficult to directly visualize the HER activity site on MoS_2 nanosheets. Therefore, it is necessary to develop a measurement technology to connect the relationship between the spatial distribution and the electrochemical activity of the HER active sites.

As an electrochemical imaging tool, the combination of scanning probe microscopy and microelectrode is effective to sense the surface reactivity of the catalysis with a micrometer scale. Scanning electrochemical microscopy (SECM[*2]) has been demonstrated to be one of the powerful tools for determining the relationship between the surface morphology of a sample and its electrochemical activities for screening highly catalytically active sites in catalytic materials.[3] However, the spatial resolution of

SECM is the issue for characterizing local electrochemical activity because of the difficulty of the miniaturization of the microelectrode. Scanning electrochemical cell microscopy (SECCM), which uses a nanopipette as a probe in a local and movable electrochemical cell, is an effective tool for operando characterization of surface structures electrochemically in a submicron spatial resolution.[4] The advantages of SECCM are that it is a reproducible and reliable technique for fabricating nanoprobes together with fast electrochemical characterization due to its small capacitive current and its ability to prevent sample contamination during scanning.

In this report, the inhomogeneous HER activity on a triangular 1H-MoS_2 monolayer nanosheet, a heterostructures of MoS_2 and WS_2 nanosheets were visualized by using SECCM.[5] Our data provides information about the local catalytic properties as well as electrochemical images of the HER current, Tafel slope, and overpotential by measuring the cyclic voltammograms (CVs) at all measurement points during the imaging. These SECCM measurement unveiled heterogeneous reactivity, relationship of layer number and HER activity, and aging effect.

*1 Transition-metal dichalcogenides (TMDs) are composed of three atomic planes and often two atomic species: a metal and two chalcogens.

*2 SECM uses microelectrode as a probe to detect a oxidation/reduction current on sample surface.

Scanning electrochemical cell microscopy (SECCM)

The SECCM uses a moveable nanopipette probe containing a 0.5 M H_2SO_4 solution and a Pd-H_2 quasi-reference counter electrode (QRCE) (Figure 1a). In the case of chloride ion free solutions, Pd-H_2 QRCE was generally used for SECCM experiments. All the potentials were converted into electric potentials when the reversible hydrogen electrode was used for the reference electrode. The following procedure was used to bring the nanopipette towards the sample surface so that the liquid meniscus just made contact at a series of predefined positions, with an electrochemical measurement at each point. First, the nanopipette (meniscus) was withdrawn from its existing position by a specified distance, typically 0.3 µm. Next, the vertical position of the probe was maintained for 60 ms, while the nanopositioning stage moved the specimen to a new imaging point in the xy plane. Then, the nanopipette was lowered at constant fall rate of 7 nm ms^{-1} while monitoring the current. Immediately after detecting a current (2 pA threshold) by forming the electrical contact between the nanopipette and the sample through the nanopipette meniscus, the approach was stopped and the vertical position of the nanopipette was saved along with the x,y co-ordinate to form a topography map. Local cyclic voltammogram was performed by sweeping the applied voltage (scan rate was set at 130-150 V/s, the measurement time was 20 ms/point) after 0.2 ms wait for suppression of capacitive current. After the electrochemical measurement, the nanopipette was quickly withdrawn by the specified distance to start a new measurement cycle. In this way, simultaneous pictures of topography and redox activity were built up.

HER reactivity mapping on MoS_2 nanosheet

1H-MoS_2 nanosheets were characterized by measuring the cyclic voltammograms (CVs) at all measurement points during the SECCM imaging. CV scan rate was set at 130 V/s, the measurement time was 20 ms/point, and the imaging time (128 × 128 points) was typically 40 min. The current image was obtained by picking up the current signal from CV or applied DC voltage (-1.3 V vs. RHE). An electrode surface area with a radius of 50 nm in the electrochemical cell was used to calculate the current density. The overpotential was evaluated at a 30 mA/cm^2 current density. The CV measurement was done at all of the scanning points, and SECCM provided three electrochemical mapping images of the HER current, Tafel slope, and overpotential, produced simultaneously. SECCM images and a graph of the electrochemical properties of the 1H-MoS_2 nanosheets are shown in Figure 1 (b-d). At the edge region, 1H-MoS_2 nanosheets showed a high current response, a low overpotential, and a low Tafel slope. Notably, it was also observed that there were some activities as a line on the HOPG, which corresponds to the HOPG step edges showing slightly high current responses. In order to characterize the HER catalytic activity of the edge and terrace regions of the 1H-MoS_2 nanosheets, CV curves were selected and averaged from the edge and terrace regions, respectively, shown in Figure 1(e-g). An overpotential with a HER current density at 30 mA/cm^2 and a Tafel slope of 1H-MoS_2 nanosheets edge region, terrace region, and HOPG step are 0.94 V (versus RHE), 1.06 V (versus RHE), and 1.15 V (versus RHE) and 130 mV/dec, 130 mV/dec, and 121 mV/dec, respectively. The relatively larger overpotentials were obtained by the SECCM measurement than typical bulk measurement. In the case of SECCM measurement, the IR drop effect was neglectable because of the small faradaic current. The origin of the overpotentials would be due to the difference of the number of catalytic active sites. These results indicate that the edge region of the 1H-MoS_2 nanosheets show low overpotential but the Tafel slope was not seen remarkble

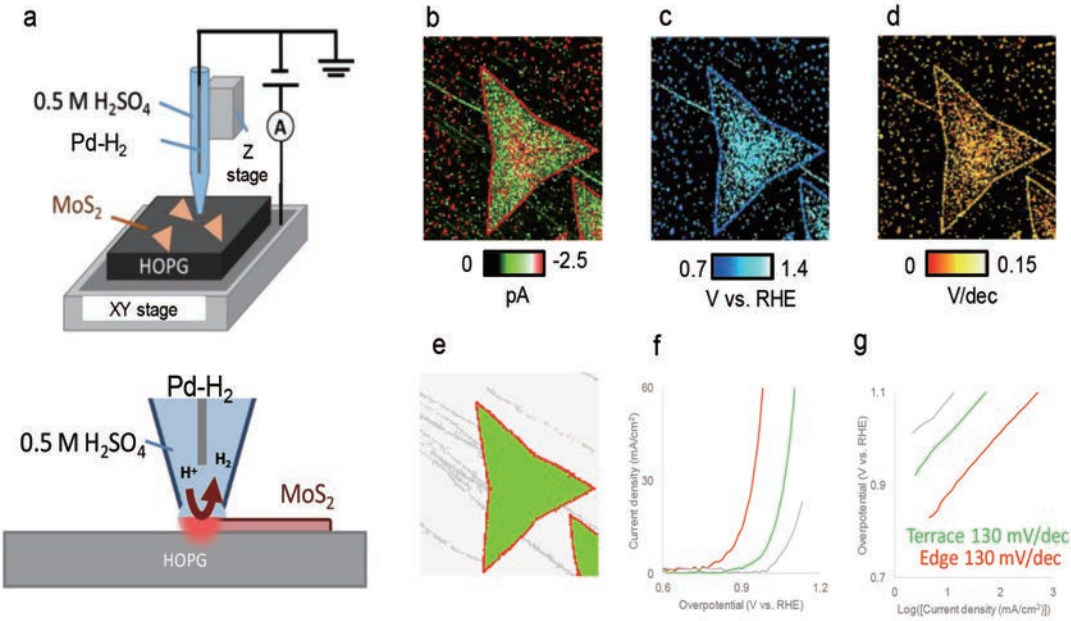

Figure 1 (a) Schematic illustration of SECCM measurements of MoS_2 nanosheets. Pd-H_2 used as a quasi-reference electrode. Nanopipette filled with 0.5 M H_2SO_4. SECCM (b) current, (c) overpotential (30 mA/cm^2), (d) Tafel slope images of 1H MoS_2 nanosheets on HOPG substrate. Scansizes were 15 × 15 μm^2. Scan rate is 130 V/s. Sweep Voltage were -1.3 V vs. RHE. (e) MoS_2 nanosheets edge(red), terrace(green), and HOPG edge(grey) tricolor images. Graphs showing the (f) overpotential and (g) Tafel slope on the 1H MoS_2 edge (red), terrace (green), and HOPG edge(grey) regions.

difference between edge and terrace region for HER catalysis. The current image shows a three highly active lines contrast at the center, which may correspond to grain boundaries or nanowires in the chemical vapor deposition grown 1H-MoS_2 nanosheets, in addition to the highly active edges.

Electrochemical activation of MoS_2 nanosheet for enhance the HER activity

The improvement of the HER activity is an important research target for dichalcogenide catalysts. Frank and coworkers recently reported that the electrochemical generation of sulfur vacancies can improve the HER activity.[6] Briefly, sulfur vacancies generated by applying a negative potential to MoS_2 are more stable than sulfur on the basal plane. At these sulfur vacancies sites, hydrogen adsorption is thermodynamically favoured than sulfur resorption. Therefore, electrochemically generated sulfur vacancies are stable and work as HER catalytic active sites. We have performed similar experiment using SECCM to improve HER activity at a local area on the MoS_2 nanosheets in order to investigate the position-dependent activation properties. The local SECCM CV imaging of a 1H-MoS_2 nanosheet was performed in three different regions with different scan voltages of −1.10, −1.20, and −1.40 V versus RHE to investigate the relationship between the applied voltage and the activation. After electrochemical activation, CV measurements and imaging were performed over a large-scale scanning area to capture a whole 1H-MoS_2 nanosheet in order to characterize the local SECCM activation effects. Figure 2(a-c) shows the electrochemical images of the activated 1H-MoS_2 nanosheet. The electrochemically activated area shows a high current response, a low overpotential, and a low Tafel slope. A high HER activity was observed in the area activated by the scan of up to −1.40 V versus RHE, whereas no significant improvement was observed in the HER activity when the scan was reversed at −1.20 V versus RHE. It was also observed that there was SECCM electrochemical treatment induced homogeneous HER activation in the treated area. These results suggest that the electrochemical activation has a threshold voltage (−1.40 vs. RHE) for improving the HER activity. Defect engineering is also a well-known technique that has been used to improve the HER activity of MoS_2, but its mechanism is unclear. As a demonstration of a defect-engineered sample measurement, we have imaged the HER activity of an over-annealed 1H-MoS_2 nanosheet (300°C in a sulfur atmosphere for 30 min), which had a lot of cracks. Figure 2(d-f) shows the SECCM images of the overannealed 1H-MoS_2 nanosheet. The cracked regions show a low overpotential response and a similar response at their edges. SECCM is also useful for evaluating the treatment effect for improving the catalytic activity of the MoS_2 nanosheet.

HER activity of the MoS_2 - WS_2 heteronanosheet

Atomic-layer semiconducting heterostructures is an important for tuning the band width.[7] However, electrochemical reactivity is closely related to adsorption / dissociation of molecules and electron transfer and Tafel–Volmer reaction is the bottle neck process of HER reaction. To characterize the heterostructures HER activity, we visualized lateral and stacked heterostructure based on MoS_2 and WS_2 heteronanosheet using SECCM and conformed nanosheet topography using AFM (Figure 3(a,b)). The mono or bilayer level lateral and stacked MoS_2 and WS_2 heteronanosheet structure was clearly visualized by AFM. Specific catalytic ability was not observed at the heterojunction, but different current signal was obtained on MoS_2 and WS_2 heteronanosheet (Figure 3(c)). To investigate the detail of HER activity difference, we performed high magnification SECCM imaging. The current response is corresponding with the region and clearly categorize the current response of MoS_2 edge (green), WS_2 terrace(red), MoS_2 terrace(blue), and kish graphite terrace(grey).

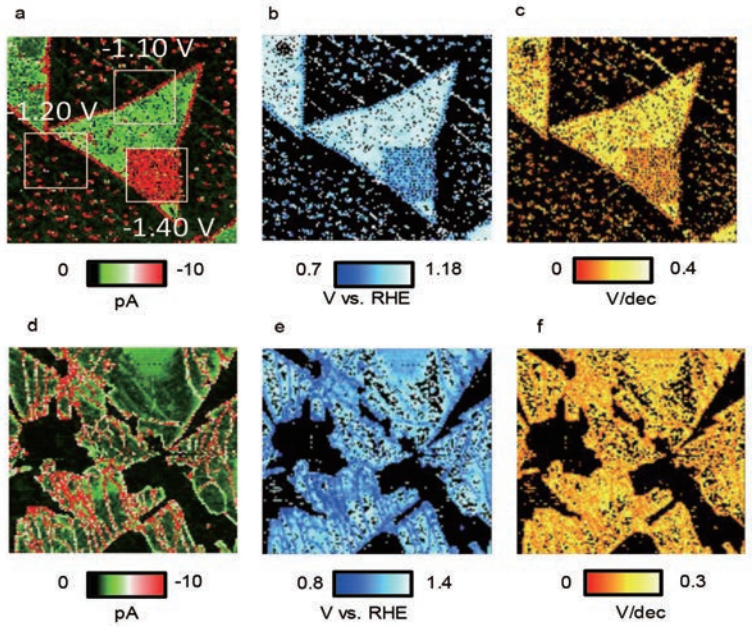

Figure 2 (a) current (b) overpotential (30 mA/cm^2) and (c) tafel slope images of electrochemical activation and imaging of 1H MoS_2 nanosheets on HOPG substrate. Scansize was 10 × 10 mm^2 and -1.2 V vs. RHE. (d) current (e) overpotential (30 mA/cm^2) and (f) tafel slope images of heating activated 1H MoS_2 nanosheets on HOPG substrate. Scansize was 10 × 10 mm^2. -1.1 V vs. RHE.

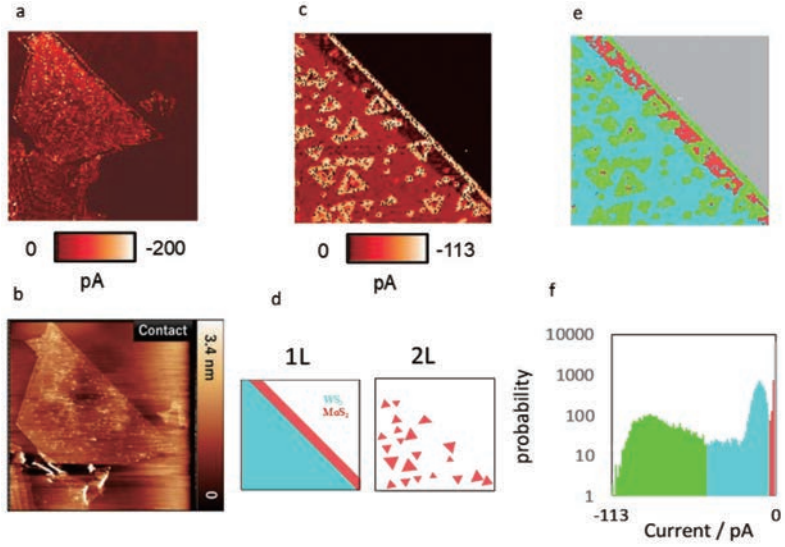

Figure 3 (a) SECCM and (b) AFM images of MoS_2 and WS_2 heteronanosheet on kish graphite. Scansizes were 20 × 20 mm^2 and 18 × 18 mm^2. Applied voltage was -1.0 V vs. RHE. (c) High magnification SECCM, (d) Schematic illustration, and (e) Four color of MoS_2 and WS_2 heteronanosheet image divided based on current and (f) Data from the SECCM images current plotted as histograms. Scansize was 5 × 5 mm^2 and -1.1 V vs. RHE.

Characterization of the Layer number related HER activity

The layer number is also reported as an important factor for HER activity because of the electron conductivity related with layer number.[8] Therefore, as a next experiment, we characterized the relation of layer number and HER activity. Figure 4(a) shows the multi layered MoS_2 and WS_2 heteronanosheet. To investigate the layer dependent HER activity, we categorized the 1st (red), 2nd(green), and 3rd (grey) layer and characterize the overpotential and Tafel slope. Surprisingly, we could not see clear difference of overpotential (30 mA/cm^2) and Tafel slope, 0.91 vs. RHE. and 185 mV/dec, at each layer number. (Figure 4 (d, e)). SECCM local electrochemical imaging is important to directly visualizing and characterizing the local catalytic activity without being buried in the average response.

Characterization of local aging phenomena

Understanding the aging phenomena is very important to use the catalytic material for long time. Nikhil and coworkers reported the aging effect of MoS_2 and WS_2 nanosheets by photoluminescence and XPS.[9] They have reported that the origin of the aging of MoS_2 was due to oxidation process of the transition metals at the edge parts and adsorption of organic contaminants. However, these methods are difficult to characterize the catalytic activity. SECCM can directly visualize the aging effect on transition metal dichalcogenide nanosheet. We characterized HER activity of fresh and partially degraded following room-temperature storage in air for 11 month after the initial synthesis MoS_2 and WS_2 heteronanosheet. The fresh sample shows high activity at the edge. In the case of the pyramid and spiral shape structure WS_2 nanosheets, top regions showed significantly high HER activity (Figure 5(a, b)). On the other hand, edge region of aging sample showed lower current signal compared to terrace region (Figure 5(c)). We also characterize the sample using CV mode SECCM for characterizing overpotential and Tafel slope (Figure 5(d)). The overpotential (30 mA/cm^2) of edge region (0.91 vs. RHE) was higher than terrace region (0.88 vs. RHE). About the Tafel slow, we could not see significant difference between edge and terrace of MoS_2 and WS_2 heteronanosheet. The degradation of MoS_2 and WS_2 heteronanosheet may be expected to derive from the reaction with oxygen, water, and adsorbed organic contamination. These result mean that characterization of progress of the heterogeneous degradation of HER activity is also important application of SECCM.

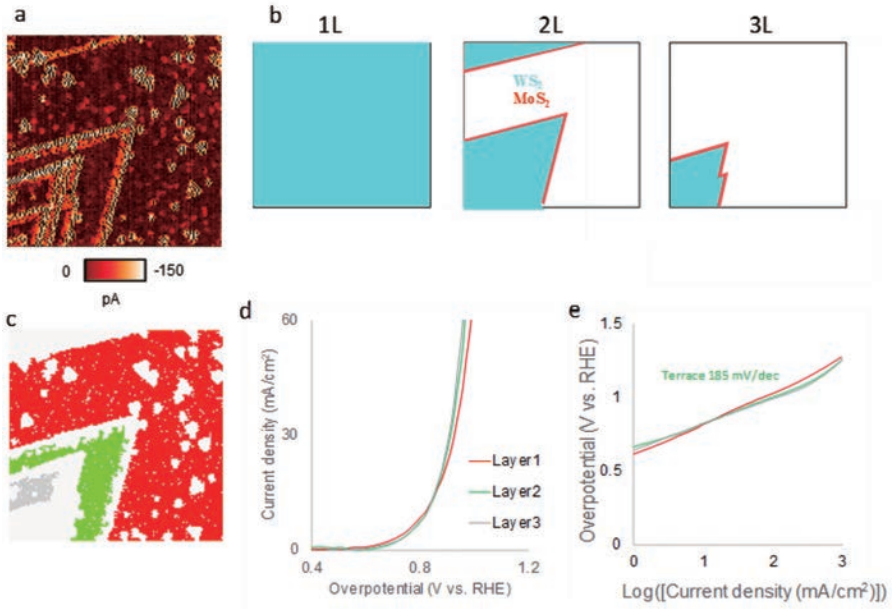

Figure 4 (a) SECCM and (b) Schematic illustration and (c) tricolor images of 1st (red), 2nd (green), 3rd (grey) of MoS_2 and WS_2 heteronanosheet on kish graphite. Scansize was 6 × 6 mm^2 and -1.0 V vs. RHE. Graphs showing the (d) overpotential and (e) Tafel slope of the 1st (red), 2nd (green), 3rd (grey) regions.

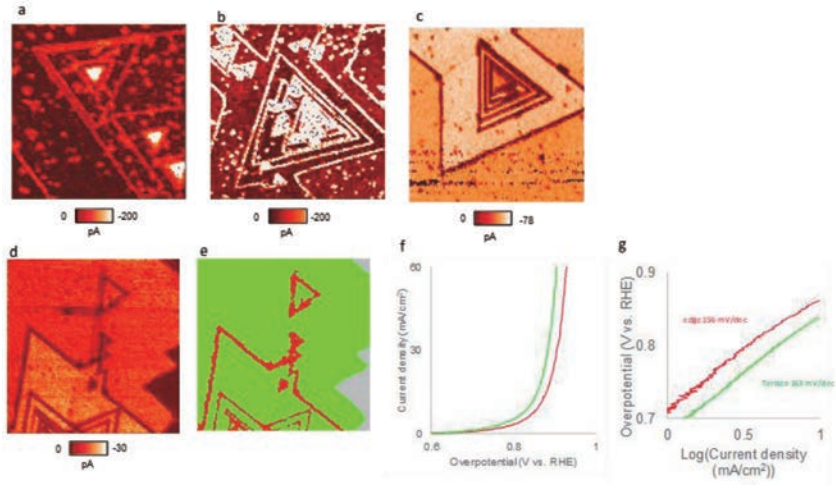

Figure 5 SECCM images of (a, b) fresh and (c) aging MoS_2 and WS_2 heteronanosheet on kish graphite. Scansize were (a) 8 × 8 mm^2 and (b-e)10 × 10 mm^2, respectively. Applied voltage were -0.4 V vs. RHE and -0.9 V vs. RHE, respectively. SECCM (d) current imaging of the aging MoS_2 and WS_2 heteronanosheet and (e) tricolor images of edge (red), terrace (green), and HOPG terrace. Scansize was 7 × 7 mm^2 and -0.4 V vs. RHE and -0.9 V vs. RHE. Graphs showing the (f) overpotential and (g) Tafel slope of the aging MoS_2 and WS_2 heteronanosheet edge (red) and terrace (green) regions.

Conclusion

We have developed SECCM for visualizing HER catalytically active sites in real-space on MoS_2 nanosheets by measuring the distributions of the current, overpotential, and Tafel slope with a submicroscale spatial resolution. The visualization of the HER active sites provides solid experimental evidence to support the previous theoretical prediction and assumption that there is an inhomogeneous catalytic activity between the edges and terraces of 1H-MoS_2 nanosheets. Moreover, the high spatial resolution of SECCM reveals an inhomogeneous HER activity from grain boundarys, small nanosheets, and electrochemically activated regions, which indicates that the HER catalysis of MoS_2 nanosheets may be improved by structure engineering. This study also demonstrates that SECCM is a powerful tool for evaluating the local HER activity for designing the suitable catalytic active structure, phase and can be widely applied for the characterization of 2D catalytic materials.

References

[1] Jaramillo, T. F.; Jorgensen, K. P.; Bonde, J.; Nielsen, J. H.; Horch, S.; Chorkendorff, I. Identification of active edge sites for electrochemical H_2 evolution from MoS_2 nanocatalysts. *Science* **2007**, *317* (5834), 100-102. DOI: 10.1126/science.1141483.

[2] Li, H.; Tsai, C.; Koh, A. L.; Cai, L. L.; Contryman, A. W.; Fragapane, A. H.; Zhao, J. H.; Han, H. S.; Manoharan, H. C.; Abild-Pedersen, F.; et al. Activating and optimizing MoS_2 basal planes for hydrogen evolution through the formation of strained sulphur vacancies (vol 15, pg 48, 2016). *Nat Mater* **2016**, *15* (3). DOI: 10.1038/NMAT4564.

[3] Fernandez, J. L.; Walsh, D. A.; Bard, A. J. Thermodynamic guidelines for the design of bimetallic catalysts for oxygen electroreduction and rapid screening by scanning electrochemical microscopy. M-Co (M : Pd, Ag, Au). *Journal of the American Chemical Society* **2005**, *127* (1), 357-365. DOI: 10.1021/ja0449729.

[4] Takahashi, Y.; Kumatani, A.; Munakata, H.; Inomata, H.; Ito, K.; Ino, K.; Shiku, H.; Unwin, P. R.; Korchev, Y. E.; Kanamura, K.; et al. Nanoscale visualization of redox activity at lithium-ion battery cathodes. *Nature communications* **2014**, *5*, 5450. DOI: Artn 5450
Doi 10.1038/Ncomms6450.

[5] Takahashi, Y.; Kobayashi, Y.; Wang, Z.; Ito, Y.; Ota, M.; Ida, H.; Kumatani, A.; Miyazawa, K.; Fujita, T.; Shiku, H.; et al. High-Resolution Electrochemical Mapping of the Hydrogen Evolution Reaction on Transition-Metal Dichalcogenide Nanosheets. *Angewandte Chemie* **2020**, *59* (9), 3601-3608. DOI: 10.1002/anie.201912863 From NLM PubMed-not-MEDLINE.

[6] Tsai, C.; Li, H.; Park, S.; Park, J.; Han, H. S.; Norskov, J. K.; Zheng, X.; Abild-Pedersen, F. Electrochemical generation of sulfur vacancies in the basal plane of MoS_2 for hydrogen evolution. *Nature communications* **2017**, *8*, 15113. DOI: 10.1038/ncomms15113.

[7] Kobayashi, Y.; Yoshida, S.; Maruyama, M.; Mogi, H.; Murase, K.; Maniwa, Y.; Takeuchi, O.; Okada, S.; Shigekawa, H.; Miyata, Y. Continuous Heteroepitaxy of Two-Dimensional Heterostructures Based on Layered Chalcogenides. *Acs Nano* **2019**, *13* (7), 7527-7535. DOI: 10.1021/acsnano.8b07991.

[8] Yu, Y. F.; Huang, S. Y.; Li, Y. P.; Steinmann, S. N.; Yang, W. T.; Cao, L. Y. Layer-Dependent Electrocatalysis of MoS_2 for Hydrogen Evolution. *Nano Lett* **2014**, *14* (2), 553-558. DOI: 10.1021/nl403620g.

[9] Gao, J.; Li, B.; Tan, J.; Chow, P.; Lu, T.-M.; Koratkar, N. Aging of Transition Metal Dichalcogenide Monolayers. *Acs Nano* **2016**, *10* (2), 2628-2635. DOI: 10.1021/acsnano.5b07677.

[10] Chen, L.; Liu, B. L.; Abbas, A. N.; Ma, Y. Q.; Fang, X.; Liu, Y. H.; Zhou, C. W. Screw-Dislocation-Driven Growth of Two-Dimensional Few-Layer and Pyramid-like WSe_2 by Sulfur-Assisted Chemical Vapor Deposition. *Acs Nano* **2014**, *8* (11), 11543-11551. DOI: 10.1021/nn504775t.

[11] Fan, X. P.; Jiang, Y.; Zhuang, X. J.; Liu, H. J.; Xu, T.; Zheng, W. H.; Fan, P.; Li, H. L.; Wu, X. P.; Zhu, X. L.; et al. Broken Symmetry Induced Strong Nonlinear Optical Effects in Spiral WS_2 Nanosheets. *Acs Nano* **2017**, *11* (5), 4892-4898. DOI: 10.1021/acsnano.7b01457.

Dr. TAKAHASHI Yasufumi
高橋 康史
Professor,
Department of Electronics,
Graduate School of Engineering,
Nagoya University

Development of Electrochemical Techniques for Defect Engineering on Advanced Energy Materials

電気化学に基づく欠陥エンジニアリング技術の開発

NAKAMURA Takashi
中村 崇司

Highly efficient energy storage/conversion devices such as fuel cells and advanced batteries are expected as key technologies for carbon-neutral and sustainable society by utilizing clean hydrogen. In energy functional materials for above-mentioned applications, defects like oxygen vacancy play an important role for their material functionalities. Therefore, understanding true properties of defect is essentially important for defect engineering. The author has been working on the establishment of electrochemical techniques which enable direct evaluation on defect functionality. Furthermore, we have been developing defect control technologies. In this paper, some examples of defect engineering on catalysts and battery materials are given.

燃料電池や次世代型蓄電池などの高効率エネルギー貯蔵・変換技術は，クリーン水素の利用によるカーボンニュートラル実現の中核を担う重要な技術と期待されている。上記デバイスを構成するエネルギー機能材料では，材料中の欠陥が機能発現の鍵となることが知られている。つまり，欠陥を軸とした機能性の理解と材料開発は重要な研究開発項目の一つであると言える。著者は電気化学セルの出力電圧が対象材料の化学ポテンシャルに対応するという現象に着目し，機能性酸化物中の欠陥生成機構を解明するための評価手法を開発してきた。さらにその技術を材料合成に応用する検討も進めている。本稿では触媒および蓄電池材料を対象とした著者らの取り組みについて述べる。

Introduction

For the realization of carbon-neutral and sustainable society, efficient utilization of renewable energy is essential. For that, advancing energy conversion/storage technologies such as hydrogen production, rechargeable batteries, electrolysis and fuel cells are important. Cation doping is the most common and effective strategy to advance functionalities of the component of above-mentioned energy conversion/storage devices. However, cation doping is becoming less effective since it has been widely examined so far. For further development of energy functional materials, we focus on the utilization of defects which inherently exist in the materials and play an important role for catalytic, electric and electrochemical properties. It is important to understand decisive factors for the functionalities and establish rational guidelines for defect engineering based on fundamental sciences. Moreover, developing defect control technology is also important goal of our work to exceed the present limit of the material exploration. For the first topic, we have been working on the development of functional energy materials which inherently contain electrochemically active point defects such as oxygen vacancy (unoccupied oxygen site) and interstitial oxygen (excess oxygen at cryptographically vacant space), and for the second topic, we advanced the electrochemical cell as a reactor which can flexibly control defect structure in the target material. Impacts and future benefit of the applicant's work is summarized in Figure 1.

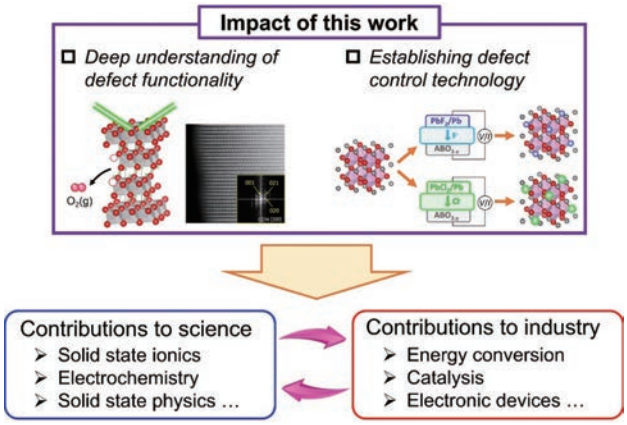

Figure 1 Impacts and future benefits of the present work.

Formation of oxygen defects in layered perovskite oxides $(La,Sr)_2NiO_{4+\delta}$

Perovskite-related oxides are regarded as promising water splitting catalysts and electrode materials for fuel cells.[1-3] Their catalytic properties are strongly influenced by oxygen defects such as oxygen vacancy and interstitial oxygen, and therefore, understanding the mechanism of oxygen defect formation is essentially important. Here, to investigate oxygen defect formation in layered perovskite oxides $(La,Sr)_2NiO_{4+\delta}$ (Figure 2-a), we applied two experimental techniques. One was the thermogravimetry (TG) which can evaluate oxygen content variation by detecting the weight change due to oxygen defect formation, Δw_s, and the other was coulometric titration (CT) which can evaluate oxygen content and equilibrium oxygen chemical potential by using the electrochemical cell composed of an oxide-ion conductor. For TG, very accurate symmetrical balance is installed into glass/ceramics chamber where temperature and atmospheric condition are controlled by a heater and gas-mixtures (Figure 2-b). Variation of oxygen content can be evaluated from the weight change by

$$\Delta\delta = \frac{M_s}{M_O}\frac{\Delta w_s}{w_s} \qquad (1)$$

where $\Delta\delta$, M_s, M_O, and w_s are the relative variation of oxygen nonstoichiometry, the formula weight of the sample and oxygen atom, and the weight of the specimen, respectively. Controllable $P(O_2)$ range by O_2-Ar gas-mixtures is 10^{-4} to 1 bar. This is not enough to evaluate the oxygen defect formation in $(La,Sr)_2NiO_{4+\delta}$.

During the CT measurement, the amount of oxygen in the specimen was controlled by the electric charge passed through the cell. After a specified amount of electric charge was passed, $\Delta\delta$ was calculated by the equation

$$\Delta\delta = \frac{C}{2FM_s} \qquad (2)$$

where C and F is the total amount of electric charge and the Faraday constant, respectively. Equilibrium oxygen partial pressure, $P(O_2)_{eq}$, corresponding to a certain oxygen content was obtained from the electromotive force between the inside and the outside of the cell, E, under the equilibrium state as

$$P(O_2)_{eq} = P(O_2)_{RE}\exp\left(\frac{4FE}{RT}\right) \qquad (3)$$

where $P(O_2)_{RE}$, R, and T are the oxygen partial pressure at the reference electrode, the gas constant and the temperature, respectively. The oxygen content was determined by the weight change of the sample after reduction decomposition under hydrogen atmosphere.

Figure 2-b, 2-c and 2-d shows the oxygen content variation of $La_2NiO_{4+\delta}$, $La_{1.8}Sr_{0.2}NiO_{4+\delta}$ and $La_{1.6}Sr_{0.4}NiO_{4+\delta}$ as a function of equilibrium oxygen partial pressure.[4] Since both TG and CT were applied complementary in this work, oxygen defect formation under wide $P(O_2)$ range was successfully evaluated. $La_{1.8}Sr_{0.2}NiO_{4+\delta}$ showed representative oxygen content variation behavior of a layered perovskite oxide. In high $P(O_2)$ atmosphere, $La_{1.8}Sr_{0.2}NiO_{4+\delta}$ showed oxygen-excess composition by accepting interstitial oxygen in the rock-salt structure, while it showed oxygen-deficient composition by oxygen vacancy formation in low $P(O_2)$ atmosphere. Plateau-like behavior of the oxygen content against $P(O_2)$ was reasonably observed near the stoichiometric oxygen composition ($4+\delta \sim 4.00$) which is consistent with thermodynamic estimation.[5] Such oxygen defect formation also depends on the acceptor concentration, Sr content in this system. As Sr concentration increases, the oxygen vacancy formation proceeds easier, while the formation of interstitial oxygen needs stronger driving force.

The observed oxygen defect formation mechanism was investigated by defect chemical and thermodynamic analyses. The defect equilibrium model was established from the site conservation, defect equilibrium reactions and charge neutrality under the rigid band approximation with p-type degenerated electronic state

$$P(O_2)^{1/2} = \frac{[O_i'']}{[V_i^{\times}]} \exp\left[\frac{\Delta G_I^{\circ} - a[O_i'']}{RT} + 2\ln\left\{\exp\left(\frac{N_A}{D_{VB}V_m}[h^{\bullet}]\right) - 1\right\}\right] \quad (4\text{-}1)$$

$$[O_i''] = \frac{-(6K_f - \delta + K_f\delta) + \sqrt{(6K_f - \delta + K_f\delta)^2 + 8K_f(1-K_f)(4+\delta)}}{2(1-K_f)} \quad (4\text{-}2)$$

where $[O_i'']$, $[V_i^{\times}]$, $[h^{\bullet}]$, ΔG_I°, ΔG_f°, K_f, a, and D_{VB} are the molar concentration of interstitial oxygen, that of vacant interstitial site, that of hole, the Gibbs free energy change of interstitial oxygen formation, that of oxygen Frenkel formation, the equilibrium constant of oxygen Frenkel defect formation, the regular solution parameter and the density of state of the valence band. The derivation of the above defect equilibrium model is summarized in our work.[4] The calculated δ-T-$P(O_2)$ relation is added in Figures 2-b, 2-c and 2-d. As illustrated, the defect equilibrium model can explain oxygen composition variation with T and $P(O_2)$ very well, meaning that the defect structure under certain T and $P(O_2)$ can be estimated precisely by this model. Such fundamental knowledge about oxygen defect formation is essentially important to design defect structures and maximize the functionalities of oxygen defects.

Lattice oxygen stability in lithium-ion battery cathode materials Li(Ni,Co,Mn)O_2

Transition metal oxides are key components of secondary batteries such as alkali metal-ion and anion batteries, sufficient stability of which is thus vitally important for ensuring high energy density and safety. However, problems attributed to the lattice oxygen instability in transition metal oxide cathodes have been widely reported, such as capacity degradation, gas generation and catastrophic thermal runaway.[6,7] These highlights the importance of insight into decisive factors for lattice oxygen stability. In this section, our recent works on the evaluation of lattice oxygen stability in layered rock-salt Li(Ni,Co,Mn)O_2 are summarized. We succeeded to evaluate the oxygen release behavior

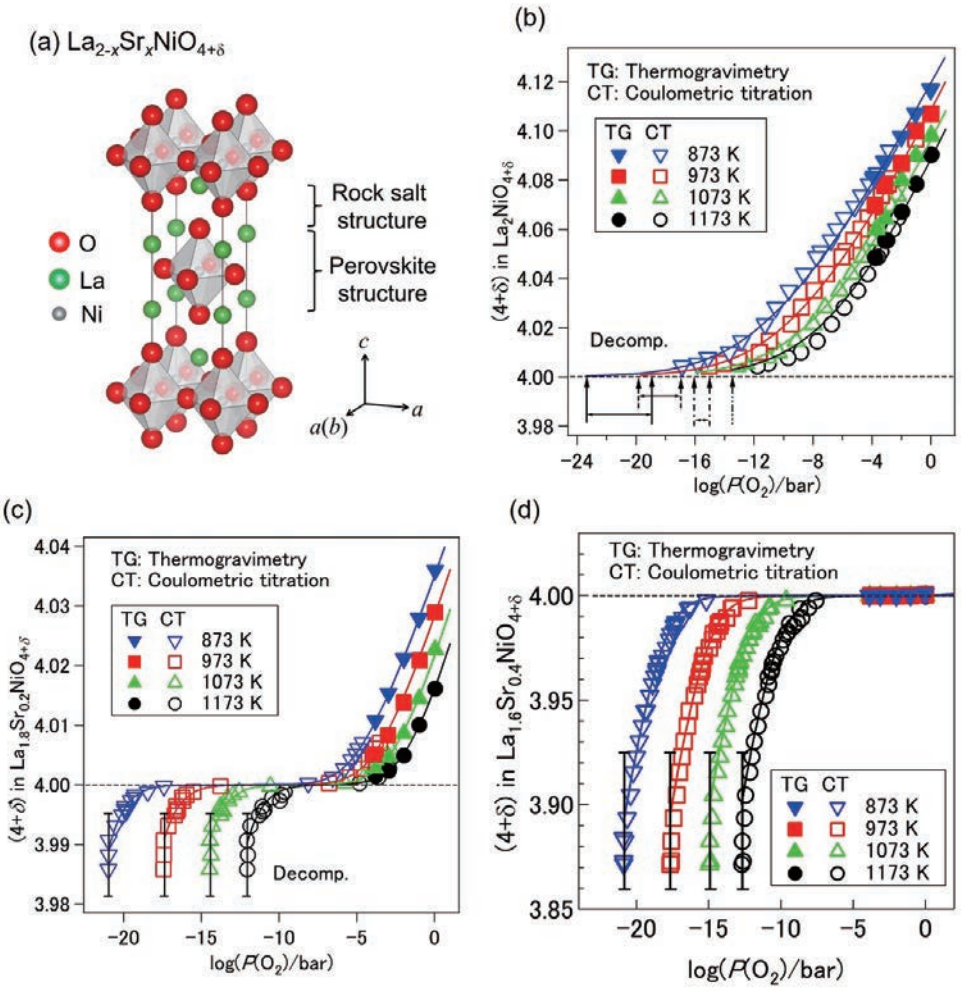

Figure 2 (a) Crystal structure of $(La,Sr)_2NiO_{4+\delta}$. Oxygen content variation (oxygen nonstoichiometry) of (b) $La_2NiO_{4+\delta}$, (c) $La_{1.8}Sr_{0.2}NiO_{4+\delta}$ and (d) $La_{1.6}Sr_{0.4}NiO_{4+\delta}$ as a function of equilibrium oxygen partial pressure. Closed and open symbols were measured by thermogravimetry and by coulometric titration, respectively. Calculated δ-T-$P(O_2)$ relation by the defect equilibrium model (Eq. 4) are shown as solid lines.

of lithium-ion battery cathode by applying the high-temperature solid-state-ionic techniques shown in the previous section, namely TG and CT. Oxygen release behavior and relevant changes in crystal and electronic structures were investigated and analyzed based on defect chemistry and thermodynamics.[8,9]

The molar ratio of oxygen over transition metal, O/TM, against $P(O_2)$ in $LiNi_{1/3}Co_{1/3}Mn_{1/3}O_2$ (NCM111) is summarized in Figure 3-a. In the figure, O/TM = 2 represents the stoichiometric oxygen composition and O/TM < 2 represents the oxygen deficient composition. The oxygen content of the pristine NCM111 was determined by iodometric titration. The oxygen content decreased along with lower equilibrium $P(O_2)$ in the gaseous phase. With totally 4.8 mol% oxygen deficiency introduced in the lattice, NCM111 remained its original layered rock-salt structure without phase transformation or reduction decomposition as confirmed by XRD (Figure 3-b). All XRD profiles of the oxygen-deficient NCM111 were indexed by $R\bar{3}m$, and no impurity peak was observed by oxygen release. However, gradual broadening of diffraction peaks was observed with increasing oxygen deficiency. This indicated the deterioration of crystallinity with oxygen deficiency, despite changes of grain size and morphology was not significant. Diffraction peaks shifted to lower angle with oxygen release, indicating the expansion of the crystal lattice. In addition, the intensity ratio the 003 and 004, I_{003}/I_{104}, declined from 1.36 in the pristine to 0.80 in the 4.8 mol% oxygen-deficient NCM111, indicating disorder of the layered structure by anti-site defect formation (exchange of Li and Ni) as reported in earlier works.[10,11] To investigate the charge compensation mechanism due to oxygen release, oxygen-deficient NCM111 (0.5 mol%, 2.0 mol%, 3.5 mol% and 4.8 mol%) were characterized by X-ray absorption spectroscopy (XAS), and transition metal L-edge spectra are summarized in Figure 3-c, 3-d and 3-e. Probing depth of the fluorescence X-ray mode is typically hundreds nanometers which is close to the size of as-synthesized primary particles, therefore obtained data reflect the bulk information. In Ni L-edge spectra, the intensity of the peak around 855 eV (L_{III} edge) decreases slightly from the pristine to the samples with 0.5 mol% and 2.0 mol% oxygen deficiency, and keep invariant with further oxygen release. These spectral changes suggest that high-valent Ni was reduced to Ni^{2+} until 2.0 mol% oxygen release, and was invariant by further oxygen release. The reduction behavior observed for Ni suggests the existence of small quantity of Ni^{3+} in the pristine sample, which can be explained by negative defects such as cation vacancy or excess Li at the transition metal site (Li''_{TM}). In Co L-edge spectra, there was no observable spectral variation until 0.5 mol% oxygen deficiency, while the shoulder peaks around 778 eV in L_{III} edge appeared with 2.0 mol% oxygen release, indicating that Co was reduced from ca. 0.5 mol% of oxygen loss. The increase of shoulder peaks with oxygen loss suggest that Co acted as the main reduction species when the amount of oxygen loss exceeded 0.5 mol%. The absorption spectra of Mn showed no significant change from the pristine to 4.8 mol% oxygen release, meaning that the contribution of Mn^{4+} reduction is negligibly small in NCM111. From the spectral changes at Ni, Co and Mn L-edge, the charge compensation mechanism due to oxygen release in NCM111 can be explained as follows. In the initial stage of oxygen release only high-valent Ni is selectively reduced followed by the selective reduction of Co^{3+} species, while the reduction of Mn^{4+} is negligible.

As discussed, the charge neutrality was balanced by selective reduction of high-valent Ni in the initial stage of oxygen release in NCM111. This strongly indicates that the presence of high-valence Ni significantly destabilizes lattice oxygen and facilitates oxygen release. To confirm this hypothesis, oxygen release from high Ni concentration NCM series, $LiNi_{0.5}Co_{0.2}Mn_{0.3}O_2$ (NCM 523) and $LiNi_{0.6}Co_{0.2}Mn_{0.2}O_2$ (NCM622), were investigated in a similar manner. Because nominal oxidation state of Ni in NCM111, NCM523 and NCM622 is 2, 2.4 and 2.667, respectively, oxygen release easily proceeds in high Ni NCM. As summarized in Figure 3-f, the δ vs. $P(O_2)$ curve of NCM622 appears in higher $P(O_2)$ region than that of NCM111, while NCM523 shows similar oxygen release behavior to NCM622 except 2-δ < 1.93. These results indicate that lattice oxygen is less stable with increasing Ni valence state and support our hypothesis that high-valent Ni destabilizes lattice oxygen. For more quantitative discussion, partial molar enthalpy of oxygen, (h_O-h_O^0), was calculated from δ-T-$P(O_2)$ relation which represents necessary energy for oxygen release. Figure 3-g shows -(h_O-h_O^0) as functions of the amount of released oxygen δ and reduction species during oxygen release; circular symbols show Ni reduction and square symbols show Co reduction. As can be clearly confirmed, -(h_O- h_O^0), in other words necessary energy for oxygen release, essentially depends on reduction transition metal. Oxygen release with Ni reduction needs less than 0.5 eV, while that with Co reduction needs more than 2.0 eV. It can be concluded that the presence of high valent Ni significantly degrades lattice oxygen stability. As demonstrated in this work, thermodynamic evaluation can pave the way for quantitative and direct discussion on lattice oxygen stability of battery materials. Undoubtedly, transition metal oxides play an important role in the next-generation batteries, including not only

advanced lithium-ion batteries but also multivalent metal-ion batteries and alkali metal-ion batteries. Oxygen release and issues induced by lattice oxygen activity are inevitable problems. We expect the methodology demonstrated in this work will establish guidelines of designing and tailoring advanced energy materials for robust and high-energy-density batteries.

Development of electrochemical reactors for anion defect engineering

Since conventional cation doping strategy is becoming less effective due to wide variety of attempts so far, anion doping gains attention as a new strategy for further advancement of energy functional materials. For efficient utilization of functionalities of anion defects, electrochemical reactors for the control of anion defect species have been developing by the authors' research team. The schematic picture of the reactor and superiorities are summarized in Figure 4. The reactor has some great advantages compared with conventional synthesis techniques such as high-pressure synthesis, mechanical milling, topochemical reaction.[12-14] First, the driving force of the anion defect doping can be controlled by the external voltage according to the Nernst equation. When A^{n-} is controlled by the electrochemical reactor, the chemical potential of the neutral A at the target material μ_A is expressed by the Nernst equation by

$$\mu_A = \mu_{A,CE} + nFE \quad (5)$$

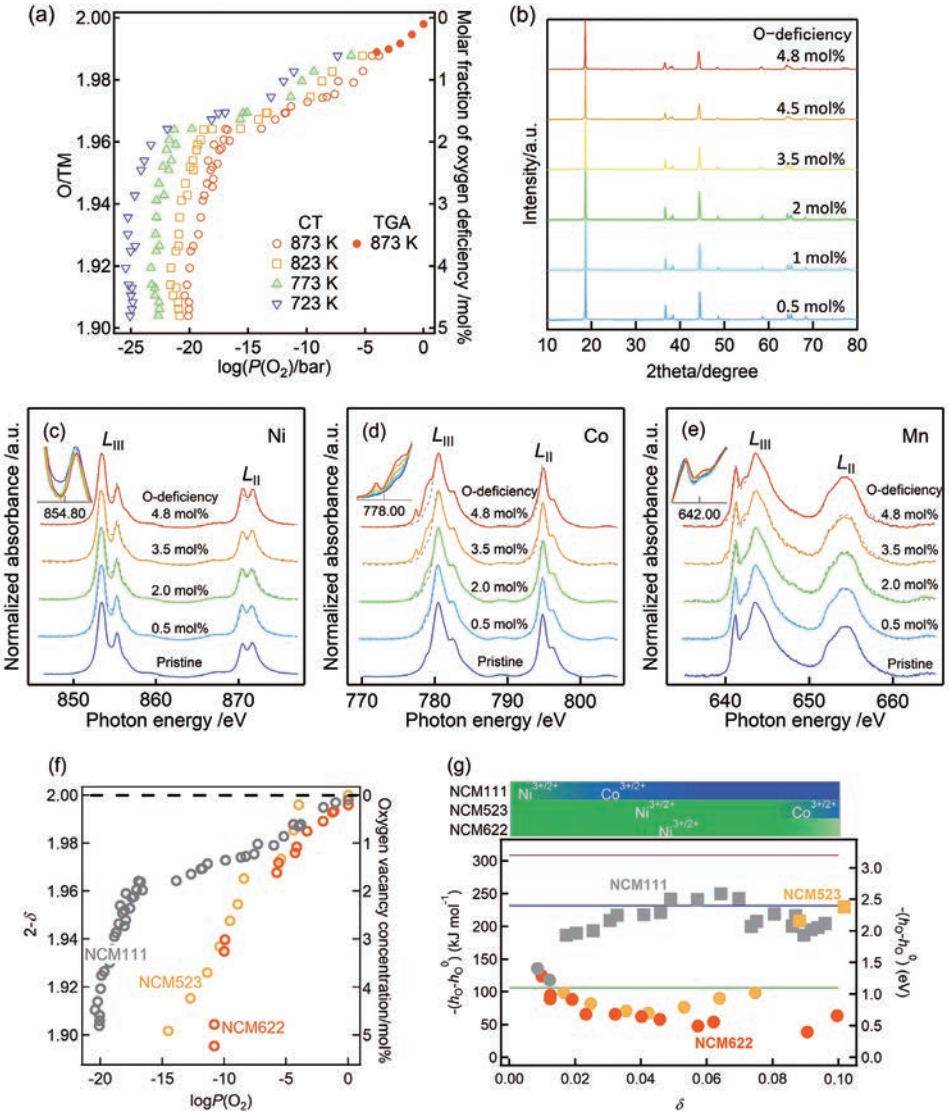

Figure 3 (a) Oxygen release behavior of NCM111 and (b) XRD patterns of oxygen-deficient NCM111. XAS spectra of oxygen-deficient NCM111 at (c) Ni L-, (d) Co L- and (e) Mn L-edge. Oxygen release behavior of NCM111, NCM532 and NCM622 measured at 873 K. (f) $-(h_O-h_O^0)$ as a function of δ. Circular symbols show $-(h_O-h_O^0)$ by Ni reduction and square symbols show that by Co reduction.

where E and $\mu_{A,CE}$ are the electrode potential and the chemical potential of A at the counter electrode, respectively. This means that the reactor can create extremely high activity condition (even impossible condition by conventional techniques) just by applying external voltage. Second, wide variety of anionic defects are controllable by changing the electrolyte. Third, the amount of doped anionic species can be quantitatively controlled by the charge passing through the cell. Considering these advantages, our electrochemical reactor can pave the way to extend the possibility of defect engineering and mixed-anion compounds.

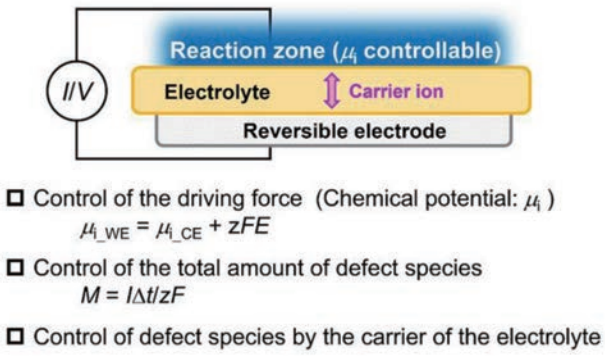

Figure 4 Schematic illustration of the electrochemical reactor for anion defect control.

Conclusions

As a new strategy for further development of energy conversion/storage technologies, we take notice of the utilization of defects in energy functional materials. To achieve this, it is necessary to establish basic sciences regarding defect formation and their functionalities, and to develop a new technology for flexible and easy control of defect species in the target material. As a case study of the first purpose, oxygen defect formation in a layered perovskite oxide $(La,Sr)_2NiO_{4+\delta}$ is summarized, since oxygen defects such as oxygen vacancy and interstitial oxygen play an important role for catalytic activity and electrochemical properties in this material. Oxygen defect formation behavior was investigated, and a defect equilibrium model based on defect chemistry and thermodynamics was proposed. The proposed model agrees very well with observed oxygen content variation with T and $P(O_2)$. Moreover, these experimental and analytical techniques are applied to understand the mechanism of oxygen release from lithium-ion battery cathodes. Although this is an unprecedented challenge in a battery research field, we, for the first time, report fruitful fundamental knowledge of oxygen release. For instance, our work revealed that reduction species (transition metal being reduced during oxygen release) essentially determine the lattice oxygen stability. For the second purpose, we are developing electrochemical reactors composed of an anion conductor which can flexibly, easily and quantitatively control anion defect species in the target material. While the concept of the reactor and schematic illustrations are shown in this paper, some promising results will be shown soon. Complementary advancement of both the establishment of fundamental sciences on defects and the development of defect control techniques is going to contribute to technological innovation of energy functional materials based on defect engineering, and consequently, contribute to the realization of carbon-neutral and sustainable society.

References

[1] A. P. Tarutin, J. G. Lyagaeva, D. A. Medvedev, L. Bi, A. A. Yaremchenko, *J. Mater. Chem. A*, 2021, 9, 154-195.
[2] P. C. Meenu, P. K. Smanta, T. Yoshida, N. J. English, S. P. Datta, S. A. Singh, S. Dinda, C. Chakraborty, S. Roy, *ACS Appl. Energy Mater.*, 2022, 5, 503-515.
[3] H. Li, Y. Chen, J. Ge, X. Liu, A. C. Fisher, M. P. Sherburne, J. W. Ager, Z. J. Xu, *JACS Au*, 2021, 1, 108-115.
[4] T. Nakamura, K. Yashiro, K. Sato, J. Mizusaki, *Solid State Ionics*, 2009, 180, 368-376.
[5] C. Wagner, *Prog. Solid State Chem.* 1971, 6, 1-15.
[6] X. Feng, M. Ouyang, X. Liu, L. Lu, Y. Xia, X. He, *Energy Storage Mater.*, 2018, 10, 246-267.
[7] S. Shrifi-Asl, J. Lu, K. Amine, R. Shahbazian-Yassar, *Adv. Ener. Mater.*, 2019, 9, 1900551.
[8] X. Hou, Y. Kimura, Y. Tamenori, K. Nitta, H. Yamagishi, K. Amezawa, T. Nakamura, *ACS Energy Lett.*, 2022, 7, 1687-1693.
[9] X. Hou, K. Ohta, Y. Kimura, Y. Tamenori, K. Tsuruta, K. Amezawa, T. Nakamura, *Adv. Energy Mater.*, 2021, 11, 2101005.
[10] T. Ohzuku, A. Ueda, M. Nagayama, *J. Electrochem.* Soc., 1993, 140, 1862-1870.
[11] J. Zheng, P. Xu, M. Gu, J. Xiao, N. D. Browning, P. Yan, C. Wang, J. G. Zhang, *Chem. Mater.*, 2015, 27, 1381-1390.
[12] N. Takeda, I. Ikeuchi, R. Natsui, K. Nakura, N. Yabuuchi, *ACS Appl. Energy Mater.*, 2019, 2, 1629-1633.
[13] M. Yang, J. A. Rodgers, L. C. Middler, J. Oró-Sró, A. B. Jorge, A. Fuertes, J. P. Attfield, *Inorg. Chem.*, 2009, 48, 11498-11500.
[14] H. Kageyama, K. Hayashi, K. Maeda, J. P. Attfield, Z. Hiroi, J. M. Rondinelli, K. R. Poeppelmeier, *Nat. Commun.*, 2019, 9, 772.

Dr. NAKAMURA Takashi
中村 崇司
Associate Professor,
Institute of Multidisciplinary Research for Advanced Materials,
Tohoku University

Development of a Highly Efficient Hydrogen Generation System by Plasmon-Induced Charge Separation Using Sunlight as an Energy Source

太陽光をエネルギー源としたプラズモン誘起電荷分離による高効率水素発生システムの開発

TAKAHASHI Yukina
髙橋 幸奈

Although the total amount of sunlight is large, the energy density per unit area is small and the supply is unstable. Therefore, it is important in practical use to devise some means to store and increase the energy density. The localized surface plasmon resonance (LSPR) of metal nanoparticles increases the density of solar energy, and the phenomenon of plasmon-induced charge separation (PICS), which occurs when metal nanoparticles are combined with semiconductors, can be used to convert light energy into electrochemical energy, which can be used to generate hydrogen from solar energy. This paper describes a research plan to develop a highly efficient hydrogen generation system using solar energy.

太陽光は総量が大きいが，単位面積あたりのエネルギー密度は小さく，供給量が不安定であるため，何らかの手段で貯めたり，エネルギー密度を高める工夫を施すことが，実用において重要である。金属ナノ粒子の局在表面プラズモン共鳴(localized surface plasmon resonance: LSPR)によって太陽光エネルギーの密度を高めるとともに，金属ナノ粒子と半導体とを組み合わせた時に生じるプラズモン誘起電荷分離(plasmon-induced charge separation: PICS)という現象を利用して光のエネルギーを電気化学エネルギーに変換することで，太陽光による高効率な水素発生システムの開発を目指す研究計画について述べる。

Introduction

A stable supply of renewable energy that does not rely on fossil resources such as oil and coal is essential to the realization of a sustainable society. Among the energy sources such as solar, wind, hydro, geothermal, tidal, and biomass, which can always be supplied from nature, solar is a particularly promising energy source. This is because the energy is obtained from outside the closed system of the earth, where the law of conservation of energy holds. The sun generates enormous amounts of energy through nuclear fusion. Only a small fraction of that energy reaches the Earth's surface. The energy reaching the surface of the earth and the sea is approximately 3 x 10^{24} J y^{-1}.[1] This value is approximately 5000 times as large as world energy consumption.[2] However, although an enormous amount of light energy falls on the earth in total, it has the disadvantage of having a small energy density per unit area. In addition, since it is dependent on nature, the supply is unstable because it is greatly affected by the seasons and weather, with the exception of some regions such as the Sahara Desert. In other words, it is an important issue in the implementation of the system to store a large amount of energy when it is supplied in large quantities, to downsize the system to produce only the necessary amount in small quantities when needed on site, and to devise ways to increase the energy density. Among them, we are focusing on ways to increase energy density.

Photoenergy harvesting in order to increase the energy density

One of the solutions is by using metal nanoparticles in order to dense the light energy. When metals are nano-sized from several nanometers to a hundred nanometers in diameter, they have the effect of trapping the photoenergy of incident light in the nanospace beyond the diffraction limit of the particle surface (Figure 1). This effect is based on a phenomenon called localized surface plasmon resonance (LSPR), and the resonance wavelength can be controlled from the UV to the near-infrared, depending on the metal species, particle size, shape, aggregation state, and refractive index of the surrounding medium. This property has been applied to sensors using the shift of plasmon peak wavelengths, and is also known to enhance both photoexcitation and emission processes of photoactive materials, such as dyes and quantum dots, on the surface of nanoparticles, which can be used for surface enhanced Raman scattering (SERS),[3] photocurrent enhancement of solar cells,[4-8] and luminescence enhancement of fluorescent dyes.[9] Theoretically, the light energy harvesting effect by LSPR is calculated to be tens to millions of times larger than that of incident light. The light energy harvesting effect of LSPR can overcome the disadvantage of sunlight, which has a low energy density per unit area.

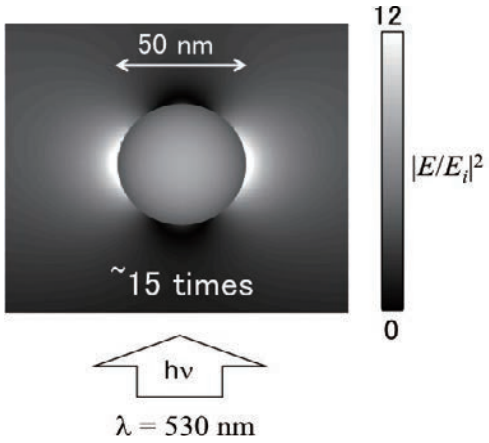

Figure 1 Photo-harvesting effect of a gold nanoparticle with the diameter of 50 nm based on LSPR (calculation).

Photoenergy conversion to other energy

There is also a method of directly utilizing light energy captured by metal nanoparticles without the use of dyes or other means. When plasmonic metal nanoparticles are combined with a semiconductor such as titanium dioxide, electrons in the metal nanoparticles transfer into the conduction band of the semiconductor under light irradiation at resonance wavelengths, a phenomenon called plasmon-induced charge separation (PICS) (Figure 2).[10] This leads to a reduction reaction on the semiconductor and an oxidation reaction on the metal nanoparticles, and is expected to be applied to sensors,[11] photoelectric conversion devices,[10,12] and visible-light-responsive photocatalysts.[10,13] In this system, light irradiation causes charge transfer to proceed directly without the use of dyes. Therefore, energy loss can be eliminated by constructing a simple system, and high conversion efficiency can be expected. This can be used in the hydrogen generation reaction by water reduction and hydrocarbon generation reaction by carbon dioxide reduction to convert light energy into chemical energy that can be stored, thereby overcoming the disadvantages of sunlight, which is unstable in supply.

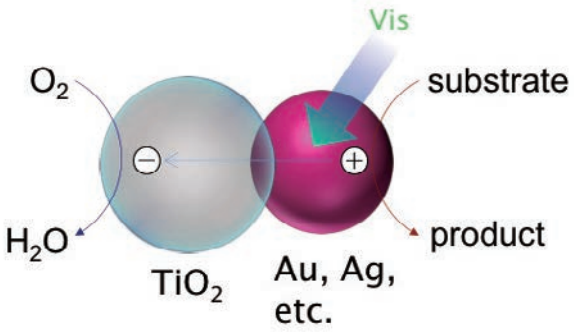

Figure 2 Schematic illustration of the conventional PICS.

Problems with conventional PICS system

However, conventional PICS has several problems due to the use of n-type semiconductors. One is the low stability of metal nanoparticles. Since oxidation reactions occur on the metal nanoparticles, it may cause the metal nanoparticles themselves to dissolve, even silver nanoparticles, which are known to be relatively stable. We have been studied to solve the problem. We succeeded in improving the thermal stability of spherical silver nanoparticles, by introducing an Al_2O_3 nanomask as a template of the nanoparticles, and the chemical stabilities by coating with a thin and dense titanium dioxide film.[14] In same way, by coating with titanium dioxide film, we improved stabilities of gold nanorods,[15] and silver nanoplates,[16] which are effective for the use of near-infrared light due to their shape anisotropy but are easily deformed into a spherical shape. However, the use of cheaper and less unstable metals was desired.

Second is the low efficiency of the charge separation. The photoelectric conversion efficiency (η) of the conventional PICS was approximately 1%.[10] In titanium dioxide photocatalysts, metal nanoparticles supported on the photocatalyst function as an electron pool that suppresses recombination of excited electrons and holes, as evidenced by their use as reduction sites.[17] Therefore, electrons transferred to the semiconductor after charge separation by conventional PICS are likely to undergo reverse electron transfer to the metal nanoparticles (recombination in the broad sense). It was supported by the reports that charge separation lifetime improved from picoseconds to microseconds by changing the semiconductor combined with the metal nanoparticles from n-type to p-type.[18]

Highly efficient hydrogen generation via PICS system with a p-type semiconductor

We therefore propose that the above problem can be solved by using a p-type semiconductor, which reverses the charge transfer, because the reduction reaction can proceed on the metal nanoparticles used in PICS (Figure 3).[19] The catalytic effect of the metal nanoparticles in the reduction reaction can also be expected. As a result, the selectivity of the reaction products can be improved. For example, copper is known to be able to reduce carbon dioxide to C2 compounds such as ethanol and ethylene when used as an electrode in electrochemical reactions.[20] Therefore, it is expected that by controlling the type of metal and crystal planes that make up the nanoparticles, arbitrary chemical reactions can be promoted, such as the generation of hydrogen and the generation of specific hydrocarbons through the reduction of carbon dioxide. In same way, as the p-type semiconductor, for example, iridium oxide is a proven material as an electrode for the electrochemical oxidation of water,[21] and is expected to water splitting into oxygen and hydrogen. The proposed system is theoretically expected to be dramatically more efficient than conventional systems.

It was noted above that conventional PICS system can be applied to sensing devices. The proposed system can also work as a sensor with higher sensitivity than conventional one. It may be possible to simultaneously detect the hydrogen generation reaction as an electrical signal in the novel system. It will be able to detect not only hydrogen generation reactions, but also the progress of beneficial chemical reactions. This sensing system will be useful in a variety of systems in the future.

Conclusion

We have described the possibility of a novel, highly efficient hydrogen generation system using PICS with a p-type semiconductor. The proposed novel system is expected to realize high-sensitivity sensing at the same time. We believe that the realization of this system, which is expected to be able to effectively harvest and utilize energy of sunlight, will contribute to solving energy problems of the world.

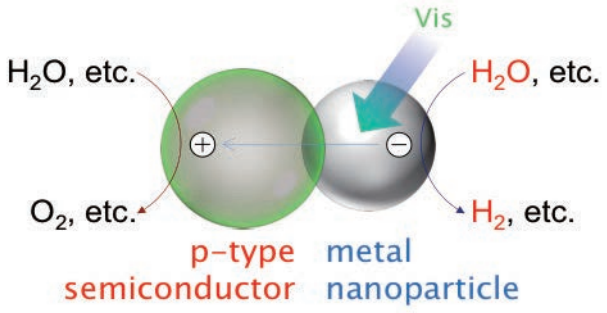

Figure 3 Schematic illustration of the PICS with p-type semiconductor.

References

[1] Solar Energy Perspectives, OECD/IEA, 2011.
[2] bp Statistical Review of World Energy 2020.
[3] M. Fleischman, P. J. Hendra, A. J. McQuillan, *Chem. Phys. Lett.*, 26, 163 (1974).
[4] C. Wen, K. Ishikawa, M. Kishima, K. Yamada, *Sol. Energy Mater. Sol. Cells*, 61, 339 (2000).
[5] S. D. Standridge, G. C. Schats, T. Hupp, *J. Am. Chem. Soc.*, 131, 8407 (2009).
[6] K. R. Catchpole, S. Pillai, J. *Luminescence*, 121, 315 (2006).
[7] D. Derkacs, S. H. Lim, P. Matheu, W. Mar, E. T. Yu, *Appl. Phys. Lett.*, 89, 093103 (2006).
[8] K. Nakayama, K. Tanabe, H. A. Atwater, *Appl. Phys. Lett.*, 93, 121904 (2008).
[9] P. Anger, P. Bharadwaj, L. Novotny, *Phys. Rev. Lett.*, 96, 113002 (2006).
[10] Y. Tian, T. Tatsuma, *J. Am. Chem. Soc.*, 127, 7632 (2005).
[11] T. Tatsuma, Y. Katagiri, S. Watanabe, K. Akiyoshi, T. Kawawaki, H. Nishi, E. Kazuma, *Chem. Commun.*, 51, 6100 (2015).
[12] Y. Takahashi, T. Tatsuma, *Appl. Phys. Lett.*, 99, 182110 (2011).
[13] E. Kowalska, R. Abe, B. Ohtani, *Chem. Commun.*, 241 (2009).
[14] Y. Takahashi, T. Tatsuma, *Nanoscale*, 2, 1494 (2010).
[15] Y. Takahashi, N. Miyahara, S. Yamada, *Anal. Sci.*, 29, 101 (2013).
[16] Y. Takahashi, K. Suga, T. Ishida, S. Yamada, *Anal. Sci.*, 32, 275 (2016).
[17] W. Kubo, T. Tatsuma, *J. Mater. Chem.*, 15, 3104 (2005).
[18] Z. Lian, M. Sakamoto, H. Matsunaga, J. J. M. Vequizo, A. Yamakata, M. Haruta, H. Kurata, W. Ota, T. Sato, T. Teranishi, *Nat. Commun.*, 9, 2314 (2018).
[19] Y. Takahashi, Y. Yamadori, T. Murayama, S. Shingo, S. Yamada, in preparation.
[20] Y. Hori, R. Takahashi, Y. Yoshinami, A. Murata, *J. Phys. Chem. B*, 101, 7075 (1997).
[21] Y. Takahashi, T. Tatsuma, *Electrochemistry*, 82, 749 (2014).

Dr. TAKAHASHI Yukina
髙橋 幸奈
Associate Professor,
International Institute for Carbon-Neutral Energy Research (I^2CNER),
Kyushu University

Data Driven Acceleration of Materials Discovery Through Integrated Correlative Spectroscopy, Synthesis, and Experimentation

相関分光法，合成，および実験の統合によるデータ駆動型材料探索の加速化

Helge Sören STEIN
ヘルゲ・ゼーレン・シュタイン

An acceleration of the transition towards renewable energy production and storage necessitates new breakthrough materials. Discovering such new and improved materials does, however, call for new paradigms that incorporate combinatorial materials science and high-throughput experimentation to fast-track materials scaling from discovery to product. Herein a brief example of materials science acceleration through integrating complex workflows is explored as implemented in the platform for accelerated electrochemical energy storage research (PLACES/R) located at the Helmholtz Institute Ulm. With the synthesis, characterization, and performance evaluation techniques, we seek to unravel the physicochemical relationships between composition, structure, processing, and performance to discover and upscale future materials for short- and long-term energy storage.

再生可能エネルギーの生産と貯蔵への移行を加速するためには，新しい画期的な材料が必要である。しかし，このような新しい材料や改良された材料を発見するためには，コンビナトリアル材料科学とハイスループット実験法を取り入れて，材料の発見から製品化までの段階を迅速に行うための新しいパラダイムが必要である。本稿では，Helmholtz Institute Ulm研究所(HIU)の電気化学エネルギー貯蔵研究加速プラットフォーム(PLACES/R)を用いた，複雑なワークフローの統合による材料科学加速の実施例を紹介する。合成，特性評価，性能評価技術を駆使することで，組成，構造，加工，性能の物理化学的な関係を解明し，短期・長期のエネルギー貯蔵のための未来の材料を発見し，スケールアップすることを目指す。

Introduction

There is a critical need for new and improved materials for intermittent renewable energy storage[1] in both stationary and mobile applications.[2] Here it is however not just important to find the highest performing[3] material for a given functional property,[4] but it is also important to discover materials that are scalable. Scalable on the TWh scale, which is the energy storage need of countries and continents, means that a material may only be comprised of earth abundant constituents and made through low-temperature green-chemistry processes.[2] Most of the currently available chemistries for Hydrogen production[5] or for batteries[6] do only fulfill this requirement in part leaving great opportunities for materials discovery and optimization.[7]

The first wave of trying to accelerate materials science was started in fact in the 1990s in Japan[8] after some early experiments in the 1950s in Germany.[9] Both times scientists tried to optimize expensive to manufacture materials like dental alloys[9],[10] containing gold or silver. The method of choice back then, and still today, was the synthesis of thin films using various CVD or PVD techniques.[11] In the 1990s there was a trend towards automation which is why there had been a trend for almost 30 years to deploy automation to materials science.[12]

The advancements in the field of “combinatorial materials science” (CMS) offered bespoke combinatorial synthesis and high-throughput characterization (using high-throughput experimentation - HTE). Many of these had the idea of connecting these systems to data management but few implemented a thorough integration.[13] In the late 2010s there was then the push for accelerated materials understanding in the so called “materials genome initia-

tive".[14],[15] There scientists sought to screen hundreds of thousands of materials using computational tools to then synthesize them using the methods available from CMS and HTE. The paradigm then was to perform so called inverse design such that one could query a functional property and receive from correlators and models a structure, composition, or processing route. Given however the vast breath and complexity of the chemical space it became evident that the descriptors and underlying physicochemical relationships were well beyond one- or two-dimensional descriptors and with the explosive rise of capabilities in data science the community shifted towards autonomous materials science. In autonomous materials science there is the idea to build so called materials acceleration platforms (MAP)[12],[16] in which research tasks such as synthesis, characterization, data-management etc. are not just accelerated through automation or use of databases but also integrated through data pipelines and robotic automation.[6] Using the perspective of accelerated and integrated research tasks one can in fact measure the acceleration of materials science through the MAP paradigm. Early demonstrations have in fact shown accelerations[4] of up to 20x but even greater accelerations should become available in the near future.

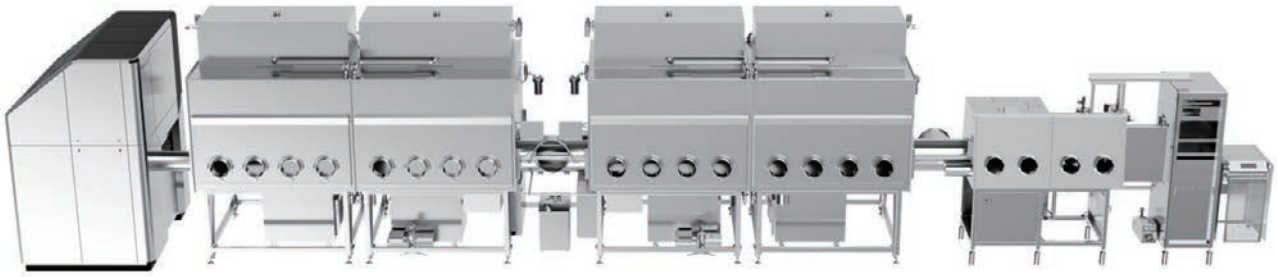

Figure 1 Rendering of the platform for accelerated electrochemical energy storage research (PLACES/R) that houses (from left to right) a near ambient pressure X-ray photoelectron spectrometer (NAP-XPS), high-throughput spectrometers and electrolyte formulation robots (left glove box), several scanning droplet cells and a coin cell assembly robot (right glovebox) as well as a sputtering system (right hand side).

Building a platform

In the following I will briefly describe an example set of measurements that highlight how the paradigm of a materials acceleration platform can be implemented. A platform is more than the sum of its parts as the overall added value is being created in the integration of its modules. Alone each setup and method can be accelerated but it is the integration that makes the difference over conventional high-throughput materials research.

Automation framework

The first and foremost important tool to build a platform that can acquire data on various of materials on different carriers using a multitude of techniques is the automation framework.[7] Given the challenge of building a laboratory[6] that utilizes instruments from a variety of vendors my current team, my coworkers from JCAP and I developed the hierarchical experimental laboratory automation and orchestration framework (HELAO). For this software we have written drivers for each and every device in our laboratory that expose them through a REST API - essentially a web server to which commands can be send. The driver functions are relatively low level i.e. turning a motor by 12 revolutions at 5 revolutions/second. More complex features are grouped into something we call action servers i.e. moving a probe by 5 mm in x-direction and 2 mm in y-direction. A sequence of actions or sequence of events makes up an experiment. A list of experiments makes up a campaign or session. Because the communication with actions and drivers can be achieved through small JSON files (essentially nested dictionaries containing instructions) an experimental session becomes programmable and interchangeable[17] between instruments (devices make up instruments).

Data management

Having all data acquisition and reporting done through code also enables fine grained data management that also entails all details of how data was acquired and processed. Any downstream processing,[18],[19] if automated, can also be integrated and be used to expand the capabilities of autonomous workflows. Currently we have drivers for stages, robots, I/O boards, potentiostats and spectrometers including even NMR. We can thus build complex workflows.

Instruments

Second are the instruments themselves. In electrochemical energy storage research there are a lot of pertinent techniques, we do however currently focus on Raman and FTIR spectroscopy in a self-build integrated setup called HITS (High-throughput spectrometer), four scanning droplet cells to perform millimeter scale high-throughput half-cell battery research (MISCHBARES), a setup for Autonomous Synthesis and Analysis of Battery electrolytes (ASAB), an automatic battery assembly robot (AutoBASS),[20] and various auxiliary and supporting techniques like high-throughput XRF and near ambient pressure XPS.

Examples

Due to the modularity of our platform,[6] there is not a single common or even "standard" workflow but several emblematic "workflow paths" through which insights can be generated. The earliest example in our laboratory was in fact the corrosion of copper and subsequent analysis using Raman and FTIR as offered through our in-house build high-throughput spectrometer (HITS) that has two Raman probes (green and red lasers) and a FTIR probe from OEM manufacturers.[21] A great benefit of high-throughput Raman spectroscopy is, that it is a relatively fast hyperspectral mapping technique that cannot just be used to fingerprint a crystal structure, but it also bears the possibility to pinpoint the location of a measurement area with great accuracy. Figure 2 shows an emblematic mapping of a materials library where the false color spots demarcate areas at which electrochemical experiments were performed. Further correlation between the Raman signals and the electrochemical protocol employed can unravel corrosion behavior. Here, we used a simple copper foil, but the possibilities are virtually unlimited in terms of materials composition through combinatorial synthesis techniques such as reactive magnetron sputtering or coating of powders.

Coating of powders is however a tedious process that requires manual finetuning of process parameters. We have however recently employed screen printing of electrodes to manufacture materials libraries for use in the scanning droplet cell (SDC). These libraries offer the benefit of being rapidly deposited and then analyzed by various subsequent methods such as X-ray fluorescence (XRF), SDC and HITS prior and post to SDC. In Figure 3 a XRF intensity map over such a materials library containing 121 Lithium iron phosphate, a common cathode material in batteries, measurement areas are shown. These measurement areas can now be analyzed using all the available techniques in our lab and be also used in full cell setups using larger area coatings (different screen-printing mask) in the AutoBASS[20] setup. The AutoBASS setup is shown in Figure 4. Here, a single battery can be assembled by a robot in under 3 minutes.

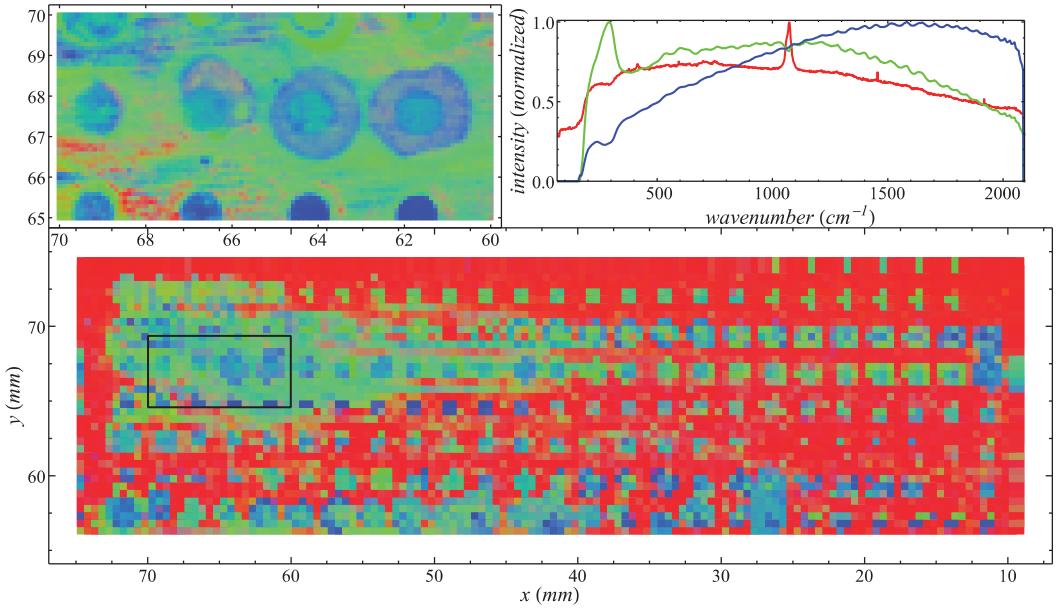

Figure 2 False color mappings using Raman spectroscopy and non-negative matrix factorization to create maps of three different phases corresponding to a background of metallic copper, and two corrosion phases. The top left image shows a zoomed in region, the top right shows the deconvoluted base spectra and the bottom part of the figure shows a large area overview of the materials library. The black box marks the area in which a high-resolution mapping was performed. The corrosion products were produced using scanning droplet cell electrochemistry.

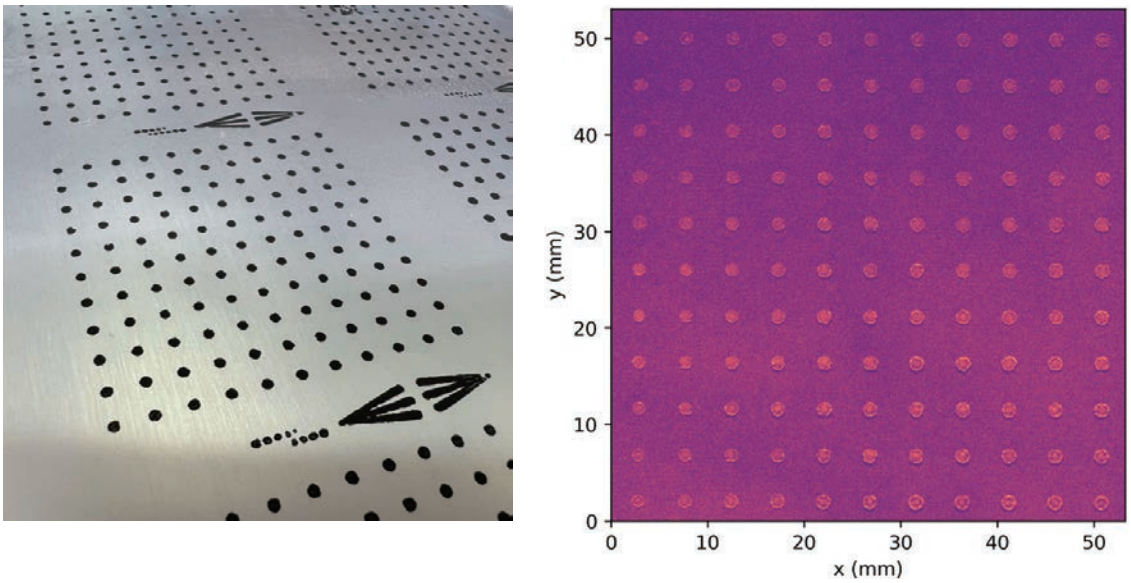

Figure 3 Left: Photograph of a screen printed materials library of Lithium iron phosphate (LFP) after drying in ambient air.
Right: X-ray fluorescence mapping of a materials library coated through screen printing after drying. Brighter spots mark the areas where LFP was deposited through the screen printing mesh. The slight gradient from the top left to the bottom right is intended as the mask contained different effective mesh sizes to vary LFP loading over the materials library. The XRF measurements were performed using a HORIBA XGT-9000 with a polycapillary probe. Using the scanning droplet cell in a similar way as shown in Figure 2 it is possible to assess real battery materials without measurement area crosstalk.

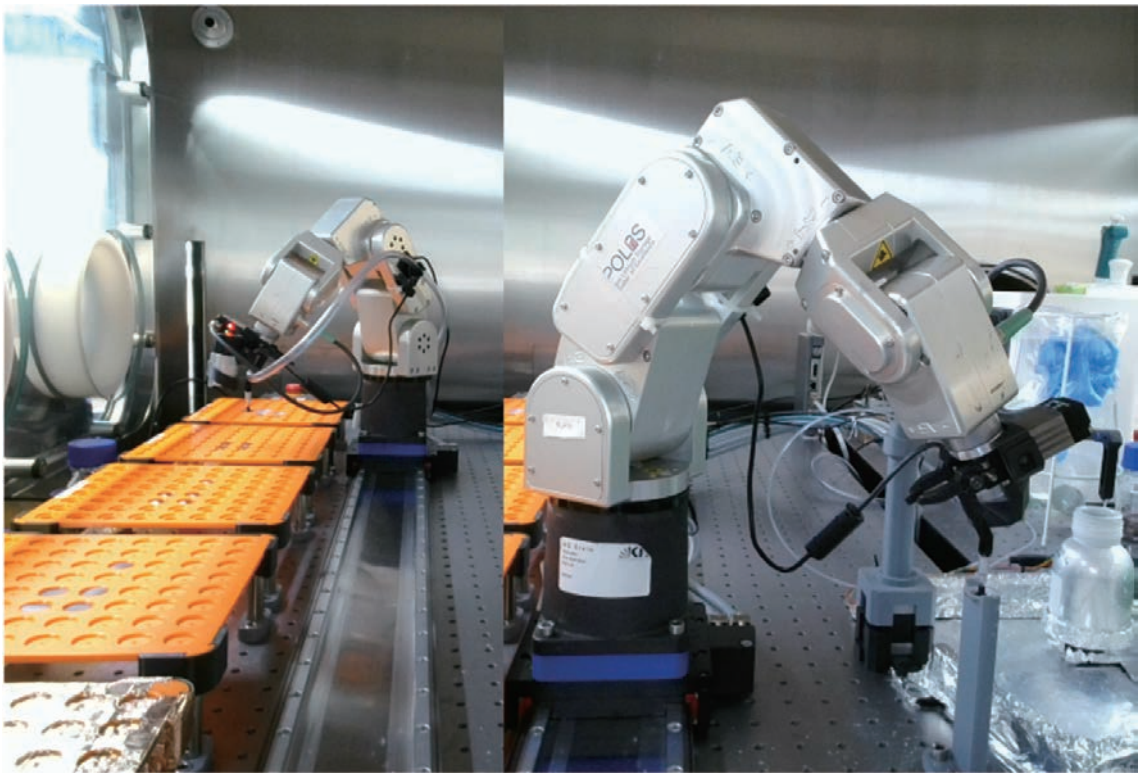

Figure 4 Photograph of the pick and placing actions of AutoBASS, a robot for the automatic assembly of coin cell batteries. On the left the robot is shown picking up cell components that are placed onto an assembly post on the right. On the assembly post additional steps such as electrolyte filling are performed. The entire process is housed inside a nitrogen filled glovebox to avoid moisture and oxygen impurities.

Conclusion

Using additional tools such as ASAB and the XPS we can thus cover the entire materials research value chain and integrate insights from all steps of battery research and even catalysis. Being able to acquire data from bulk, interface, and interphase processes in combination with system and long-term effects opens up new and interesting research directions. Through fine grained data management and automation control we also have the unique opportunity to deploy A.I. guidance of our robotic systems. With novel orchestration paradigms and software such as FINALES we can even integrate external data sources and measurement requests to build workflows across laboratories and modalities to create the lab of the future.

Acknowledgements

I thank my entire team that made this platform possible. For this technical report I'd especially thank Jackson Flowers, Fuzhan Rahmanian, Leah Nuss, Stefan Fuchs and Bojing Zhang.

References

[1] J. Amici *u. a.*, „A Roadmap for Transforming Research to Invent the Batteries of the Future Designed within the European Large Scale Research Initiative BATTERY 2030+“, Advanced Energy Materials, S. 2102785, 2022.

[2] M. Fichtner *u. a.*, „Rechargeable Batteries of the Future—The State of the Art from a BATTERY 2030+ Perspective“, *Advanced Energy Materials*, S. 2102904, 2021.

[3] A. Benayad *u. a.*, „High-throughput experimentation and computational freeway lanes for accelerated battery electrolyte and interface development research“, *Advanced Energy Materials*, Bd. 12, Nr. 17, S. 2102678, 2022.

[4] B. Rohr *u. a.*, „Benchmarking the Acceleration of Materials Discovery by Sequential Learning“, *chemrxiv*, S. 10-26434, 2019.

[5] L. Zhou *u. a.*, „Combinatorial screening yields discovery of 29 metal oxide photoanodes for solar fuel generation“, *Journal of Materials Chemistry A*, Bd. 8, Nr. 8, S. 4239-4243, 2020.

[6] H. S. Stein *u. a.*, „From materials discovery to system optimization by integrating combinatorial electrochemistry and data science“, *Current Opinion in Electrochemistry*, S. 101053, 2022.

[7] F. Rahmanian *u. a.*, „Enabling Modular Autonomous Feedback-Loops in Materials Science through Hierarchical Experimental Laboratory Automation and Orchestration“, *Advanced Materials Interfaces*, Bd. 9, Nr. 8, S. 2101987, 2022.

[8] H. Koinuma und I. Takeuchi, „Combinatorial solid-state chemistry of inorganic materials“, *Nature Mater*, Bd. 3, Nr. 7, Art. Nr. 7, Juli 2004, doi: 10.1038/nmat1157.

[9] A. Boettcher, G. Haase, und R. Thun, „Strukturuntersuchung von Mehrstoffsystemen durch kinematische Elektronenbeugung“, *Z. Metallkde.*, Bd. 46, Nr. 5, S. 386-400, 1955.

[10] J. Li *u. a.*, „Combinatorial screening of Pd-based quaternary electrocatalysts for oxygen reduction reaction in alkaline media“, *Journal of Materials Chemistry A*, Bd. 5, S. 67-72, 2016.

[11] A. Ludwig, „Discovery of new materials using combinatorial synthesis and high-throughput characterization of thin-film materials libraries combined with computational methods“, *npj Computational Materials*, Bd. 5, Nr. 1, Dez. 2019, doi: 10.1038/s41524-019-0205-0.

[12] H. S. Stein und J. M. Gregoire, „Progress and prospects for accelerating materials science with automated and autonomous workflows“, *Chemical Science*, Nr. 10.1039/C9SC03766G, 2019.

[13] L. Banko und A. Ludwig, „Fast-Track to Research Data Management in Experimental Material Science-Setting the Ground for Research Group Level Materials Digitalization“, *ACS Comb. Sci.*, Bd. 22, Nr. 8, S. 401-409, Aug. 2020, doi: 10.1021/acscombsci.0c00057.

[14] M. L. Green *u. a.*, „Fulfilling the promise of the materials genome initiative with high-throughput experimental methodologies“, *Applied Physics Reviews*, Bd. 4, Nr. 1, S. 11105, 2017, doi: 10.1063/1.4977487.

[15] A. Jain *u. a.*, „Commentary: The materials project: A materials genome approach to accelerating materials innovation“, *APL Materials*, Bd. 1, S. 011002, 2013.

[16] M. M. Flores-Leonar *u. a.*, „Materials Acceleration Platforms: On the way to autonomous experimentation“, *Current Opinion in Green and Sustainable Chemistry*, Bd. 25, S. 100370, Okt. 2020, doi: 10.1016/j.cogsc.2020.100370.

[17] M. D. Wilkinson *u. a.*, „The FAIR Guiding Principles for scientific data management and stewardship“, *Scientific Data*, Bd. 3, S. 160018-9, März 2016, doi: 10.1038/sdata.2016.18.

[18] F. Rahmanian *u. a.*, „Conductivity experiments for electrolyte formulations and their automated analysis“, *Sci Data*, Bd. 10, Nr. 1, S. 43, Jan. 2023, doi: 10.1038/s41597-023-01936-3.

[19] F. Rahmanian *u. a.*, „One-Shot Active Learning for Globally Optimal Battery Electrolyte Conductivity“, *Batteries & Supercaps*, Bd. 5, Nr. 10, S. 1-9, 2022, doi: 10.1002/batt.202200228.

[20] B. Zhang, L. Merker, A. Sanin, und H. S. Stein, „Robotic cell assembly to accelerate battery research“, *Digital Discovery*, Bd. 1, Nr. 6, S. 755-762, Dez. 2022, doi: 10.1039/D2DD00046F.

[21] S. Daboss, F. Rahmanian, H. S. Stein, und C. Kranz, „The potential of scanning electrochemical probe microscopy and scanning droplet cells in battery research“, *Electrochemical Science Advances*, S. e2100122, 2021.

Dr. Helge Sören STEIN
ヘルゲ・ゼーレン・シュタイン

Tenure Track Professor,
Institute for Physical Chemistry (IPC) & Helmholtz Institute Ulm (HIU),
Karlsruhe Institute of Technology (KIT)

エネルギーとモビリティの変革に向けた HORIBAモビリティ・コネクティビティ研究所の取組み

HORIBA Institute for Mobility and Connectivity[2] for Contributing to the Transformation of Energy and Mobility Systems

木下 明生
KINOSHITA Akio

カリフォルニア大学アーバイン校に，HORIBAモビリティ・コネクティビティ研究所がHORIBAグループの寄付により2021年7月に開設された。この研究所は，今後相互に深く関連していくエネルギーとモビリティの社会インフラストラクチャーを統合的に捉え直すことにより，新たな視点からの研究を推進することを目的としたもので，最近の世界的なエネルギー問題への注目の中，既に具体的な取組みが活発に進められている。本稿ではこの研究所の構想や研究事例について紹介する。

Figure 1 HIMaC[2] Opening Ceremony. (Oct. 11, 2022)
(from left to right) HIMaC[2] Inaugural Director Vojislav Stamenkovic, HORIBA, Ltd. Chairman & Group CEO Atsushi Horiba, UCI Chancellor Howard Gillman, HORIBA Ltd. Executive Corporate Officer Jai Hakhu, UCI Dean of Engineering Magnus Egerstedt.

はじめに　ーエネルギーとモビリティの動向ー

現在，全世界で地球温暖化への対応が喫緊の課題となっており，COP26時点ではG20を含む150か国以上の国でカーボンニュートラルの目標が期限を設けて宣言されている。これを受けて再生可能エネルギーへのシフトが大きな動きとなっており，加えて国家としてのセキュリティの観点からもエネルギー調達が大きな注目点となっている。一方，エネルギー消費の面ではモビリティが主要な一角を占めているが，電動車両の急激な拡大が進みつつあり，特に中国，欧州で顕著である。
その自動車においては，さらに自動運転化，コネクテッド化が進んでおり，それらの技術によって車群が協調的に走行することで全体としての省エネルギーを実現する試みなども始まっている。このような状況はエネルギー，モビリティおよび情報通信の三大インフラストラクチャーが統合されていく過程を示すものと見ることができる。これらの構造的な変化がHORIBAモビリティ・コネクティビティ研究所（HORIBA Institute for Mobility and Connectivity[2]，以下HIMaC[2]）の設立の基本的背景にある。

HIMaC^{2}で目指す研究　ー背景とコンセプトー

現在の社会の基盤となっているエネルギー供給の仕組みは，電力を例にとると，発電＞送電＞配電というように，少数の発電所で集中的に作った電気を広く安定供給する考え方が基本となっている。中央から全体への一方通行的ないわゆる系統電力の構造であるが，現在これに対し，再生可能エネルギーの利用拡大，エネルギーの地産地消の要請が急速に高まっている。これを背景に太陽電池や中間のエネルギー貯蔵手段である二次電池といった要素が加わるようになり，これまで一方通行的に安定に制御されていた電力ネットワークが，より分散型でインタラクティブな形態に変化しつつある。

よく知られているように再生可能エネルギーは太陽光，風力，波力など，どれも変動が大変大きく予測しにくいため，安定供給の観点からは大きな課題である。これらをどのように配置し，どう動作させるのが望ましいのか，全体のシステムの安定的運用をどのように保証していくのかは必ずしも明確ではない。発電や蓄電能力の配置や充放電スケジューリングに加えてシステムの安定保証，不測の変動に対するレジリエンス，維持更新を含めた総コストといった観点も含め，ネットワークをどう設計し，運用すべきかは十分検討すべき問題である。

他方，自動車について見ると，これまで長年そのエネルギーのほとんどを，限られた産油国に偏在する原油を精製したガソリンや軽油から得ていたが，百年に一度と言われるような変革期に入り，電動化が大きく拡大しつつある。将来の自動車は，電気エネルギーを貯蔵し電力ネットワークとの間で充放電することで相互作用する，ネットワークに統合された一部としても見ていく必要があるであろう。加えて水素がエネルギー媒体として重要な役割を担うようになり，水電解を介して電気エネルギーから変換され，エネルギー貯蔵や移動のための媒体として利用されたり，車載燃料電池により直接車両の移動のためのエネルギーとして利用される。

このような観点から，自動車を含んだエネルギーネットワークを図示してみると**Figure 2**のようになる。まず一次エネルギーとしては多様な再生可能エネルギーが提供される。また自動車には大容量蓄電池が搭載され，ハイブリッドやバッテリーEVがネットワーク側とエネルギーを直接授受することになる。このような“21世紀型”のエネルギーネットワークでは，分散型，双方向型を前提としたエネルギーマネジメント，燃焼反応に加えて電気化学反応によるエネルギー変換といった新たな技術を確立する必要がある。要素技術としてのエネルギー変換の効率化などもチャレンジすべき研究課題であるが，それにとどまらず，系全体としての動的な振る舞いの理解や制御も未解明の領域である。このように課題が学際的に広範囲にわたること，個々の要素のみならずシステムまでの多階層となることなどから，本質を理解し次世代のインフラストラクチャーの方向を検討していくためには，領域横断の観点でのアプローチが不可欠である。こうした考え方に基づき，この問題に取り組む研究所をカリフォルニア大学に新たに設立することとなった。なお，HIMaC^{2}の末尾にある“2”は，エネルギーそれ自体と情報コミュニケーションの二重の意味での接続が重要であることを意味している。

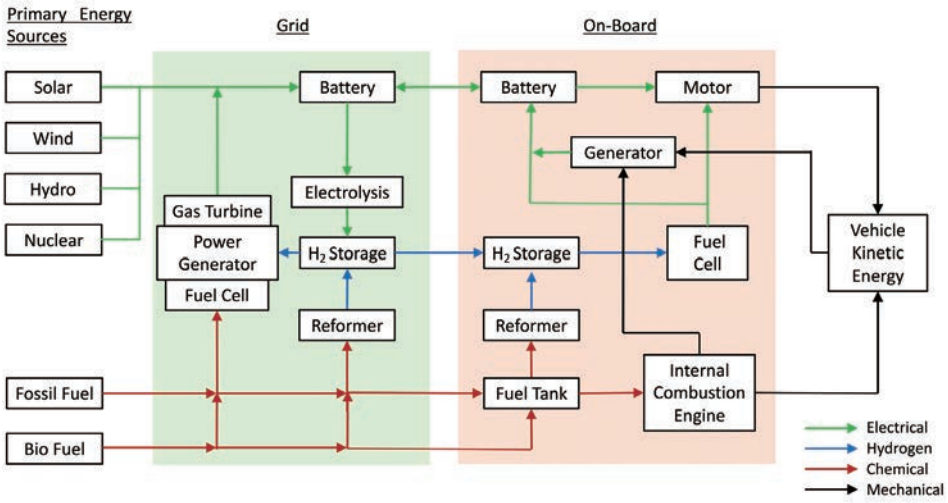

Figure 2　A Comprehensive View of Energy Network Integrated with Vehicles.

HIMaC^{2}の研究室構成

カリフォルニア大学アーバイン校(University of California, Irvine, 以下UCI)ではエネルギー分野の研究をAdvanced Power and Energy Program (以下APEP)が主導してきた実績があり, マスキー法が導入された1970年に早くも燃焼研究を立ち上げたり, 電力グリッドの研究, 水素エネルギーの利用技術など多様な研究を先駆けて推進してきた。その長年の実績の上に, 前述のようなエネルギーネットワークに対する新たな問題意識によりHIMaC^{2}が設立され, 電気化学系の材料科学分野で世界をリードする業績をあげてきたVojislav Stamenkovic教授が初代所長として着任している。
HIMaC^{2}は前章で述べた課題認識を反映し, 以下の四研究室構成となっている。

・Vehicle Evolution Laboratory (VEL) : 車載の電動車両要素やシステム技術の評価, 研究を行う。そのためHORIBAの計測システムを中心にダイナモメータ, 二次電池評価用環境チャンバーなどが設けられている(**Figure 3**)。

・Grid Evolution Laboratory (GEL) : Grid to Vehicle, Vehicle to Gridを含む電力ネットワークのダイナミクスなどグリッド階層の研究を行う。多様な電力系での動的現象を再現可能なグリッドのシミュレータを備えている。

・Connected and Autonomous Mobility Laboratory (CAML) : 車両が自動運転化されることも包含し, Vehicle to Vehicle, Vehicle to Infrastructureのコミュニケーションによる個々の車両, 交通流, エネルギー効率などへの影響, AIに基づく制御など全く新しいアプローチでの研究を行う。HORIBA MIRA社の開発による協調走行制御のシミュレーションプラットフォームを導入している。

・Analytic Laboratory (AL) : 以上のシステム, グリッドレベルでの現象の基礎となる電気化学の先端材料の分析, 研究を行うため, 以下の最新のHORIBA分析機器を設置している。
  ・LabRAM HR Evolution Nano : AFMラマン分光装置
  ・XGT-9000 : 微小部X線分析装置
  ・nanoPartica SZ-100V2 : ナノ粒子解析装置
  ・GD-Profiler2 : グロー放電発光表面分析装置

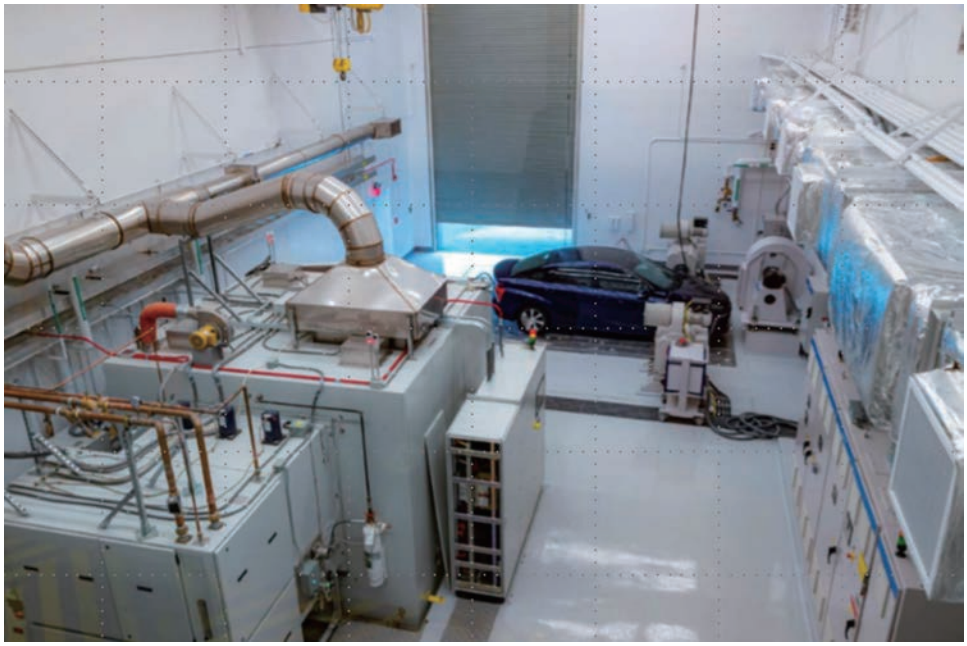

Figure 3 Vehicle Evolution Laboratory.

今後のエネルギー分野の課題は材料物性から装置，システム，さらにはグリッド全体まで深い多層構造にわたっていることから，各研究室はそれぞれの階層に対応した構成となっている。これらをさらに有機的に組み合わせることで，これまで必ずしも十分ではなかった階層を縦断する観点での新たな課題や現象に取り組むことを可能としている。さらにUCIではキャンパスのエネルギーネットワーク自体を独立したマイクログリッドとし，実際にグリッドレベルでの実験を行うこともできる。このマイクログリッドには太陽電池や水素関係の設備なども接続され，極めて広範囲で総合的な検討に対応可能な環境を備えている。以上のユニークな研究機能群と構成により，大きな研究発展の可能性を有している。

HIMaC^{2}の研究プロジェクト事例

HIMaC^{2}はまだオープニング後間もない立ち上げ期にあるが，既に様々な研究プロジェクトが開始されており，主要な政府機関からの受託研究も多く含まれている。以下に本稿執筆時点で進行中の主なプロジェクトを示す。

1. Smartville：カリフォルニア州立大学サンディエゴ校からのスピンオフ企業との使用済み電池の活用技術の研究
2. Microgrid-in-a-Meter：太陽電池を含む孤立グリッド系について，停電時などの動的事象への対応技術の研究
3. HD-ZEV Charging/Fueling Codes and Standards：電気，水素を用いるヘビーデューティ車両のエネルギー充填手段に関する標準化のための基礎研究
4. Aqueous, Air breathing long – duration energy system：非Liイオン型の新方式電池の研究
5. Smart Cities and Connected and Autonomous Vehicles：自動運転車両を視野に，AIベースの交通制御インフラ協調によるエネルギー効率向上に向けた研究
6. M^{2}CFT：Million Mile Fuel Cell Truckコンソーシアムの一環となる負極の触媒材料の研究
7. Break Dust Project：ブレーキ及びタイヤダストの影響に関する評価研究

以上の多くは公的機関の支援を受けており，例えば3はカリフォルニア州大気資源局，4，5は連邦エネルギー省の公的資金を受けている。また他大学や研究機関との共同プロジェクトも多く進められている。

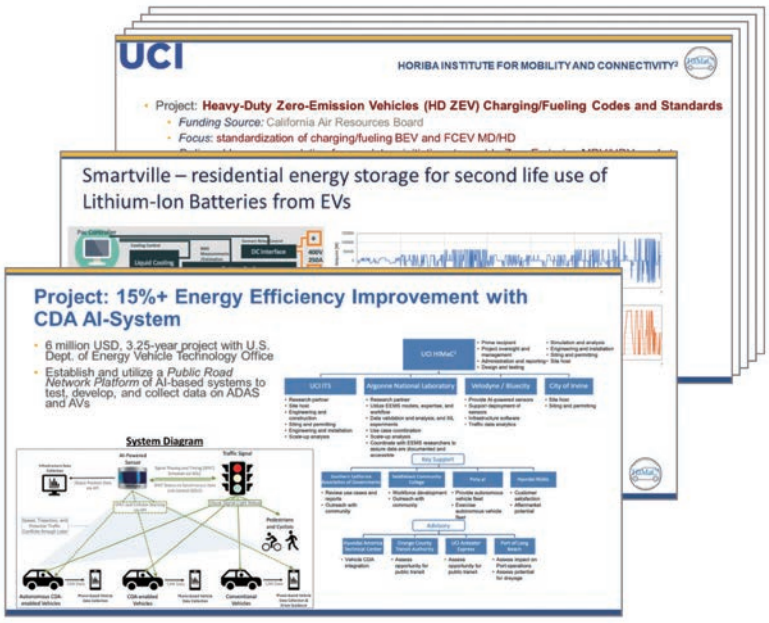

Figure 4 Examples of Research Projects at HIMaC^2.

おわりに

以上述べてきたように，HORIBAモビリティ・コネクティビティ研究所は，エネルギーとモビリティのネットワークが大きく変革し始める，時宜を得たタイミングでその活動を開始した。今後社会全体が直面する多様な問題に対し，今までにない研究に踏み込む最前線の領域で，既にリーダーシップを発揮しつつある。エネルギーやモビリティの産業を横断し，行政やアカデミアなど多様なステークホルダーとともに，具体的な研究プロジェクトを通して将来の課題解決に資する新たな知見を開拓することが期待される。

なお，この研究所の設立準備にあたっては，UCIのAdvanced Power and Energy Programの創始者であり，永年米国のエネルギー分野の研究を主導してきたScott Samuelsen教授に多くを負っている。構想検討段階からのSamuelsen教授の想像力あふれるリーダーシップに謝意を表し，本稿の結言とする。

木下 明生

KINOSHITA Akio

株式会社堀場製作所
フェロー
博士（工学）
Fellow
HORIBA, Ltd.
Ph.D.

全固体電池の研究開発に資する分析技術

Analytical Techniques Contributing to the Research and Development of All-Solid-State Batteries

坪田 隆之
TSUBOTA Takayuki
株式会社コベルコ科研
技術本部 EV・電池ソリューションセンター
EV・電池解析技術室 室長
博士(理学)

Manager
EV Battery Analysis & Evaluation section
EV Battery Solution Center
Kobelco Research Institute, inc.
Doctor of Science

走行中CO_2削減のために，自動車のEVシフトが世界的に加速しており，二次電池の需要が高まっている。高いリチウムイオン伝導を発現する固体電解質を用いた全固体電池の研究開発が進められており，その開発動向と課題について概説する。全固体電池の実用化には大気非暴露に対応した分析技術が必須であり，固体電解質の化学状態・構造解析や，全固体電池における固体粒子間の接合界面の観察技術や電子導電パス解析など，総合的な分析評価・解析技術が重要となる。

The worldwide shift to EVs in automobiles is accelerating in order to reduce CO_2 during driving, and the demand for rechargeable batteries is increasing. Research and development of all-solid-state batteries using solid electrolytes that exhibit high Li ion conduction is underway, and this paper outlines the development trends and challenges. Analytical technology corresponding to non-atmospheric exposure is essential for the practical application of all-solid-state batteries. Comprehensive analytical evaluation and analysis techniques are important, including chemical state and structural analysis of solid electrolytes, observation techniques for the junction interface between solid particles in all-solid-state batteries, and electronic conductivity path analysis.

はじめに

2015年に開催されたCOP21(国連気候変動枠組み条約第21回締約国会議)にてパリ協定が採択されて以降，世界は脱炭素社会の実現に向けて大きく舵を切った。我が国においては，2020年10月に「2050年カーボンニュートラル，脱炭素社会の実現」が宣言された。カーボンニュートラルとは，温室効果ガスの排出量と吸収量を均衡させ，実質ゼロとすることを意味している。同年12月には「2050年カーボンニュートラルに伴うグリーン成長戦略」が策定されている。

エネルギーの脱炭素化には電化・水素化・カーボンリサイクル燃料の活用などがあるが，電化の推進には蓄電池が不可欠である。自動車産業においては，欧州連合(EU)では，2035年にガソリン車などの内燃機関車の販売を事実上禁止することで合意した。我が国においても2021年に「2035年までに乗用車新車販売で電動車100%を実現する」方針が示された。ここでの電動車とは電気自動車(EV)ハイブリッド車(HV)，プラグインハイブリッド車(PHEV)，燃料電池車(FCV)である。こうした脱炭素を背景に，自動車産業においてはEVシフトが加速している。

EVには液系リチウムイオン二次電池が主に使用されているが，電池性能が航続距離や加速など車両性能に与える影響が大きいため，高容量化や高入出力化，耐久性向上のために正負極の活物質やセパレータ，電解液などの材料開発が進められている。しかしながら，液系リチウムイオン二次電池のエネルギー密度は250 Wh/kg程度が限界と言われており，さらなる高エネルギー密度となる新型電池が求められている。ポストリチウムイオン電池としてナトリウムイオン電池や，カルシウムイオン電池などの多価カチオン電池などが検討されている。

近年，高リチウムイオン伝導体である硫化物系固体電解質の開発が盛んに進められており，液系リチウムイオン電池を凌ぐエネルギー密度が期待できる新型電池として全固体リチウムイオン電池が注目され，実用化に向けた研究開発が進められている。

コベルコ科研では，リチウムイオン二次電池の試作・内部

抵抗解析技術，電池解体・機器分析による部材の劣化解析技術，コンピューターシミュレーション技術，安全性評価技術を保有しており，二次電池の総合評価・分析解析技術を構築している。全固体電池においても固体電解質の合成から電池試作・評価技術を有しており，全固体電池の研究開発を支援している。

本稿では，全固体電池の研究開発に必要な分析技術について，株式会社堀場製作所との連携事例を中心に報告する。

全固体リチウムイオン電池の特徴と課題

全固体リチウムイオン電池は，電解液を高イオン伝導体である固体電解質に置き換え，正極合材層，固体電解質層，負極合材層がすべて固体で構成されていることが特徴である。固体電解質は主に$Li_7P_3S_{11}$，$Li_{10}GeP_2S_{12}$(LGPS)に代表される硫化物系[1-7]と，$Li_7La_3Zr_2O_{12}$(LLZ)に代表される酸化物系[8]に大別される。電解液と比較して高電位での電気化学的安定性を有している固体電解質を選択することで，液系電池では適用が難しかった$LiNi_{0.5}Mn_{1.5}O_4$などの5V級活物質を使用することができ，エネルギー密度を上げることができる。

また，良好な入出力特性も期待されている。電解液ではリチウムイオンに加えてアニオンも伝導に寄与するため輸率が低くなるが，固体電解質のアニオンは骨格を形成しているのみで伝導には寄与しない。つまり固体電解質はリチウムイオンのシングル伝導体であり輸率は1となるため高いイオン伝導率となる。

硫化物ガラス電解質の$Li_7P_3S_{11}$[1,2]や，結晶性電解質の$Li_{10}GeP_2S_{12}$(LGPS)[3-5]，アルジェロダイト型Li_6PS_5X(X＝Cl, Br, I)[6,7]に代表される硫化物系固体電解質はイオン伝導性に優れ，有機電解液を超える10^{-2} S/cmオーダーのイオン伝導率を示す固体電解質も報告されている。当社にて合成した固体電解質のイオン伝導率を**Figure 1 (a)**に示す[9]。結晶性電解質を代表してアルジェロダイト型硫化物系固体電解質のLi_6PS_5Clの結晶構造を**Figure 1 (b)**に示す。塩化物イオンは面心立方格子(4a, 4c)を形成し，リチウムイオンは四面体位置にランダムに分布している。Pは四面体サイト(4b)を占有し，SはPS_4^{3-}四面体ユニットを形成した構造となっている。

全固体リチウムイオン電池は高エネルギー密度化や高入出特性が期待される一方で，実用化には材料や製造プロセスに課題があり，その観点から研究開発が進められている。全固体電池は構成要素がすべて固体であるが故に，固体電解質と活物質界面との良好な接合界面を形成し維持することが求められる。電池の成型時の変形や，充放電に伴う活物質の膨張収縮に追随することが重要であり，柔軟な変形能力を持つ硫化物系固体電解質を用いた全固体電池の開発が車載用途を中心に進められている。硫化物系固体電解質は反応性が高く，大気中の水分により容易に加水分解し硫化水素が発生するため，厳密に水分管理された低露点Ar雰囲気グローブボックス中にて取扱う必要がある[10]。各種分析においてもサンプリングから分析機器までの輸送，測定まで一貫して大気非暴露の取扱いが必須となる。全固体電池の研究開発に必要な分析技術の一覧を**Table 1**に示す。

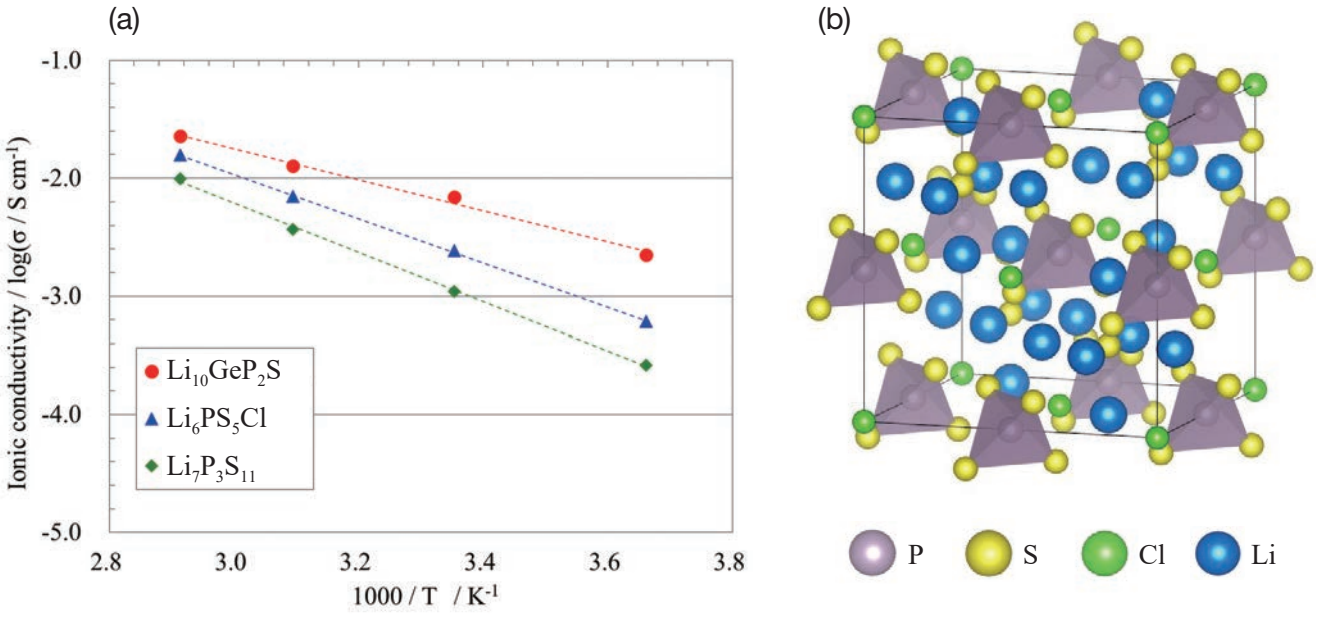

Figure 1 (a) Ion conductivity of sulfide-based solid electrolytes. (b) Crystal structure of Li_6PS_5Cl solid electrolytes.

Table 1 Analysis technology for secondary batteries.

Development issues		Focus points	Analytical methods
Optimization of solid-state electrolytes	Improvement of ionic conductivity	・Crystal structure ・Chemical state	・XRD, in-situ XRD ・Raman, in-situ Raman
	Improvement of stability	・Atmospheric stability	・Exposure test + Gas analysis
Optimization of the coating layer	Improvement of coverage Homogenization of the coating	・Coverage, uniformity	・XPS, TOF-SIMS
Optimization of electrode and cell structures	Improvement of the dispersibility of materials	・Dispersion state, unevenness	・SEM + image analysis
	Improvement of the flowability of materials	・Flowability, adhesion	・Flowability test
	Understanding of material and electrode strengths	・Crushing strength, hardness ・Modulus of elasticity	・Crushing test, Nanoindentation ・SPM, Nanoindentation
	Improvement of the adhesion of each layer	・Interface adhesion	・SAICAS, peel test
	Optimization of Li ion and electron paths	・Electrode structure observation ・Effective conductivity analysis	・3D-FIB-SEM ・Image analysis ・Symmetric cells + resistance analysis
Battery characteristics Optimization of battery characteristic control and management	Understanding of battery characteristics	・Cycle characteristics, temperature characteristics	・Creating prototype cells + charge/discharge test
	Clarification of the degradation mechanism	・Composition distribution in the electrode ・Chemical state distribution in the electrode ・Reaction phase at the interface between solid electrolyte and active material ・Valence and local structure of active material ・Morphological changes during charge/discharge	・GD-OES ・Diagonal cutting XPS ・Cryo biaxial Cs-STEM ・XAFS/Synchrotron radiation ・In-situ SEM
	Understanding of thermal properties	・Thermal conductivity ・Specific heat	・Hot disk method, heat transfer analysis ・DSC, external heating evaluation of cells
	Understanding of safety	・Reaction heat evaluation	・DSC ・Safety test

固体電解質合成におけるラマン分光法の活用

固体電解質の合成は，固相プロセスと液相プロセスに大別される。固相プロセスに代表されるメカニカルアロイング（MA）は，機械的にエネルギーを加えることにより化学反応を促進させ，非晶質や熱力学的準安定相の固体電解質を得る手法である。一方，液相プロセスは，出発原料を有機溶媒に浸漬し，加振や攪拌により化学反応を促進した後に，加熱により有機溶媒を揮発させ固体電解質を得る手法である。今回は固相プロセスを採用し，車載用全固体電池への適用が検討されているアルジェロダイト型硫化物系固体電解質Li_6PS_5Clの合成を行った。露点－70℃以下のAr雰囲気グローブボックス中で出発原料をLi_2S：P_2S_5：LiCl＝0.625：0.125：0.25 at%のモル比にて混合した後，遊星型ボールミルを用いたMAプロセスにより前駆体を調整した。MA時間は5 h，13 h，20 h，30 hとした。

MAプロセス中の化学結合状態の把握は，化学反応の進行状況を知る上で極めて重要である。X線回折（XRD：X-ray Diffraction）による結晶構造解析結果を**Figure 2(a)**に示す。前駆体合成が進むほどLi_2S，LiClの原料由来のピークが減少するが，アモルファス化も進行するためXRDでの状態帰属が困難となる。つまり結晶性評価が得意なXRDでは化学反応の進行状況が判断できず，MAプロセス後の熱処理により結晶化した後で，XRDやイオン伝導率測定により評価することとなる。その後にMA時の化学反応不足が判明した場合には，大きくやり直しの工数が発生し，製造現場においては生産性を低下させることとなる。そこで当社と堀場製作所は，MA後の固体電解質についてインラインで評価可能な小型ラマン分光装置の検討を進めている。ラマン分光法はラマン散乱光を用いて物質の評価を行う振動分光法である。散乱光には入射光と同波長のレイリー散乱光に加え，入射光と物質の相互作用により入射光と異なる波長のラマン散乱光が含まれる。波長差は対象物質が持つ分子振動のエネルギー分に相当し，ピーク位置からは化学結合状態，スペクトル形状から分子構造情報や結晶構造，ピークの半値幅からは結晶性，ピーク位置のシフトから応力や歪みなどの物性情報を得ることができる。

堀場製作所製の小型レーザーラマン分光装置による結晶構造解析結果を**Figure 2(b)**に示す。レーザー波長は532 nm，レーザー出力は3 mWとした。MAにより前駆体合成が進むほど原料であるLi_2S，P_2S_5由来のピークが減少し，Li_6PS_5ClのPS_4^{3-}四面体ユニット由来のピークが出現し，シャープになっていくことが確認された。このようにラマン分光法によりMAにおける化学反応の進行状況を捉えることが可能であり，固体電解質合成における有用な分析手法である。

固体電解質の観察技術

固体電解質の結晶構造は球面収差補正機能付き走査透過型

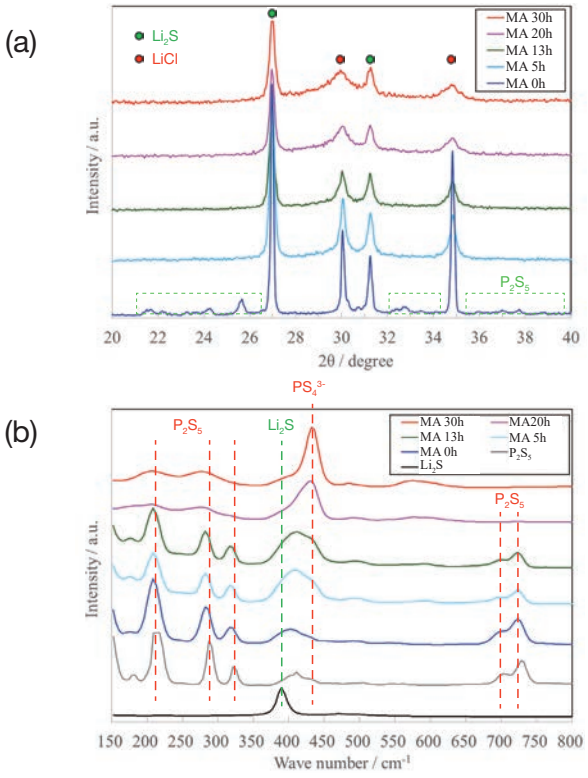

Figure 2　(a) Ion conductivity of sulfide-based solid electrolytes.
(b) Crystal structure of Li_6PS_5Cl solid electrolytes.

電子顕微鏡(Cs-STEM：Spherical aberration corrected Scanning Transmission Electron Microscope)にて観察を行う。固体電解質は水分と反応し容易に状態が変化するため，低露点Ar雰囲気グローブボックスにてサンプリングし，不活性ガス雰囲気を保持したまま収束イオンビーム加工装置(FIB: Focused Ion Beam)に挿入し，断面マイクロサンプリング法によりTEMサンプルを摘出し，FIB加工により薄片化する。酸化物系固体電解質であるLLZのCs-STEM観察結果を**Figure 3**に示す。LLZは酸化物であるが電子線のダメージに弱く，容易に変質するため，常温での観察は困難である。我々は観察中の冷却による熱ダメージの低減に加えて，二軸傾斜による晶帯軸観察が可能な大気非開放冷却二軸ホルダにより，LLZの原子コラム像の撮影に成功している。

全固体電池の電極試作と電極構造の評価技術

液系リチウムイオン電池では多孔質電極にて電解液が染み込み活物質／電解液界面が自発的に形成される。硫化物系全固体電池では固体電解質と活物質，導電助剤を予め混合し，均一分散させる必要がある。活物質の利用率の向上や高い入出力特性を得るためには，電子伝導経路，イオン伝導経路それぞれを最適化した電極構造が必要となる。そのため，電極の深さ方向の元素分析や，活物質，固体電解質，導電助剤の3次元構造の可視化や，導電性マッピングなど種々の分析を用いて総合的に評価している。

一方，電池の観点では作製方法・取り扱いの簡便さから粉体を乾式で混合しプレス・積層することで得られる小型の圧粉型全固体電池が用いられることが多い。しかしながら，電池のサイクル劣化解析や安全性評価といったより実使用に近い評価を行うためには，実機を模擬した大容量の電池が必要となる。大容量電池とするための大面積の電極を作製する手法として，液系リチウムイオン二次電池と同様のプロセスである，電極合材をスラリー化し湿式塗工する方法が挙げられる。当社では電極合材をスラリー化し，塗工，乾燥，プレスによる密度調整，積層化により，塗工型の硫化物系全固体電池の試作を行っている。$Li(Ni_{1/3}Mn_{1/3}Co_{1/3})O_2$の表面に$LiNbO_3$をコーティングした正極活物質と，合成した$Li_6PS_5Cl$固体電解質，導電助剤，バインダーの重量比を74：23：3：3 wt%となるようにバインダーと溶剤を加えて混合・スラリー化させた後，集電箔に塗工・乾燥させることで塗工型の正極を作製した。

塗工型正極の深さ方向の元素分析は，高周波グロー放電発光分析(GD-OES：Glow Discharge Optical Emission Spectroscopy)にて実施した。GD-OESは大気非暴露ユニットを取り付けた堀場製作所製のGD-Profiler2を使用した。電極の評価に用いられるSEM-EDXにおいては，軽元素であるLiの検出は困難であるが，GD-OESではLiの発光を高感度に検出することができるため分析可能である。分析エ

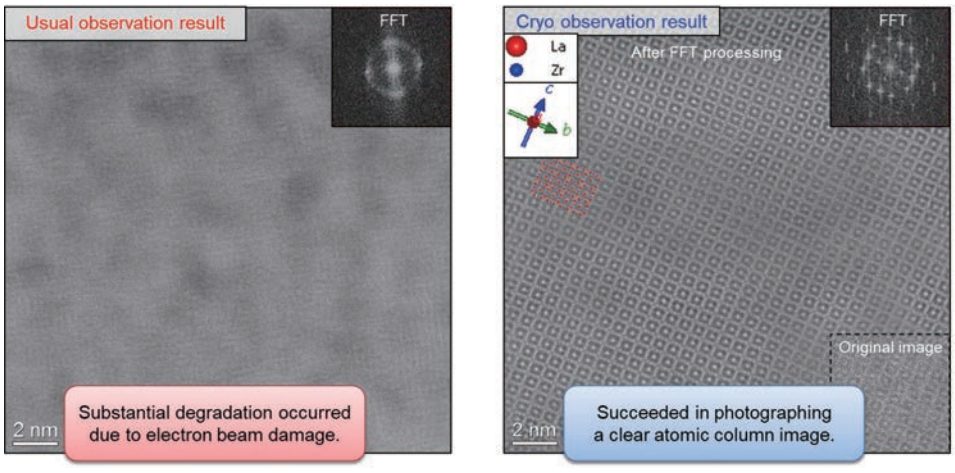

Figure 3　Cs-STEM images of $Li_7La_3Zr_2O_{12}$ solid electrolyte.

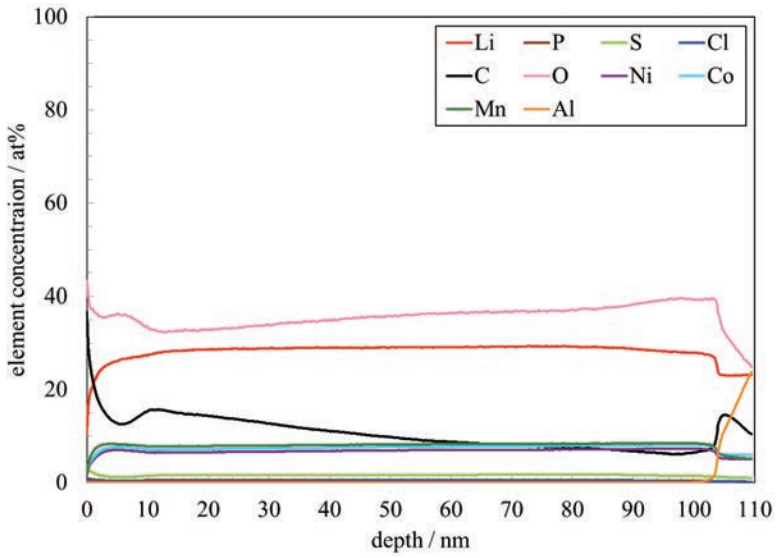

Figure 4　Depth profile analysis of cathode by GD-OES.

リアは例えばΦ4 mmなど広いこと，Arスパッタリングにより表層から100 μmの深部まで測定できるなどユニークな特徴を有しており，電極の深さ方向分析に有用な分析手法である。低露点Ar雰囲気のグローブボックス内で電極をサンプリングし，大気非暴露対応のトランスファーベッセルにて輸送し，GD-OESにセットした。塗工型正極の深さ方向の元素分析結果を**Figure 4**に示す。塗工厚みが約100 μmの電極について，表層から集電箔まで，構成元素であるLi，P，S，Cl，C，Ni，Co，Mn，Alを捉えており，活物質や固体電解質，バインダーの混合状態を評価することができる。

電極の3次元構造は，FIB-SEM（Focused Ion Beam Scanning Electron Microscopes）を用いて解析を行っている。FIBにより断面加工を行い，断面SEM像を取得する。続いて加工面をさらに削り，新たな断面SEM像を取得することを繰り返し，複数の2次元断面像から3次元構築像を取得する。さらに画像解析により各構成部材の体積比率や部材間の接触面積の評価することで構造の最適化を行っている。固体電解質は断面加工時の熱により容易に変質してしまうことから，熱影響を抑えるため冷却加工（クライオ加工）が必要となる。断面観察時もサンプルへのダメージを抑えるため低加速電圧やクライオ対応など観察条件を最適化することで初めて全固体電池の断面観察が可能となる。一方，製造プロセスの観点では，電極形成や粉体充填プロセス中の粒子の振る舞いの把握が重要であり，固体電解質の流動性や付着性は電極合材の設計や製造プロセスを考える上で非常に重要なパラメータとなる。流動性が高い固体電解質ほど電極合材作製時の分散性は高くなるが，一方で流動性が高いほど粒子同士の界面形成や維持に必要な付着性は低くなるため適切な粉体設計が必要である。我々は流動性評価とせん断試験が同一の装置で評価でき，比較的少量のサンプルで測定が可能なパウダーレオメータをドライルームに設置し，動的流動性試験により固体電解質の流動性を，せん断試験にて付着・凝集性を評価している[11]。

固体電解質の弾性率は活物質/固体電解質界面形成の容易さを評価するための重要な物性値であるが，測定手法によって固体電解質ペレットのマクロな構造の影響を受け，固体電解質そのものの弾性率の測定が難しい場合がある。我々は低露点Ar雰囲気グローブボックス内に設置した走査型プローブ顕微鏡法（SPM：Scanning Probe Microscopy）により，微小領域の弾性率マッピングを行うことで，固体電解質そのものの弾性率を評価している。

全固体電池の試作・評価技術

正極活物質Li（$Ni_{1/3}Mn_{1/3}Co_{1/3}$）O_2と合成した固体電解質Li_6PS_5Cl，導電助剤の合材からなる塗工正極と，負極活物質であるグラファイトと固体電解質Li_6PS_5Cl，導電助剤の合材からなる塗工負極を，固体電解質を挟んで対向させ，プレスにより緻密化・界面形成を行うことで塗工型全固体電池を作製した。

放電レート特性試験の結果を**Figure 5（a）**に示す。電圧範囲を2.0 Vから4.2 Vとし，環境温度25℃にて定電流-定電圧充電の後，Cレートを変えて放電を行った。なお，1Cは定格容量を1 hで放電する電流であり，2C，3Cは定格容量をそれぞれ1/2 h，1/3 hで放電する電流である。5C放電においても高い容量維持率を示し，良好な出力特性であった。

1Cにおける充放電サイクル試験の結果を**Figure 5（b）**に示す。300サイクルでの容量維持率は98%であり，充放電効率は約100%であった。このように1Cにて300サイクルの繰り返し充放電が可能であり，長期の耐久性評価が可能である。

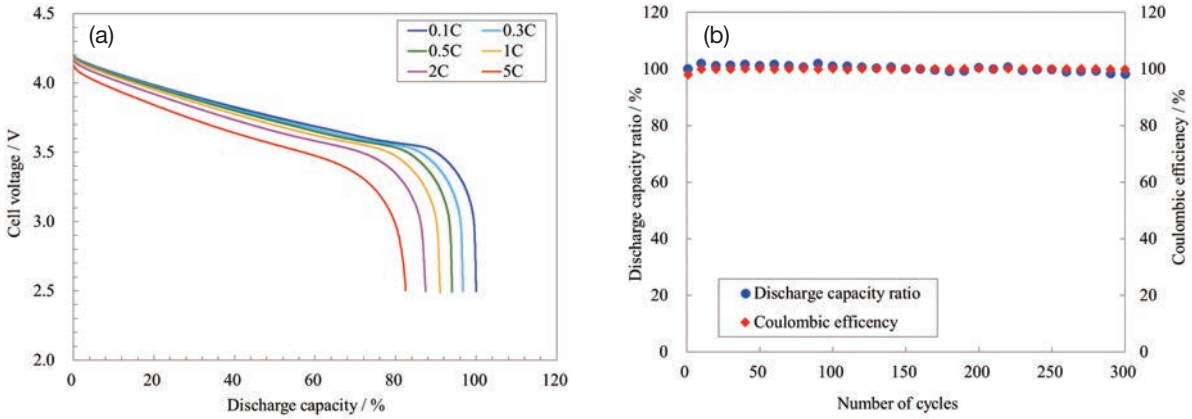

Figure 5　Electrochemical performances of solid-state battery. (a) Discharge rate performance. (b) Charge-discharge cycle performance.

おわりに

次世代電池として期待される全固体電池について，材料開発やプロセス開発開発に資する分析技術を紹介した。硫化物系全固体リチウムイオン電池は液系リチウムイオン電池と比較して，高エネルギー密度，優れた入出力特性が期待できることから，車載用途を中心に実用化に向けた研究開発が加速している。全固体電池のキーマテリアルである固体電解質では，合成プロセスに応じた大気非暴露の分析技術が必要であり，MAプロセスにおける小型ラマン分光装置での評価事例を紹介した。全固体電池はすべて固体粒子から構成されることから良好な電池特性を得るには，固体/固体界面形成と維持，電極内の導電パス・リチウムイオンパスの形成が必要である。FIB-SEMによる電極構造の3D構造解析やTEM観察によるナノ構造解析，GD-OESによる電極の深さ方向分析，SPMによる電子伝導パスの評価など，種々の分析手法を組み合わせて総合的に評価していく必要がある。

我々は二次電池の試作，物理解析や化学分析を駆使した解体調査，安全性試験，および計算科学との複合解析により，全固体電池をはじめとする二次電池の研究開発に貢献していく。

参考文献

[1] F. Mizuno, A. Hayashi, K. Tadanaga, and M. Tatsumisago: Adv. Mater., 17(2005)918.
[2] M. Tatsumisago, M. Nagao, and A. Hayashi, J. Asian Ceram. Soc., 1(2013)17.
[3] 菅野了次，イオン伝導体創出から固体電池構築へ，応用物理，第90巻 第1号，(2021)6.
[4] Y. Kato, S. Hori, T. Saito, K. Suzuki, M. Hirayama, A. Mitsui, M. Yonemura, H. Iba, and R. Kanno, Nat. Energy, 1(2016)16030.
[5] N. Kamaya, K. Homma, Y. Yamakawa, M. Hirayama, R. Kanno, M. Yonemura, T. Kamiyama, Y. Kato, S. Hama, K. Kawamoto, and A. Mitsui, Nature Materials, 10(2011)682.
[6] S. Boulineau, M. Courty, J.-M. Tarascon and V. Viallet, Solid State Ionics, 221(2012)1.
[7] H.J. Deiseroth, S.T. Kong, H. Eckert, J. Vannahme, C. Reiner, T. Zaiss, and M. Schlosser, Angew. Chem., Int. Ed., 47(2008)755.
[8] R. Murugan, V. Thangadurai, and W. Weppner, Angew. Chem. Int. Ed., 46(2007)7778.
[9] K. Momma and F. Izumi, J. Appl. Cryst., 44(2011)1272.
[10] H. Muramatsu, A. Hayashi, T. Ohtomo, S. Hama, M. Tatsumisago, Solid State Ionics, 182(2011)116.
[11] 阿知波敬，全固体電池の性能向上のための粉体物性評価技術，粉体工学会誌，第59巻 第11号，(2022)575.

水素燃焼ガスタービン開発における水素濃度計測

Hydrogen Concentration Measurement in Hydrogen Combustion Gas Turbine Development

都留 智子
TSURU Tomoko
川崎重工業株式会社 航空宇宙システムカンパニー
航空エンジンディビジョン エンジン技術開発部 エンジン熱技術課 課長
Manager
Engine Thermal Engineering Section
Engine Technology Development Department,
Aero Engine Business Division, Aerospace Systems Company
Kawasaki Heavy Industries, Ltd.

堀川 敦史
HORIKAWA Atsushi
川崎重工業株式会社 技術開発本部 技術研究所
エネルギーシステム研究部 研究一課 課長
Manager
Section 1, Energy System Research Department
Technical Institute, Corporate Technology Division
Kawasaki Heavy Industries, Ltd.

内山 悠太
UCHIYAMA Yuta
川崎重工業株式会社 技術開発本部 技術研究所
エネルギーシステム研究部 研究一課 主事
Section 1, Energy System Research Department
Technical Institute, Corporate Technology Division
Kawasaki Heavy Industries, Ltd.

近年機運が高まってきている脱炭素社会の実現に向けた，産業用ガスタービンや航空エンジンの水素対応化に対する当社の取り組みを紹介し，水素燃焼器の開発における水素ガス濃度計測に期待する役割について述べた。また，航空機エンジン向け水素燃焼器の開発において水素濃度を計測するため，HORIBA HyEVO-1000を導入する計画だが，デモ機による試計測では精度よくリアルタイム計測できることを確認できた。

キーワード：水素ガスタービン，NOx，未燃水素

This report introduces the efforts of Kawasaki Heavy Industries for developments of hydrogen-fueled industrial gas turbines and aircraft engines toward the realization of a decarbonized society. In the hydrogen-fueled combustor development, accurate measurement of hydrogen concentration in the exhaust gas will play more important role. Trial measurement results of hydrogen concentration using HORIBA HyEVO-1000, performed in KHI Akashi works, demonstrated favorable accuracy and time response.

Keywords: Hydrogen gas turbine, NOx, unburned hydrogen

はじめに

2018年7月の第五次エネルギー基本計画[1]では，国際的な水素サプライチェーンの構築と共に，安定的かつ大量に水素を消費する水素発電の開発を進めることが重要と記載された。また，2021年10月の第六次エネルギー基本計画[2]では，2050年カーボンニュートラル実現に向け，火力発電の脱炭素化として，水素・アンモニアを燃料とした発電は有力な選択肢の一つと記され，水素およびアンモニア発電については，2050年には電力システムの中の主要な供給力・調整力として機能すべく，技術的な課題の克服を進めると記載された。加えて，航空機分野においては，2035年以降の水素航空機の実現に必要となる水素燃焼器などのコア技術の開発を推進していくことが記された。

当社では，**Figure 1**に示す国際水素サプライチェーンを構築するための水素の製造・輸送・貯蔵・利用の各種技術開発と実証を進めている[3]。具体的には，褐炭や再生可能エネルギーから水素を製造し，液化して輸送・貯蔵し，炭化水素系燃料に代わる燃料として利用するまでの一気通貫の開発・実証である。

本稿では，産業用ガスタービンや航空エンジンに用いられる水素燃焼器の開発における当社の取り組みを紹介し，こ

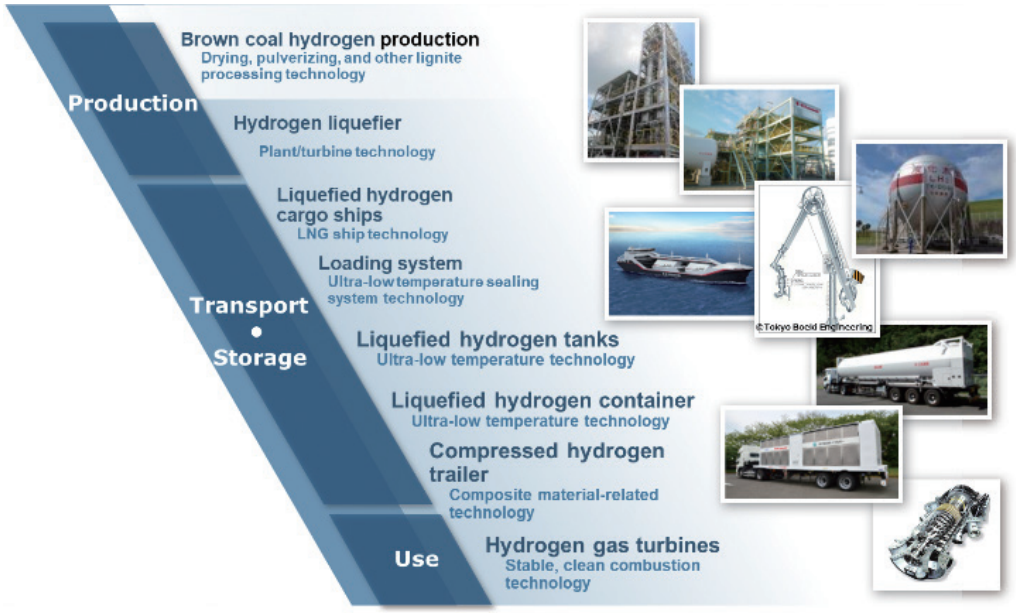

Figure 1　Technology developments for Hydrogen Society in Kawasaki Heavy Industries, Ltd.

れらの開発に必要となる水素ガス濃度計測について述べる。最後に，航空機エンジン向け水素燃焼器の開発における水素濃度計測の事例として，水素ガス測定装置 HORIBA HyEVO-1000の活用事例を紹介する。

水素燃焼の課題

水素と天然ガスの主成分であるメタンとの燃焼特性の比較や，燃焼時の水素特有の問題を**Table 1**に示す。水素はメタンに比べ，最大燃焼速度が速く，消炎距離も小さいことから燃焼器部品に水素火炎が近づき，金属部品の高温化や酸化，焼損を起こす可能性が高い。また，水素では可燃範囲も広くなることから，予混合燃焼は逆火の発生リスクが高まる。加えて，水素の燃焼速度の速さや火炎温度の高さは局所的な高温の燃焼ガスの発生を招くため，NOx（窒素酸化物）の増大につながる。これらの水素特有の燃焼特性を考慮し，水素の安定燃焼と低NOx性を兼ね備えた燃焼器の開発が求められる。一方で，従来の炭化水素系燃料に比べ反応性の高い水素は，未燃焼のまま排出されることが極めて少ないというメリットがある。ガスタービンの安定した燃焼状態では未燃水素が発生しないことを当社の燃焼試験において確認している。しかしながら，不安定な燃焼状態や，過濃条件，負荷変化や着火や消炎などの過渡条件においては未燃水素が発生する。燃焼器よりも下流に未燃水素が堆積し，意図しない燃焼や爆発に至ることは避けねばならぬため，開発の過程で未燃水素の発生有無や濃度を把握することが重要である。

Table 1　Combustion characteristics of methane and hydrogen and problems with hydrogen combustion

燃焼特性	メタン	水素	水素燃焼における問題
燃焼速度[m/s]（量論混合比，0.1 MPa）	0.4	2.65	異常燃焼（逆火，燃焼振動）
消炎距離[mm]	2.2	0.64	金属部品の高温化による，酸化や焼損
可燃限界[Vol%]	5〜15	4〜75	異常燃焼（逆火）
火炎温度[degC]（空気中）	1875	2045	サーマルNOx増大

Micro-mix水素燃焼技術と産業用ガスタービン実証試験

当社では，ドイツ・アーヘンにあるAcUAS（Aachen University Applied Sciences）が保有する微小な水素火炎を用いたmicro-mix水素専焼ドライ低NOx燃焼技術に着目し，B&B-AGEMA社と共同で，産業用ガスタービン燃焼器への適用検討ならびに燃焼器の概念設計を実施した[4-6]。

Figure 2（a）にmicro-mix水素専焼ドライ低NOx燃焼技術の概念図ならびに**Figure 2（b）**に燃焼数値流体解析結果例を示す[7]。微小な水素噴射孔から水素を噴射し，直交する空気噴流と急速に混合させ，水素火炎を形成する。微小な水素火炎を形成することで，局所的な高温域の発生を無くし，反応時間を短くしてNOxの発生を抑制する。また，水素噴射孔背後ならびに空気通過部（Air Guiding Panel：AGP）と水素供給部の背後に形成される循環域の間のせん断域にて，活性化学種であるOHラジカルやH原子が生成され水素火炎が保持される。このため，水素供給部内への水素火炎の侵入ならびにAGP上流側への逆火は発生しない。

当社の産業用ガスタービンでは，逆流缶型燃焼器を用いて

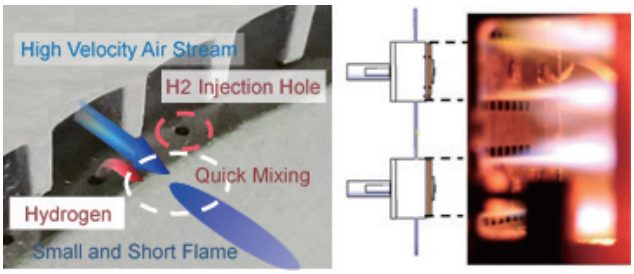

Figure 2(a) Micro-mix hydrogen flame.

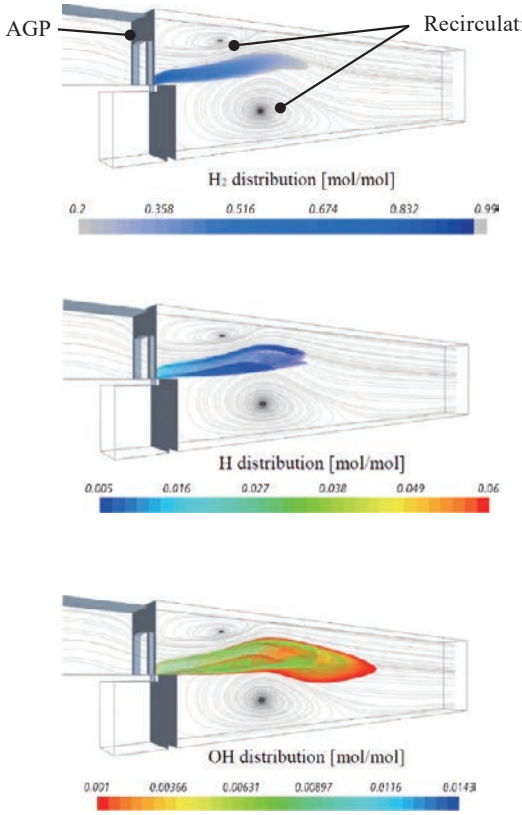

Figure 2(b) Structure of hydrogen flame and flame holding (Examples of CFD analysis).

いる。このため，AcUASでの水素燃焼試験で用いていた矩形micro-mixバーナを缶型燃焼器形状に合うようにリング形状とした。**Figure 3**にmicro-mixバーナモジュールを搭載した燃焼器の形状図（初期構想段階）を示す[8]。

当社は，国立研究開発法人新エネルギー・産業技術総合開発機構（NEDO : New Energy and Industrial Technology Development Organization）の助成事業において，本micro-mix水素専焼ドライ低NOx燃焼技術を用いた1MW級水素ガスタービン発電設備での水素発電，および地域社会への熱電供給実証を2020年に成功している[9]。

航空エンジンの脱炭素化に向けた動き

近年，航空業界でのカーボンニュートラル実現に向けて，燃料電池や代替航空燃料（SAF：Sustainable Aviation Fuel）に加え，水素燃料への対応についても機運が高まっている。2020年に仏エアバス社が2035年の運行開始を目指した水素航空機開発プロジェクトをスタートさせた[10]のをきっかけに，エンジンや装備品，空港でのインフラ整備など様々な分野で水素対応化に対する取り組みが活発化している。

当社においても，脱炭素化に大きく寄与すると想定される路線距離2,000～3,000 km，乗客数200人程度をターゲットとした水素航空機向けのコア技術開発を2021年度にNEDOの委託を受けて開始した[11]。航空エンジン用燃焼器及びエンジンシステム，液化水素燃料タンク及び装備システム，機体の構造検討をコア技術と設定し，2028年度まで各構成品の開発を推進する。2029～2030年度にはそれらを統合した一気通貫の統合システム地上試験を行い，水素航空機を社会実装するための主要技術を実証することを目指す。

航空エンジン用燃焼器の開発においても，産業用ガスタービンと同様高い環境適合性が求められ，ICAO（International Civil Aviation Organization）で厳しい規制が設けられている。航空エンジンを脱炭素化することによりCO_2やスモークという観点では環境負荷低減に大きく寄与できるが，NOxや水蒸気の発生は避けることができない。

特に，航空エンジンの内部は産業用ガスタービンと比較して圧力が高く，NOxを低減させることが難しいとされてい

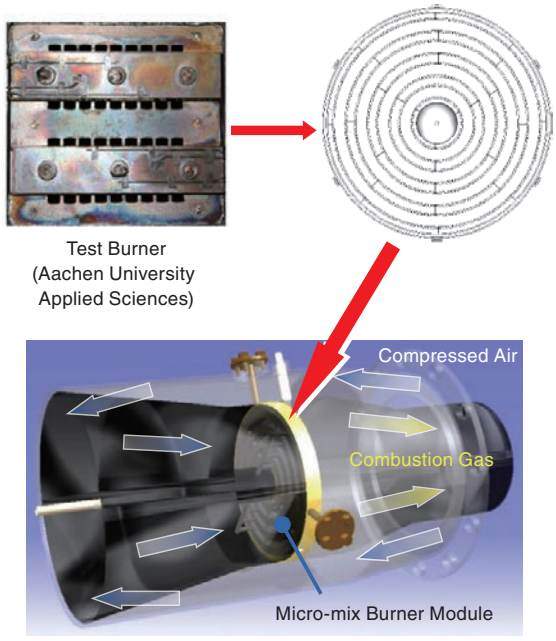

Figure 3 Schematic view of the first conceptual design of hydrogen Dry Low Emission combustor with micro-mix burner module.

る。さらに，運転中の出力変動が大きく急速であることから，燃焼条件の変化に追随しながら有害物の排出を低減できる燃焼器の開発が，水素航空機の実用化に向けて非常に重要となると考えられる。

ガスタービン燃焼器開発における未燃水素濃度計測

冒頭で述べた通り，水素は可燃範囲が広く安定燃焼していれば未燃水素はほとんど発生しない。しかし，エンジンの低負荷時，過渡状態（起動，出力変動時）は燃焼が不安定になりやすく，未燃水素の発生要因となる。特に航空エンジンは産業用ガスタービンと比べて空気流量，圧力，空気過剰率が短時間で大きく変化するので，一時的に多くの未燃水素が発生するリスクがある。

水素燃焼器の開発においては，前述した安定燃焼時のNOx排出量の低減だけでなく，低負荷時や過渡運転時でも一定以上の燃焼効率を確保しなければならず，開発試験用の計測機器としては応答性（0.5秒程度）と精度（数ppmオーダの解像度）の両方に対応できるものが求められる。

HyEVO-1000を用いた未燃水素濃度計測事例の紹介

当社では，航空エンジン用燃焼器向けにリアルタイムで精度の高い水素濃度計測ができる機器として2023年度に販売開始予定のHORIBA HyEVO-1000を導入することを計画している。導入に向けて，2022年12月にデモ機での試計測を実施したので，その事例を紹介する。

Figure 4に試験装置外観を示す。水素ガス燃料は燃料マニホールドを介して燃焼器ケーシング内に配置された燃料ノズルから噴射され，ライナと呼ばれる円環状の内筒の中で火炎を形成する。排ガスは燃焼器出口からサンプリングし，加熱フィルタを通って濃度計本体へ供給される。計測データの検証のため，ガスクロマトグラフィによる水素濃度計測も並行して実施した。

Figure 5に，HyEVO-1000とガスクロマトグラフィで計測した水素濃度の比較を示す。一連の空燃比条件において両者は良い一致を示し，水素濃度を精度良く計測できていることを確認した。また，連続計測における応答性も良く，スムーズに燃焼試験を実施することができた。

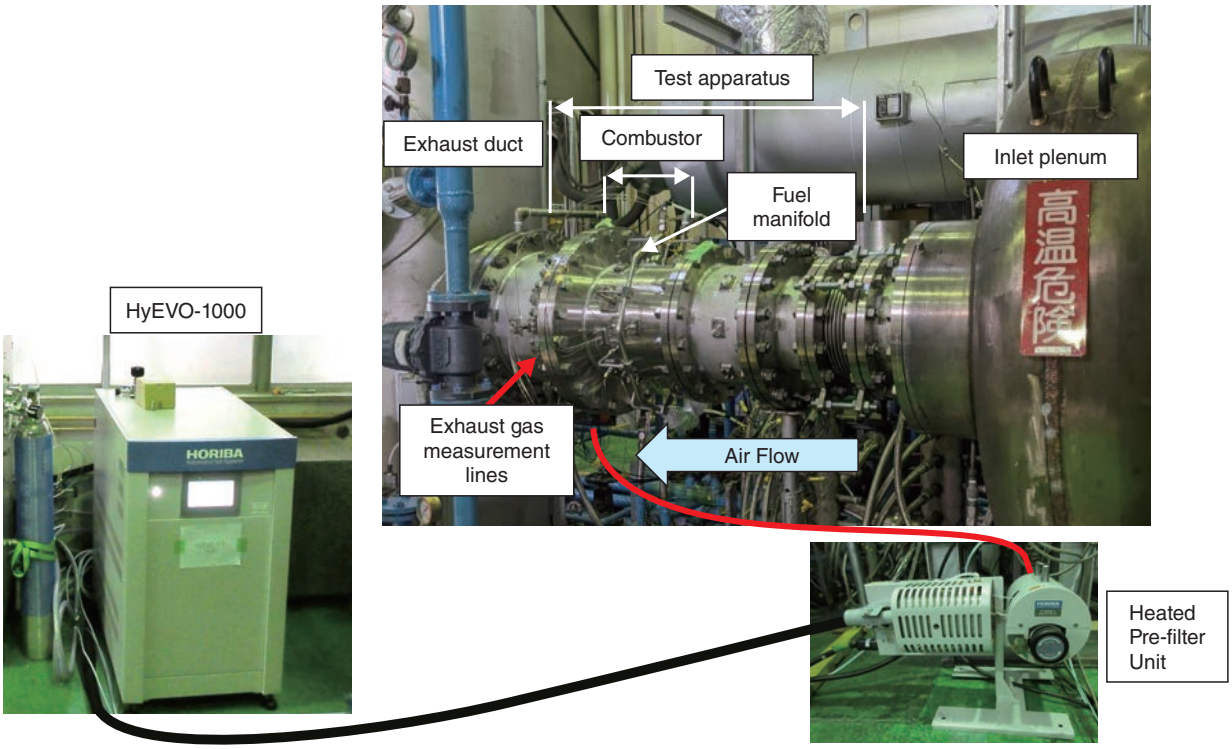

Figure 4　Test apparatus of hydrogen combustor for aeroengine.

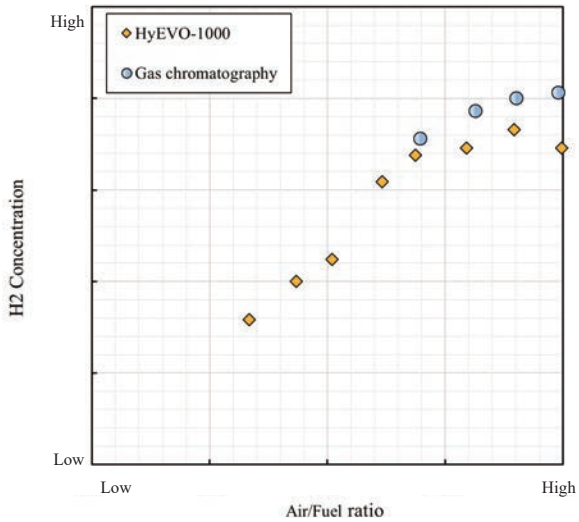

Figure 5 Comparison of hydrogen concentration between HyEVO-1000 and gas chromatography.

おわりに

産業用・航空用ガスタービン向け水素燃焼器の開発における当社の取り組みを紹介し，燃焼器開発のための水素濃度計測の位置づけについてHyEVO-1000を用いた水素濃度計測事例紹介を交えて述べた。従来の水素濃度計にはなかった高い計測能力を有効に活用することで，水素燃焼器の開発促進につなげられるものと期待している。水素利活用による脱炭素化がこれからさらに活発化するであろうことを考えると，水素濃度計測に対して様々な分野で需要が高まると予想される。ユーザの立場としては，計測能力もさることながら，機器の扱いやすさやコストも重要なポイントであり，更なるコンパクト化，静音構造，柔軟な作動レンジへの対応など，期待する部分が大きい。メーカとユーザが互いに協力しながら，より高度で使いやすい計測機器を実現できれば将来の環境負荷低減技術の実証に大きく寄与できるものと期待している。

謝辞

水素専焼ドライ低NOx燃焼技術を用いた水素発電，熱電供給実証においては，NEDO課題設定型産業技術開発費助成事業「水素社会構築技術開発事業／大規模水素エネルギー利用技術開発／ドライ低NOx水素専焼ガスタービン技術開発・実証事業」にご支援をいただきました。また，水素濃度計の導入および燃焼試験は，NEDOグリーンイノベーション基金事業「次世代航空機の開発プロジェクト／水素航空機向けコア技術の開発」における航空機エンジン向け水素燃焼器の研究の一部として，NEDOの委託を受けて実施しました。ここに謝意を表します。

参考文献

[1] 国立国会図書館 インターネット資料収集保存事業，経済産業省 ニュースリリース ウェブサイト；新しいエネルギー基本計画が閣議決定されました，https://warp.da.ndl.go.jp/info:ndljp/pid/11126101/www.meti.go.jp/press/2018/07/20180703001/20180703001.html（アクセス日2022年2月20日）

[2] 経済産業省 ニュースリリース ウェブサイト；第6次エネルギー基本計画が閣議決定されました，https://www.meti.go.jp/press/2021/10/20211022005/20211022005.html（アクセス日2021年10月25日）

[3] 西村元彦，水向健太郎，洲河誠一；国際液化水素サプライチェーンの技術構築の現状，エネルギー・資源学会誌，通巻229号，Vol.39 No.3，(2018)，153-157.

[4] Funke, H., et al; Numerical and Experimental Characterization of Low NOx Micromix Principle for Industrial Hydrogen Gas Turbine Applications, Proceedings of ASME Turbo Expo 2012, Copenhagen, Denmark, GT2012-69421.

[5] Funke, H., et al; Experimental and Numerical Characterization of the Dry Low NOx Micromix Hydrogen Combustion Principle at Increased Energy Density for Industrial Hydrogen Gas Turbine Applications, Proceedings of ASME Turbo Expo 2013, San Antonio, Texas, GT2013-94771.

[6] Haj Ayed, A., et al; Numerical Study on Increased Energy Density for the DLN Micromix Hydrogen Combustion Principle, Proceedings of ASME Turbo Expo 2014, Dusseldorf, Germany, GT2014-25848.

[7] Kroniger, D., et al; Numerical Study of Hydrogen-fueled Micromix Combustion and Experimental Validation of NOx Emissions, 第48回ガスタービン学会定期講演会（オンライン開催），講演論文集A-14，(2020)

[8] 堀川敦史，他；ドライ水素低NOx燃焼技術の開発，第43回ガスタービン学会定期講演会（米子），講演論文集A-7，(2015)

[9] NEDO ニュースリリース ウェブサイト；世界初，ドライ低NOx水素専焼ガスタービンの技術実証試験に成功，https://www.nedo.go.jp/news/press/AA5_101337.html（アクセス日2023年2月20日）

[10] https://www.airbus.com/en/innovation/zero-emission/hydrogen/zeroe（アクセス日：2023年2月27日）

[11] NEDOニュースリリース ウェブサイト；グリーンイノベーション基金事業で，次世代航空機に関する研究開発事業に着手―水素航空機向けコア技術の確立と，主要構造部品の飛躍的軽量化を目指す―
https://www.nedo.go.jp/news/press/AA5_101488.html（アクセス日2023年2月27日）

量子カスケードレーザと独自の濃度演算手法を用いたガス分析技術「IRLAM」の開発
～高感度・低干渉・高速応答ガス分析の実現～

Development of a Gas Analysis Technology “IRLAM” Using Quantum Cascade Laser and Unique Concentration Calculation Method
~ Realization of High-Sensitivity, Low-Interference, and Fast-Response Gas Analysis ~

渋谷 享司
SHIBUYA Kyoji

HORIBAが新たに開発した量子カスケードレーザ(QCL)を用いたガス分析手法，赤外レーザ吸収変調法(IRLAM)は，サンプルガスの吸収信号から，濃度定量に重要な情報を，特徴量として抽出して演算を行うことで，従来のスペクトルフィッティング手法に比べ，劇的に演算時間を短縮することができる。この独自の濃度演算アルゴリズム(特許登録済)を自社製造のQCLと小容量で長い光路長が得られる独自構造のヘリオットセルと組み合わせることで，高感度で干渉ガス影響に強く，高速に測定が可能なガス分析計を完成させた。IRLAMは，QCLを用いたガス分析の産業適用範囲を大きく広げることに成功し，世界初のQCLを用いた車載排ガス計測装置を実現し，石油化学プロセスのリアルタイム監視などに適用されている。

キーワード
ガス分析，赤外吸収分光法，量子カスケードレーザ，スペクトル解析，特徴量

HORIBA’s newly developed gas analysis method using a quantum cascade laser (QCL), infrared laser absorption modulation (IRLAM), dramatically reduces calculation time compared to conventional spectral fitting methods by extracting information important for concentration determination from the absorption signal of the sample gas as features (patent registered). By combining this method with QCLs manufactured in-house and a uniquely structured Herriott cell with a small volume and long optical path length, we have completed a gas analyzer with high sensitivity, small influence of interfering gases, and fast response. IRLAM has succeeded in greatly expanding the industrial application range of gas analysis using QCL, realizing the world’s first QCL-based onboard exhaust gas measurement and real-time monitoring of petrochemical processes.

Keywords
gas analysis, infrared absorption spectroscopy, quantum cascade laser, spectral analysis, features

はじめに

HORIBAは，赤外吸収を用いたガス分析技術を自動車や工場の排ガス計測，大気環境計測，プロセス監視・制御などに古くから適用し，様々な産業分野の環境負荷低減や生産性向上に貢献してきた。従来の赤外ガス分析技術としては，非分散型赤外吸収法(NDIR)と呼ばれる手法が広く用いられてきた[1]。NDIRは，加熱したフィラメント等からの熱輻射を光源とし，測定対象ガスの吸収帯に合わせて，光学バンドパスフィルターで利用する波長帯を切り出し，その赤外光の吸収量から測定対象ガスの濃度を求める。NDIRは光源の波長分解能が高くないため，測定対象ガスと吸収帯が重なる干渉ガスの影響を除去することが原理的に難しい。そこで，測定対象ガスを封入したセルで赤外光を検出

するニューマティック型検出器[2]を用いることで，ある程度のガス選択性を持たせることができる。またフーリエ変換赤外分光法（FT-IR）を用いたガス分析手法は，サンプルガスの赤外領域全体の吸収スペクトルを取得することができるため，多変量解析などを適用することで，多くのガス成分を同時に計測することが可能となり，自動車の排ガス計測などに広く用いられている[3]。一方，単一波長の量子カスケードレーザ（QCL）を光源とする吸収分光法（QCL-IR）を用いたガス分析では，高い波長分解能で計測が可能なため，計測に用いる波長をうまく選定することで，干渉ガスの影響を大きく抑えることができる。また光源の単位波長辺りのエネルギー密度が高く，レーザ光の直進性から，長い光路長が得られる多重反射セルとの相性も良いため，NDIRやFT-IRに比べ，より高感度な計測が可能となる。HORIBAは，QCL-IRを用いたガス分析計を自動車排ガス計測に世界に先駆けて適用してきた[4,5]。QCL-IRは，原理的に干渉ガス影響に強い特長を持つが，自動車排ガス計測など，多数の干渉ガスが共存し，それらの濃度がダイナミックに変化するようなアプリケーションでは，波長の選択だけでは，完全に干渉ガス影響を排除することは難しい。そこで，従来のQCL-IRでは，測定により得られたサンプルガスの吸収スペクトルに対して，予め用意した測定対象ガスや干渉ガスのモデルスペクトルとのカーブフィッティングによって，干渉ガス影響を補正した測定対象ガスの濃度を算出していた。さらに干渉ガス影響だけでなく，環境温度・圧力の変動，レーザ発振波長のドリフト，共存ガスとの相互作用によるスペクトルブロードニングなど様々な外乱影響が吸収スペクトルに変化を与えるため，これらの非線形な外乱影響の補正まで含めようとすると，繰り返し演算を伴う複雑なフィッティング処理が必要となり，このような演算をリアルタイムで高速に実行するために，高性能で大掛かりなコンピュータを装置に搭載する必要があった。しかし，このような要求は，装置コストやサイズの増加だけでなく，過酷な環境においても安定した動作が求められる工業計器としては，適用範囲に制約がかかることになる。

そこで我々は，機械学習などで用いられる「特徴量」という概念をQCL-IRの濃度演算アルゴリズムに適用することを着想し，測定で得られた吸収信号から目的ガスや干渉ガス，その他の外乱影響の特徴量を抽出して，濃度定量に必要な情報量を保ったまま，説明変数の数を大幅に減らすことで，濃度演算処理の負荷を劇的に軽減することに成功した。これにより，基板組込型の汎用マイクロコンピュータでも，測定精度に影響を与える様々な外乱影響を除去しながら，十分に高精度かつリアルタイム計測を実現できるようになった。我々はこのガス分析手法を赤外レーザ吸収変調法（Infrared Laser Absorption Modulation：IRLAM™*1）[6]と名付け，この原理を用いたガス分析計の製品化に成功した。以下に，IRLAMの原理や構成，従来技術との比較について述べ，IRLAMを適用した製品例について紹介する。

*1 IRLAMは株式会社堀場製作所の日本及びその他の国における登録商標または商標です。

IRLAMの原理と構成

IRLAMを含め，吸収分光法によるガス分析は，以下の式で表されるランベルト・ベールの法則に基づいて，サンプルガスへの入射光量Iinと透過光量Ioutの比の対数で定義される吸光度Aが，ガス濃度cと光路長Lに比例する関係を基本原理として用いている。

$$A = -\log\left(\frac{I_{out}}{I_{in}}\right) = \varepsilon \cdot c \cdot L$$

ここで，ε は，吸光係数と呼ばれるガス固有の比例定数である。

Figure 1にIRLAMガス分析計の基本構成の模式図を示す。IRLAMでは，QCLからの光をヘリオットセルと呼ばれるサンプルガスを導入する分析セルに入射させ，サンプルガス透過後の出射光を赤外検出器で受光し，吸収信号を取得する。そして得られた吸収信号から特徴抽出を伴う独自の濃度演算アルゴリズムによって，測定対象ガスの濃度を算出する。IRLAMガス分析計を特徴づける重要な要素は，QCLとヘリオットセルと濃度演算アルゴリズムの3つであり，以下に各要素について説明を加える。

量子カスケードレーザ

QCLは，中赤外領域（4～12 μm程度）で，室温レーザ発振が可能な比較的新しい半導体レーザの一種である[7]。多くのガス分子は，中赤外領域で最も強い吸収を示すため，この波長領域をレーザ発振できるQCLは，ガス分析にとって，最も適した光源と言える。QCLは，数百層から成る多層の半導体薄膜から構成され，材料組成・膜厚を制御することで，発振波長を自在に設計できることが特長である。HORIBAは，このQCLを自社製造する技術を確立しており，測定対象ガスの種類や濃度レンジに応じた最適な波長のQCLを設計・製造することが可能で，様々なガス分析ニーズに柔軟に対応することができる。

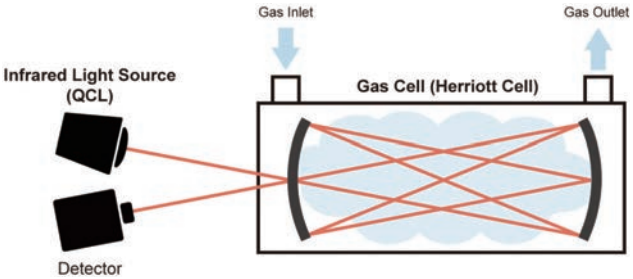

Figure 1 Schematic diagram of the basic configuration of the IRLAM gas analyzer.

ヘリオットセル

吸収分光法によるガス分析計では，ランベルト・ベールの法則からわかるように，光がサンプルガスを透過する距離（光路長）が長いほど，大きな吸光度が得られ，感度が向上する。そこで，IRLAMガス分析計では，**Figure 1**に示すように内部に設置した対向するミラーによって，光を多重反射させることで長い光路長が得られるヘリオットセルと呼ばれるガスセルを採用している。

従来のヘリオットセルでは，円形の球面ミラーを用いるものが一般的であったが[8]，我々は，細長形状の球面ミラーを用いることで，十分な光路長を確保した上で，セルの内部容積を大幅に低減することに成功した[9]。セルの内部容積を低減すると，ガス置換時間によって律速される分析計の応答速度が改善する。この細長球面ミラーを用いたヘリオットセルでは，5 mの光路長をわずか40 mLの内部容積で実現することができ，IRLAMガス分析計の応答速度の向上と装置の小型化に寄与している。

濃度演算アルゴリズム

IRLAMガス分析計にとって，最も特徴的な要素が，濃度演算アルゴリズムにある。IRLAMの濃度演算アルゴリズムには，機械学習などで用いられる「特徴量」という概念を適用している。**Figure 2**に，IRLAMのガス分析手順の模式図を示す。測定対象ガスの吸収スペクトルのピークを中心として，QCLの波長を一定の周期で変調すると，吸収スペクトルの形状を反映した周期的な吸収信号が検出器より得られる。この吸収信号に対して，抽出したい特徴に合わせて予め用意した複数の参照信号との相関を取ることで，特徴量の抽出を行い，得られた各特徴量と，校正ガスを用いて予め取得した参照用の特徴量と比較して，最小二乗法により，濃度定量を行う[6,10]。

機械学習では，多くの教師データを学習することで，アルゴリズムが抽出する特徴量を自動的に決定するが，IRLAMにおいては，設計者が濃度定量に重要な因子を経験に基づいて選択し，それらが吸収信号に与える影響を物理的性質に基づいて把握して，抽出する特徴量を決定している点が異なる。具体的な濃度定量に重要な因子としては，測定対象ガスと干渉ガスの吸収信号の形状，QCLの発振波長のドリフトの影響，そして，圧力や共存ガスの濃度変化により生じるスペクトルブロードニングの影響などが挙げられる。IRLAMの実際のガス分析応用においては，これらの因子に関する特徴量を中心に，10個程度の特徴量を用いて，濃度定量を行っている。

以上のような特徴量を用いた濃度演算の手順の利点は，特徴抽出によってスペクトル情報を圧縮することで，従来の吸収スペクトルを直接カーブフィッティングする場合に比べて，大幅に少ない説明変数で，干渉ガス影響やその他の外乱影響の補正機能を持った濃度演算を提供できることである。一般的なスペクトルカーブフィッティングでは，数百点からなる吸収スペクトルデータを用いるため，数百の連立一次方程式からなる最小二乗法を実行する必要がある。一方，IRLAM の場合，連立一次方程式の数は数個から10個程度であるため，演算負荷は10～100分の1に軽減される。そのため，高速なリアルタイム計測が必要な場合にも高性能なコンピュータは必要なく，汎用の組み込みプロセッサーで十分である。これにより，IRLAMでは，PC不要の装置構成が可能となり，装置の小型化が容易となると共に，過酷な環境においても安定した連続運転が可能な工業計器として，適用範囲を広げられるようになった。

IRLAMと従来技術との性能比較

IRLAMは，従来の赤外吸収を用いたガス分析技術に対して，検出や干渉ガス影響の性能において，大きく改善がなされている。以下に具体的な測定例を元に，従来技術と比較した結果を示す。

検出感度

Figure 3は，IRLAMガス分析計と従来技術であるFT-IRガス分析計で，自動車排ガス中のホルムアルデヒド（HCHO）を同時に測定した結果を比較したものである。赤線がFT-IRでの測定結果であり，青線がIRLAMでの測定結果である。まず右図を見ると，両者の全体的な濃度変化の傾向は一致していることがわかる。しかし，ノイズの大きさが大きく異なることがよくわかる。右図の一部を拡大した

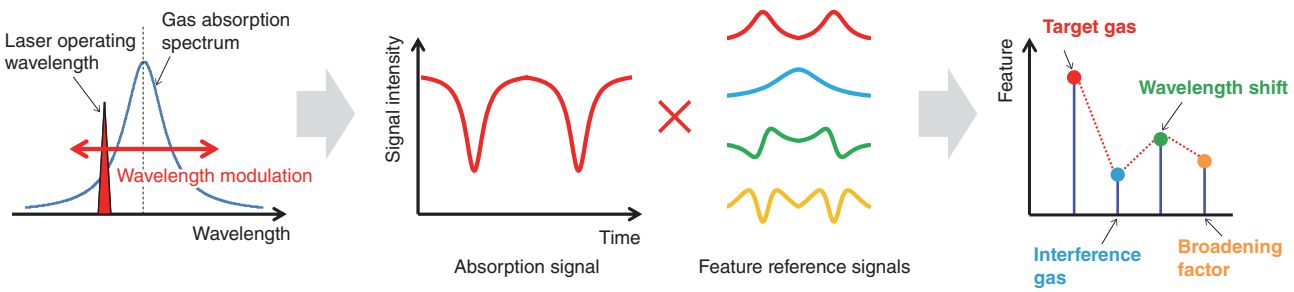

Figure 2　Conceptual diagram of the gas analysis procedure in IRLAM.

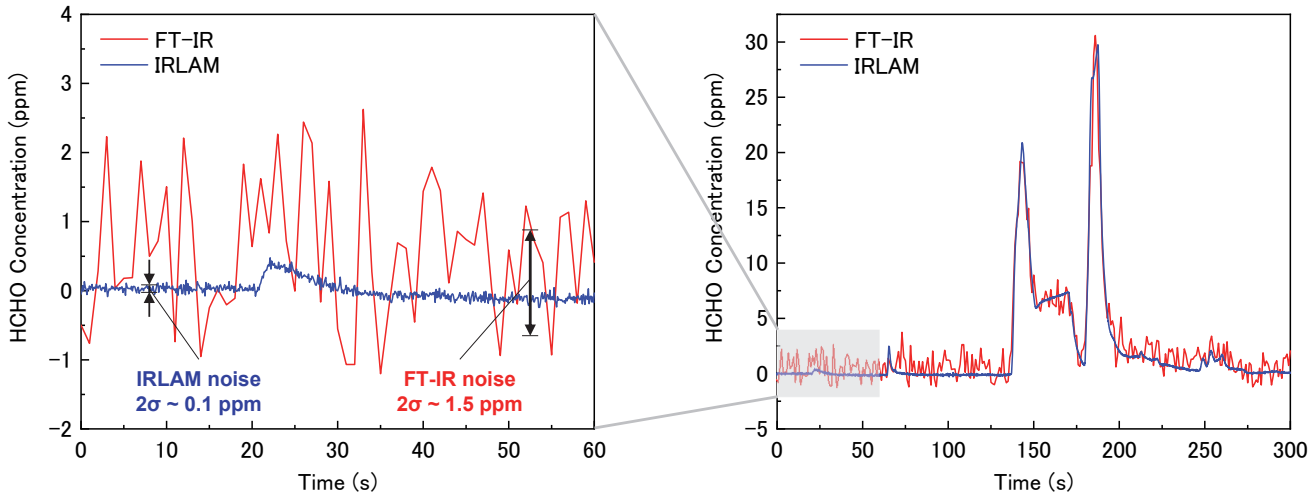

Figure 3 Comparison of detection sensitivity between IRLAM and FT-IR for HCHO measurement (the left figure is enlarged from 0 to 60 s in the right figure).

左図に示すように，IRLAMはFT-IRの10分の1以下のノイズ幅になっており，FT-IRではノイズに埋もれて検出できないわずかな濃度変化も正確に測定できている。このようにIRLAMは，従来技術のFT-IRに比べて検出感度が10倍以上改善していることが示された。

干渉ガス影響

Figure 4は，IRLAMガス分析計と従来技術であるNDIRガス分析計で，測定対象ガスである一酸化二窒素（N_2O）と干渉ガスである二酸化炭素（CO_2）を順番に分析セルに導入した時の分析計の濃度指示値の変化を比較したものである。左図の赤線のグラフがNDIRでの測定結果であり，右図の青線のグラフがIRLAMでの測定結果である。まず左図のNDIRの測定結果を見ると，測定対象ガスのN_2Oを導入した時だけでなく，干渉ガスであるCO_2を導入した時にも大きく指示値が変化しており，CO_2が混在する状態では，CO_2の干渉ガス影響を大きく受けて，N_2Oの濃度を正しく測れないということを示している。一方，右図のIRLAMの測定結果を見ると，NDIRの時の試験の10倍の濃度のCO_2を導入しているにも関わらず，全くと言っていいほど，干渉ガス影響が出ていない結果が得られており，干渉ガスのCO_2が高濃度で混在する状態であってもN_2Oの濃度を正確に計測することができることがわかる。このように，IRLAMは，従来技術のNDIRでは不可能だった干渉ガス影響をほぼゼロにすることを実現した。

IRLAMを適用した製品例

以上で述べたような特徴を持つIRLAMは，自動車の排ガス計測や石油化学プロセスなどの高精度でリアルタイムの計測が必要な分野ですでに使われている。以下では，それらの現在製品化されているIRLAMガス分析計について紹介する。

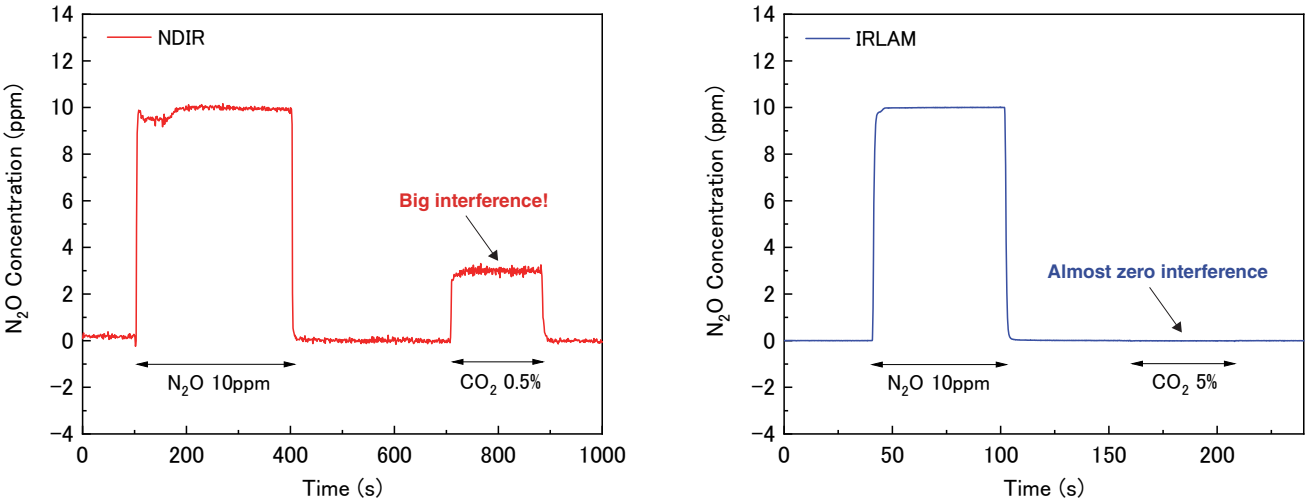

Figure 4 Comparison of interfering gas influence between IRLAM and NDIR for N_2O measurement (left: NDIR, right: IRLAM).

エンジン排ガス分析計
MEXA-ONE IRLAM

MEXA-ONE IRLAMは，定置型の自動車排ガス計測用のIRLAMガス分析計である。エンジン排ガス測定装置MEXA-ONEに搭載されるタイプ（XLA-11，XLA-13H）と単独ユニットのタイプ（MEXA-ONE-XL-NX）がラインナップされており，完成車の排ガス認証試験やエンジンの環境性能改善のための研究開発などに用いられている。

XLA-11は，温室効果ガスで規制対象物質であるN_2Oを測定対象としており，認証試験法である定量希釈サンプリング装置（CVS）を用いた計測に対応するため，ppbレベルの計測精度でN_2Oを計測できるように設計されている。またMEXA-ONE-XL-NXは，従来からの規制対象物質の窒素酸化物（NOx）や近年PM2.5の原因物質の一つとして注目されているアンモニア（NH_3）なども含め，NO，NO_2，N_2O，NH_3の4つの窒素化合物を同時に高精度にリアルタイム計測することが可能で，低環境負荷車の開発にはなくてはならない製品として自動車メーカー等で広く用いられている。

そしてXLA-13Hは，有害物質で米国等ではすでに規制対象物質になっており，欧州等でも規制化が検討されているHCHOを測定対象としており，従来技術では難しかった自動車排ガス試験サイクルでの高精度な連続計測を可能にした[11]。本製品は，欧州の排ガス規制などの政策に指針を与える欧州委員会の共同研究センター（JRC）においても評価され，実際の排ガス計測に十分に耐えうる性能を持つことが示された[12]。

車載型排ガス計測システム
OBS-ONE IRLAM

近年，実路走行中の排ガスを計測する実路走行排ガス（Real Driving Emission：RDE）試験を認証試験法とするRDE規制が欧州で導入された。RDE試験を行うためには，可搬型排ガス計測システム（Portable Emission Measurement System：PEMS）と呼ばれる小型で耐環境性が強い分析装置が求められる。特に車載型の分析計では，試験室内の分析計と異なり，激しい振動や温度・気圧の変動など，過酷な環境下でも安定した計測を実現する必要がある。そのような厳しい要求に対して，IRLAMのロバスト性の高い濃度演算アルゴリズムと堅牢なハードウェア設計によって応えることができ，QCLを用いたガス分析計としては世界初となる車載型専用設計の自動車排ガス分析装置（OBS-ONE-XL）の製品化に成功した。**Figure 5**に本装置の外観写真を示す。

本製品では，欧州の次期自動車排ガス規制Euro 7において導入が検討されているN_2OとNH_3を測定対象とし，前述した細長球面ミラーを用いた小型ヘリオットセルとPC不要の濃度演算アルゴリズムのおかげで，車載に耐えうる小型化を実現した[13]。そして，本製品は欧州委員会のJRCにも注目され，Euro 7の検討に向けて評価され，定置型分析計と良い相関を示し，PEMSとして十分に実用に足る性能を持っていることが示された[14,15]。

プロセス用レーザガス分析計
PLGA-1000

PLGA-1000は，石油化学プロセスのリアルタイム監視・制御に用いるためのIRLAMガス分析計である。**Figure 6**に本分析計の外観写真を示す。従来は，ガスクロマトグラフィー（GC）を用いたプロセス監視が主流であったが，GCの場合，リアルタイム性に欠けるため，プロセスの異常が発生した際の検知に遅れが生じ，場合によっては大きな原材料のロス，生産性の低下に繋がる課題があった。そこで，よりリアルタイム性の高い計測手法が求められていたが，石油化学プロセスでは，多くの炭化水素類が高濃度で混在するため，お互いの干渉ガス影響やブロードニング影響が強く，GC以外のガス分離を伴わない手法での計測は困難であった。

しかしIRLAMはそのような困難なガス条件においても，独自の濃度演算アルゴリズムにより，干渉ガス影響やブロードニング影響を除去して，目的とするガスを高精度にリアルタイム計測できることを実証した。本成果は海外の大手石油化学メーカーにも認められ，エチレン（C_2H_4）製造プロセスにおける不純物であるアセチレン（C_2H_2）等を計測するために，PLGA-1000が採用されている。

Figure 5 Photograph of the on-board emission measurement system, OBS-ONE-XL.

Figure 6 Photograph of the petrochemical process gas analyzer, PLGA-1000.

IRLAMのカーボンニュートラル社会への貢献

IRLAMを用いたガス分析技術は，水素を中心としたカーボンニュートラルな代替エネルギーの利活用においても様々な適用が検討されている。例えば，水素を燃料電池に利用する際，水素中の不純物が燃料電池の性能や寿命に影響を与えるため，水素の製造時や利用時に，水素中のppm～ppbレベルの不純物を管理したい要求がある。また水素や水素を元に合成される水素キャリアの一つであるNH_3は，カーボンフリーな燃料として，直接燃焼させて利用することも検討が進んでいる。水素やNH_3を燃焼させる際，CO_2は発生しないが，NOxや未燃のNH_3が排出されうるので，これらの排出を抑える燃焼制御が重要となる。さらに，排出されたCO_2を回収して，再利用することでカーボンニュートラルを実現するCCU（Carbon Capture and Utilization）の取り組みにおいても，回収したCO_2を再利用するための純度管理や回収したCO_2と水素から，エネルギーとして有用なメタン（CH_4）を合成するメタメーションのプロセス管理などで，ガス分析が重要な役割を担う。このような要求や課題に対して，IRLAMは高感度・低干渉で連続分析が可能なガス分析によって，ソリューションを提供することができる。

おわりに

以上で述べてきたように，IRLAMは，自社製造のQCLを光源とし，独自構造のヘリオットセル，そして吸収変調信号からの特徴量の抽出に基づく独創的な濃度演算アルゴリズムにより，従来技術では困難な条件下においても高精度なリアルタイム計測を実現し，QCLを用いたガス分析の産業適用範囲を大きく広げることに成功した。

IRLAMの特長をまとめると以下のように言うことができる。

①高感度・低干渉：QCL-IRの原理的な特長と独自の濃度演算アルゴリズムで，サンプルガスに含まれる様々な干渉ガスの影響を受けず，高感度な計測を実現。

②ダイレクト・リアルタイム：サンプルガスの前処理不要で，小容量ヘリオットセルによる速いガス置換と高速な濃度演算アルゴリズムで，高精度なリアルタイム計測が可能。

③高安定・高ロバスト性：独自の濃度演算アルゴリズムと堅牢なハードウェア設計で，過酷な使用環境（温度・圧力変動，振動大）でも安定に計測が可能。

IRLAMは，今後もあらゆる産業のガス分析ニーズに応え，各産業の環境負荷低減や生産性向上，そしてカーボンニュートラル社会の実現に大きく貢献することが期待される。なお，本論文で述べた内容の詳細について，さらに理解を深めたい読者は，筆者がIRLAM技術について総合的にまとめた参考文献[16]も合わせて参照されたい。

＊編集局注：本内容は特段の記載がない限り，本誌発行年時点での自社調査に基づいて記載しています。

参考文献

[1] 石田耕三：赤外線ガス分析計の開発，Readout, vol.32, 60（2006）.
[2] 青木潤次：ニューマチック赤外検出器，Readout, vol.7, 64（1993）.
[3] M. Adachi et al.: Automotive Emission Analyses using FTIR Spectrophotometer, SAE Technical Paper, 920723（1992）.
[4] 原健児：中赤外レーザ吸光法自動車排ガス分析計QL-N_2O，Readout, vol.43, 65（2014）.
[5] K. Hara et al.: Development of Nitrogen Components Analyzer Utilizing Quantum Cascade Laser, SAE Technical Paper, 2009-01-2743（2009）.
[6] K. Shibuya et al.: High-sensitivity and low-interference gas analyzer with feature extraction from mid-infrared laser absorption-modulated signal, Measurement Science and Technology, vol.32, 035201（2021）.
[7] J. Faist et al.: Quantum Cascade Laser, Science, vol.264, 553（1994）.
[8] D. Herriott et al.: Off-Axis Paths in Spherical Mirror Interferometers, Applied Optics, vol.3, 523（1964）.
[9] 堀場製作所：日本特許公報，多重反射セル，ガス分析装置，及び多重反射セルの構成方法，特許第7094467号（2022）.
[10] 堀場製作所：日本特許公報，分析装置，分析装置用プログラム及び分析方法，特許第6886507号（2021）.
[11] K. Hara et al.: Formaldehydes Measurement Using Laser Spectroscopic Gas Analyzer, SAE Technical Paper, 2021-01-0604（2021）.
[12] R. Suarez-Bertoa et al.: Real-Time Measurements of Formaldehyde Emissions from Modern Vehicles, Energies, vol.15, 7680（2022）.
[13] Y. Onishi et al.: Development of On-Board NH_3 and N_2O Analyzer Utilizing Mid-Infrared Laser Absorption Spectroscopy, SAE Technical Paper, 2021-01-0610（2021）.
[14] R. Suarez-Bertoa et al.: NH_3 and N_2O Real World Emissions Measurement from a CNG Heavy Duty Vehicle Using On-Board Measurement Systems, Applied Sciences, vol.11, 10055（2021）.
[15] T. Selleri et al.: Measuring Emissions from a Demonstrator Heavy-Duty Diesel Vehicle under Real-World Conditions—Moving Forward to Euro VII, Catalysts, vol.12, 184（2022）.
[16] 渋谷享司：赤外レーザー吸収変調法による高精度・リアルタイムガス分析技術の開発と産業応用，分析化学，Vol.72，受理済 掲載準備中（2023）.

渋谷 享司
SHIBUYA Kyoji
株式会社堀場製作所
開発本部
テクノロジーイノベーションセンター 先行開発部
博士（工学）
Advanced R&D Department,
Technology Innovation Center, R&D Division
HORIBA, Ltd.
Ph.D.

Thermal Runaway: Can Ultrasound Finally Solve Li-ion Cells' Most Dangerous Challenge?

熱暴走：超音波はリチウムイオンセルの最も危険な課題を解決できるか？

Michele BRAGLIA
ミシェル ブラグリア

Richard STOCKER
リチャード ストッカー

The occurrence of several battery-related accidents over the years has risen public awareness of risks and safety issues around electric vehicles (EVs). Current safety features implemented on battery management systems (BMSs) heavily depend on thermocouples instrumented to the surface of the cell. However, for an effective early warning system, the ability to record or detect internal changes of a cell is vital. One technique that may be ideally suited to this is ultrasonic measurement. As part of a European Automobile Manufacturers' Association (ACEA)-funded project, HORIBA MIRA has been collaborating with University College of London (UCL) to explore the use of ultrasound to detect internal changes in a cell to pre-emptively warn about thermal runaway (TR). This article reports on experimental studies aimed at evaluating the application of ultrasonic sensors to detect abuse conditions and early TR signals in battery cells. The changes in acoustic behaviours of battery cells have been monitored and evaluated during temperature-controlled, nail penetration, and overcharge as well as homogeneous and localised heating tests. Finally, ultrasound's ability to capture key events during thermal runaway propagation scenarios has been assessed by triggering TR in a cell of a small prototype module.

近年，バッテリーに関連する事故が頻発し，電気自動車(EV)のリスクと安全性に対する社会的な認識が高まっている。バッテリー管理システム(BMS)に搭載されている安全機能は，セル表面に取り付けられた熱電対に大きく依存している。しかし，効果的な早期警告システムのためにはバッテリーの内部変化を記録・検出する能力が不可欠であり，そのために最適な技術の一つが超音波測定である。欧州自動車工業会(ACEA)が資金提供するプロジェクトの一環として，HORIBA MIRAはロンドン大学(UCL)と共同で，熱暴走(TR)を事前に警告するためにセルの内部変化を検出する超音波の利用法を研究している。本稿では，バッテリーセル内部の異常状態の検出や熱暴走の兆候の早期検出のために超音波センサーを応用した実験研究を報告する。

Introduction

In lithium-ion batteries (LIBs), accidents stem from two broad issues. In the first type, a cell or a battery pack can fail due to mechanical, thermal, or electrical abuse. During mechanical abuse, the two electrodes connect due to nail penetration, fracture of the separator, or deformation of the electrode. When the battery is subject to electrical abuse, such as over-discharge, metallic dendrites (mainly lithium or copper) grow on the anode surface and may penetrate the separator. Thermal abuse occurs when the cells are cycled/stored at excessive temperature, triggering the thermal decomposition of the materials inside the cells.

The second type of safety accident is generally the most feared since it occurs during the seemingly normal operations of the battery. These faults give no clear warning signals and are the most difficult to predict and detect. Such accidents are often due to the presence of internal short circuits (ISCs) caused by foreign metal particles that contaminate the electrode materials during the manufacturing process. These contaminants, in electrochemical contact with the cathode, are oxidized and dissolved into the electrolyte during cycling. They then diffuse and plate on the anode, piercing the separator and causing an ISC (grown-in internal shorts). When a large area ISC is formed, the electric energy is released at a high rate in

that area, rapidly increasing the internal temperature and, possibly, triggering TR. ISC has been the main cause of recalls of automotive LIBs.[1] This class of safety accidents is particularly eared as safety components incorporated in today's lithium-ion cells and battery packs are not effective.

What is Thermal Runaway and Why it is Challenging to Avoid

Both classes of safety accidents can trigger TR. During thermal runaway (Figure 1) the cell temperature increases due to exothermic reactions. In turn, the increased temperature accelerates the decomposition reactions and the system quickly destabilizes. At the end of the TR, temperatures higher than 1000 °C can be reached and high amounts of flammable and harmful gases are released.[2]

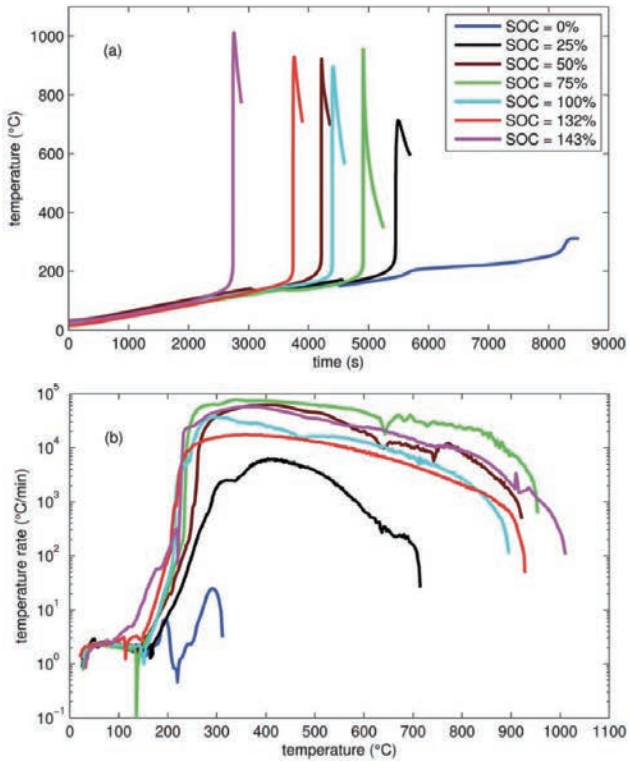

Figure 1 TR induced by thermal ramp experiments on NCA cathode cells at different states of charge.
(a) Cell temperature profiles, (b) Cell temperature rate vs. cell temperature. Adapted from.[2]

If a cell fails in a battery pack it can lead the surrounding cells to also fail, causing a chain reaction within the pack with potentially serious consequences which is known as thermal runaway propagation (TRP). Such an event is particularly scary in the automotive industry where high-capacity cells present in battery pack modules are often spaced less than 1 mm and, in some cases, there might even be direct contact among adjacent cells. In modules with banks of cells in parallel, if one cell experiences an ISC it can act as a short for the entire bank, leading to an external short for the remaining cells.

The BMS is a key safety component of the battery pack as, if properly designed, it can keep the battery pack from operating in unsafe conditions. However, some relevant issues arise when considering its implementation on EV battery packs. Standard BMSs rely on temperature readings from thermocouples located on the surface of the cell which, in the case of large cells, can be very different from the temperature of their centre. The formation of an internal cell temperature gradient can create local gassing and accelerated cell degradation. The cooling system, regardless of its efficiency, has limited efficacy on temperature gradients as it can only cool the cell surface. If not properly considered by the BMS, ageing can also cause cell unbalance which can limit cell capacity, accelerate degradation, or cause electrical abuse of some of the cells. The number of safety-related accidents that have occurred recently indicates that in some cases current BMSs alone can be inadequate.[3][4] For an effective early warning system, the ability to detect internal temperature changes is vital.

Legislation

On the 12th of May 2020, China issued three mandatory standards for EVs safety that relate to the EV battery, the EV itself and electric buses. The battery regulations mandate improved battery system safety regarding thermal diffusion, external fire, mechanical shock, simulated collision, thermal and humidity cycling, external short circuit, overcharge, and over-temperature. In addition, in the case of TR of one cell, no fire or explosion should occur in the cabin for at least 5 minutes, allowing for occupants to escape the vehicle. The battery system is required to notify the vehicle occupants of a thermal incident immediately. More stringent requirements for preventing water ingress, ensuring proper insulation and battery monitoring are also included. Due to their larger battery packs, the new standards for electric buses have more rigorous demands on battery casing collision, charging and water ingress. The standards request for appraisal of the flame-retardant performance, TR prevention and the battery management unit.[5]

To date, there exists a wide variety of battery designs and thermal management strategies across the various EVs. Manufacturers have varied between cylindrical, pouch and prismatic cells with air, water-glycol, or refrigerant-based cooling. As regulations like these are enforced it may well push the industry towards one solution. Emerging technologies like immersion cooling, where the cells are immersed in a flame-retardant dielectric fluid,

may start to take a larger share of the market. Detecting thermal events in vehicles is also a widely unexplored area of the market. Another consideration is how to notify passengers and if an active method of extinguishing the battery pack should be incorporated into the design. Crucially, all the methods have their limitations and it is imperative to avoid false positives and potentially extinguish a battery that is working correctly, as this is often the most expensive component in the vehicle.[5]

Factors of Risk

In current LIBs the cathode chemistry plays a major role with regard to proneness to TR. Transition metal oxides commonly employed as a cathode in LIBs become structurally unstable if their thermal decomposition temperature (TR onset temperature) is reached. The consequent release of the oxygen present in their crystalline structure prompts the combustion of the liquid electrolyte sustaining a rising heating rate that leads the cell to irreversibly enter TR. Among the commercially employed cathode materials, lithium iron phosphate (LFP) presents highest thermal stability. Nickel manganese cobalt oxide 111 (NMC111), has slightly better thermal stability than nickel cobalt aluminium oxide (NCA), which, combined with its good energy density, makes it one of the most widespread cathode materials in current LIBs. The thermal decomposition with associated oxygen release occurs at around 350 °C for LFP, 280 °C for NCA and 300 °C for NMC 111. The thermal stability of the high Ni-content cathodes as NMC 811 drastically decreases, with thermal decomposition starting already at 150 °C in the case of the NMC 811.[6]

The thermal stability of carbonaceous and transition metal oxides is a function of the state of charge (SoC). This becomes particularly evident in the case of overcharge where TR onset temperatures decrease sharply as SoC increases. The onset temperatures of thermal decomposition in overcharged NCA cells can go as low as 65 °C.[6]

Cell design is also crucial for safety. Nanomaterial- level design strategies can allow the usage of thermally unstable materials (Ni-core rich, Mn-shell rich active materials). A crucial design parameter for safety is the capacity load ratio. The anode should be present in slight excess with respect to the cathode to avoid lithium plating due to loss of anode active material during ageing. Kinetics mismatch between anode and cathode must also be avoided and the porosity of the electrodes must be properly implemented.

The geometry of the cell also has some important consequences on safety. Pouch cells are sometimes considered safer since they can freely expand and release pressure. However, safety vents are installed on rigid prismatic and cylindrical cells. The design and size of the vent are critical to ensure suitable pressure management. An important parameter is also the cell size. Larger cells contain more chemical energy, exhibit higher temperature gradients and their cooling is less effective due to the lower surface-to-volume ratio.

Experimental TRP studies have shown that cell spacing, tab connection, vents location/design and thermal barriers are the key parameters to mitigate TRP risks. However, the empirical nature of such tests makes their validity limited to the specific assembly and configuration tested. Small differences in cell designs, cell manufacturing methods and ageing states can severely affect the results of such tests.

Methods to Monitor Battery Packs

Optimal combinations of cell materials, design and advanced BMS strategies can reduce but not eradicate the risk of TR. Thus, it is crucial to develop methods that can promptly detect nascent TR to give the BMS more time to take suitable countermeasures or to passengers to leave the vehicle. Some TR detection methods are presented and schematically illustrated in Table 1:

- Gas/pressure/strain gauge sensors: gas generation starts occurring in the very early stages of TR, regardless of the cell type, chemistry, and format. During overheating, the liquid electrolyte expands, the internal pressure increases, and the gas is vented out of the cell. Gas and pressure sensors were proven to be capable to detect TR onset more quickly than non-embedded temperature sensors and in a stage in which TR can still be impeded if suitable countermeasures are adopted.[9] Each sensor type has its characteristic detection speed, signal clarity and actual deployment feasibility. A combination of different sensors could be instrumented to a cell to correlate each measured signal with the TR onset and the best sensors setup to detect TR identified.
- Other techniques based on self-discharge current detection, cell modelling (equivalent circuits, Kalman filters), consistency analysis of parameters within the battery pack and electrochemical impedance spectroscopy have been successfully implemented and applied to detect ISC or thermal abuse and have good potential to be implemented onboard.[10]-[20]

Table 1 Matrix summarising the TR detection methods listed in this document and their relative pros and cons.

·Detection methods	Advantages	Disadvantages
·Self-discharge measurement	- Simple, quick, and effective in detecting ISC	- Conventional methods to measure self-discharge are time-intensive (typically taking days or even weeks), costly, complex and/or not well-difined - TR triggered by thermal, mechanical, and electrical abuse is not directly detected
·Consistency within the battery pack	- Cheap and easy to implement onboard	- Relies on external temperature readings - Threshold for deviations from normal conditions might cause unacceptably frequent stops and too loose conditions might be ineffective in timely detecting TR
·Multi-sensors	- A suitable combination of different types of sensors can provide an early warning of TR	- Temperature and voltage sensors are not effective to detect TR under certain conditions. Their combination with other sensors increases system cost and complexity - More prone to sensor failure - The interpretation of the sensore's readings might not be so straightforward and false alarms can be generated since gas and pressure increases can occur also during normal battery operation
·Internal short circuit modelling	- Does not require additional sensors onboard (only I, V and T sensors needed)	- Complexity, computational resources - Can be hard to verify/adapt to different cell types
·Impedance spectroscopy	- Can infer the internal temperature of a cell - In the case of certain I, V input signals (i.e. square waves) it can be applied onboard	- Its adaptation and interpretation for different cell chemistries might be cumbersome since the SoC and the ageing of the battery can be difficult to separate from the temperature effect

A Novel Approach: Acoustic Impedance

Ultrasonic testing is a non-destructive technique based on monitoring how ultrasound waves propagate through an object of interest. In industry, ultrasound is typically used to test for cracks within materials, measure thicknesses and monitor corrosion of pipes. Another common use is in underwater range finding (Sonar) in which by measuring the difference in time between the pulse being transmitted and the echo being received, it is possible to determine the distance of an object. In medical imaging, ultrasound is used to visualize muscles, tendons, and many internal organs to capture their size, structure and any pathological lesion with real-time tomographic images. The technology is relatively inexpensive and portable, especially when compared with other techniques, such as magnetic resonance imaging and computed tomography. Recently, ultrasound is gaining attention for the study of electrochemical devices.[21]-[23] The main advantages of this technique are that it is non- destructive, can be conducted operando, it is relatively cheap, and measurements are very quick, taking only microseconds to complete.

Working Principle and Potential for Monitoring Batteries Safety

In the battery test bench used for acoustic analysis, a cell equipped with an ultrasonic transducer and a thermocouple is placed inside a thermal chamber and connected to an external battery cycler and an ultrasonic multiplexer which generates and record the electrical and acoustic signals. When conducting an ultrasonic measurement, a very short ultrasonic pulse wave is generated by a piezoelectric transducer. The signal then travels through the object of interest and the wavefront is a influenced by the properties of the object's component materials. The signal is then either received by a second transducer on the other side of the object (Transmission) or the reflected waves are received by the same transducer that generated them (Pulse Echo). An important acoustic wave property is the time of flight (ToF) which is the time taken for the generated wave to travel through the object and is affected by the speed of sound through the material through which it propagates.

Typical waveforms obtained for pulse-echo mode and transmission set-ups performed on the same cell are shown in Figure 2.[30] In pulse-echo mode Figure 2a, the initial signal at a ToF below 1 µs is due to the generation of the initial ultrasonic pulse and is not influenced by the cell under study. The peaks at ToF values higher than 1 µs are reflection peaks related to the internal structure and the interfaces present within the cell. Acoustic peaks corresponding to higher ToFs reflect the properties of interfaces located farther from the acoustic emitting device. The amplitude of these internal reflection peaks decreases steadily with penetration depth due to signal attenuation and reflection in previous layers. At ca 8.7 µs a peak with a slightly higher amplitude is observed. This is referred to as the first echo peak and corresponds to the part of the ultrasonic signal that has travelled all the way through the cell and hit the back case. Due to the large difference in acoustic impedance between the cell and the external air, nearly all the signal is reflected resulting in the slightly higher amplitude observed. In the transmission set-up (Figure 2b) a strong peak is observed at a ToF approximately half of that observed for the pulse-echo experiments. The strong multiple peaks observed at lower ToFs in pulse-echo mode are no longer observed as these are due to reflections from the internal layers within the cell.

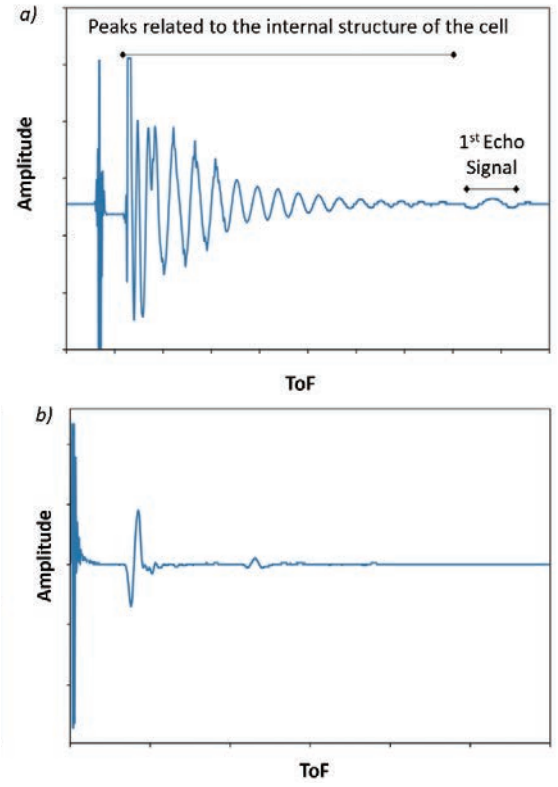

Figure 2 Typical acoustic waveform generated from a) pulse- echo mode and b) transmission mode setups. Adapted from.[30]

LIBs present a typical layered structure in which the anode is constructed of a carbon material supported on a copper current collector, the cathode consists of an active material, typically a metal oxide such as NCA or NMC supported on an aluminium current collector, and a separator which ensures that no direct contact is made between the anode and the cathode. Such layers are then wrapped together to form the so-called jelly roll. All components in the pouch cell are soaked in an electrolyte solution which acts as an acoustic couplant between different layers and allows the acoustic signal to travel through the cell. When an ultrasound waveform is generated by the transducer placed on the surface of the cell, the wavefront travels through the cell. At every material interface, some of the signal is transmitted and some is reflected back towards the transducer. The percentage reflected and transmitted is dependent on the difference between the acoustic impedance of the two materials. As the material properties change with cycling, the speed of sound through the materials will also be affected resulting in a shift in peak's ToFs. In addition, the electrode layers expand and contract as lithium ions move, also resulting in shifts in peak's ToFs.

The capability of acoustic waves to unveil information about internal interfaces and material properties of batteries has recently led to initial studies in which ultrasound and acoustic sensors have been employed to estimate SoC and state of health (SoH),[22]-[27] but only few have reported the use of acoustic measurements to monitor abuse testing of LIBs.[28] For the interested reader, the experimental studies here reported have been published in specialised scientific journals.[29][30]

Experimental Work Between HORIBA MIRA and UCL

This study aimed to assess the practical capability of acoustic-based techniques to promptly inform about abusive operating conditions occurring within battery cells. It explored the method's potential to be effectively employed in real-world applications as an early TR detection method, benchmarking it against currently employed sensors such as thermocouples and voltage sensors. A broad range of techniques for inducing TR (including nail penetration, overcharge as well as uniform and localised heating) was tested on several 210 mAh pouch cells based on a lithium cobalt oxide cathode (LCO) and a graphite anode. The acoustic measurements were compared with voltage and temperature readings and X-ray radiography was employed to give further physical insight and support findings from acoustic measurements. The TRP through a small module of cells was investigated with the use of multiple transducers.

Results

Internal Temperature

To determine how the temperature of the cell affects the waveform generated by ultrasonic analysis, a 210 mAh pouch cell was set up in an environmental chamber and the acoustic signal was monitored as the temperature was varied.[30] Figure 3a shows a plot of how the temperature was altered with time . To investigate the cell behaviour in mildly abusive conditions, the temperature was varied beyond the window temperature assigned by cell manufacturers (0-40 °C). A colourmap plot of how the acoustic signal changes during this period is shown in Figure 4b. This plot is effectively a top-down view of how the typical signal varies with temperature. Each line shows a peak, with the colour indicating the amplitude and its position in the y-direction indicating the ToF.

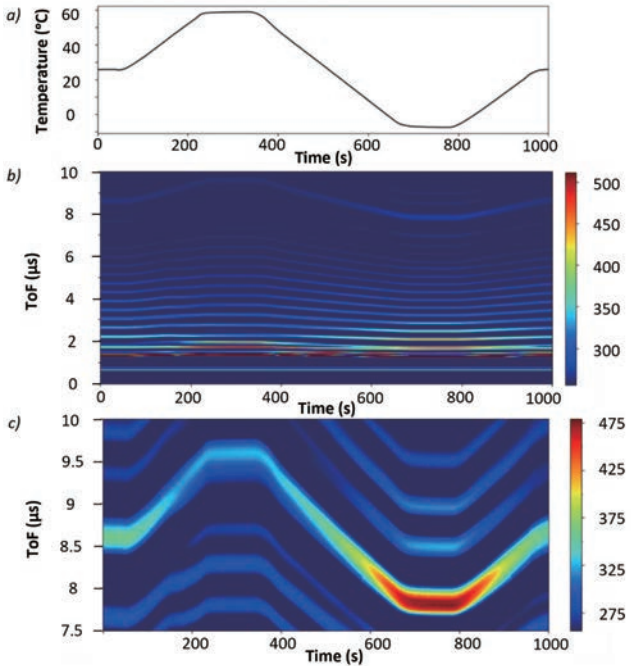

Figure 3 (a) A plot of how cell temperature varied over the course of the experiment. (b) A colourmap plot showing how the received acoustic waveform varied over the course of the temperature experiment. (c) A colourmap plot of how the first echo peak varies as the temperature is varied over the duration of the experiment. Adapted from.[30]

As the temperature is initially held constant, no variation in amplitude or ToF is observed with any peak. During heating the ToF of each peak increased due to the individual anode and cathode layers expansion, causing the entire cell to swell accordingly. The effect becomes more pronounced as the ToF of the peak increases since for reflections from deeper interfaces the signal must travel farther through the changing battery materials and the effects are increased. As the cell is cooled the changes are reversed due to the contracting of the cell, while the amplitude of all peaks increases. The first echo peak, located at 8.75 µs, shows the largest shift in ToF with temperature.

For the temperature to be accurately predicted using the acoustic techniques, an understanding of how the SoC of the cell affects the relationship is required. To investigate this, the previous experiment was repeated at various SoCs and the results are summarised in Figure 4.[30] For all SoCs, a linear relationship between the first echo peak's ToF and the temperature is observed, with a similar gradient between 0 and 50 °C, which allows to easily measure the internal temperature of a given cell. At higher and lower temperatures, the correlation deviates from linearity suggesting cell ageing/damage. This damage is likely due to taking the cell outside of the manufacturer's temperature specifications. Small deviations from the predicted linear relationship between ToF and temperature could then be used to detect and measure the extent of cell damage. This may represent a powerful tool for predicting the onset of irreversible cell degradation and TR.

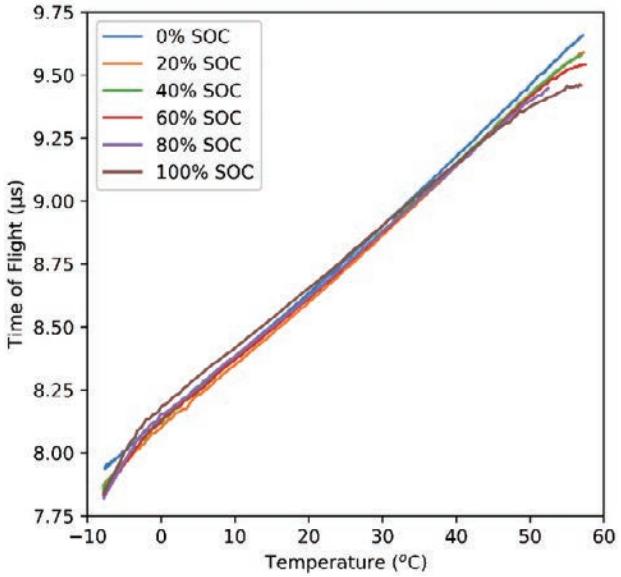

Figure 4 The variation of ToF of the first echo peak at various SOCs. Adapted from.[30]

For the applicability of ultrasound in automotive, the technique must apply to a wide range of cell geometries and capacities. As a proof of concept to show the flexibility of the technique, a range of cell geometries and capacities from a range of manufacturers were also tested. Tests on a 400 mAh cell with same cell chemistry and construction techniques from the same manufacturer and on a 20 Ah A123 pouch cell using both through-transmission and pulse-echo experiments gave consistent results with higher ToFs than the 210 mAh cell as would be expected.

The effect of the cell geometry was also explored via cylindrical cell testing in pulse-echo and transmission mode. Pulse-echo measurements did not prove successful with no repeatable readings obtained whereas tests in transmission mode did prove successful. Transducers were set up at 180º configuration. It was also found that if the transmit and receive transducers are not aligned (180º set-up) and instead are placed with a slight angle between them, the obtained results vary. The propagation of lamb waves around the outer can of the cylindrical cell results in two additional wavelets that appear in the waveform. Depending on the angle of the receiver transducer relative to the transmission transducer the ToF of these lamb waves is altered. This feature shows the potential to detect can swelling as well as surface defect formation by monitoring how the two lamb waves behave.[29]

Detection of Internal Defects

To determine the ability of acoustics to detect any defects that may be present in cells or formed during operation/abuse, acoustic tests were run on two 400 mAh pouch. One of the cells was unused whereas the other had been cycled multiple times during which a sudden failure had occurred. Typical waveforms obtained from transmission experiments for both the 'good' and 'defective' cell are shown in Figure 5.[29]

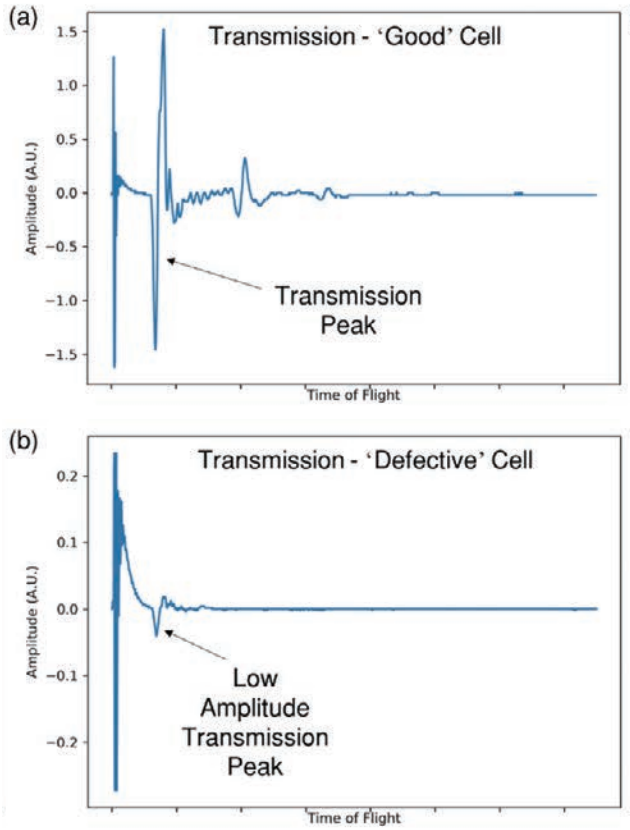

Figure 5 The difference in transmission results for a 'good' 400 mAh cell (a) and a 'defective' cell (b). Adapted from.[29]

The 'good' cell shows a high amplitude transmission peak (Figure 5a) whereas the 'defective' cell also shows the transmission peak at the same ToF but the amplitude has dropped significantly. These results suggest the presence of a defect since the formation of any gases or defect would inhibit good acoustic contact between the electrode layers. To investigate this, the defective cell was studied using X-ray computed tomography.[29] Figure 6 shows visible layer separation at 160 µm. These tests show that even small defects can lead to significant changes in the acoustic signal.

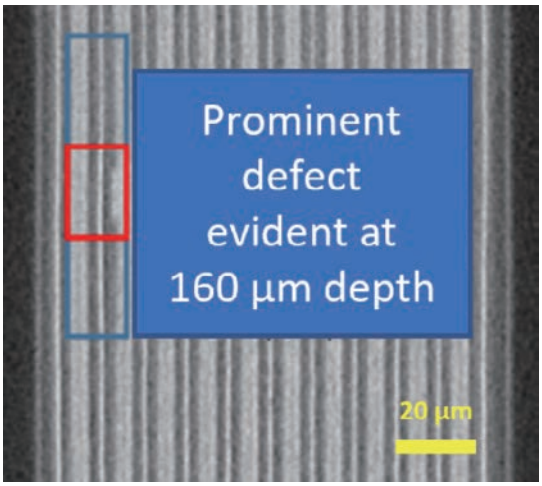

Figure 6 X-ray computed tomography results showing the internal structure of the 'defective' 400 mAh cell shows the prominent defect.. Adapted from.[29]

Thermal Runaway Studies at Cell Level

To acoustically monitor TR in individual cells and its propagation through a module or pack consisting of multiple cells, a method for triggering TR which is reliable, repeatable, and representative of EVs in real- world applications is required. Several methods were tested with a focus on those that would most closely replicate a TR event triggered by an ISC.

The first method tested was nail penetration. Nail penetration is generally regarded as the industry standard test for replication of ISCs. For internal shorts, the highest rates of reaction and largest temperature increases are expected to occur around the nail. Thus, the surface temperature of the cell is not representative of the higher temperatures within the cell. To assess the ability of ultrasound to measure the extent of damage that occurs during TR, several tests were conducted with the chosen cell, a 210 mAh LCO pouch cell, at various SoCs under the assumption that a higher SoC would release more energy during failure and cause more damage. The results showed a sudden loss of acoustic signal in all tests regardless of the SoC of the cell or the amount of damage induced, proving its high sensitivity to the structural damage caused by a nail penetration in the cell.

Another method for inducing TR is by overcharge. Overcharge of LIBs in constant current mode can lead to rapid temperature increase and eventually induce TR. For these tests, C-rates significantly above those recommended by the manufacturer's specification were chosen. A fully charged cell (4.2 V) was overcharged at 10 C followed by 20 C while acoustic measurements were conducted. A strong influence on the acoustic signal was observed. However, the complex nature of the processes occurring within the cell made this technique unsuitable as a method of triggering TR. The overcharge tests did

however suggest that the acoustic methodology could be useful for understanding the process occurring within the cell during overcharge.

Thermally-induced TR, i.e. TR triggered by heating the cell until it fails, is one of the simplest methods for inducing cell failure. To study the ability of acoustic sensors to monitor thermally-induced TR, a cell with a transducer attached was heated between two heating plates. While repeatable and consistent acoustic signals were observed for cells operating under normal conditions, when the cells were pushed outside these limits toward dangerous temperatures, clear changes in acoustic signals were visible. At lower temperatures, additional peaks were observed indicating the presence of additional interfaces within the cell as thermal damage occurs. When the temperature increased further, the ToF of the first echo peak shifted quite drastically before disappearing completely at ca. 100 °C, when the electrolyte likely evaporated. Importantly all these distinct and measurable changes occurred long before the cell entered irreversible TR.

Thermally-induced TR was proved to be a useful method for inducing TR. However, homogeneous heating of the cell is less representative of the type of thermal abuse that would likely occur in a real-world application caused by an ISC, where higher thermal gradients would be more localised within the cell. To make the tests more representative, a heating cartridge was used to heat a small area of the cell to represent the area where a short is occurring. A fully charged cell was heated from the bottom of the cell with a heating cartridge, while an acoustic transducer was placed on the top of the cell. The results of the experiment showed that the voltage remained relatively consistent until the cell entered TR, proving that monitoring cell voltage does not reveal damaging processes occurring within the cell. Over the first 150 seconds, while there was little to no change observed in the temperature recorded by the thermocouple placed on the top of the cell by the transducer, significant changes in the acoustic signal were observed. The echo peak (close to the heating cartridge) was the first peak to disappear, followed sequentially by peaks at lower ToFs, about 500 seconds before the cell entered TR. Importantly, readings from the thermocouples only showed a mild temperature rise throughout.

Thermal Runaway Propagation at Module Level

For higher power operations battery modules or packs are often used, in which multiple cells are connected in series to provide higher voltages and in parallel to provide higher currents (Figure 7).

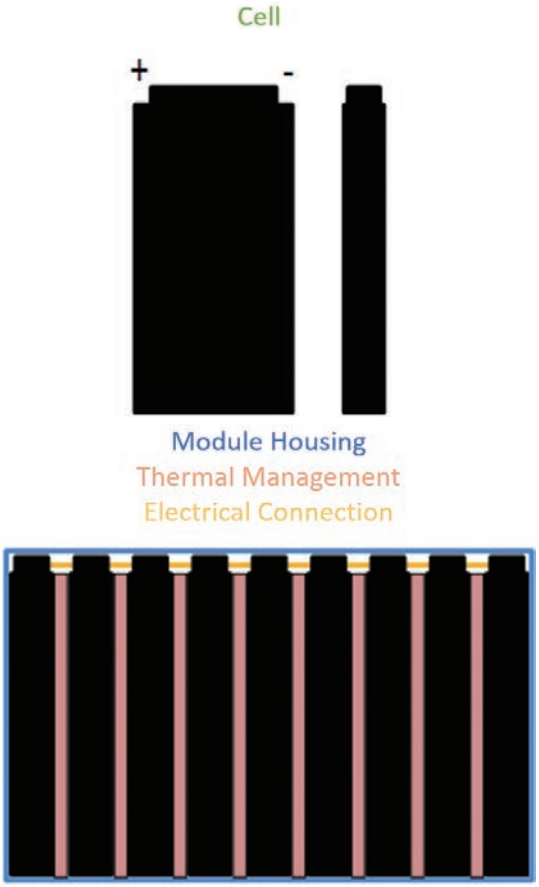

Figure 7 Single-cell and multiple cells assembled in the module configuration.

Understanding the operation of these packs and the inherent risks is of vital importance. Failure of a single cell can easily trigger the rapid heating and consequential failure of neighbouring cells causing a thermal propagation chain reaction.

To study the effectiveness of the ultrasonic technique in pack applications, a small four-cell demonstration module was constructed. Each of the four cells was placed side by side and connected in parallel with a transducer placed on the surface of each of the cells. Thermocouples were placed on the top and bottom of each cell to monitor the temperature of each cell and the thermal gradient from the top of the cell to the bottom.

To determine the expected variation in acoustic signal during normal operation the pack was first left at rest or 15 min before being discharged at 1 C, then immediately charged again at 1 C. All cells exhibited similar acoustic signatures, with changes in the acoustic signals which were measurable but not significant compared to the changes observed in the TR tests.

The four-cell module was then subjected to an abuse test (Figure 8). A heating cartridge was placed on the underside of Cell 4 to trigger localised damage followed by TR. Initially, all cells were held at room temperature for ca.

400 seconds. Then, the heating cartridge in contact with the base of Cell 4 was switched on. All cells were supported on a heat-proof mat with the heating cartridge only in contact with Cell 4. The results from this test are summarised in Figure 9, with the acoustic behaviour of the cells shown along with the temperature of the bottom of each cell.

During rest at room temperature, no shift in any of the acoustic signals is observed. As soon as the localised heating on Cell 4 is initiated, the acoustic signal of this cell begins to change. For clarity, the change in ToF of the first echo peak has been plotted for all cells in Figure 10 and compared to the temperature of the top and bottom of the cell. During heating, the ToF of the first echo peak of Cell 4 rapidly increases beyond any change that would be expected under normal operation.

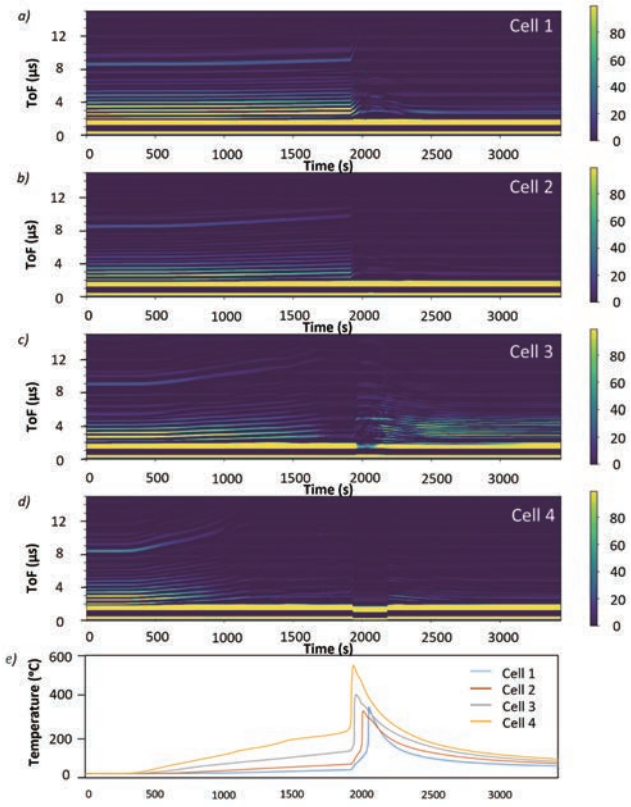

Figure 8 The propagation of thermal failure through a four-cell pack. The acoustic behaviour of Cell 1 (a), Cell 2 (b), Cell 3 (c) and the thermally abused Cell 4 (d) are shown as well as the temperature of the bottom of each cell (e).

After ca. 1000 seconds, the peak amplitude drops and the signal is lost. Meanwhile, the top of the cell is at 70 °C and the bottom at 117 °C, sufficient for electrolyte evaporation. At this point, the acoustic signal has indicated that a significant thermal event and/or damage has occurred to Cell 4. The cell, however, is heated for a further 900 seconds (15 minutes) before it enters TR. The ToF of the first echo peak in Cell 3 also begins to shift as soon as the heating of Cell 4 begins, albeit at a slower rate. After 1400 seconds, 400 seconds slower than Cell 4, the amplitude of the first echo peak in Cell 3 is also lost. The temperature at the bottom of the cell is ca. 100 °C at this point. As Cell 4 enters TR, the heat produced also causes Cell 3 to rapidly heat and enter TR. Cell 2 and Cell 1 also follow similar dynamics although at slower rates due to their farther location from the cell that first undergoes TR. However, the ToF of the first echo peak remains visible until the cells enter TR, suggesting they were still relatively undamaged until the flames coming from the other cells reached them.

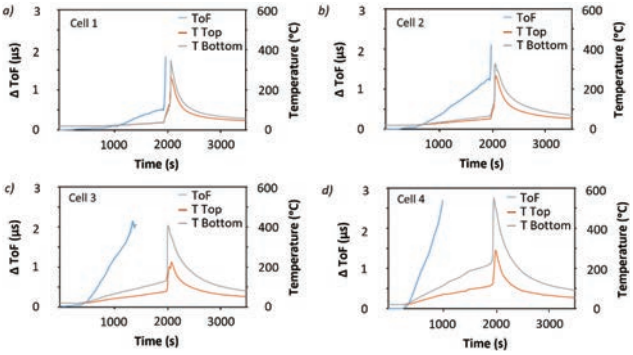

Figure 9 The temperature and ToF variation of the module cells (a) Cell 1, (b) Cell 2, (c) Cell3, (d) Cell 4.

Since the change in ToF of the first echo peak can be both measured using acoustics and predicted based on thermocouple measurements, a potential method to detect unexpected heating or damage is to look for any changes in ToF that are unexpected based on thermocouple readings. To explore this, the ToF of the first echo peak was tracked and the predicted ToF change calculated based on a thermocouple measurement. The predicted value was then subtracted from the measured one. When the cell was operated in normal conditions a value of zero was returned. Conversely, when any change in temperature that wasn't measured by the thermocouple occurred, the predicted and measured values differed, resulting in a deviation from zero. This deviation indicated that a temperature shift not recorded by the top thermocouple was occurring. This type of measurement seems promising to detect any internal temperature changes, such as those caused by ISCs.

Repeatability and Susceptibility to False Positives

For this technology to be implemented in a BMS, the measurements must be robust, repeatable, and not susceptible to false positives. While more work needs to be done before the acoustic temperature measurement technique can be employed commercially, initial results are promising. All tests reported in this study show consistent results with similar acoustic behaviours observed in all TR experiments. The acoustic waveform observed is consistent from cell to cell and the changes observed during

failure are significantly larger than any changes observed in normal use, as shown in Figure 10. The cell to cell variation under normal operation (cycling at the cell's max C rate) is significantly smaller than the changes observed for all cells in the module tested. The point at which each cell reached 60 °C, the cell's maximum working temperature, is also marked on the plot and demonstrates that, based on acoustic readings, an indication of an issue with each cell would have been recorded long before the cell entered an irreversible self-heating process or TR.

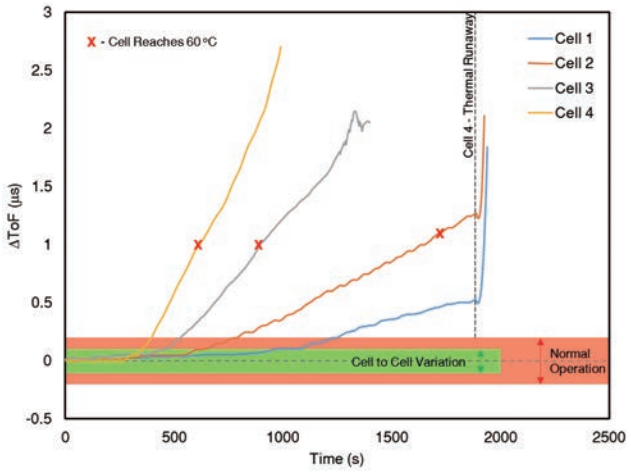

Figure 10 The changes in ToF for each peak relative to cell-to- cell variation and changes in ToF during regular operation.

Conclusions and Further Research

This study demonstrated the ability of ultrasound measurements to accurately monitor the internal temperature of a cell, detect rapid heating and indicate when a cell is about to enter TR well before conventional methods based on voltage and temperature readings. In the module setup, the acoustic signature of the first echo pulse is lost is ca. 900 seconds before the cell enters TR. It was shown that ultrasonic testing can be used to probe virtually all types of batteries. A range of techniques for inducing TR was tested. The significant structural damage caused by a nail penetration experiment instantly causes a loss in acoustic signal due to the gaps appearing between layers and stopping acoustic transmission. Thermally-induced heating of the cell proved to be the most effective and reproducible method for inducing cell failure. The changes in ToF of the first echo peak correlate with cell temperature and give a clear indication of when a cell is heating. In these tests the electrolyte evaporation resulted in a loss of acoustic signal, providing a clear indication that significant cell heating and damage were occurring. To replicate more representatively real-world applications, the thermally induced TR experiments were repeated by heating only a small area of the cell. These tests showed that the technique could detect internal temperature changes long before the thermocouples placed on the surface of the cell. With the use of multiple transducers, it was also possible to detect the propagation of TR through a small module of cells. Indications that the cells were reaching dangerous temperatures were evident from acoustic measurements long before the first cell failed triggering a chain reaction through the pack and causing all cells to fail. Finally, acoustic measurements were proven to be particularly reliable, delivering consistent acoustic signals across different cells and significantly larger ToF changes than any observed in normal use in the case of abuse conditions.

From the results here presented, a short-term application could be to include ultrasonic monitoring as part of HORIBA MIRA's abuse testing approach to provide real-time access to internal states of the cell as well as more informative data and consultancy on test outcomes. With regards to onboard battery pack applications, while these results are very encouraging, there is a long way to go before "smart" batteries (i.e. containing an ultrasonic diagnostic system) can be commercially manufactured. To take the technology forward on the journey to mass-production, more comprehensive ultrasonic tests on a wide variety of batteries (encompassing the complete spectrum of battery types), looking across the complete range of operational variables (temperature, age, charging history, battery construction, etc) shall be performed. All tests will need to be repeated multiple times to statistically have confidence that the ultrasonic data can reliably show the condition of the battery. A cost-effective integrated ultrasonic transducer system including transducers, electrical connectivity, transducer drive electronics and signal analysis will need to be developed for each class of cell/battery.

Finally, an analysis needs to be made as to what proportion of cells within the battery pack needs to be monitored. A battery-analysis system that relied on a few cells within the pack being ultrasonically active would significantly reduce costs and greatly simplify the system connectivity. With this regard, a promising technique currently under investigation at UCL for monitoring electrochemical devices is acoustic emission. While the techniques discussed thus far rely on the generation of an ultrasonic pulse to probe the device and another, or the same transducer, to receive the altered acoustic signal, emission uses a single transducer to 'listen' for any sounds generated by the cell itself. In the typical setup used for an acoustic emission experiment, an acoustic emission sensor, effectively a transducer similar to those used for ultrasound testing, is placed on the cell of interest and sounds generated by the cell are monitored. This approach presents several advantages for battery pack

monitoring where it has the potential to sensibly reduce costs and system complexity.

Acknowledgments

The authors would like to acknowledge the European Automobile Manufacturers' Association (ACEA) for support in funding the experimental work here presented.

* Editorial note: This content is based on HORIBA's investigation at the year of issue unless otherwise stated.

References

[1] Q. Wang, B. Mao, S. I. Stoliarov, and J. Sun, "A review of lithium ion battery failure mechanisms and fire prevention strategies," Prog. Energy Combust. Sci., vol. 73, pp. 95-131, Jul. 2019.

[2] A. W. Golubkov et al., "Thermal runaway of commercial 18650 Li-ion batteries with LFP and NCA cathodes - Impact of state of charge and overcharge," RSC Adv., vol. 5, no. 70, pp. 57171-57186, 2015.

[3] Faiz Siddiqui, "A Tesla Model S erupted 'like a flamethrower.' It renewed old safety concerns about the trailblazing sedans," The Washington Post, 2020.

[4] Heekyong Yang, "Kona EV owners say Hyundai mishandling recall for battery fires," Reuters, 2020.

[5] James Edmondson, "China to Enforce Electric Vehicle Safety by 2021," 2020. [Online]. Available: https://www.idtechex.com/en/research- article/china-to-enforce-electric-vehicle-safety-by-2021/20707.

[6] M. Braglia, "Thermal Runaway and Thermal Propagation Detection," 2019.

[7] C. Mikolajczak, K. White, M. Kahn, and R. T. Long, Lithium-Ion Batteries Hazard and Use Assessment. SpringerBriefs in Fire, 2013.

[8] J. Garche and K. Brandt, Eds., Electrochemical Power Sources: Fundamentals, Systems, and Applications Li-Battery Safety. Elsevier, 2019.

[9] S. Koch, K. Birke, and R. Kuhn, "Fast Thermal Runaway Detection for Lithium-Ion Cells in Large Scale Traction Batteries," Batteries, vol. 4, no. 2, p. 16, 2018.

[10] X. Feng, C. Weng, M. Ouyang, and J. Sun, "Online internal short circuit detection for a large format lithium ion battery," Appl. Energy, vol. 161, pp. 168-180, 2016.

[11] C. Wu, C. Zhu, Y. Ge, and Y. Zhao, "A diagnosis approach for typical faults of lithium-ion battery based on extended Kalman filter," Int. J. Electrochem. Sci., vol. 11, no. 6, pp. 5289-5301, 2016.

[12] N. S. Spinner, C. T. Love, and S. G. Rose-Pehrsson, Susan L. Tuttle, "Expanding the Operational Limits of the Single-Point Impedance Diagnostic for Internal Temperature Monitoring of Lithium-ion Batteries," Electrochim. Acta, vol. 174, pp. 488-493, 2015.

[13] Z. Liao, S. Zhang, K. Li, G. Zhang, and T. G. Habetler, "A survey of methods for monitoring and detecting thermal runaway of lithium-ion batteries," J. Power Sources, vol. 436, no. June 2019, p. 226879, 2019.

[14] L. H. J. Raijmakers, D. L. Danilov, J. P. M. Van Lammeren, M. J. G. Lammers, and P. H. L. Notten, "Sensorless battery temperature measurements based on electrochemical impedance spectroscopy," J. Power Sources, vol. 247, pp. 539-544, 2014.

[15] L. H. J. Raijmakers, D. L. Danilov, J. P. M. Van Lammeren, T. J. G. Lammers, H. J. Bergveld, and P. H. L. Notten, "Non-Zero Intercept Frequency: An Accurate Method to Determine the Integral Temperature of Li-Ion Batteries," IEEE Trans. Ind. Electron., vol. 63, no. 5, pp. 3168- 3178, 2016.

[16] R. Srinivasan, P. A. Demirev, and B. G. Carkhuff, "Rapid monitoring of impedance phase shifts in lithium-ion batteries for hazard prevention," J. Power Sources, vol. 405, no. September, pp. 30-36, 2018.

[17] R. Srinivasan, B. G. Carkhuff, M. H. Butler, and A. C. Baisden, "Instantaneous measurement of the internal temperature in lithium-ion rechargeable cells," Electrochim. Acta, vol. 56, no. 17, pp. 6198-6204, 2011.

[18] B. G. Carkhuff, P. A. Demirev, and R. Srinivasan, "Impedance-Based Battery Management System for Safety Monitoring of Lithium-Ion Batteries," IEEE Trans. Ind. Electron., vol. 65, no. 8, pp. 6497-6504, 2018.

[19] R. Schwarz, K. Semmler, M. Wenger, V. R. H. Lorentz, and M. Marz, "Sensorless battery cell temperature estimation circuit for enhanced safety in battery systems," IECON 2015 - 41st Annu. Conf. IEEE Ind.

Electron. Soc., pp. 1536-1541, 2015.
[20] J. P. Schmidt, S. Arnold, A. Loges, D. Werner, T. Wetzel, and E. Ivers-Tiffée, "Measurement of the internal cell temperature via impedance : Evaluation and application of a new method," J. Power Sources, vol. 243, pp. 110-117, 2013.
[21] Y. S. Chou, N. Y. Hsu, K. T. Jeng, K. H. Chen, and S. C. Yen, "A novel ultrasonic velocity sensing approach to monitoring state of charge of vanadium redox flow battery," Appl. Energy, vol. 182, pp. 253-259, 2016.
[22] B. Sood, C. Hendricks, M. Osterman, and M. Pecht, "Health monitoring of lithium-ion batteries," Electron. Device Fail. Anal., vol. 16, no. 2, pp. 4-16, 2014.
[23] A. G. Hsieh et al., "Electrochemical-acoustic time of flight: In operando correlation of physical dynamics with battery charge and health," Energy Environ. Sci., vol. 8, no. 5, pp. 1569-1577, 2015.
[24] S. Bhadra, A. G. Hsieh, M. J. Wang, B. J. Hertzberg, and D. A. Steingart, "Anode Characterization in Zinc-Manganese Dioxide AA Alkaline Batteries Using Electrochemical-Acoustic Time-of-Flight Analysis," J. Electrochem. Soc., vol. 163, no. 6, pp. A1050-A1056, 2016.
[25] G. Davies et al., "State of Charge and State of Health Estimation Using Electrochemical Acoustic Time of Flight Analysis," J. Electrochem. Soc., vol. 164, no. 12, pp. A2746-A2755, Sep. 2017.
[26] L. Gold et al., "Probing lithium-ion batteries' state-of-charge using ultrasonic transmission - Concept and laboratory testing," J. Power Sources, vol. 343, pp. 536-544, 2017.
[27] P. Ladpli, F. Kopsaftopoulos, R. Nardari, and F.-K. Chang, "Battery charge and health state monitoring via ultrasonic guided-wave-based methods using built-in piezoelectric transducers," Smart Mater. Nondestruct. Eval. Energy Syst. 2017, vol. 10171, no. March, p. 1017108, 2017.
[28] Y. Wu, Y. Wang, W. K. C. Yung, and M. Pecht, "Ultrasonic Health Monitoring of Lithium-Ion Batteries," Electronics, vol. 8, no. 7, p. 751, 2019.
[29] J. B. Robinson et al., "Identifying Defects in Li-Ion Cells Using Ultrasound Acoustic Measurements," J. Electrochem. Soc., vol. 167, no. 9626352, 2020.
[30] R. E. Owen et al., "Operando Ultrasonic Monitoring of Lithium-Ion Battery Temperature and Behaviour at Different Cycling Rates and under Drive Cycle Conditions," J. Electrochem. Soc., vol. 169, 2022.

Michele Braglia
ミシェル ブラグリア
Energy Systems Innovation Lead
Mobility Innovation Hub
HORIBA MIRA

Richard Stocker
リチャード ストッカー
Principal Engineer (Battery Solutions)
HORIBA US,
Mobility Innovation Hub
HORIBA MIRA

Materials Analysis of SOFC/SOEC Stack's Components using HORIBA's Scientific Instruments

HORIBAの科学機器によるSOFC/SOECスタック構成部材の材料分析

Guillaume KESSLER
ギオーム ケスリ

This article summarises measurements done on Solid Oxide Fuel Cell (SOFC)/Solid Oxide Electrolysis Cell (SOEC) in HORIBA application lab using inhouse scientific instruments. It also gives an analysis of SOFC and SOEC market trend in testing, and summarises insights from research literature. The focus of this review was introducing materials analysis in SOFC/SOEC sector and explaining application of HORIBA's scientific instruments in this sector. It was highlighted that SOFC/SOEC markets not only needs materials analysis at the R&D step, but also along the production line. This includes measurements from the preparation of raw materials to in-line quality control and post-mortem analysis. HORIBA can provide scientific instruments to make a large number of these measurements. These measurements will help to improve SOFC/SOEC cells, stacks and systems performance and durability, which can be determined with HORIBA test stations and Balance of Plants.

HORIBAの科学機器を使用したアプリケーションラボでの測定結果，文献，固体酸化物形燃料電池(SOFC)/固体酸化物形電解槽(SOEC)の市場動向に関するHORIBAの分析結果をまとめて紹介する。このレビューの焦点はSOFC/SOEC分野における材料分析の紹介と，HORIBAの科学機器の応用について説明する。SOFC/SOEC市場では，研究開発段階での材料分析だけでなく，生産ラインでの材料分析も必要であることが強調された。これには原材料の準備からインラインの品質管理，事後分析までの測定が含まれる。HORIBAはこれらの測定を数多く行うための科学機器を提供することができ，これらの測定はSOFCセル，スタック，システムの性能と耐久性の向上に役立ち，HORIBAのテストステーションやBalance of Plantsで判定することが可能である。

Introduction

Due to climate change, Alternative Energy Solutions (AES) are under investigation to decarbonize societies. Among these solutions, fuel cells and electrolysis cells are considered as promising solutions to participate in the energy transition. Fuel cells (Solid Oxide Fuel Cell, Proton Exchange Membrane Fuel Cell…) convert certain fuels into electricity via an electrochemical reaction. Electrolysis cells (Solid Oxide Electrolysis Cell, Proton Exchange Membrane Electrolysis Cell, Alkaline Electrolysis Cell, Anion Exchange Membrane Electrolysis Cells…) convert electricity and certain fuels into other fuels (Figure 2, for SOFC and SOEC).

Fuel cells are promising because they can use renewable fuels such as Green Hydrogen, and their fuel to electricity efficiencies are higher than many energy systems such as gas turbine, Steam turbine and Diesel engine.[2] Many technologies of fuel cells exist, they are summarised in Table 1.

Electrolysers are promising because they can produce Hydrogen from water and electricity by emitting less CO_2 than the conventional steam-methane reforming process.[3] Also, electrolysers can produce synthetic fuels from non-fossil energy sources: CO_2 and H_2O.[4] Alkaline Electrolysis Cell (AEC), Proton Exchange Membrane Electrolysis Cell (PEMEC), Solid Oxide Electrolysis Cell (SOEC) and Anion Exchange Membrane Electrolysis Cell (AEMEC) are the four types of electrolyser technologies that are used today.

Table 1 Fuel Cell technologies.[2]

Type of fuel cell	Electrolyte	Operating Temperature	Fuel	Oxidant	Electrical Efficiency	Application
PEM (Proton Exchange Membrane)	Polymer: proton exchange membrane	50-80°C	Pure Hydrogen produced from hydrocarbons, melthanol or electrolysis	O_2/Air	40-50%	Transportation, H2 production.
AFC (Alkaline Fuel Cell)	Potassium hydroxide (KOH)	50-200°C	Pure Hydrogen or hydrazine liquid or methanol	O_2/Air	50-55%	Stationary (Apollo).
AEM (Anion Exchange Membrane)	Polymer	25-70°C	Hydrogen, methanol, maybe other alcohols and N-fuels (research)	O_2/Air	60%	Transportation, H2 production.
PAFC (Phosphoric Acid Fuel Cell)	Phosphoric Acid	160-210°C	Hydrogen produced from hydrocarbons or methanol	O_2/Air	40-50%	Stationary 100-400kW, Heavy duty, Air-independent propulsion (submarine)
MCFC (Molten Carbonate Fuel Cell)	Molten salts such as NO_3, SO_4, and CO_3	630-650°C	Hydrogen, CO, natural gas, propane, marine diesel	CO_2/O_2/Air	50-60%	Stationary
DMFC (Direct Methanol Fuel Cell)	Polymer	60-200°C	Liquid methanol	O_2/Air	40-55%	Power for man-portable tactical equipment, Battery chargers, and Autonomous power for test and training instrumentation
SOFC (Solid Oxide Fuel Cell)	Ceramic such as YSZ or CGO	600-1000°C	Hydrogen, natural gas or propane	O_2/Air	45-70%	Stationary, H2 production, CHP, Integrated coal gasification sysems, Integrated steam turbines, Electric vehicles (APU)

Components of a SOFC/SOEC Stack

Fuel Cells and Electrolysis Cells technologies differ in the materials used to make them. These technologies (Table 1) are not necessarily in direct competition; they can have different applications. This article focuses on the Solid Oxide Fuel Cell (SOFC) and Solid Oxide Electrolysis Cell (SOEC) technologies which are publicly known as High temperature Fuel Cell and High temperature Electrolysis Cell. When these technologies are used, they are part of a system made of a stack and auxiliaries. A stack is made of cells (fuel cells or electrolysis cells), stacked together with interconnectors, glass sealings, end plates and compression rods (not shown) (Figure 1). Interconnectors conduct gases through the stack and connect electrically cells together. Glass sealings seal gases compartment (H_2/air, H_2/atmosphere, and O_2/atmosphere compartments). End plates participate in the compression of the stack, provide electrical insulation between adjacent cells, and enable the stack to be connected to gases and electricity. Compression rods maintain the stack compressed. Depending on the kind of Solid Oxide Cells used (High temperature, Intermediate temperature, Low temperature), SOFC and SOEC stacks use different materials for the cathode, electrolyte, anode, and interconnectors. The most common materials used in SOFC stacks are listed in Table 2.

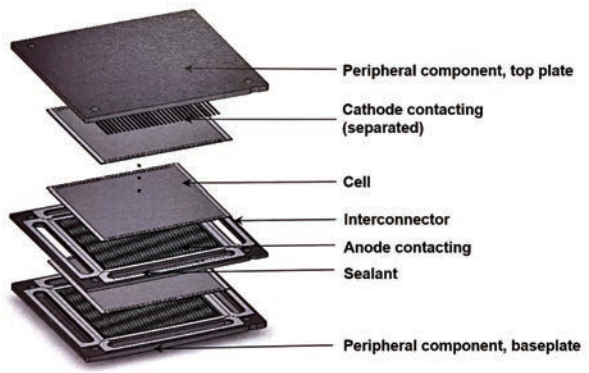

Figure 1 Exploded view of an assembled SOFC/SOEC planar cell,[5] where four rods and nuts at each corner crimp these planar cells together.

SOFCs and SOECs

SOFCs and SOECs are made of solid oxides, especially electroceramics. Some SOFC are reversible, so they can be used as SOEC.[7] The SOFC technology is well-known for its fuel tolerance and flexibility, high electrical efficiency (45-70%)[2] and high operating temperature (600-1000°C).[2] Three families of SOFC exist:

- High temperature SOFC, operating between 900°C and 1000°C;
- Intermediate temperature SOFC, operating between 700°C and 900°C;
- Low temperature SOFC, operating between 500°C and 700°C.

High temperature SOFCs are mostly used in Integrated

Table 2 Main materials used in SOFC.[6]

	Cathode	Electrolyte	Anode	Interconnect
High temperature SOFC (900-1000°C)	$La(Sr)MnO_3$	$Zr(Y)O_{2-x}$	$Ni\text{-}Zr(Y)O_2$	$LaCr(Mg)O_3$
Intermediate temperature SOFC (700-900°C)	$La(Sr)MnO_3$, $La(Sr)Co(Fe)O_{3-x}$	$Zr(Y)O_{2-x}$, $Ce(Gd)O_{2-x}$, $La(Sr)Ga(Mn)O_{3-x}$	$Ni\text{-}Zr(Y)O_2$	$Cr\text{-}Fe(Y_2O_3)$, $Inconel\text{-}Al_2O_3$
Low temperature SOFC (500-700°C)	$La(Sr)Co(Fe)O_{3-x}$	$Ce(Gd)O_{2-x}$, $La(Sr)Ga(Mn)O_{3-x}$	$Ni\text{-}Zr(Y)O_2$, $Ni\text{-}Ce(Gd)O_{2-x}$	Stainless steel

coal gasification systems and grid power distribution.[4] Intermediate temperature SOFCs are mainly used in Combined Heat and Power (CHP) systems,[8] integrated gas turbines[9] and vehicles (Auxiliar Power Unit).[10],[11] Low temperature SOFCs are principally used in Combined Heat and Power (CHP) systems, Auxiliary Power Units (APU) of electric vehicles.

SOFCs can use hydrogen as fuel, this will produce electricity and water (Figure 2): at the cathode $O_2(g)$ is reduced to O^{2-}; in the electrolyte O^{2-} ions are transported from the cathode to the anode and at the anode $H_2(g)$ is oxidised to $H_2O(g)$. Hydrogen can be produced by Solid Oxide Electrolysis Cell (SOEC) (Figure 2): at the cathode $H_2O(g)$ is reduced to $H_2(g)$ and O^{2-} ions; in the electrolyte O^{2-} ions are transported from the cathode to the anode and at the anode O^{2-} ions are oxidised to $O_2(g)$.

SOFC/SOEC Materials Analysis

Along the development cycle of a SOFC/SOEC stack, all constituting materials (interconnector, glass sealing, end plate, compression rod, cells) are analysed. In this article, a focus is made on the materials analysis of cells (SOFC/SOEC).

SOFC/SOEC Materials Properties and Performance

SOFCs/SOECs are characterised in terms of performance and durability. The performance of a SOFC/SOEC relates to its electrical efficiency, fuel utilisation, and power density at different current densities. The durability of a SOFC/SOEC has to do with the degradation of the performance over time and test cycles, in certain test conditions. The SOFC/SOEC performance and durability depend on the cell design, intrinsic properties of materials (electronic conductivity, ionic conductivity, thermal expansion coefficient, Oxygen self-diffusion coefficient, Surface exchange coefficient, Area Specific Resistance, porosity content, grains size, thickness, …)[12] and operating conditions (air and fuel compositions, temperature, gas pressure, …). To optimise SOFC/SOEC materials, the link between materials composition and microstructure, and performance and durability tests must be understood. For this, the materials composition and microstructure are analysed along the manufacturing steps, drafted in Figure 3, where firstly powders are prepared from raw materials, secondly inks are produced from powders, dispersants, solvents, and binders, thirdly inks are coated on a support and dried, fourthly cut to the right dimensions, and then fifthly coated layers are sintered.

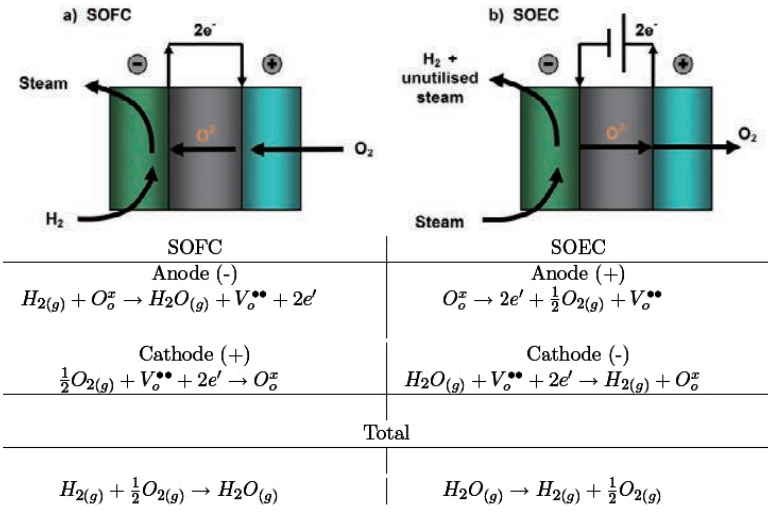

Figure 2 Schematics and electrochemical reactions taking place in a SOFC and a SOEC.[1]

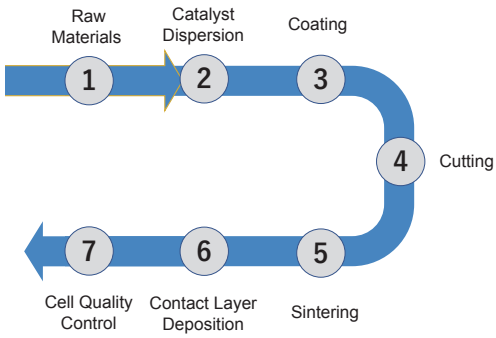

Figure 3 Schematic of the SOFC cell manufacturing.

Raw Materials Characterisation

Raw materials particles are characterised at line with instruments such as HORIBA XploRa™ PLUS confocal Raman microscope (Figure 4), HORIBA Partica LA-960V2 laser scattering particle size distribution analyzer (Figure 5), HORIBA nanoPartica SZ-100V2 Series nanoparticle analyzer (Figure 6) and HORIBA Partica CENTRIFUGE CN-300 centrifugal nanoparticle analyzer (Figure 7) to know their composition, crystallinity, size and distribution.

Ink Characterisation

Inks are characterised at line to know the particles size distribution in ink with HORIBA Partica LA-960V2 laser scattering particle size distribution analyzer (Figure 5) or with HORIBA SZ-100V2 Series nanoparticle analyzer (Figure 6) or with HORIBA Partica CENTRIFUGE CN-300 centrifugal nanoparticle analyzer (Figure 7), their rheology, viscosity, and zeta potential with HORIBA SZ-100V2 Series. Figure 8 shows results from HORIBA Partica LA-960V2 using the high concentration cell on an ink.

Figure 8 shows the results of the relationship between the scanning electron microscope (SEM) morphology of a PEFC (polymer electrolyte fuel cell), (not of SOFC here) cell coated layer and the particle size distribution of the ink analyzed by HORIBA Partica LA-960V2 using a high concentration cell. By using the high concentration cell, the particle size distribution of ink can be measured without diluting the ink as much as possible. Figures 8(a), (b), and (c) show that the particle size distribution is approximately 20 to 300 µm for Sample A, 0.2 to 1 µm for Sample B, and 0.1 µm for Sample C, respectively. Figures 8-(d), (e), and (f) show surface SEM images of the coated layers of Sample A, B, and C. Figures 8-(g), (h), and (i) show cross-sectional SEM images. The results show that the surface morphology of the coated layer becomes rougher and the variation of film thickness becomes larger when the inks with large particle size distribution are applied, that clearly confirms the effect of the catalyst dispersion solution on the microstructure of the coated layer.

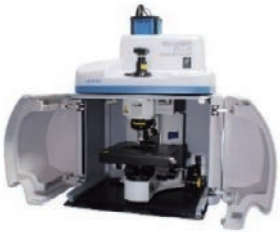

Figure 4 XploRA PLUS Raman Spectrometer - Confocal Raman Microscope.

Figure 5 Partica LA-960V2 Laser Scattering Particle Size Distribution Analyzer.

Figure 6 nanoPartica SZ-100V2 Series Nanoparticle Analyzer.

Figure 7 Partica CENTRIFUGE CN-300 Centrifugal Nanoparticle Analyzer.

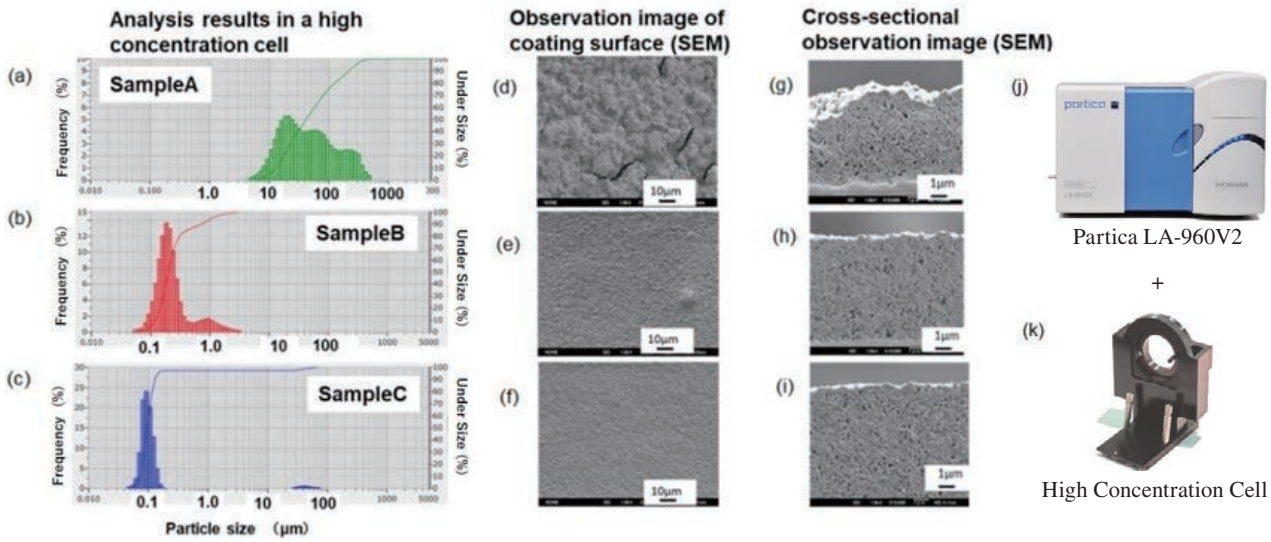

Figure 8 Particle size distributions (a-c) and SEM (d-i) data from different ink preparations. Particle size distributions were obtained with HORIBA Partica LA-960V (j) using High Concentration Cell (k) [Data provided by: Hirai & Sasabe Laboratory, Tokyo Institute of Technology, FC-Cubic].

Coating Characterisation

Nowadays, cells manufacturers want to measure the coated catalyst film thickness and catalyst loading inline, and ensure that the coated film shows a homogeneous distribution of the catalyst and the binder from the coating step to the drying step. Also, they want to detect defects (over thicknesses, impurities, pinholes, bubbles …).

HORIBA can provide an inline XRF solution to measure the amount and thickness of catalyst coated films inline. Figure 9 shows a photograph of the X-ray analysis head section (a) and an image of its X-ray analysis unit when installed in a roll-to-roll facility (b). As shown in Figure 9-(c), multiple X-ray analysis heads can be installed on the roll-to-roll coating film, or the X-ray analysis head can scan over the film while making measurements. HORIBA can also provide Raman solutions to detect defects and control the homogeneity of catalyst and binder in coated films. The example in Figure 10 shows Raman mapping (a) of the surface of a humid SOFC/SOEC air electrode using a HORIBA LabRAM Soleil Raman Spectrometer (c). The colour of each spectrum shown in Raman spectrum (b) corresponds to the colour of Raman mapping (a), where blue shows materials X, red shows materials X+C-H (polymer), and green and orange show Fe_3O_4 or Fe_2O_3 (impurity) respectively.

Sintering Characterisation

Today's market looks for inline instruments to detect defects and fast offline instruments to measure the thickness of sintered cells. HORIBA can provide inline XRF (Figure 9) or offline XRF solutions for defect detection and inline measurement of sintered layer thickness. Figure 11 shows the elemental composition analysis of dark impurity spots (b) on the SOFC anode surface using the HORIBA XGT-9000 (c), a micro X-ray fluorescence analyzer capable of elemental analysis and elemental mapping of small areas as small as φ10 μm. Figure 11-(a) shows the results of five elemental analyses, and it was found that a higher concentration of Fe_2O_3 was detected in the dark spot area than in the reference area, indicating that it was the cause of the dark spot. HORIBA can also provide a Raman solution to detect defects in the sintered layer. Figure 12 shows a microscope image and Raman mapping of a sintered SOFC anode surface by HORIBA LabRAM soleil. The colour of the Raman mapping image (a) corresponds to the colour of the Raman spectrum (b), showing red: materials X; red: ZrO2 ; blue: NiO; yellow: $BaTiO_2$ (impurity).

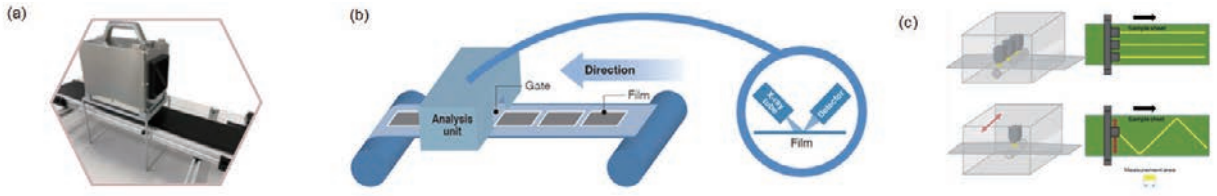

Figure 9 Photo (a) and Schematics (b and c) of inline XRF system.

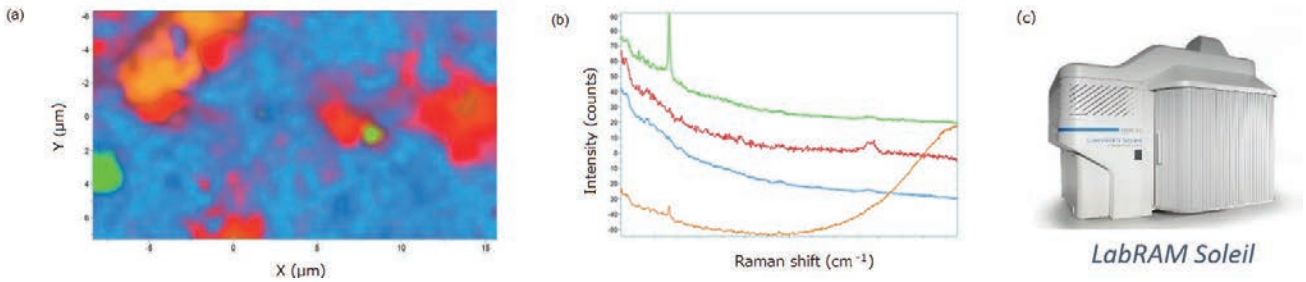

Figure 10 Raman mapping (a) and Raman spectrum (b) of a humid SOFC/SOEC air electrode measured with HORIBA LabRAM Soleil Raman Spectrometer (c). In blue: materials X; in red: materials X + C-H (polymer); in green and orange: Fe_3O_4 or Fe_2O_3 (impurity).

Post-mortem analysis

Once cells have been tested (performance and durability tests) with test stations such as the one produced by HORIBA FuelCon (Figure 13), some post-mortem analyses are done. In research, this is very common to do post-mortem analysis on cross sections with Scanning Electron Microscope (SEM)/Energy Dispersive X-ray (EDX) and Focused Ion Beam (FIB)-SEM. SEM-EDX enables to identify the chemical composition of layers (undesired phases, impurities…) and estimate both the quality of contacts and the porosity content. The FIB-SEM gives access to the 3D structure of layers (porosity content, contact surface, tortuosity…).[13] These data obtained from SEM are used to understand performance and durability tests results. For example, a loss of performance can be explained by the formation of an insulating phase at the electrode/electrolyte interface[14] or the electrode delamination[15] or the diffusion of species[14],[16] or something else. The post-mortem analysis can be completed with other characterisation technics such as Raman spectroscopy, X-ray Fluorescence spectroscopy and Glow Discharge Optical Emission Spectrometer (Figure 16), developed by HORIBA.

Raman spectroscopy was used to detect phase transformation in YSZ electrolyte enhanced by Nickel reduction.[17] It can also be used to monitor Cr poisoning behaviour of $La_{0.6}Sr_{0.4}Co_{0.2}Fe_{0.8}O_3$ (LSCF) cathodes.[18]

X-ray fluorescence spectroscopy can be used to identify, in a non-invasive way, Ni-S compound formed within a Ni-YSZ fuel electrode of a SOFC in contact with H_2S.[19] It can also be used to monitor the depletion and agglomeration of Ni in Ni-YSZ electrode[16] or a crack formation inside the YSZ electrolyte.[20]

In addition to composition and microstructural analyses, there is an interest in the industry to measure the mechanical properties of SOFC and SOEC cells.

SOFC/SOEC Stack and Hot-Box Materials Analysis

Current SOFC research is not only searching for new cathode, anode and electrolyte materials with greater performance and durability, but also for better interconnectors, glass sealings, end plates, compression rods and stack designs. That is why not only single cells are tested and characterised but also stacks and hot-box systems. Stacks and hot-box systems performance and durability can be determined with test stations such as HORIBA FuelCon test stations (Figures 14 and 15). The performance and durability test results will again be completed with measurements done from the raw materials preparation to the post-mortem analysis.

(a)

	Fe2O3	NiO	Y2O3	ZrO2	HfO2	CaO	Cr2O3	Cl	SO3
reference	0.05	28.4	7.9	61.1	2.2	0.3	0.03	0.00	0.00
Dark points									
N°1	0.11	30.2	7.8	59.3	2.2	0.3	0.02	0.02	0.00
N°2	0.18	28.7	7.9	60.6	2.2	0.3	0.03	0.03	0.00
N°3	0.09	29.9	7.8	59.9	2.2	0.2	0.02	0.00	0.00
N°4	0.24	32.3	7.5	57.4	2.2	0.2	0.05	0.05	0.00
N°5	0.21	29.6	7.8	59.9	2.1	0.2	0.04	0.05	0.00

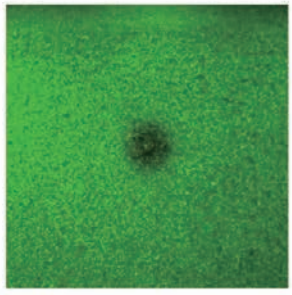

Figure 11 X-ray fluorescence signature (a) of a dark impurity spot (b) on a SOFC anode. A high concentration of Fe_2O_3 was detected with HORIBA XGT-9000 (c).

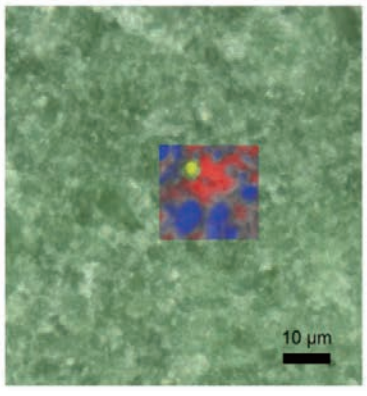

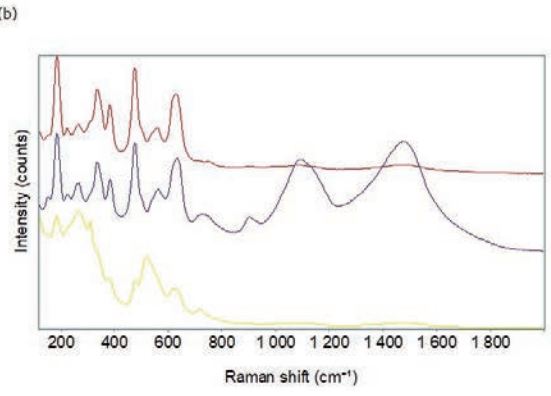

Figure 12 Microscope image and Raman mapping (a), and Raman spectrum (b) of a sintered SOFC anode measured with HORIBA LabRAM soleil (c). In red: materials X; in red: ZrO_2 ; in blue: NiO; in yellow: $BaTiO_2$ (impurity).

PEMFC/PEMEC cells, stacks, and systems Materials Analysis

Like HORIBA testing capability of SOFC/SOEC components and systems, HORIBA is capable of characterising PEMFC/PEMEC components and systems from materials to performance level. HORIBA GD-Profiler 2, coupled with HORIBA XploRa Plus Microscope are, for example, very useful to characterise the Bipolar Plates (PEM interconnectors) coating. By combining the elemental depth profile and the Raman spectrum of the Bipolar Plate coating, they helped to understand the impact of the coating morphology on the coating thickness (Figure 16).

Figure 16 shows an example of the characterization of a DLC coated film on a bipolar plate (PEM interconnector) using HORIBA GD-Profiler 2 (d) and the HORIBA XploRa Plus Microscope (e). The coated film of the bipolar plate must have a quality and thickness that satisfies high conductivity and corrosion resistance. Figure 16-(a) shows the Raman spectrum of the surface of the DLC-coated film of the bipolar plate (b). The quality of the DLC film can be evaluated by the ratio of the peak intensity of the G-band around 1580 cm-1 and the D-band around 1360 cm-1, which is derived from carbon, and the width at half maximum. Figure 16-(c) shows the elemental depth profile of a DLC-coated film on a bipolar plate. The vertical axis is indicated by the elemental emission intensity, or elemental concentration, and the horizontal axis is indicated by the sputtering time, which can be converted to the depth from the surface. The red line is the profile of carbon derived from the DLC film, and the black line is the profile of titanium, the base material of the bipolar plate. From this depth profile, the thickness of the DLC coated film can be analyzed. Thus, by combining the elemental depth profiles and Raman spectra, the influence of the DLC film quality of the bipolar plate on the thickness of the coating can also be investigated.

Conclusion

The main focus of research in SOFC/SOEC today, is the development of improved materials and designs to increase the efficiency and reduce the cost of these systems. This includes the development of new electrodes materials, electrolytes, and fuel cell components (interconnectors, glass sealings, end plates). Researchers are looking at ways to optimise the performance and durability of SOFCs/SOECs by analysing materials and their performance. The materials analysis can be made by Raman spectroscopy, X-ray Fluorescence, Dynamic light scattering, Glow Discharge Optical Spectrometer, Energy-dispersive X-ray spectroscopy and other technics. The main challenge of SOFC/SOEC industrials is the upscaling of SOFC/SOEC stacks production. To support this growth, HORIBA is offering inline monitoring solutions to control the quality of the process. Also, HORIBA is suppling end-of-line test stations to sinter stacks and validate their performance. Additionally, HORIBA provides measurement and test equipment for fuel cells and electrolysers systems development.

* Editorial note: This content is based on HORIBA's investigation at the year of issue unless otherwise stated.

Figure 13 Evaluator C1000-HT SOFC Fuel Cell Test Station.

Figure 14 EVALUATOR S25-HT.

Figure 15 S25-HT for Hot-Box systems.

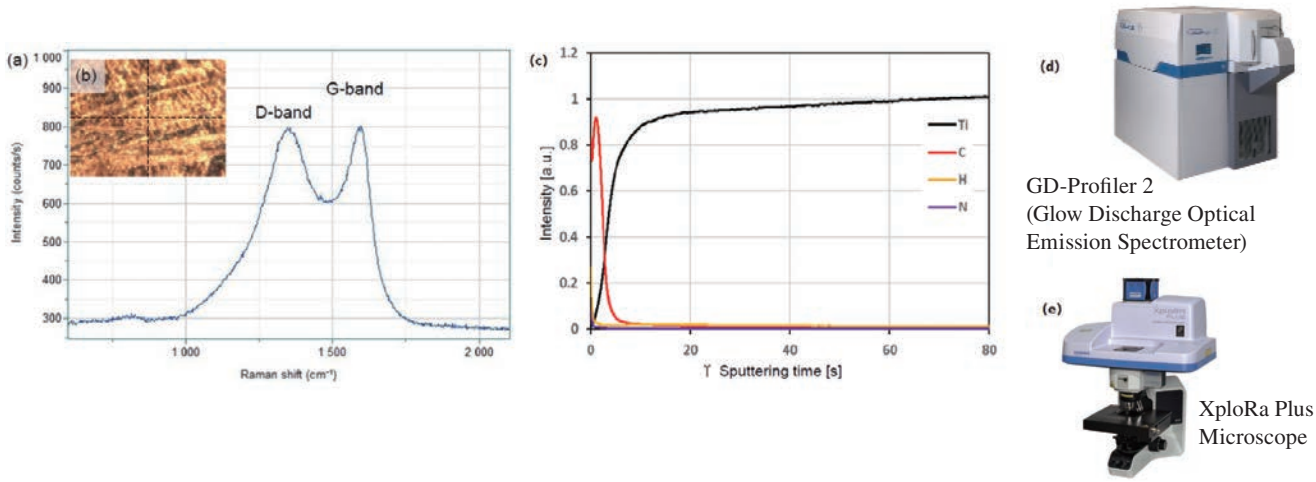

Figure 16 Raman spectrum obtained with HORIBA XploRa Plus Microscope (e) on a carbon coated surface of a bipolar plate and Optical image of the measurement area (a), and Elemental depth profile of the bipolar plate analysed by GD-Profiler 2 (d).[21]

References

[1] S. Skinner, 'Lecture 8', presented at the Lecture 8, Imperial College London, 2021.

[2] S. Skinner, 'MSE 411 Lecture 2 Fuel Cell Technology', presented at the MSE 411 Lecture 2 Fuel Cell Technology, Imperial College London, 2021.

[3] M. Katebah, M. Al-Rawashdeh, and P. Linke, 'Analysis of hydrogen production costs in Steam-Methane Reforming considering integration with electrolysis and CO2 capture', *Clean. Eng. Technol.*, vol. 10, p. 100552, Oct. 2022, doi: 10.1016/j.clet.2022.100552.

[4] S. H. Jensen, X. Sun, S. D. Ebbesen, R. Knibbe, and M. Mogensen, 'Hydrogen and synthetic fuel production using pressurized solid oxide electrolysis cells', *Int. J. Hydrog. Energy*, vol. 35, no. 18, pp. 9544-9549, Sep. 2010, doi: 10.1016/j.ijhydene.2010.06.065.

[5] M. Kusnezoff *et al.*, 'Progress in SOC Development at Fraunhofer IKTS'.

[6] S. Skinner, 'MSE 411 Lecture 6', presented at the MSE 411 Lecture 6, Imperial College London, 2021.

[7] M. Shen, F. Ai, H. Ma, H. Xu, and Y. Zhang, 'Progress and prospects of reversible solid oxide fuel cell materials', *iScience*, vol. 24, no. 12, p. 103464, Dec. 2021, doi: 10.1016/j.isci.2021.103464.

[8] E. J. Naimaster and A. K. Sleiti, 'Potential of SOFC CHP systems for energy-efficient commercial buildings', *Energy Build.*, vol. 61, pp. 153-160, Jun. 2013, doi: 10.1016/j.enbuild.2012.09.045.

[9] V. Zaccaria, D. Tucker, and A. Traverso, 'Gas turbine advanced power systems to improve solid oxide fuel cell economic viability', *J. Glob. Power Propuls. Soc.*, vol. 1, p. U96IED, Jun. 2017, doi: 10.22261/U96IED.

[10] D. J. L. Brett, A. Atkinson, N. P. Brandon, and S. J. Skinner, 'Intermediate temperature solid oxide fuel cells', *Chem. Soc. Rev.*, vol. 37, no. 8, pp. 1568-1578, Jul. 2008, doi: 10.1039/B612060C.

[11] J. Lawrence and M. Boltze, 'Auxiliary power unit based on a solid oxide fuel cell and fuelled with diesel', *J. Power Sources*, vol. 154, no. 2, pp. 479-488, Mar. 2006, doi: 10.1016/j.jpowsour.2005.10.036.

[12] G. Kessler, S. Skinner, and P. D. Z. Xie, 'Optimising the performance of the electrolyte barrier layer in Ruddlesden-Popper based fuel cells', MEng Thesis, Department of Materials Imperial College, Jun. 2021.

[13] O. Celikbilek, 'An experimental and numerical approach for tuning the cathode for high performance IT-SOFC', PhD thesis, Université Grenoble Alpes, 2018.

[14] S. Zarabi Golkhatmi, M. I. Asghar, and P. D. Lund, 'A review on solid oxide fuel cell durability: Latest progress, mechanisms, and study tools', *Renew. Sustain. Energy Rev.*, vol. 161, p. 112339, Jun. 2022, doi: 10.1016/j.rser.2022.112339.

[15] Z. Pan et al., 'On the delamination of air electrodes of solid oxide electrolysis cells: A mini-review', *Electrochem. Commun.*, vol. 137, p. 107267, Apr. 2022, doi: 10.1016/j.elecom.2022.107267.

[16] J. Villanova, S. Schlabach, A. Brisse, and A. Léon, 'X-ray fluorescence nano-imaging of long-term operated solid oxide electrolysis cells', *J. Power Sources*, vol. 421, pp. 100-108, May 2019, doi: 10.1016/j.jpowsour.2019.02.084.

[17] T. Ishiyama, H. Kishimoto, K. D.- Bagarinao, K. Yamaji, T. Horita, and H. Yokokawa, 'Gradual Conductivity Degradation of Nickel Doped Yttria Stabilized Zirconia by Phase Transformation at Operating Temperature', *ECS Trans.*, vol. 78, no. 1, pp. 321-326, May 2017, doi: 10.1149/07801.0321ecst.

[18] Y. Chen *et al.*, 'An effective strategy to enhancing tolerance to contaminants poisoning of solid oxide fuel cell cathodes', *Nano Energy*, vol. 47, pp. 474-480, May 2018, doi: 10.1016/j.nanoen.2018.03.043.

[19] W. M. Harris *et al.*, 'Three-Dimensional Microstructural Imaging of Sulfur Poisoning-Induced Degradation in a Ni-YSZ Anode of Solid Oxide Fuel Cells', *Sci. Rep.*, vol. 4, no. 1, p. 5246, Jun. 2014, doi: 10.1038/srep05246.

[20] L. Bernadet *et al.*, 'Enhanced diffusion barrier layers for avoiding degradation in SOFCs aged for 14000 h during 2 years', *J. Power Sources*, vol. 555, p. 232400, Jan. 2023, doi: 10.1016/j.jpowsour.2022.232400.

[21] C. Nishimura, T.-H. Wu, E. Iso, A. Fujimoto, P. Chapon, and J. Hirose, 'Proton Exchange Membrane Fuel Cell Bipolar Plate Analyses by GD-OES and Raman', *HORIBA Sci.*.

Guillaume KESSLER
ギオーム ケスリ
Hydrogen Product Specialist,
ATS (Automotive Test Systems) - AES (Alternative Energy Systems- Hydrogen),
HORIBA FRANCE SAS

Production of Solid Oxide Fuel Cell and Electrolyzer Stacks using HORIBA FuelCon's Sintering Equipment

HORIBA FuelCon製焼結装置を用いた固体酸化物形燃料電池および電解槽スタックの製造

Mathias RACHAU
マティアス ラハウ

Fuel cell and electrolyzer solutions will play a major role in the development of the future Hydrogen economy helping to replace fossil fuels. Specifically, high temperature solid oxide cell (SOC) technology has important advantages such as increased efficiencies and the extended range of applications based on its fuel flexibility. The production of solid oxide cells and stacks is a key aspect on the way to an increased number and higher power level of system installations. HORIBA FuelCon provides SOC sintering, reduction and testing equipment that helps to scale-up the production to an industrial level and by that, to minimize the production costs. The present article provides insides on HORIBA FuelCon's solutions based on the specific SOC production steps.

燃料電池と電解槽のソリューションは，化石燃料に代わる将来の水素経済の発展に大きな役割を果たす。特に高温固体酸化物形燃料電池(SOC)技術には，効率向上や燃料の柔軟性に基づく応用範囲の拡大など，重要な利点がある。固体酸化物形燃料電池とスタックの製造はシステムの設置台数と出力レベルを向上させるための重要な要素となっている。HORIBA FuelConはSOCの焼結，還元，試験装置を提供し，工業レベルまで生産をスケールアップすることで生産コストを最小化することに貢献している。本稿ではSOCの製造工程に基づいたHORIBA FuelConのソリューションについて紹介する。

Introduction

The "Paris Agreement" from 2015 that determined to limit global warming clearly below 2 K compared with pre-industrial times motivates the recently raised international activities aiming for reduction of global CO_2 emissions.

Reaching that goal will require to establish a throughout interaction between different energy sectors such as electricity, heat, chemistry and mobility based on alternative energy sources, mainly renewables.

The nature of renewable energy sources like wind and solar power implies the need for seasonal energy storage solutions.

Also, the associated reduction of fossil fuel utilization down to zero will only be successful if there is a way to substitute today's fossil feedstock sources in the chemical industry, the agri-food sector as well as the cement and steel production.

A basic and key and element for the implementation of all three mentioned aspects sector coupling, energy storage and fossil feedstock substitution will be Hydrogen.

A major part of the Hydrogen amounts required will be provided by electrolysis solutions. Amongst different electrolyzer technologies, the high-temperature Solid Oxide Electrolysis (SOEC) shows the highest efficiencies for pure water electrolysis and allows even to utilize CO_2 for provision of a $CO + H_2$ mixture, termed syngas, a major feedstock gas in the chemical industry. Moreover, the efficiency can be increased by heat coupling with subsequent exothermal processes like methanation and ammonia synthesis which play an important role for higher hydrocarbon production as well as for the agri-food sector.

The escalating Hydrogen demand leads to a rapidly rising request for electrolysis facilities, already now. Scaling up the capacities for SOEC cell and stack production requires specifically optimized and fully automated production equipment.

HORIBA FuelCon, as a provider of fuel cell and electrolyzer evaluation and manufacturing equipment for more than 20 years, offers a wide line-up of SOEC testing and production solutions in the full scope from cells to stacks. The same equipment is able to produce and test SOFC fuel cell stacks as well as rSOC reversible solid oxide stacks as these are just two more variants of the solid oxide technology.

The following article gives a detailed overview about solid oxide cell design and stack manufacturing processes. HORIBA FuelCon's associated production equipment will be illustrated providing insides of the applied technologies.

R&D and Quality tests for Cells

Solid oxide cells basically consist of a thin, sintered electrolyte foil that is applied with specific fuel and air electrode materials on each side.

A common electrolyte material is yttrium-oxide-stabilized zirconium dioxide (YSZ), a ceramic material that is gas tight in order to separate the reactants being in contact with the cell. While the electrolyte needs to be a good electrical insulator, it allows O^{2-} ions to pass. Aside from the high temperature that is needed to activate the O^{2-} ion conductivity (min. 600 °C), the O^{2-} ion transport is the main difference to PEM technology which is based on the transport of H^{+} ions (protons).

The fuel and air electrode materials are highly porous allowing the reacting gases to reach the three-phase boundary (electrolyte, electrode and gas). Also, a good electrical conductivity is desired to lead the electrons being released when O_2 split into O^{2-} ions. In order to assure the electrodes staying attached at the electrolyte when operating at high temperatures, the thermal expansion coefficients (TEC) of the electrodes need to be aligned to the electrolyte's properties.[1]

Commonly, the fuel and air electrode materials are printed on the electrolyte (e.g. by screen printing or tape casting) in form of a paste or slurry. After printing, the materials need to dry before they will be sintered at 1,000-1,400 °C. The materials being typically used are Nickel for the fuel electrode and lanthanum strontium manganite (LSM) for the air electrode.[1] Their main job is to catalyze the reactions, O^{2-} ion generation on air side and oxidation of the supplied fuel on the fuel side. In order to increase the electrochemical active zones and for TEC optimization, both electrodes are provided as a composite (cermet = ceramic + metal) of the basic materials mentioned above and electrolyte material (YSZ).[1]

To provide mechanical support to the cell, one of the layers need to be made thicker and by that representing a distinctive feature of the cell concept. Most manufactures use one of these 3 common cell types:

- Electrolyte supported cells (ESC, e.g. IKTS, Sunfire)
- Anode supported cells (ASC, e.g. Topsoe, Elcogen) or
- Metal supported cells (MSC, e.g. Ceres Power)

HORIBA FuelCon's cell test equipment accommodates all these cell types by using the integrated, fully ceramic cell

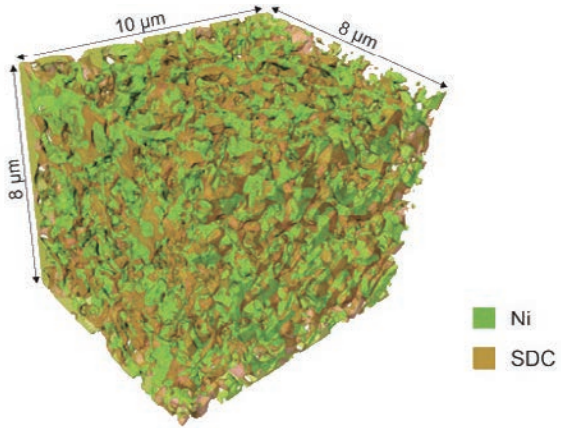

Figure 1 3D example of a Ni/SDC cermet, Gregor Kapun, Ljubljana.[3]

Cell type	Electrolyte Supported Cells (ESC)	Anode Supported Cells (ASC)	Metal Supported Cells (MSC)
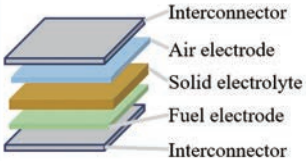	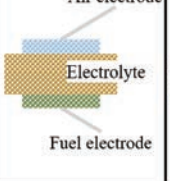	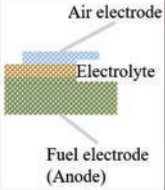	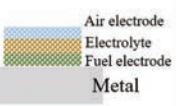
Example	IKTS, Sunfire	Topsoe, Elcogen	Ceres Power

Figure 2 SOC cell types.

housing for standard 5 × 5 cm cell designs as well as button cells. The all-ceramic cell housing approach provides a clean testing environment avoiding impurities. Mirror-finishing the ceramic surface improves the adhesion between ceramics. Thus, there is no need to use gaskets or glass sealing which allows to operate the cell in another test run or to apply academic examinations using HORIBA Scientific's wide range of sophisticated equipment such as Raman Spectroscopy.

Cell tests are supported by a number of proprietary features including a direct injection humidifier providing steam with a minimized noise or a direct combustion humidifier with zero noise, both for fuel cell and electrolysis operation at up to 100% steam.

Desulfurizer and reformer units being available for integration in HORIBA FuelCon's test stations allow for reformat fuel cell tests while a number of diverse supply media, such as H_2, CO_2, CO, CH_4, NH_3, support reformat simulation as well.

Electrolysis and reverse SOC operation based on steam and/or CO_2 is just another operation mode as the integrated 2-quadrant load provides smooth changing through the current origin.

Specific cell properties are determined by the integrated high-performance impedance spectrometer (EIS).

Stack Sintering

In order to receive an adequate power output for a specific SOFC/EC application, the single cells are piled on top of each other. The so called "stack" provides a higher voltage, equivalent to the number of cells, while the current through the complete stack is identical with the one applicable to a single cell.

In most cases, the cells are stacked in a bipolar manner meaning that the anode of one cell faces directly to the cathode of the next cell. The advantage of that method is a very simple electrical interconnection. However, since both air and fuel electrode need to be supplied with air and fuel gas just at the point of common contact, an additional interconnector layer is required to separate the two gas sections.

The interconnector plate has multiple functions as it needs to assure an optimal electrical contact and conductivity between the cells, provide main gas channels and stabilization to the stack and carries contacting and tightening elements. The interconnector material should have a high thermal conductivity to keep the temperature gradients inside the stack low and, at the same time, its thermal expansion coefficient (TEC) needs to meet the associated cell properties to prevent mechanical stress.[1] Finally, the interconnector's surface needs to build a tight oxide layer being protected from further oxidation and evaporation of metal contents while still keeping a good electrical conductivity in reducing and oxidizing atmospheres. A proven and widely used material for all these purposes is Crofer22APU, a ferritic high-temperature stainless steel.[1]

To contact the interconnector plate to the anode and cathode electrodes, additional materials are desired to fill the space between the rough surfaces of electrodes and interconnector.[1] Nickel foam or grids provide good results in reducing atmospheres at the fuel electrode.

The oxidizing atmosphere at the air electrode does not allow to use similar metal foams or grids due to their large active surface. A common solution is using electrically well conducting oxide ceramics with perovskite or spinell structures. Elements like manganese, lanthanum, strontium, chromium, kobold, copper or iron are part of these structures to obtain the required properties like the

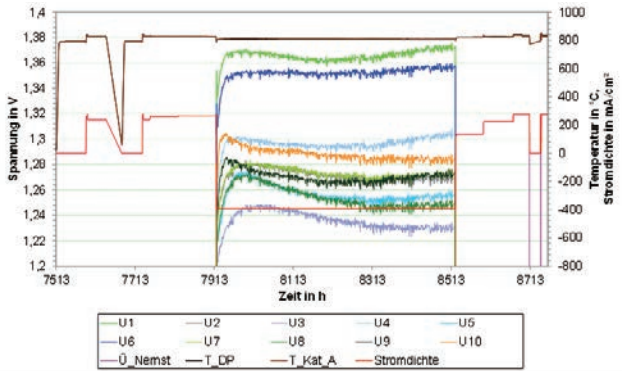

Figure 3 SOEC cell voltages @ 10...20 g/min steam over 600 h, IKTS.

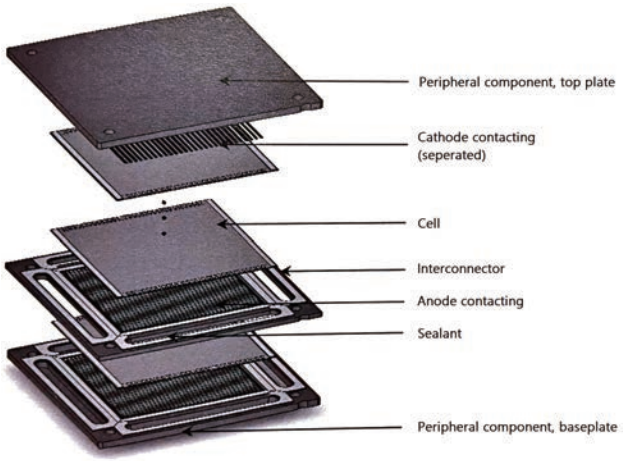

Figure 4 Explosion view of a planar, bipolarly assembled stack.[1]

good electrical conductivity.[1]

Usually, these contacting materials are applied in green state to the interconnector plate or to the air electrode where they build ceramic contacting bars. In this way, the oxide ceramics also represents a favored local barrier between interconnector and cathode that complicates evaporated chromium to reach the air electrode where it would harm the long-term cell performance.[1]

The air electrode connecting bars have contact to the opposite side after stack assembly already. Depending on the stack concept, they will be sintered (substance-to-substance bonds) or pressed with high pressure (force-fit bonds) at the next step.[1]

Before sintering can take place, the interconnector plates and the cell electrodes need to receive a sealant to keep the air and fuel gas inside the channels. Commonly, a glass solder, a special glass composition that allows to achieve the optimal TECs, is applied to the interconnector plate as a foil or paste. Beside sealing, the glass provides a leveling effect between the cells.[1]

Using HORIBA FuelCon's sintering stations, the stack is heated above typical operating temperatures up to 1.000 °C while air is supplied to both fuel and air side. During the sintering process, the stack releases organics coming from the glass solder binders which need to be removed safely. HORIBA FuelCon integrates purging and trace heating features as well as exhaust incinerator solutions.

The furnaces provided by HORIBA FuelCon come with multi-zone control to assure optimal heat distribution and can be arrange to accompany multiple stacks. Once the desired temperature is reached, the proprietary mechanical load design applying compression forces from above or from below the stack allows to compress the stack uniformly in order to secure the intended stack geometry. The maximum force level depends on the specific stack design and can reach up to 40 kN which is kept safely by HORIBA FuelCon's load concept, even at power outage or emergency shut down.

It is important to calculate the optimal glass amount, in order to receive optimal electrical contact after sintering without having surplus glass entering other parts of the stack. Using an open air side concept allows to waive the glass sealant at the air electrode which simplifies air side contacting as the green connecting bars described above can be sintered onto the air electrode, directly.[1]

Partly glass crystallization during the sintering process shifts the TEC toward the value of the cell. In addition, by crystallization, the glass viscosity increases by magnitude which provides the stack with the desired mechanical stability even at maximum operation temperatures.[1]

Stack Reduction

In preparation to the first real stack operation after sintering, the fuel electrode must be reduced using Hydrogen. The catalytic component, a nickel-containing material, forms nickel oxide (NiO) in air, although the nickel compound must be in the metallic state. Reduction with Hydrogen reduces nickel oxide to nickel. The reduced fuel electrode must have enough porosity to transfer the fuel gases. Good electrical conductivity is needed for decreasing the area specific resistance.

The time allowed to conduct the overall anode reduction process is a critical variable in stack production as this step may causes thermal and mechanical stress to the single cells and to the interconnection with other cells. Thus, Hydrogen is commonly diluted with nitrogen in order to control the speed of reduction and by that to protect the stack integrity.[1]

Using HORIBA FuelCon's sintering and reduction stations, the operator can control both the Hydrogen dilution and the flow rate of Hydrogen mixture in a well-defined way. A typical starting ratio is 20 % H_2 and 80 % N_2.[4] The test stand automation allows to control the duration and a continuous increase of Hydrogen content perfectly in accordance with manufacture's requirements.

The reduction process takes place at furnace temperatures between 700 - 800 °C which is below the sintering temperature. The sintering station's multi-zone furnace control follows the given temperature curves and limits precisely.

Stack Test

After sintering and reduction, one important test is to verify the stack's gas tightness. The glass sealant between cells and interconnectors needs to provide reliable leak protection.

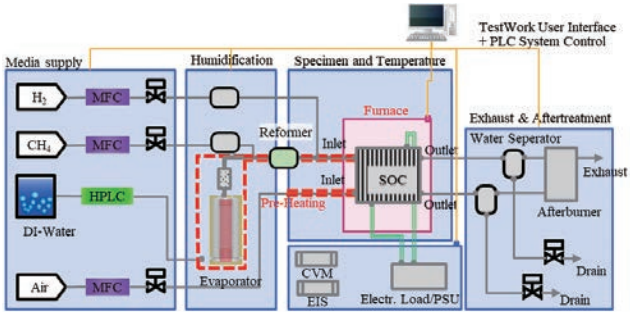

Figure 5 Overview of an SOC evaluation system.

HORIBA FuelCon's test stations offer diverse methods for leak testing. One is the fully automated online leakage test allowing to check for fuel and air electrode and for cross-over leakages during hot operation, depending on stack design. Another method is injecting noble gas like helium to fuel and/or air side. Helium traces found in the opposite gas compartment does indicate a cross-over leakage.

Once Hydrogen is supplied by 100 %, the OCV provides a more detailed picture about successful gas channel sealing as the OCV level highly depends on cross-over leak tightness. HORIBA FuelCon's sintering stations allow to measure the overall stack voltage as well as potentials of single cells or cell groups by multiple cell voltage measurement (CVM) options. By this means, manufacturing quality can be checked down to each single cell. High voltage measurement accuracy by superior input resistances for a large number of cells is the basis.

Polarization tests are a standard to receive quick information on the stack performance after manufacturing.[2] Typically, these tests are conducted under part load of the stack's nominal power. Depending on the intended application, the stack is operated in either fuel cell, electrolysis or reversible mode.

HORIBA FuelCon's sintering stations support all these operation variants in one rig. In most cases, focusing on Hydrogen and steam provision is sufficient for quality checks. If required, additional gases are available, e.g. NH_3 and CH_4 for ammonia and carbon fuel operation or CO_2 for co-electrolysis.

HORIBA FuelCon's proprietary direct injection humidifier provides large amounts of steam with a minimized noise. Together with the fully integrated 2-quadrant load concept, the stations support to change smoothly between fuel cell and electrolysis mode.

For all sintering and testing steps, HORIBA FuelCon supports closed stack concepts as well as open air or fuel side stack designs by proprietary furnace solutions that take care about chromium and silica prevention at the same time. Exhaust gases are cooled down and led to outside the station safely while sample ports allow manufacturers to check gas compositions continuously using gas analyzers from HORIBA. Defined exhaust interfaces enable operators to remove exhausts or to connect to sub-sequent processes.

Scaling-up Stack Production

The worldwide increasing CO_2 reduction goals will motivate the fuel cell and electrolyzer manufacturers to scale-up their production, rapidly. This concerns the cell and stack production in equal measure.

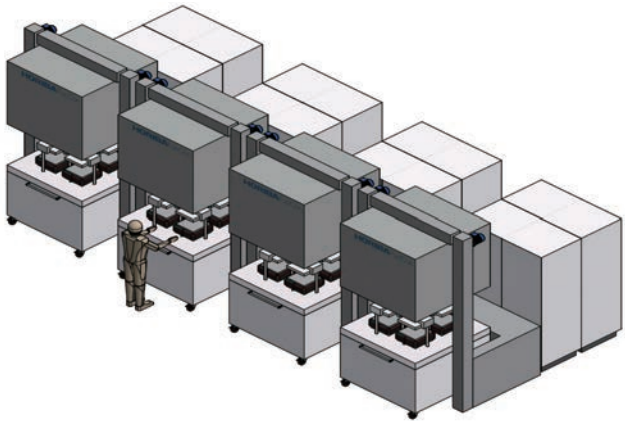

Figure 7 HORIBA FuelCon's Multiple Sintering Stations with 4-fold trolleys.

Higher volumes can be reached by installing additional production capacities. Optimizing the manufacturing processes and logistics does need to take place at the same time in order to increase the output of one production line to an optimum.

HORIBA FuelCon does provide next generation sintering and reduction stations, already now. Larger furnaces with space for multiple stacks are just a first step.

HORIBA FuelCon's proprietary trolley concept supports manufacturers with a movable and universal multi-stack platform that can be used for the whole range from stack assembly down to stack sintering, reduction and testing. As the trolleys include mechanical load systems for each

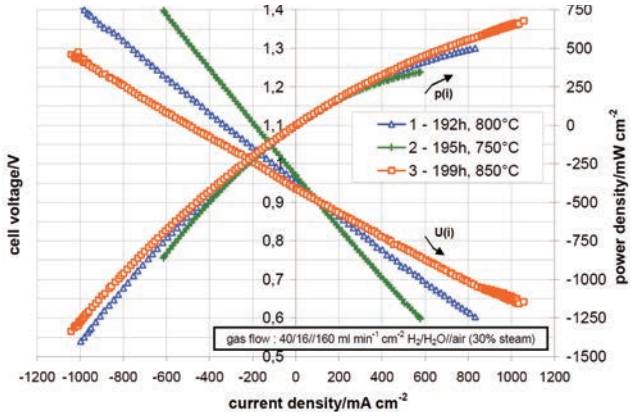

Figure 6 Polarization and i-p curves for reversible SOC operation at different temperatures.[2]

single position, the assembled stacks can be pre-compressed for safe stack transfer. Prepared like that, a trolley is in pool position for docking with the next allocated sintering station once the previous trolley is ready. That might be the case even if the cool down procedure has not finished yet as a quick cool down by furnace opening and stack transport may be acceptable at intermediate temperatures already to shorten the station's occupation time. Moreover, docking the trolley to HORIBA FuelCon's multiple sintering stations is conducted without manual help as they come with an automated docking solution. The described handling covering a number of compatible stack trolleys does allow to reduce the setup and production time to a minimum.

Conclusion

A detailed outline of solid oxide technological principles with HORIBA FuelCon's associated testing and production equipment and their upscaling concepts has been provided.

Solid oxide cell technologies comprise a number of sophisticated methods on cell and stack level, developed over the last decades. Diverse manufacturing steps are required, specifically differentiated according to the concrete SOC type and its fuel cell or electrolyzer application.

HORIBA FuelCon provides proven and progressive sintering, reduction and testing solutions for the broad range of existing SOC variants. Cell and stack manufacturers receive strong support for SOC production and for their upscaling strategy - saving time and resources.

* Editorial note: This content is based on HORIBA's investigation at the year of issue unless otherwise stated.

References

[1] Megel, S.: *Kathodische Kontaktierung in planaren Hochtemperatur-Brennstoffzellen*, Fraunhofer Verlag, **2009**

[2] Schiller, G.; Ansar, A.; Patz, O: *High Temperature Water Electrolysis Using Metal Supported Solid Oxide Electrolyser Cells (SOEC)*, Advances in Science and Technology Vol. 72, **2010**

[3] G. Kapun, S. Šturm, M. Marinšek, M. Gaberščcek: *Three-dimensional characterization of Ni-Sm0.2Ce0.8O2-δ cermet for SOFC anodes by high-resolution FIB-SEM Tomography*, The 16th European Microscopy Congress, **2018**

[4] Hagen, A.; Caldogno, R.; Capotondo; F.; Sun X.: *Metal Supported Electrolysis Cells*, energies, **2022**

Mathias Rachau
マティアス ラハウ
Application Expert
HORIBA FuelCon GmbH

Column

コラム

東京大学とHORIBAがカーボンニュートラル実現に向け独自のソリューションに挑む

Tokyo University and HORIBA Tackle Carbon Neutrality Through Unique Approaches

森 春仁
MORI Haruhito

2022年4月，堀場製作所は東京大学大学院工学系研究科と「環境調和型エネルギーシステム社会連携講座」を開設しました。地球環境保全の重要性に対する認知が拡がり，世界各地で環境対応技術の研究開発が推進される中，近年はエネルギーセキュリティの観点からも自然エネルギーの利活用に対する期待値が高まっています。地球環境に影響を及ぼす温室効果ガスをコントロールするために，温室効果ガスの多くを占める二酸化炭素を増やさないカーボンニュートラル活動が重要とされ，その実現に向け，LCA（ライフサイクルアセスメント）など，環境負荷評価の必要性がさらに増してきています。そして製品の製造過程における二酸化炭素排出量がその製品の価値を決める時代も迫っています。

これまで日本ではエネルギーの使用量を抑制することで二酸化炭素排出量を削減する「省エネ」の活動が推進され世界をリードしてきました。各家庭でも高効率なエアコンやコージェネレーションシステム，太陽光パネルの設置などHEMS（Home Energy Management System）が導入され，化石燃料による発電量の抑制に取り組んできました。またオフィスではBEMS（Building Energy Management System），工場ではFEMS（Factory Energy Management System）による二酸化炭素の排出量削減が進められています。そのような状況の中，HORIBAが協働させて頂くことの多いお客様の研究開発現場に目を向けると，複雑・多様な試験を行う中で，エネルギー利用の効率性や，リソースの効率性よりもデータ取得が優先される，という現場を垣間見ることがあります。そこで本連携講座では，たとえ研究開発であってもエネルギー使用量を勘案した開発が必要になることを見据え，「急峻なエネルギー需要を伴う研究開発現場におけるエネルギーマネジメントシステム」の構築に取り組みます。

今回の取り組みでは，電力システムの研究に強みをもち，最先端の予測技術により最適なエネルギー需給バランスの解明に取り組む東京大学と，自動車開発設備メーカーとしての顔を持ち現場を知り尽くすHORIBAが長年培ってきた「分析・計測技術」を掛け合わせ，研究開発現場の実態に即した新しい「エネルギーマネジメントシステム」を創り上げます。

そして，ここで構築したシステムの事業化と，自動車の研究開発現場のみならず，あらゆる産業界の研究開発施設への社会実装を通して，エネルギーの最適利用・CO_2削減に貢献します。なお，研究活動における各種実証実験は，堀場製作所のびわこ工場「HORIBA BIWAKO E-HARBOR」（滋賀県大津市）内にある自動車開発の総合試験設備「E-LAB」で実施します。バッテリーや燃料電池，内燃機関といったユニット単体から完成車に至るまで，複合的な試験を行うことができる「E-LAB」は，液体／ガス燃料の供給や建屋空調といったインフラを含め，自動車の研究開発現場を想定した最適な「実験場」としての資質を備えています。「E-LAB」内の分析・計測装置および付帯設備の計測データを一括管理する堀場製作所のデータマネジメントシステム「STARS Enterprise」と，東京大学の予測技術を掛け合わせ，CO_2排出量や電力使用量，設備発熱量などのデータを効率よく「見える化」し，「管理」します。

東京大学大学院 工学系研究科 SCHOOL OF ENGINEERING THE UNIVERSITY OF TOKYO × HORIBA Explore the future

Figure 1　（写真左より）東京大学大学院工学系研究科 教授 熊田 亜紀子，同大学院工学系研究科長 染谷 隆夫，堀場製作所 代表取締役会長 兼 グループCEO 堀場 厚，同社 コーポレートオフィサー CTO 兼 ビジネスインキュベーション本部 本部長 中村 博司

※所属・役職は開設当時のものです。（2022年4月5日）

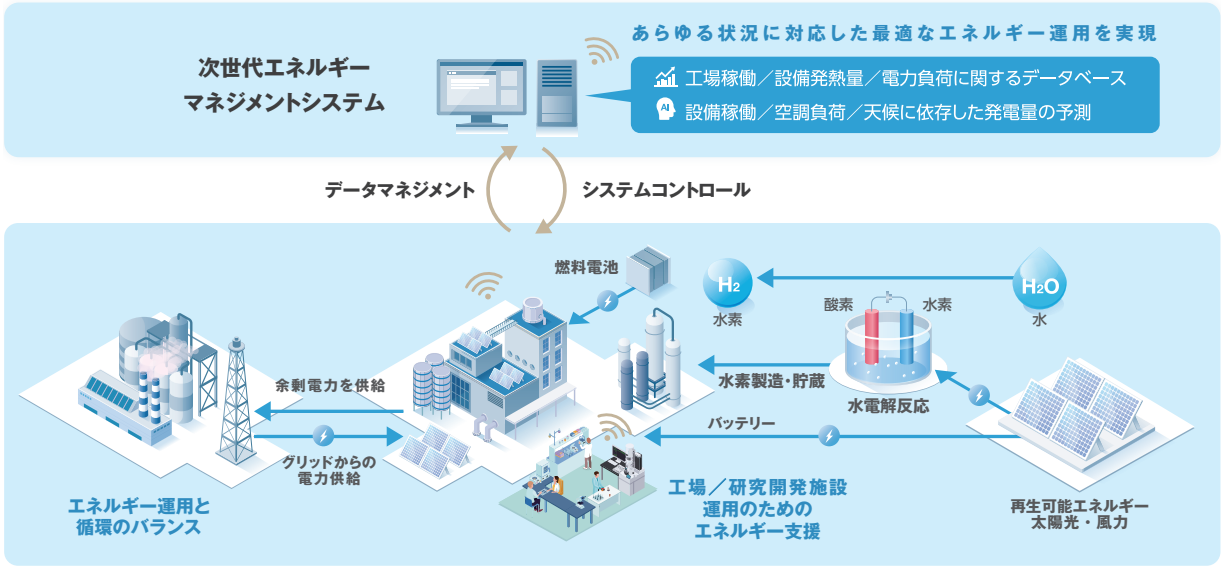

Figure 2　社会実装のイメージ

連携講座スタートから，「E-LAB」において複雑に絡み合うエネルギー消費量の分離，各コンポーネント間の相関関係・因果関係の見える化を実現し，設備稼働計画に対する消費エネルギーの最小化，自然エネルギーの効果的な導入の道筋を見い出しています。また，エネルギーの利活用で重要な役割を担うエネルギーキャリヤとしての水素にも着目し，自然エネルギーとの親和性，例えば変動する太陽光発電量に対する電解水素製造の追従性，電気化学反応セルの劣化との関係解明から，エネルギーマネジメントシステムに対する水素のポテンシャルを明確にしていきます。

加えてこの取り組みを通した東京大学との交流により，エネルギーマネジメントに関する研究開発をリードし，次世代を担うことができる高度人財を育成します。さらに，蓄積したノウハウを役立て，新たな産学連携などへ繋げることで，「智慧」の輪を拡げ，持続的な技術革新へ発展させていきます。

社会実装に向けては，産業界の実態把握と，学術界の最先端の知見と，双方をうまく組み合わせることが極めて重要です。皆さまからのサポートも頂きながら，社会にお役に立てるソリューション提供を目指していきます。

＊編集局注：本内容は特段の記載がない限り，本誌発行年時点での自社調査に基づいて記載しています。

森 春仁
MORI Haruhito
株式会社堀場製作所
ジュニアコーポレートオフィサー（理事）
エネルギー・環境本部　副本部長
Deputy General Manager
Energy & Environmental Division
Junior Corporate Officer
HORIBA, Ltd.

公益社団法人日本分析化学会による表彰
Awarded by the Japan Society for Analytical Chemistry

第71年会(2022年)公益社団法人日本分析化学会による表彰

表彰の概要

公益社団法人日本分析化学会による表彰制度において，株式会社堀場製作所 渋谷 享司が「先端分析技術賞(JAIMA機器開発賞)」を，株式会社堀場テクノサービス 大石 誠が「有功賞」を受賞した。

先端分析技術賞とは：先端的分析技術開発(機器開発，分析・評価技術開発，分析用新規物質の開発，など)や実用化において，優秀なる業績と展開性を示した個人あるいはグループに贈呈される。本賞は，一般社団法人 日本分析機器工業会(JAIMA)のスポンサーシップによるJAIMA機器開発賞により構成されている。今年度は1名と1グループが受賞。

有功賞とは：多年にわたり分析の実務に従事し，又は分析に欠くべからざる機械，器具並びに試薬などの製造等の実務に従事して功労のあった者に贈呈される。今年度は49名が受賞。

2022年度受賞者

◆先端分析技術賞 JAIMA機器開発賞
株式会社堀場製作所　ビジネスインキュベーション本部
Technology Innovationセンター
先行開発部 Common IRLAMチーム
渋谷 享司　博士(工学)

＜研究業績＞
量子カスケードレーザーを用いたガス分析技術：
赤外レーザー吸収変調法の実用化

◆有功賞
株式会社堀場テクノサービス
Solution Marketing Strategy Department
大石 誠

＊編集局注：本内容は特段の記載がない限り，受賞時点での自社調査に基づいて記載しています。

Figure 1　渋谷 享司(左)大石 誠(右)

「2022年度光化学協会技術賞」を受賞

Introduction of Awardees of the Japanese Photochemistry Association in 2022

2022年度光化学協会技術賞

Figure 1　(後列中央)光化学協会 会長　池田 浩教授
(後方右)光化学協会 元理事　玉井 尚登教授
(前列左から)北川 雄一，原 清明，Adam Gilmore

光化学協会とは

光化学協会(1976年発足)は，光化学および光技術領域の基盤研究から幅広い応用技術を担う学会。
個人会員1000名余，賛助会員43社

表彰の概要

光化学協会技術賞は，光化学を応用した技術の開発あるいは工業化などで特に顕著な業績のあった者に授与される賞で，会員(理事)の他薦により選出される。

受賞テーマ・受賞者

時間分解機能を有する超高感度モジュール型蛍光分光測定装置の開発とその応用
Development of Ultra-Sensitive Modular Fluorescence Spectrometer with Time-Resolved Function and its Applications

原 清明(株式会社堀場製作所／株式会社堀場エステック／日本)
業績：時間相関単一光子計数法を用いた蛍光寿命測定装置(NAES-1100)を日本で初めて市販製品化。光化学・半導体分野で時間分解発光の技術をリード。

Adam Gilmore(HORIBA Instrument Inc.／米国)
業績：HII Piscataway(旧Edison)にてモジュール型蛍光分光装置の開発プロジェクトリーダーを担当。
SWCNTs※などのナノテクノロジー分野の研究向けにNanologを上市。さらにAqualog/DuettaのA-TEEM技術を応用した蛍光アプリケーションの開発に従事。

北川 雄一(株式会社堀場テクノサービス／日本)
業績：フィールドエンジニアとしてHII Piscataway(旧Edison)での研修後，HTS Analytical Solution Plazaにて蛍光アプリケーションエンジニアとして依頼分析・独自の分析技術開発に従事。

＊編集局注：本内容は特段の記載がない限り，受賞時点での自社調査に基づいて記載しています。

ご推薦者
光化学協会 元理事
玉井 尚登教授

HORIBAは時間分解発光測定装置NAESを日本で初めて市販製品化したことが業績として非常に大きい。さらにその後，米国SPEX社がグループに加わり，紫外，可視，近赤外というワイドレンジのモジュール型蛍光分光光度計を開発発売，さらにその上に時間分解機能を融合した装置にまで改良してきたことは高く評価される。

※SWCNTsはSingle Wall Carbon Nano Tubes(単層カーボンナノチューブ)の略式。半導体性のSWCNTsを溶液中で分散するとNIR領域で蛍光を発光することがわかっている。

2022年度光化学協会技術賞 受賞への想い

株式会社堀場製作所／株式会社堀場エステック
フェロー
原 清明　博士(工学)

大昔の製品が関係しての受賞に驚きを禁じ得ない。蛍光・りん光の過渡応答波形を計測する“時間相関単一光子計数法の発展系システム”として，蛍光・りん光寿命を算出し，また時間分解発光測定が可能なNAES-1100を1983年に世界に先駆けて上市した。本システムにはナノ秒パルス光源，試料室含む低迷光分光モジュール，偏光測定可能機能，光電子パルス検出用時間電圧計測部／マルチチャンネル波高分析部，寿命算出アルゴリズムとソフトウエア含む総合的な技術が開発され実装された。ちなみに製品名のNAESは，Nano-sec Emission Spectrometerの頭文字をとったもので，蛍光(Fluorescence)だけでなく，りん光(Phosphorescence)や固体からの光ルミネセンス(Photoluminescence)をも包含した発光(Emission)を意識し，英語の“nice”(ナイス)に似た発音から名付けた。

1980年代には，現在のような取扱が簡易で高周波数の紫外可視域のパルスレーザーやLEDは無く，低繰返しパルス光源でも高効率で発光波形の検出を実現するかが課題であった。NAESは，多チャンネル時間電圧計測システムにより，多重光電子パルス列を時間分解して計測し，光源波形と蛍光波形を同時に計測することで，この課題を克服し，寿命演算も応答波形測定も同時に容易に実現できるシステムとなった。光源としては，最初はフラッシュランプ(数kHz,)のみだったが，700シリーズからは，従来の市販品に比べて一桁以上早い繰り返し周波数1 kHzの窒素レーザー(337.1 nm)を，さらに窒素-色素レーザーを組み込むことで，広い発振波長帯(360 nm～750 nm)をもち，更なる微弱光やサブナノ秒の発光寿命測定を可能とした。これにより化合物半導体のPhotoluminescence研究の応用に展開できた。

Figure 2　1983年 NAES-1100販売開始
時間相関単一光子計数法を用いた蛍光寿命測定装置

筆者が本賞受賞者の一人として推薦されたのは以下のような理由によるらしい：①NAESシリーズが日本の光化学・光物理の研究分野に大きく貢献をしたこと，②NAESシリーズが“モジュール型蛍光分光測定装置の礎”となっていること，③HORIBAの蛍光分光の技術文化を醸成し，Dr. Birchが育てた英国JYIBH(Glasgow)や米国HII(Piscataway)の技術とのシナジーにより，先進的で高性能な蛍光分光装置として発展してきたこと。

開発開始から約10年間で3世代のNAESシリーズを上市できたのは，優秀で熱意あるプロジェクトメンバーに恵まれたからである。当時の北海道大学 応用電子研究所の進藤善雄先生，社内では開発・設計の横山一誠氏を中心に田中優氏，吉田夏紀氏，大槻久仁雄氏，米田有利氏，下野善弘氏，三笠木千里氏，粉川雅至氏，樽井克泰氏，南孝明氏，伊串達夫氏たちである。私がその代表として賞を頂いた形になったが，受賞の栄誉を皆さんと分かち合いたい想いである。本賞受賞に当たり，光化学協会に推薦文をご提出いただきました関西学院大学教授 玉井尚登先生に心から感謝申し上げます。

Adam Gilmore's Achievements for Fluorescence Instrumentation and Analysis at HORIBA Instruments Inc.

HORIBA Instrument Inc.
Adam Gilmore, Ph. D.

HORIBA's Fluorolog instrument line had already played a seminal role in the discovery and development of semiconducting photoluminescent nanomaterials1 including organic light emitting diodes (OLEDs), quantum dots (QDs) and single wall carbon nanotubes (SWCNTs). Importantly, the new preferred analytical method for SWCNTs involved measuring a near infrared (NIR) photoluminescence excitation-emission matrix or EEM. The EEM provided important information about the individual structures within complex mixtures of SWCNTs, including their concentrations, diameters, chiralities, aggregation states and even lengths that were not possible to determine with any other method.

Figure 3　2010年代 Nanolog販売開始
（モジュール型蛍光分光装置）
紫外・可視域から近赤外までの蛍光
およびりん光および寿命測定が可能

Conventional single-channel NIR detectors and scanning monochromators, however, required extensive data acquisition times (up to hours) and were often prone to drift due to temperature instability associated with liquid nitrogen dewar hold-times. The long acquisitions and difficulties maintaining the detector's temperature limited throughput requirements needed to analyze different SWCNT synthesis and purification samples. The conceived solution based on the Fluorolog platform was trademarked in 2005 as the Nanolog® and involved developing software and hardware to interface a multichannel NIR detector, known as an InGaAs array, coupled to a high- resolution imaging spectrograph and scanning excitation monochromator. The Nanolog was equipped with optics to facilitate scanning the primary absorbance and excitation bands (500-800 nm) for the SWCNTs in the 0.8 to 1.3 nm diameter range by rapidly collecting the complete NIR PL emission spectrum (800-1500 nm) at each excitation wavelength. Extension of the excitation NIR range and power with a tunable CW Ti-S laser and an extended NIR InGaAs array allowed for measurements of larger diameter SWCNTs important for device manufacturing applications. In general, the Nanolog reduced the SWCNT EEM collection often to less than 15 minutes and thus became globally popular with numerous researchers and institutions studying SWCNTs, NIR emitting QDs and other nanomaterials.

Another key element of the SWCNT analysis problem was the inherent difficulty of qualitatively and quantitatively interpreting the complex EEM data which comprised numerous spectral peaks each associated with up to dozens of SWCNT species, depending on the synthesis or purification method. The Nanolog's imaging spectrograph configuration also facilitated incorporation of UV-VIS multichannel (CCD) detectors which expanded the capacity to study a much wider variety of PL nanomaterial using the EEM method1.

I would like to conclude by expressing my sincerest gratitude for my colleagues in HORIBA for helping to promote my nomination and for the members and administrators of the Japanese Association of Photochemistry for the acknowledgement of my work with the 2022 Technical Award with my distinguished colleagues Drs. Hara and Kitagawa. I felt very honored and truly enjoyed the experience of the award ceremony.

光化学の可能性について

株式会社堀場テクノサービス
北川 雄一

光化学は物理学，生物学，さらには医学，電子工学にも深く関連する学際的な研究分野です。また，光化学が関連するのは基礎研究分野のみに限られるものではありません。光化学は応用分野・産業界とも深くつながり，科学技術に貢献して発展してきました。太陽電池，LED，光触媒，癌の蛍光マーカー等の私たちの身近な製品や技術を見ても，光関連の科学技術の重要性は確実に増してきていると感じます。光化学は今後もますます発展すると確信しています。

事実，HORIBAの蛍光・りん光分光測定装置は，半導体や光触媒を含む先端材料，製薬や食品を含むライフサイエンス，河川や海洋の水中溶存有機物やマイクロプラスティック等の環境分析など様々な分野で活用されています。

発光のエネルギーに相当するスペクトル測定に加え，励起状態がどの程度の時間維持されるか取得する発光寿命測定は，発光特性を表す重要なパラメータとなります。HORIBAには，超高感度な定常発光スペクトル測定の技術と，時間相関単一光子計数法をベースにした時間分解発光測定の技術があり，この二つを組み合わせたFluorolog-TCSPCはこれまで分析困難であった光変換事象を詳細に解き明かす強力分析析ツールとして役立っています。

例えば，GaN，YAGなどの化合物半導体や，太陽電池材料として注目を集めるペロブスカイト化合物，放射線を可視光に変換するRPLガラス等の分析においては，発光波長は価電子帯と伝導帯のバンドギャップエネルギーに関する情報，発光寿命は光励起した電子の生存時間（キャリア寿命）に関する情報などを含みます。また，発光デバイスなどとして利用される際には，不純物がドープされて新たな電子準位，即ち新たな発光特性が発現します。一つの試料が複数の発光特性を有していることから，照射波長と観測発光波長の両方を掃引する測定は発光特性の全容を掴む上で強力な手がかりとなります。更に，通常の発光スペクトル測定では重複して見えたピークも，時間分解測定により個別の異なるスペクトルとしてより詳細に解析することが可能です。『時間分解機能を有する超高感度モジュール型蛍光分光測定装置』は，通常検出が困難な微弱発光も高いS/N比でデータを取得でき，様々な発光特性評価に貢献しています。

蛍光分光分析のアプリケーション開発に携わる身として，本光化学協会技術賞の受賞は大変名誉であり身に余る光栄です。偉大な先輩方が築かれた技術を基盤としてHORIBAの蛍光分光技術で実現できる研究分野から応用分野にわたる幅広いソリューション提供に努めます。

＊編集局注：本内容は特段の記載がない限り，記事執筆時点での自社調査に基づいて記載しています。

Figure 4　表彰盾

令和4年度近畿地方発明表彰
Kinki Region Invention Awards 2022

京都発明協会会長賞

粒度分布測定装置（特許第5937956号）

表彰の概要

本発明表彰は，近畿地方における発明の奨励・育成を図り，科学技術の向上と地域産業の振興に寄与することを目的としており，近畿地方において優秀な発明，考案，又は意匠（以下「発明等」という。）を完成された方々，発明等の実施化に尽力された方々，発明等の指導，奨励，育成に貢献された方々の功績を称え顕彰するものである。この度，HORIBAの特許第5937956号（光学分析装置）が京都発明協会会長賞を受賞した。

表彰案件の概要

本発明は，装置のダウンタイム削減とユーザビリティ向上に寄与する半導体製造プロセス用薬液濃度モニターの校正機構に関する発明考案である。本発明は，光ファイバ式　薬液濃度モニター CS-600F（**Figure 1**）に採用されている。

Figure 1　受賞した技術を用いた製品
「光ファイバ式薬液濃度モニター CS-600F」

従来発明等の課題

半導体製造プロセス用薬液濃度モニターは，光源からの光を光ファイバで測定セルまで導き，測定セルを通過した光を光ファイバで検出器に導き，検出器で得られた光量から薬液の濃度を求める装置である。このような装置では，光ファイバ及び光源の経時変化や測定セルの汚れなどが検出器で得られる光量に影響するため，定期的にそれらによる光量変動分を校正する必要がある。従来の装置は，反射ミラーを用いて，「光ファイバと測定セルを含めた光学系全体に起因する光量変動分の校正【光路A】」と，「光源に起因する光量変動分の校正【光路B】」を行う構成であった（**Figure2**）。光路Aの校正を行う際は，校正液を測定セルに流さなければならないため，校正の度にダウンタイムが生じていた。さらに，測定セルの汚れによる光量変化は比較的ゆっくり起こる一方で，光ファイバに起因する光量変化は一日で大きく変動するため，光ファイバの校正周期に合わせて光路Aの校正を行う必要があった。

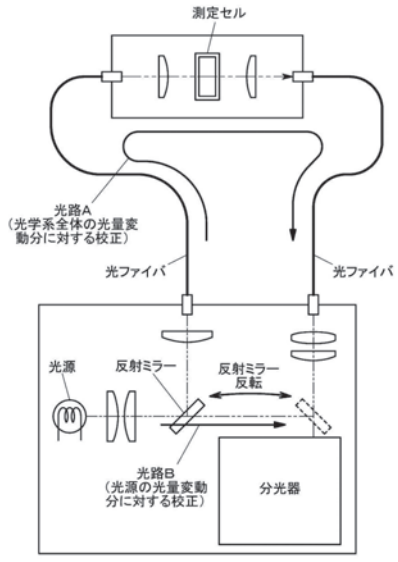

Figure 2　従来の光学分光装置の校正を示す模式図

本発明等の特徴

本発明では，比較的短周期で校正が必要な「光源と光ファイバに起因する光量変動分の校正【光路①】」と，比較的長周期での校正で良い「測定セルに起因する光量変動分の校正【光路②】」を別々に行うことのできる光学系とした（**Figure3**）。光路①においては「光源側の光ファイバから出た光が測定セルを通過せずに検出器側の光ファイバに入る測定セル非通過状態（**Figure4**）」，光路②においては「光源側の光ファイバから出た光が測定セルを通過して検出器側の光ファイバに入る測定セル通過状態（**Figure5**）」とし，２つの状態を自在に切り替えられる構成とした。この構成によって，比較的短周期で行う必要がある光路①の校正を測定セルに校正液を流すことなく行えるようになった。さらに比較的長周期で起こる測定セルに起因する光量変動が測定に影響を与えるようになった段階で初めて，光路②の状態で測定セルに校正液を流して測定セルに起因する光量変動を校正すればよくなった。これによってダウンタイムの削減およびユーザビリティ向上を実現した。

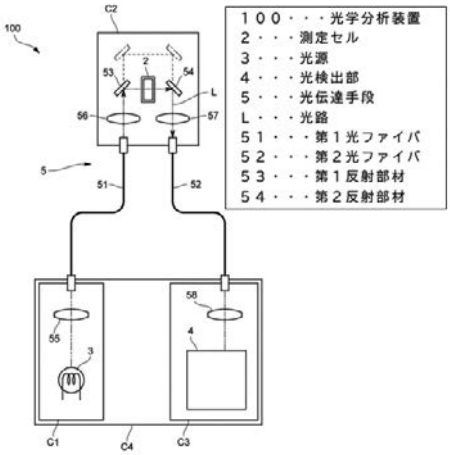

Figure 3　本発明の光学分析装置の校正を示す模式図

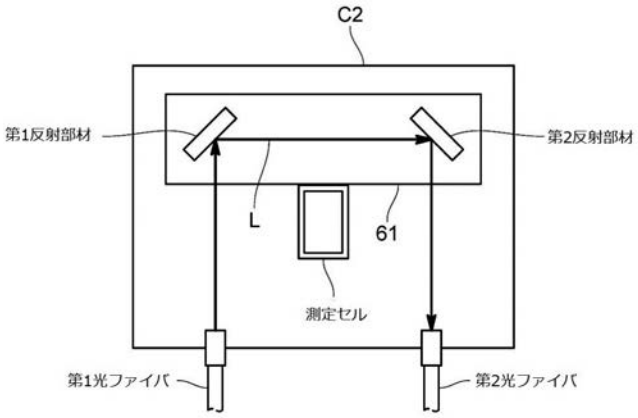

Figure 4　光源及び光ファイバに起因する光量変化を校正する光路（光路①，測定セル非通過状態）を示す模式図

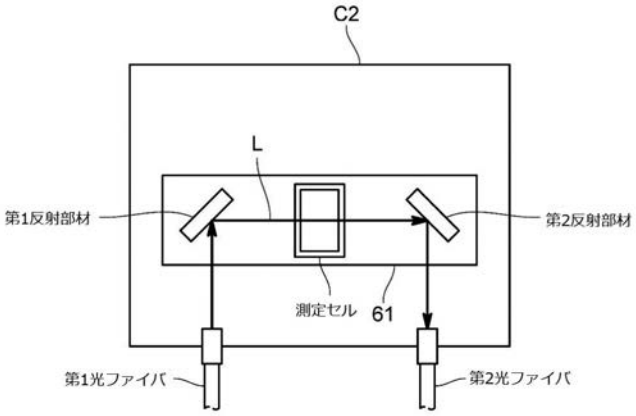

Figure 5　測定セルに起因する光量変化を校正する光路（光路②，測定セル通過状態）を示す模式図

【登録番号】
特許第5937956号
【発明者】
有本 公彦
高木 想

Figure 6　京都発明協会会長賞受賞　有本 公彦（右）

その他受賞案件

受賞名	特許番号	発明の名称	発明者氏名
発明奨励賞	特許第6605807号	元素分析装置の清掃機構	谷口 平八朗，黒住 拓司，平田 泰士，山田 雄大
発明奨励賞	特許第6646476号	排ガス計測装置及び排ガス計測方法	大槻 喜則
発明奨励賞	特許第6106773号	流量測定装置及び流量制御装置	安田 忠弘，高倉 洋

Figure 7　令和4年度近畿地方発明表彰式
（左より　谷口 平八朗，有本 公彦，大槻 喜則）

＊編集局注：本内容は特段の記載がない限り，本誌発行年時点での自社調査に基づいて記載しています。

第12回 HORIBA Group IP World Cup Gold Award受賞IPの紹介

Award Winners of 2022 HORIBA Group IP World Cup

IP World Cup

HORIBAグループで生まれた数々の独創的な技術や知的財産（以下，Intellectual Propertyの略語として「IP」ともいう）が事業の推進力となってきた。技術開発とその成果たる知的財産がHORIBAブランドの本質的な要素であり，HORIBA Group IP World Cup（**Figure 1**）は，HORIBA Group is One Companyの精神のもと，事業を牽引する技術・知的財産をグループ全体で賞賛し，次なる成長の起爆剤となる技術・知的財産の創出をさらに奨励していくことを趣旨として創設された。

第12回HORIBA Group IP World Cup[*1]では，海外を含むHORIBAグループの開発拠点で選考された14件の応募があり，株式会社堀場アドバンスドテクノの「Method for measuring residual chlorine concentration during washing of vegetables」がGold Awardを受賞した。この知的財産は，電極に付着する測定妨害物質であるアニオン性有機物と残留塩素の液体中の移動度の違いを利用することで，測定前にアニオン性有機物を取り除き，残留塩素のみを電極表面で検知することができる発明考案であり，今後のHORIBAグループのバイオ・ヘルスケア分野の事業を牽引する技術として以下に紹介する。

＊1 第12回では，2021年6月1日から2022年5月31日の間に創作，出願，論文発表，特許登録，または外部表彰を受賞したなどの知的財産を対象としている。

Figure 1　HORIBA Group IP World Cup

Method for measuring residual chlorine concentration during washing of vegetables

IP：（特許）特願2021-099730
（発明の名称：電気化学測定装置及び電気化学測定方法）
受賞者：宮村 和宏（株式会社堀場アドバンスドテクノ／日本）

Figure 2　Gold Awardを受賞した宮村和宏（右）

Gold Award受賞IPの概要

食品の衛生管理はHACCP*2の義務化もあり，より厳密な管理が必要とされている。たとえば，カット野菜洗浄時の工程管理において，野菜の種類，量や洗浄液の温度，Ph，残留塩素（有効塩素）濃度等の記録を行う。その中でも残留塩素は洗浄中に濃度が低下するため，頻繁に洗浄液を汲み取り，比色法や試験紙を用いて測定・記録を行い，必要に応じて濃度調整を行う必要があった。

これは多大な労力を要し，加えて作業者による測定誤差や測定忘れ，記入ミスなどが懸念される。また，急速に普及している工程管理のIoT化には，現状の手作業は不向きである。これらの課題を打開する手段として，測定作業を自動化でき，データ通信も可能な残留塩素濃度モニターの開発が求められた。

連続的にモニタリングをするにあたり，課題の一つに野菜から溶出するマイナスに電荷をもったアニオン性有機物により，測定値が徐々に低下することが挙げられる。これは，アニオン性有機物と残留塩素の多くを占める次亜塩素酸イオンが同じ電荷を持つため，電極表面に付着するからである。

本受賞発明は，上記のような課題を克服したものであり，妨害物質がある状況下でも測定対象物を測定出来る残留塩素濃度モニターに関するものである。具体的には，**Figure 3**に示すような，アニオン性有機物と残留塩素の移動度の差を利用する。測定前にマイナスに電圧を印加することで，マイナスに電荷をもったアニオン性有機物を電極表面から引き離し，直後に次亜塩素酸イオン濃度を計測することで，アニオン有機物の影響を低減している。

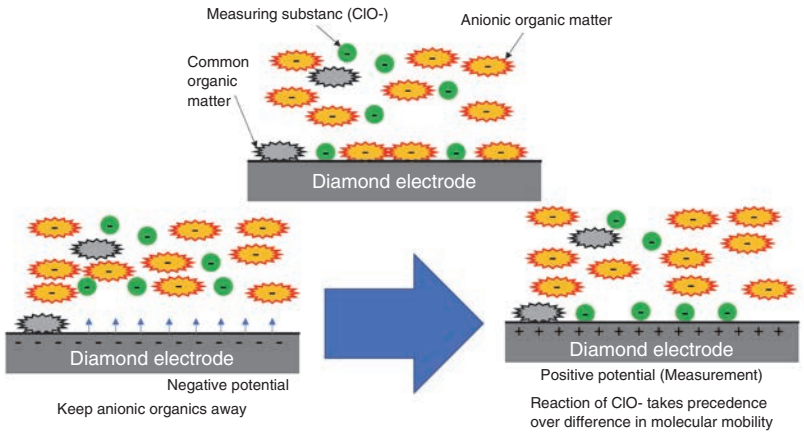

Figure 3　残留塩素の測定手順

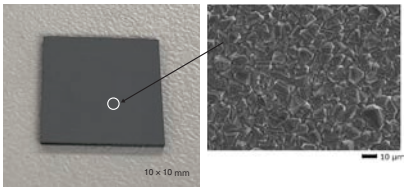

Figure 4　ダイヤモンド電極

また，本発明の電極に慶應義塾大学の栄長泰明教授と開発を進めてきたダイヤモンド電極（BDD；Boron-Doped Diamond）（**Figure 4**）を採用した場合，プラスとマイナスに，数Vの電圧の印加を長期間行っても電極へのダメージを考慮する必要が無くなる。

＊2 HACCP：Hazard Analysis and Critical Control Point

その他受賞IP

【Silver Award】

AI Profiling：Screening for diseases from standard blood analysis

IP：(論文)Malar J. 2020 Nov 23; 19(1): 429. doi: 10.1186/s12936-020-03502-3, Malaria Journal

受賞者：Dr. Sebastien RAIMBAULT(HORIBA ABX SAS／フランス)
(論文名称：Performance evaluation of machine learning-based infectious screening flags on the HORIBA Medical Yumizen H550 Haematology Analyzer for vivax malaria and dengue fever)

概　要：血液検体がマラリアに感染しているかデング熱に感染しているかを予測するための技術。従来の手法では人が顕微鏡で血液検体を観察していたが非常に時間がかかるうえ，マラリア感染をデング熱と間違えずに診断することが難しかった。本IPでは機械学習を用いて血球計数装置で得られた測定値から感染の有無を予測する予想モデルを構築した。この予測モデルを搭載した血球計数装置を用いることで従来よりも迅速に感染した検体をスクリーニングでき，一部においてマラリアとデング熱の区別も可能となった。このことから特にインド等での医療負荷低減に貢献した。

【Bronze Award】

Quick installation method for ADS(Automatic Driving System)by using ISOFIX

IP：(特許)特許第7008615号(発明の名称：保持装置及びそれが備える搭載台の固定方法)

受賞者：古川和樹，松原由明(株式会社堀場製作所／日本)

概　要：人間の代わりにシャシダイナモメータ上で車両を自動で運転する自動運転ロボット(ADS)に関する技術。従来製品は，ベルトとスティックを用いて3箇所で座席に固定しており，車両への搭載に時間がかかっていた。本技術はチャイルドシートを固定するのに十分な強度を持つISOFIXを活用することで，座席との固定箇所を1箇所に削減しても安定した固定を実現した。本IPは，ADSのセールスポイントである車両への搭載性を改善し(従来製品と比較して固定時間を80%削減，全体の搭載時間を52%削減)，利用者の利便性に大きく寄与した。

【Honorable Mention】

MULTI-TRACK RAMAN WELL PLATE READER

IP：(特許)US63/293733(発明の名称：MULTI-TRACK RAMAN WELL PLATE READER)

受賞者：Dr. Aashish TULADHAR, Nicolas VEZARD, Beth FINAMORE(HORIBA Instruments Incorporated／アメリカ)

概　要：ラマンプローブが複数本配置されたウェルプレートリーダーに関する技術であり，Life Science等の成長市場への展開が期待され，選定された。プローブはウェルプレート上で互いに隣接しないように配置され，ラマン信号をHII製の冷却scientific CMOSカメラ(SylentTM)を使ったイメージング分光器の独立離間したチャンネルに導く。この構造により，ラマン信号の同時取得が可能となり，クロストークを抑えつつ測定速度と測定感度の大幅向上を実現した。本IPの適用製品(PoliSpectraTM Raman Plate Reader)により，ハイスループットスクリーニングが必要となる創薬等のユーザーの要求に答えることができた。

Figure 5　表彰式

＊編集局注：本内容は特段の記載がない限り，本誌発行年時点での自社調査に基づいて記載しています。

Scientific Research Papers from HORIBA Group

From July 1, 2022 to March 31, 2023 on ScienceDirect

Towards tailpipe sub-23 nm solid particle number measurements for heavy-duty vehicles regulations

a: Barouch Giechaskiel, b: Matthias Schwelberger, c: Linus Kronlund, d: Christophe Delacroix, e: Logan A. Locke, f: M. Yusuf Khan, g: Tobias Jakobsson, Hua Lu Karlsson, h: Yoshinori Otsuki, i: Sawan Gandi, j: Stefan Keller, Benedikt Grob, k: Christos Dardiodis, Athanasios Mamakos

a: European Commission, Joint Research Centre (JRC)
b: Daimler Truck AG
c: Volvo GTT
d: Volvo Powertrain Engineering
e: Cummins Ltd
f: Cummins Inc.
g: Scania
h: Horiba Europe GmbH
i: Sensors Europe GmbH
j: AIP GmbH Co. KG
k: AVL List GmbH
Transportation Engineering Volume 9, September 2022, 100137

Indocyanine green conjugated phototheranostic nanoparticle for photodiagnosis and photodynamic therapy

a: Kenta Shinoda, Akane S. Suzuki, Toshinori Nakayama, bc: Akiko Suginami, Yutaka Tamura, d: Yasumitsu Moriya, e: Masamichi Yamashita, e: Tsutomu Tanaka, Yoshiharu Okamoto, f: Hiroshi Suito, Yasunori Akutsu, Hisahiro Matsubara, g: Kengo Saito, Hiroshi Shirasawa, h: Yoko Shinozaki, i: Kazuoki Isojima, j: Naohito Nakamura, Yasushi Miyauchi

a: Department of Immunology, Graduate School of Medicine, Chiba University
b: Department of Bioinformatics, Graduate School of Medicine, Chiba University
c: Molecular Chirality Research Center, Chiba University
d: Department of General Thoracic Surgery, Graduate School of Medicine, Chiba University
e: Department of Veterinary Clinical Medicine, School of Veterinary Medicine, Tottori University
f: Department of Frontier Surgery, Graduate School of Medicine, Chiba University
g: Department of Molecular Virology, Graduate School of Medicine, Chiba University
h: HORIBA Techno Service Co., Ltd.
i: Tateyama Machine Co., Ltd.
j: Kamakura Techno-Science, Inc.
Photodiagnosis and Photodynamic Therapy Volume 39, September 2022, 103041

Electro-thermal modelling of redox flow-batteries with electrolyte swapping for an electric ferry

a: Richard Woodfield, Stephan Glover, b: Robert Watson, c: Peter Nockemann, d: Richard Stocker

a: School of Mechanical and Aerospace Engineering, Queen's University Belfast
b: School of Aeronautical and Automotive Engineering, Loughborough University
c: School of Chemistry, The QUILL Research Centre, Queen's University Belfast
d: HORIBA MIRA
Journal of Energy Storage Volume 54, October 2022, 105306

Determination of Cabernet Sauvignon wine quality parameters in Chile by Absorbance-Transmission and fluorescence Excitation Emission Matrix (A-TEEM) spectroscopy

a: Jorge Zincker, Alvaro Gonzalez, ac: Doreen Schober, b: Adam Gilmore, Linxi Chen

a: Center for Research and Innovation, Vina Concha y Toro
b: HORIBA Instruments Inc.
c: Emiliana Organic Vineyards
Food Chemistry Volume 392, 30 October 2022, 133101

Quantitative assessment of visual microscopy as a tool for microplastic research: Recommendations for improving methods and reporting

a: Syd Kotar, Kristine Gesulga, Wenjian Lao, Leah M. Thornton Hampton, Stephan B. Weisberg, Charles S. Wong, b: Rae McNeish, c: Clare Murphy-Hagan, Andrew B. Gray, Samiksha Singh, d: Violet Renick, e: Chih-Fen T. Lee, Theresa Slifko f: Clare Steele, g: Bert van Bavel, gh: Amy Lusher, i: Charles Moore, Win Cowger, j: Elizabeth Minor, k: Paul Helm, m: Keith Rickabaugh, n: Hannah De Frond, Keenan Munno, Chelsea M. Rochman, o: Gaurav Amarpuri, p: Robert C. Andrews, q: Steven M. Barnett, rs: Silke Christiansen, s: Florian Vollnhals, t: Kevin Crampond, u: Fangni Du, v: Jeanne Hankett, w: Kay Ho, x: Julia Jaeger, y: Claire Lilley, z: Lei Mai, aa: Odette Mina, ab: Eunah Lee, ac: Sebastian Primpke, ad: Joakim Skovly, ae: Suja Sukumaran, af: Jennifer Van Brocklin, ag: Chenxi Wu

a: Southern California Coastal Water Research Project Authority
b: Department of Biology, California State University
c: Department of Environmental Sciences, University of California-Riverside
d: Orange County Sanitation District
e: Water Quality Laboratory, Metropolitan Water District of Southern California
f: Environmental Science and Resource Management, California State University
g: Norwegian Institute for Water Research
h: Department of Biological Sciences, University of Bergen
i: The Moore Institute for Plastic Pollution Research
j: Department of Chemistry and Biochemistry and Large Lakes Observatory, University of Minnesota Duluth
k: NatureWorks LLC
l: Environmental Monitoring & Reporting Branch, Ontario Ministry of the Environment
m: RJ Lee Group
n: Department of Ecology and Evolutionary Biology, University of Toronto
o: Eastman Chemical Company
p: Department of Civil and Mineral Engineering, University of Toronto
q: Barnett Technical Services
r: Fraunhofer Institute for Ceramics Technology and Systems (IKTS)
s: Institute for Nanotechnology and Correlative Microscopy (INAM)
t: Institut des Sciences de la Mer de Rimouski, Universite du Quebec a Rimouski
u: State Key Laboratory of Estuarine and Coastal Research, East China Normal University
v: BASF Corporation
w: US Environmental Protection Agency, Atlantic Coastal Environmental Sciences Division
x: Eurofins Environment Testing Australia
y: Eurofins SF Analytical Laboratories, Inc.
z: Center for Environmental Microplastics Studies, Guangdong Key Laboratory of Environmental Pollution and Health, School of Environment, Jinan University
aa: The Energy and Environmental Sustainability Laboratories, The Pennsylvania State University

ab: Horiba Instruments, Inc.
ac: Alfred Wegener Institute, Helmholtz Centre for Polar and Marine Research
ad: Eurofins Environmental Testing Norway AS
ae: Thermo Fisher Scientific
af: Department of Fisheries, Wildlife, and Conservation Sciences, Oregon State University
ag: State Key Laboratory of Freshwater Ecology and Biotechnology, Institute of Hydrobiology, Chinese Academy of Sciences
Chemosphere Volume 308, Part 3, December 2023, 136449

Isothermal crystallization of polyhydroxyalkanoate (PHA) utilizing Raman spectroscopy to follow chain packing as well as molecular motion

a: Fran Adar, b: Reva Street, c: Isao Noda

a: HORIBA Scientific, USA
b: Drexel University
c: University of Delaware
Spectrochimica Acta Part A: Molecular and Biomolecular Spectroscopy Volume 285, 15 January 2023, 121861

pH response and mechanical properties of Fe_2O_3-TeO_2-based glass/stainless steel enamel electrodes for pH sensors

a: Tadanori Hashimoto, Tomonari Kuno, Daiki Ito, Atsushi Ishihara, b: Yuji Nishio

a: Division of Chemistry for Materials, Graduate School of Engineering, Mie University
b: HORIBA Advanced Techno, Co., Ltd.
Heliyon Volume 9, Issue 1, January 2023, e12966

Non-destructive estimation of the cation composition of natural carbonates by micro-Raman spectroscopy

ab: Shu-hei Urashima, Hiroharu Yui, c: Mayu Morita, Shintaro Komatani

a: Department of Chemistry, Faculty of Science, Tokyo University of Science
b: Water Frontier Research Center, Research Institute for Science & Technology, Tokyo University of Science
c: HORIBA Techno Service Co., Ltd.
Analytica Chimica Acta Volume 1242, 15 February 2023, 340798

What determines accuracy of chemical identification when using microspectroscopy for the analysis of microplastics?

a: Hannah De Frond, b: Win Cowger, c: Violet Renick, d: Susanne Brander, e: Sebastian Primpke, f: Suja Sukumaran, g: Dounia Elkhatib, h: Steve Barnett, i: Maria Navas-Moreno, j: Keith Rickabaugh, k: Florian Vollnhals, l: Bridget O'Donnell, m: Amy Lusher, n: Eunah Lee, o: Wenjian Lao, p: Gaurav Amarpuri, q: George Sarau, kq: Silke Christiansen

a: Department of Ecology & Evolutionary Biology, University of Toronto
b: Moore Institute for Plastic Pollution Research
c: Environmental Services Department, Orange County Sanitation District
d: Department of Fisheries, Wildlife, and Conservation Sciences, Coastal Oregon Marine Experiment Station, Oregon State University
e: Alfred Wegener Institute, Helmholtz Centre for Polar and Marine Research, Biologische Anstalt Helgoland

f: Thermo Fisher Scientific
g: Oak Ridge Institute of Science Education, c/o U.S. Environmental Protection Agency, ORD/CEMM Atlantic Coastal Environmental Sciences Division
h: Barnett Technical Services
i: Lever Photonics
j: RJ Lee Group
k: Institute for Nanotechnology and Correlative Microscopy - INAM
l: HORIBA Scientific, USA
m: Norwegian Institute for Water Research, Oslo, Norway, Department of Biological Sciences, University of Bergen
n: HORIBA Instruments Inc.
o: Southern California Coastal Water Research Project Authority
p: Eastman Chemical Company
q: Fraunhofer Institute for Ceramics Technology and Systems - IKTS
Chemosphere Volume 313, February 2023, 137300

Absorbance-transmission and fluorescence excitation-emission matrix (A-TEEM) with multi-block data analysis and machine learning for accurate intraregional classification of Barossa Shiraz wine

a: Ranaweera K.R. Ranaweera, ab: Susan E.P. Bastian, Dimitra L. Capone, David W. Jeffery, c: Adam M. Gilmore

a: Department of Wine Science and Waite Research Institute, The University of Adelaide (UA)
b: Australian Research Council Training Centre for Innovative Wine Production
c: HORIBA Instruments Inc.
Food Control Volume 144, February 2023, 109335

Effect of natural and forced charge air humidity on the performance and emissions of a compression-ignition engine operating at high warm altitude

a: Jose Ramon Serrano, Jaime Martin, Pedro Piqueras, Roberto Tabet, b: Javier Gomez

a: Universitat Politecnica de Valencia, Spain
b: HORIBA Europe GmbH, Germany
Energy Volume 266, March 2023, 126409

Machine learning for classifying and predicting grape maturity indices using absorbance and fluorescence spectra

ab: Claire E.J. Armstrong, Vinay Pagay, David W. Jeffery c: Adam M. Gilmore, ad: Paul K. Boss

a: Australian Research Council Training Centre for Innovative Wine Production, The University of Adelaide
b: School of Agriculture, Food and Wine, and Waite Research Institute, The University of Adelaide
c: HORIBA Instruments Inc.
d: CSIRO Agriculture and Food
Food Chemistry Volume 403, 1 March 2023, 134321

Influence of nitro group on solvatochromism, nonlinear optical properties of 3-morpholinobenzanthrone: Experimental and theoretical study

a: Anup Thomas, b: Elena M. Kirilova, c: B.V. Nagesh, B. Siddlingeshwar, d: Krishna Chaitanya, e: Reji Philip, f: S.R Manohara, g: H.C. Sudeeksha

a: Centre for Computational Research in Clean Energy Technologies, Sree Chitra Thirunal College of Engineering

b: Department of Chemistry, Daugavpils University

c: Department of Physics, M.S. Ramaiah Institute of Technology, (Autonomous Institute affiliated to VTU)

d: School of Chemical Sciences, SRTM University

e: Light and Matter Physics Group, Raman Research Institute

f: Nano-Composites and Materials Research Lab, Department of Physics, Siddaganga Institute of Technology, (Autonomous Institute affiliated to VTU)

g: HORIBA India Scientific

Journal of Photochemistry and Photobiology A: Chemistry Volume 437, 1 March 2023, 114434

* Editorial note: This content is based on HORIBA's investigation at the year of issue unless otherwise stated.

HORIBA World-Wide Network

JAPAN

HORIBA, Ltd.

2 Miyanohigashi-cho, Kisshoin, Minami-ku, Kyoto, 601-8510, Japan
Phone : (81)75-313-8121 Fax : (81)75-321-8312

Biwako Factory
1-15-1, Noka, Otsu, Shiga, 520-0102, Japan
Phone : (81)-77-548-6130 Fax : (81)-77-548-6193

Saiin Factory
43-1 Nishimizosaki-cho, Saiin, Ukyo-ku, Kyoto, 615-0046, Japan
Phone : 81-75-323-7067 Fax : 81-75-323-7085

Tokyo Branch
Kanda Awaji-cho Nichome Building, 2-6 Kanda Awaji-cho, Chiyoda-ku, Tokyo, 101-0063, Japan
Phone : 81-3-6206-4711 Fax : 81-3-6206-4720

Tokyo Sales Office
Kanda Awaji-cho Nichome Building, 2-6 Kanda Awaji-cho, Chiyoda-ku, Tokyo, 101-0063, Japan
Phone : 81-3-6206-4721 Fax : 81-3-6206-4730

Hokkaido Sales Office
6F Park East Sapporo, 1-3 Minami Ichijo Higashi, Chuo-ku, Sapporo, Hokkaido, 060-0051, Japan
Phone : 81-11-207-1800 Fax : 81-11-207-1802

Tohoku Sales Office
4-21-8 Izumichuo, Izumi-ku, Sendai, Miyagi, 981-3133, Japan
Phone : 81-22-776-8251 Fax : 81-22-772-6727

Tochigi Sales Office
1F Flora Building, 1-9-15 Higashishukugo, Utsunomiya, Tochigi, 321-0953, Japan
Phone : 81-28-634-7051 Fax : 81-28-634-6099

Yokohama Sales Office
1F ShinYokohama Mineta Building, 2-3-19 Shinyokohama, Kohoku-ku, Yokohama, 222-0033, Japan
Phone : 81-45-478-7017 Fax : 81-45-478-7029

Nagoya Sales Office
4F BIZrium Nagoya, 3-1-17 Noritakeshinmachi, Nishi-ku, Nagoya, Aichi, 451-0051, Japan
Phone : 81-52-433-3450 Fax : 81-52-433-3460

Toyota Sales Office
2-23 Tsukasa-cho, Toyota, Aichi, 471-0831, Japan
Phone : 81-565-37-8510 Fax : 81-565-37-8511

Hamamatsu Sales Office
221-1 Sanjino-cho, Minami-ku, Hamamatsu, Shizuoka, 430-0816, Japan
Phone : 81-53-468-7780 Fax : 81-53-468-7781

Osaka Sales Office
4F ShinOsaka UenoToyo Building, 7-4-17 Nishinakajima, Yodogawa-ku, Osaka, 532-0011, Japan
Phone : 81-6-6390-8011 Fax : 81-6-6390-8012

Shikoku Sales Office
9-9 Imazato-cho, Takamatsu, Kagawa, 760-0078, Japan
Phone : 81-87-867-4800 Fax : 81-87-867-4801

Hiroshima Sales Office
1F Furuta Building, 2-5-27 Miyanomachi, Fuchu-cho, Aki-gun, Hiroshima, 735-0005, Japan
Phone : 81-82-288-4433 Fax : 81-82-286-0761

Kyusyu Sales Office
1F Hakata Fukoku Seimei Building, 8-30 Tenyamachi, Hakata-ku, Fukuoka, 812-0025, Japan
Phone : 81-92-292-3593 Fax : 81-92-292-3594

HORIBA Advanced Technology Center
11-5 Hokotate-cho, Kamitoba, Minami-ku, Kyoto, 601-8116, Japan
Phone : 81-75-693-2300 Fax : 81-75-693-2350

Kutsuki Training Center
335-10 Tochu, Kutsuki, Takashima, Shiga, 520-1425, Japan
Phone : 81-740-38-3127 Fax : 81-740-38-3126

HORIBA STEC, Co., Ltd.

11-5 Hokotate-cho, Kamitoba, Minami-ku, Kyoto, 601-8116, Japan
Phone : (81)-75-693-2300 Fax : (81)-75-693-2350

Aso Factory
Torikokogyodanchi, 358-11, Koumaibata, Toriko, Nishiharamura, Aso-gun, Kumamoto, 861-240, Japan
Phone : (81)-96-279-2921 Fax : (81)-96-279-3364

Fukuchiyama Technology Center
11-1 Miwa-cho Miwa, Fukuchiyama, Kyoto, 620-1445 Japan
Phone : (81)-773-59-2070 Fax : (81)-773-59-2074

Tokyo Sales Office
5F Kanda Awaji-cho Nichome Building, 2-6 Kanda Awaji-cho, Chiyoda-ku, Tokyo, 101-0063, Japan
Phone : 81-3-6206-4731 Fax : 81-3-6206-4740

Tohoku Sales Office
4-21-8 Izumichuo, Izumi-ku, Sendai, Miyagi, 981-3133, Japan
Phone : 81-22-772-6717 Fax : 81-22-772-6727

Yamanashi Sales Office
3F Daita Building, 2-14-13, Marunouchi, Kofu, Yamanashi, 400-0031, Japan
Phone : 81 55-231-1351 Fax : 81- 55-231-1352

Nagoya Sales Office
4F BIZrium Nagoya, 3-1-17 Noritakeshinmachi, Nishi-ku, Nagoya, Aichi, 451-0051, Japan
Phone : 81-52-433-3451 Fax : 81-52-433-3461

Kyushu Chuo Sales Office
Torikokogyodanchi, 358-11 Koumaibata, Toriko, Nishiharamura, Aso-gun, Kumamoto, 861-2401, Japan
Phone : 81-96-279-2922 Fax : 81-96-279-3364

HORIBA Advanced Techno, Co.,Ltd.

2 Miyanohigashi-cho, Kisshoin, Minami-ku, Kyoto, 601-8551, Japan
Phone : (81)-75-321-7184 Fax : (81)-75-321-7291

Factory
2 Miyanohigashi-cho, Kisshoin, Minami-ku, Kyoto, 601-8551, Japan
Phone : 81-75-321-1215 Fax : 81-75-321-1079

Tokyo Sales Office
Kanda Awaji-cho Nichome Building, 2-6 Kanda Awaji-cho, Chiyoda-ku, Tokyo, 101-0063, Japan
Phone : 81-3-6206-4751 Fax : 81-3-6206-4760

Tohoku Sales Office
4-21-8 Izumichuo, Izumi-ku, Sendai, Miyagi, 981-3133, Japan
Phone : 81-22-776-8253 Fax : 81-22-772-6727

Nagoya Sales Office
4F BIZrium Nagoya, 3-1-17 Noritakeshinmachi, Nishi-ku, Nagoya, Aichi, 451-0051, Japan
Phone : 81-52-433-3452 Fax : 81-52-433-3462

Osaka Sales Office
4F ShinOsaka UenoToyo Building, 7-4-17 Nishinakajima, Yodogawa-ku, Osaka, 532-0011, Japan
Phone : 81-6-6390-8211 Fax : 81-6-6390-8222

Shikoku Satellite Office
9-9 Imazato-cho, Takamatsu, Kagawa, 760-0078, Japan
Phone : 81-87-867-4841 Fax : 81-87-867-4842

Kyusyu Sales Office
1F Hakata Fukoku Seimei Building, 8-30 Tenyamachi, Hakata-ku, Fukuoka, 812-0025, Japan
Phone : 81-92-292-3595 Fax : 81-92-292-3596

Kyushu Chuo Sales Office
Torikokogyodanchi, 358-11, Koumaibata, Toriko, Nishiharamura, Aso-gun, Kumamoto, 861-240, Japan
Phone : 81-96-234-8035 Fax : 81-75-321-7291

HORIBA TECHNO SERVICE Co., Ltd.

2 Miyanohigashi, Kisshoin, Minami-ku, Kyoto, 601-8305, Japan
Phone : (81)-75-313-8125 Fax : (81)-75-321-5647

Tokyo Service Station
4F Kanda Awaji-cho Nichome Building, 2-6 Awaji-cho, Kanda, Chiyoda-ku,Tokyo, 101-0063, Japan
Phone : 81-3-6206-4750 Fax : 81-3-6206-4742

Hokkaido Sevice Station
6F Park East Sapporo, 1-3 Minami Ichijo Higashi, Chuo-ku, Sapporo, Hokkaido, 060-0051, Japan
Phone : 81-11-207-1801 Fax : 81-11-207-1802

Tohoku Service Station
4-21-8 Izumichuo, Izumi-ku, Sendai, Miyagi, 981-3133, Japan
Phone : 81-22-776-8252 Fax : 81-22-772-6727

Fukushima Service Station
101 Office Tatsumi, 5-13-17 Saikon, Koriyama, Fukushima, 963-8862, Japan
Phone : 81-24-925-9311 Fax : 81-24-925-9312

Tochigi Service Station
1F Flora Building, 1-9-15 Higashishukugo, Utsunomiya, Tochigi, 321-0953, Japan
Phone : 81-28-634-6098 Fax : 81-28-634-6099

Chiba Service Station
1-8-12 Goichuo-higashi, Ichihara, Chiba, 290-0054,Japan
Phone : 81-436-24-3914 Fax : 81-436-24-0642

Kashima Service Station
1-4-35 Kamisu, Kamisu, Ibaraki, 314-0143, Japan
Phone : 81-299-91-0808 Fax : 81-299-92-9561

Tsukuba Service Station
203 Tsukuba Cityia Moi Building, 5-20-2 Kenkyugakuen, Tsukuba, Ibaraki, 305-0817, Japan
Phone : 81-29-863-7311 Fax : 81-29-859-5221

Saitama Service Station
1F Higashikawaguchi Garden Plaza, 1-6-1 Totsukahigashi, Kawaguchi, Saitama, 333-0802, Japan
Phone : 81-48-298-6871 Fax : 81-48-298-6880

Nishitokyo Service Station
1F The-Macrocosm, 3-37-34 Izumi, Kokubunji, Tokyo, 185-0024, Japan
Phone : 81-42-322-3211 Fax : 81-42-322-3210

Yokohama Service Station
1F Plime ShinYokohama Building, 2-3-19 Shinyokohama, Kohoku-ku, Yokohama, Kanagawa, 222-0033, Japan
Phone : 81-45-478-7018 Fax : 81-45-478-7029

Fuji Service Station
1F Suzuki Building, 4-7 Suzukawahigashi-cho, Fuji, Shizuoka, 417-0012, Japan
Phone : 81-545-33-3152 Fax : 81-545-33-3159

Hamamatsu Service Station
221-1 Sanjino-cho, Minami-ku, Hamamatsu, Shizuoka, 430-0816, Japan
Phone : 81-53-464-1339 Fax : 81-53-464-6528

Tokai Service Station
2-23 Tsukasa-cho, Toyota, Aichi, 471-0831, Japan
Phone : 81-565-37-3510 Fax : 81-565-37-3520

Nagoya Service Station
1F Riverpage, 3-203 Kamiyashiro, Meito-ku, Nagoya, Aichi, 465-0025, Japan
Phone : 81-52-705-0711 Fax : 81-52-705-0710

Hokuriku Service Station
1F Ichigo-Toyama-Eki-Nishi Building, 1-1-19 Jintsu-Honmachi, Toyama, 930-0008, Japan
Phone : 81-76-422-6112 Fax : 81-76-422-6446

Mie Service Station
1F Taiyo-Seimei Yokkaichi Building, 1-1-18 Unomori, Yokkaichi, Mie, 510-0074, Japan
Phone : 81-59-340-6061 Fax : 81-59-340-6063

Kyoto Service Station
2 Miyanohigashi, Kisshoin, Minami-ku, Kyoto, 601-8305, Japan
Phone : 81-75-325-5291 Fax : 81-75-321-5647

Osaka Service Station
4F ShinOsaka UenoToyo Building, 7-4-17 Nishinakajima, Yodogawa-ku, Osaka, 532-0011, Japan
Phone : 81-75-325-5291 Fax : 81-75-321-5647

Hyogo Service Station
381 Nnjyo, Himeji, Hyogo, 670-0952, Japan
Phone : 81-79-284-8320 Fax : 81-79-284-8321

Shikoku Service Station
9-9 Imazato-cho, Takamatsu, Kagawa, 760-0078, Japan
Phone : 81-87-867-4821 Fax : 81-87-867-4822

Okayama Service Station
1-12-35 Tsurajima, Kurashiki, Okayama, 712-8012, Japan
Phone : 81-86-448-9760 Fax : 81-86-446-5637

Hiroshima Service Station
1F Furuta Building, 2-5-27 Miyanomachi, Fuchucho, Aki-gun, Hiroshima, 735-0005, Japan
Phone : 81-82-283-3378 Fax : 81-82-286-0761

Yamaguchi Service Station
1F 3rd Hanada Building, 1-72 Hashimoto, Shunan, Yamaguchi, 745-0022, Japan
Phone : 81-834-34-8684 Fax : 81-834-34-8685

Kyusyu Service Station
1F Hakata Fukoku Seimei Building, 8-30 Tenyamachi, Hakata-ku, Fukuoka, 812-0025, Japan
Phone : 81-92-292-3597 Fax : 81-92-292-3598

Oita Service Station
1F Tsuruwa Building, 2-2-37 Hagiwara, Oita, 870-0921, Japan
Phone : 81-97-551-3982 Fax : 81-97-551-3889

Kumamoto Service Station
Toriko-kogyodanchi, 358-11, Koumaibata, Toriko, Nishiharamura, Aso-gun, Kumamoto, 861-2401, Japan
Phone : 81-96-279-2985 Fax : 81-96-279-2986

HORIBA World-Wide Network

BRAZIL

HORIBA Instruments Brasil, Ltda.
Rua Presbitero Plinio Alves de Souza, 645, Loteamento Multivias, Jardim Ermida II - Jundiai Sao Paulo - CEP 13.212-181 Brazil
Phone : (55)-11-2923-5400 Fax : (55)-11-2923-5490

TCA/HORIBA Sistemas de Testes Automotivos Ltda.
Avenida Luigi Papaiz, 239 - Campanário, Diadema, São Paulo, Brazil CEP: 09931-610
Phone : (55)-11-4224-0200 Fax : (55)-11-4227-3133

CANADA

HORIBA Canada, Inc.
Unit102, 5555 North Service Road Burlington, Ontario, Canada, L7L 5H7
Phone : (1)-905-335-0234 Fax : (1)-905-331-2362

London Office
347 Consortium Court, London, Ontario, Canada, N6E 2S8
Phone : 1-519-668-6920 Fax : 1-519-668-8437

U.S.A.

HORIBA Americas Holding Incorporated
9755 Research Drive, Irvine, CA 92618, U.S.A.
Phone : (1)-949-250-4811

HORIBA Instruments Incorporated
9755 Research Drive, Irvine, CA 92618, U.S.A.
Phone : (1)-949-250-4811 Fax : (1)-949-250-0924

Ann Arbor Office
5900 Hines Drive, Ann Arbor, MI 48108, U.S.A.
Phone : (1)-734-213-6555 Fax : (1)-734-213-6525

Austin Office
9701 Dessau Road, Suite 605, Austin, TX 78754, U.S.A.
Phone : (1)-512-836-9560 Fax : (1)-512-836-8054

Canton Office
5449 Research Drive Canton, MI 48188, U.S.A.
Phone : (1)-800-445-9853 Fax : (1)-734-483-1592

Fletcher Office
270 Rutledge Road, Unit D Fletcher, NC 28732, U.S.A.
Phone : (1)-828-676-2801 Fax : (1)-828-676-2805

Houston Office
5390 Bay Oaks Drive, Pasadena, TX 77505, U.S.A.
Phone : 1-281-482-4334 Fax : 1-281-674-6058

Novato Field Office
359 Bel Marin Keys Blvd, #18, Novato, CA 94949, U.S.A.

HORIBA New Jersey Optical Spectroscopy Center
20 Knightsbridge Rd, Piscataway, NJ 08854, U.S.A.
Phone : +(1)-732-494-8660 Fax : +(1)-732-549-5125

Portland Office
7007 S.W. Cardinal Lane, Suite 185, Portland, OR 97224, U.S.A.
Phone : +(1)-503-624-9767 Fax : +(1)-503-968-3236

HORIBA Reno Technology Center
3740 Barron way Reno, Nevada 89511, U.S.A.
Phone : +(1)-775-358-2332 Fax : +(1)-775-358-0434

Sunnyvale Office
430 Indio Way, Sunnyvale CA 94085, U.S.A.
Phone : +(1)-408-730-4772 Fax : +(1)-408-730-8975

Tempe Office
1515 West University Drive, Suite 101 Tempe, AZ 85281, U.S.A.
Phone : +(1)-480-791-2203

Troy Office
2890 John R Road, Troy, MI 48083, U.S.A.
Phone : +(1)-248-689-9000 Fax : +(1)-248-689-8578

AUSTRIA

HORIBA (Austria) GmbH
Kaplanstrasse 5, A-3430 Tulln, Austria
Phone : +(43)-2272-65225 Fax : +(43)-2272-65225-45

CZECH

HORIBA Czech Olomouc Factory
Zeleznicni 512/7, 779 00 Olomouc, Czech Republic
Phone : +(420) 588 118 365 + (420) 588 118 393

HORIBA Czech Prague Office
Prumyslova 1306/7, CZ-10200, Praha 10, Czech Republic
Phone : +(420) 246 039 265

FRANCE

HORIBA Europe Holding SASU
14 Boulevard Thomas Gobert - CS 45002 - 91120 Palaiseau - France

HORIBA Europe Research Center
14 Boulevard Thomas Gobert - Passage Jobin Yvon CS 45002 - 91120 Palaiseau - France
Phone : +(33)-1-69-74-72-00 Fax : +(33)-1-69-31-32-20

HORIBA FRANCE SAS, Longjumeau Office
16-18, rue du Canal, 91165 Longjumeau Cedex, France
Phone : +(33)-1-69-74-72-00 Fax : +(33)-1-69-09-07-21

HORIBA FRANCE SAS, Lille Office
455 avenue Eugène Avinée - 59120 LOOS - France
Phone : +(33)-1-69-74-72-00 Fax : +(33)-3-20-59-18-08

HORIBA ABX SAS
Parc Euromédecine, rue du Caducée, BP7290, 34184 Montpellier Cedex 4, France
Phone : +33 (0)4 67 14 15 16 Fax : +33 4-67-14-15-17

GERMANY

HORIBA Europe GmbH / Oberursel Office
Hans-Mess-Str.6, D-61440 Oberursel, Germany
Phone : +(49)-6172-1396-0 Fax : +(49)-6172-1373-85

HORIBA Europe GmbH, Darmstadt Office
Landwehrstrasse 55, D-64293, Darmstadt, Germany
Phone : +(49)-6151-5000-0 Fax : +(49)-6151-5000-3865

HORIBA Europe GmbH, Dresden Office
Hugo-Junckers-Ring 1, 01109 Dresden, Germany
Phone : +(49)-351-8896807 Fax : +(49)-351-8896808

HORIBA Europe GmbH, Florsheim Office
Mariechen-Graulich-Straße 10-12a, 65439 Flörsheim, Germany
Phone : +49 6145 37699-12

HORIBA Europe GmbH, Hanover Office
Frankenring 14, D-30855 Langenhagen, Germany
Phone : +49 511-65523987 Fax : +49 511-54571751

HORIBA Europe GmbH, Korschenbroich Office
Friedrich-Ebert-Str. 9-11, D-41352 Korschenbroich, Germany
Phone : +(49)-2161-47537-0

HORIBA Europe GmbH, Leichlingen Office
Julius-Kronenberg-Str. 9, D-42799 Leichlingen, Germany
Phone : +(49)-2175-8978-0 Fax : +(49)-2175-897850

HORIBA Europe GmbH, Munich Office
Waldmeisterstr. 72-74/Robinienstr. 66, D-80935 Munich, Germany
Phone : +(49)-89-2444779-0 Fax : +(49)-89-2444779-10

HORIBA Europe GmbH, Potsdam Office
Dennis-Gabor-Str. 2, D-14469 Potsdam, Germany
Phone : +(49)-3316-4900-70 Fax : +(49)-3316-4900-74

HORIBA Europe GmbH, Stuttgart Office (Boeblingen)
Hanns-Klemm-Str. 56, D-71034 Boeblingen, Germany
Phone : +(49)-7031-677-9440 Fax : +(49)-7031-677-9450

HORIBA Europe GmbH, Stuttgart Office (Neuhausen)
Zabergaeustr. 3, D-73765 Neuhausen, Germany
Phone : +(49)-7158-933-800 Fax : +(49)-7158-933-899

HORIBA Europe GmbH, Wolfsburg Office
Klauskamp, Heinenkap II 38444 Wolfsburg, Germany
Phone : +(49)-5361-38653-16 Fax : +(49)-5361-38653-24

HORIBA Jobin Yvon GmbH
Neuhofstrasse 9, D_64625, Bensheim, Germany
Phone : 49(0)62-51-84-750 Fax : 49(0)62-51-84-7520

HORIBA FuelCon GmbH
Otto-von-Guericke-Allee 20, 39179 Barleben, Germany
Phone : +49 39203 514 400 Fax : +49 39203 514 409

BeXema GmbH
Otto-von-Guericke-Allee 20, 39179 Barleben, Germany
Phone : +49 39203 964 200

HORIBA Tocadero GmbH
Johann-Hittorf-Str. 8 12489 Berlin Germany
Phone : +49 (0)30 6392 3150 Fax : +49 (0)30 6392 3151

ITALY

HORIBA ITALIA Srl
Via Luca Gaurico 209 - 00143 ROMA,Italy
Phone : +(39)-6-51-59-22-1 Fax : +(39)-6-51-96-43-34

Torino Office
Via Feroggio, 30, 10151 Torino, Italy
Phone : +(39)-1-19-04-06-01 Fax : +(39)-1-19-00-04-48

HORIBA ABX SAS, Italy Branch
Viale Luca Gaurico 209/211, 00143 Roma, Italy
Phone : +(39)-6-51-59-22-1 Fax : +(39)-6-51-96-43-34

NETHERLANDS

HORIBA Europe GmbH, Netherlands Branch
Science Park Eindhoven 5080 (Industrial park " Ekkersrijt ") 5692 EA, Son, Netherlands
Phone : +(31)-40-2900240 Fax : +(31)-40-2900624

POLAND

HORIBA ABX Sp. z o.o.
Aleja Niepodleglosci 18, 02-653 Warszawa (Warsaw), Poland.
Phone : +(48)-22-673-2022 Fax : +(48)-22-673-2026

PORTUGAL

HORIBA ABX SAS, Portugal Branch
Alfrapark - Estrada de Alfragide n° 67, Edificio F - Piso 0 Sul, 2610-008 Amadora, Portugal
Phone : +(35)-12-14-72-17-70 Fax : +(35)-12-14-72-17-89

ROMANIA

HORIBA (Austria) GmbH, Romania Branch
B-dul.Republicii, nr. 164, Etaj Parter, Birourile nr. 3 si 4, Pitesti, 110177, Judetul Arges, ROMANIA
Phone : +(40)-348-807117 Fax : +(40)-348-807118

RUSSIA

HORIBA OOO
Altufievskoe shosse, 13, building 5, 127106, Moscow, Russia
Phone : +(7)-495-221-87-71 Fax : +(7)-495-221-87-68

Zelenograd Office
Office 106, 2nd West st., 1, build 1, 124460, Zelenograd city, Moscow, Russia
Phone : (+7)-499-995-09-54

SPAIN

HORIBA ABX SAS, Spain Branch
Calle Apolonio Morales. Num. 6 (Bajos), 28036 Madrid, Spain
Phone : +(34)-91-353-30-10 Fax : +(34)-91-353-30-11

HORIBA MIRA SPAIN, S.L.
Calle Oficios, nave 22, 04620 Vera (Almería), Spain
Phone : +(34)-950-39-11-53

SWEDEN

HORIBA Europe GmbH, Sweden Branch (Gothenburg)
Grimboasen 10 A, S-417 05 Gothenburg, Sweden
Phone : +(46)-10-161 1500 Fax : +(46)-10-161 1503

HORIBA Europe GmbH, Sweden Branch (Sodertalje)
Sydhamnsvagen 55-57, SE- 15138, Sodertalje, Sweden
Phone : +(46)-8-550-80701 Fax : +(46)-8-550-80567

TURKEY

HORIBA Europe GmbH, Istanbul Office
Veysel Karani Mahallesi, Colakoglu Sokak No: 10, Rings Rezidans D:23, PK: 34885, Sancaktepe / Istanbul, Turkey
Phone : +90 216 572 1166 Fax : +90 216 572 1167

HORIBA World-Wide Network

UNITED KINGDOM

HORIBA UK Limited
Kyoto Close Moulton Park Northampton NN3 6FL UK
Phone : +44 (0)1604 542500 Fax : +44 (0)1604 542699

HORIBA UK Finance Limited
Kyoto Close Moulton Park Northampton NN3 6FL UK
Phone : +(44) 1604 542500

HORIBA Jobin Yvon IBH Ltd.
133 Finnieston St. Glasgow G3 8HB, UK
Phone : +(44)-141-229-67-89 Fax : +(44)-141-229-67-90

HORIBA Test Automation Limited
Brook Court Whittington Hall Worcester WR5 2RX, UK
Phone : +(44)-1905-359359 Fax : +(44)-1905 359332

HORIBA MIRA Limited
Watling Street, Nuneaton, Warwickshire, CV10 0TU, United Kingdom
Phone : +(44)-24-7635-5000

Quatro Park
Unit 1, Quatro Park, Paycocke Road, Basildon, Essex, SS14 3GH, United Kingdom
Phone : +(44)-1268-290100

HORIBA MIRA Certification Limited
Watling Street, Nuneaton, Warwickshire, CV10 0TU, United Kingdom
Phone : +(44)-24-7635-5000

MIRA Service Limited
Watling Street, Nuneaton, Warwickshire, CV10 0TU, United Kingdom
Phone : +(44)-24-7635-5000

MIRA Technology Park Limited
Watling Street, Nuneaton, Warwickshire, CV10 0TU, United Kingdom
Phone : +(44)-24-7635-5000

MIRA UGV Limited
Suite 1.03, Technology Centre Nw05 Mira Technology Park, Watling Street, Nuneaton, Warwickshire, United Kingdom, CV10 0TU

CHINA

HORIBA INSTRUMENTS (SHANGHAI) CO., LTD
No.99, Chunxiu Rd, Anting Town, Jiading District, Shanghai, China 201804
Phone : +(86)-21-6952-2835 Fax : +(86)-21-6952-2823

HORIBA Technology (Suzhou) Co.,LTD.
No.1 building, Industry park, No.101 Chenmenjing Rd, Taicang, Jiangsu, China (215400)
Phone : +(86)-0512-3306-6388

HORIBA (China) Co., Ltd.
Room 1604, Building 1, No.185 Moyu Road, Anting Town, Jiading District, Shanghai, China, 201805
Phone : +(86)-21-6289-6060 Fax : +(86)-21-6289-5553

HORIBA (China) Trading Co., Ltd.
Unit D, 1F, Building A, Synnex International Park, 1068 West Tianshan Road, 200335, Shanghai, China
Phone : +(86)-21-6289-6060 Fax : +(86)-21-6289-5553

Beijing Branch
12F, Metropolis Tower, No.2, Haidian Dong 3 Street, Beijing, 100080, China
Phone : +(86)-10-8567-9966 Fax : +(86)-10-8567-9066

Guangzhou Branch
Room 1611/1612, Goldlion Digital Network Center, 138 Tiyu Road East, Guangzhou 510620, China
Phone : +(86)-20-3878-1883 Fax : +(86)-20-3878-1810

HORIBA Precision Instruments (Beijing) Co., Ltd.
Building1, No.3 yuan, Xixing Road, Houshayu Town, Shunyi District, Beijing, 101318 China
Phone : +86-10 8492 9402 Fax : +86-10 8492 7216

MIRA China Ltd.
Unit E, B1F, Building A, Synnex International Park, No. 1068 Tianshan West Road, Shanghai 200335, China
Phone : +(86)-21-6220-6377 Fax : +(86)-21-6220-6379

Xiangyang Workshop
A27-1, Jiahai industrial park, High-tech District, Xiangyang, Hubei, 441004, China
Phone : +(86)-710-2578-268

INDIA

HORIBA India Private Limited
246, OKHLA INDUSTRIAL ESTATE, PHASE 3 NEW DELHI - 110020, India
Phone : +91-11-4646-5000 Fax : +91-11-4646-5020

Bangalore Office
3rd, No.504, 22nd Cross HSR Club Road Sector-3, Bengaluru, Karnataka, 560102, INDIA
Phone : +(91)-80-4127-3637

Chennai Office
No.9, 01 & 02 Floor,Ganapathy Colony,Thiru-Vi-Ka Industrial Estate,Guindy, Chennai ,600032 India
Phone : +(91)-44-42077899

Haridwar Factory
Plot No. 26, Sector-7, IIE, SIDCUL, Haridwar, Uttarakhand - 249403, India
Phone : +(91)-1334-239139

Kolkata Office
EK Tower/6th Floor/Office -4A, Action Area-II D, Newtown, Pin Code 700161,India
Phone : +(91)-90073-63356

Nagpur Factory
Plot No B-3, C-32, MIDC Industrial Area, Butibori, Phase 2, Nagpur, Maharashtra, 441122, India
Phone : +(91) 71-0328-0200

Technical Center
D-225,Chakan MIDC Phase-II, Bhamboli Village, Pune-410501., India
Phone : +(91) 21-3567-6000

INDONESIA

PT HORIBA Indonesia
Jl. Jalur Sutera Blok 20A, No. 16-17, Kel. Kunciran, Kec. Pinang Tangerang - 15144, Indonesia
Phone : +62-21-3044 8525 Fax : +62-21-3044 8521

KOREA

HORIBA KOREA Ltd.
25, 94-Gil, Iljik-Ro, Manan-Gu, Anyang-Si, Gyeonggi-Do, 13901, Korea
Phone : +(82)-31-296-7911 Fax : +(82)-31-296-7913

Ulsan Office
613, Doosan We've the Zenith, 1877, Sinjeong-Dong, Nam-Gu, Ulsan-Si, 44679, Korea
Phone : +(82)-52-275-0122 Fax : +(82)-52-276-0136

HORIBA STEC KOREA, Ltd.
98, Digital valley-ro Suji-gu, Yongin-si Gyeonggi-do 16878 Korea
Phone : +(82)-31-8025-6500 Fax : +(82)-31-8025-6599

PHILIPPINES

HORIBA INSTRUMENTS (SINGAPORE) PTE LTD., MANILA OFFICE
27/F Tower 2, The Enterprise Center, 6766 Ayala Avenue corner Paseo de Roxas, Brgy. San Lorenzo, Makati City, Philippines, 1226
Phone : +63 2 8885 8468 Fax : None

SINGAPORE

HORIBA Instruments (Singapore) Pte Ltd
3 Changi Business Park Vista #01-01, Singapore 486051
Phone : +(65)-6-745-8300 Fax : +(65)-6-745-8155

West Office
83 Science Park Drive, #02-02A, The Curie, Singapore 118258
Phone : +(65)-6-908-9660

TAIWAN

HORIBA Taiwan, Inc.
8F.-8, No.38, Taiyuan St. Zhubei City, Hsinchu County 30265, Taiwan (R.O.C.)
Phone : +(886)-3-5600606 Fax : +(886)-3-5600550

Tainan Office
1F., No.90 Ziyou Rd., Shanhua Dist., Tainan City, 74158, Taiwan (R.O.C.)
Phone : +(886)6-581-1108 Fax : +(886)6-581-1160

THAILAND

HORIBA (Thailand) Limited
46/8 Rungrojthanakul Bld., 1st, 2 nd Floor Ratchadapisek Road., Huai Khwang, Bangkok 10310, Thailand
Phone : +66 (0) 2 861 5995 ext.123 Fax : +66 (0) 2 861 5200

HORIBA Holding (Thailand) Limited
46/8 Rungrojthanakul Bld., 1st, 2 nd Floor, Ratchadapisek Road., Huai Khwang, Bangkok 10310, Thailand
Phone : +(66)-2-861-59-95 Fax : +(66)-2-861-52-00

VIETNAM

HORIBA Vietnam Company Limited
Lot 3 and 4, 16 Floor, Detech Tower II, No. 107 Nguyen Phong Sac Street, Dich Vong Hau Ward, Cau Giay District, Hanoi, Vietnam
Phone : +(84)-24-3795-8552 Fax : +(84)-24-3795-8553

Branch in Ho Chi Minh city
7th Floor, No 09 Dinh Tien Hoang Street, Da Kao Ward, District 1, Hochiminh City, Vietnam
Phone : +84 2871095386

Readout HORIBA Technical Reports May 2023 No.57

発行日　2023 年 5 月 31 日
発行人　中村 博司
発行元　株式会社堀場製作所
〒 601-8510
京都市南区吉祥院宮の東町 2
https://www.horiba.com/jp/publications/readout/

DTP・製版・印刷・製本　株式会社 写真化学

お問い合わせ先
株式会社堀場製作所
開発本部　R&D プランニングセンター
オープンイノベーション推進室
TEL：075-313-8121（代）
E-mail：readout@horiba.co.jp

HORIBA

Explore the future